VISTAS IN GEOLOGICAL RESEARCH

VISIONS IN GEOLOGICAL SCIENCES (VIGS 2023)

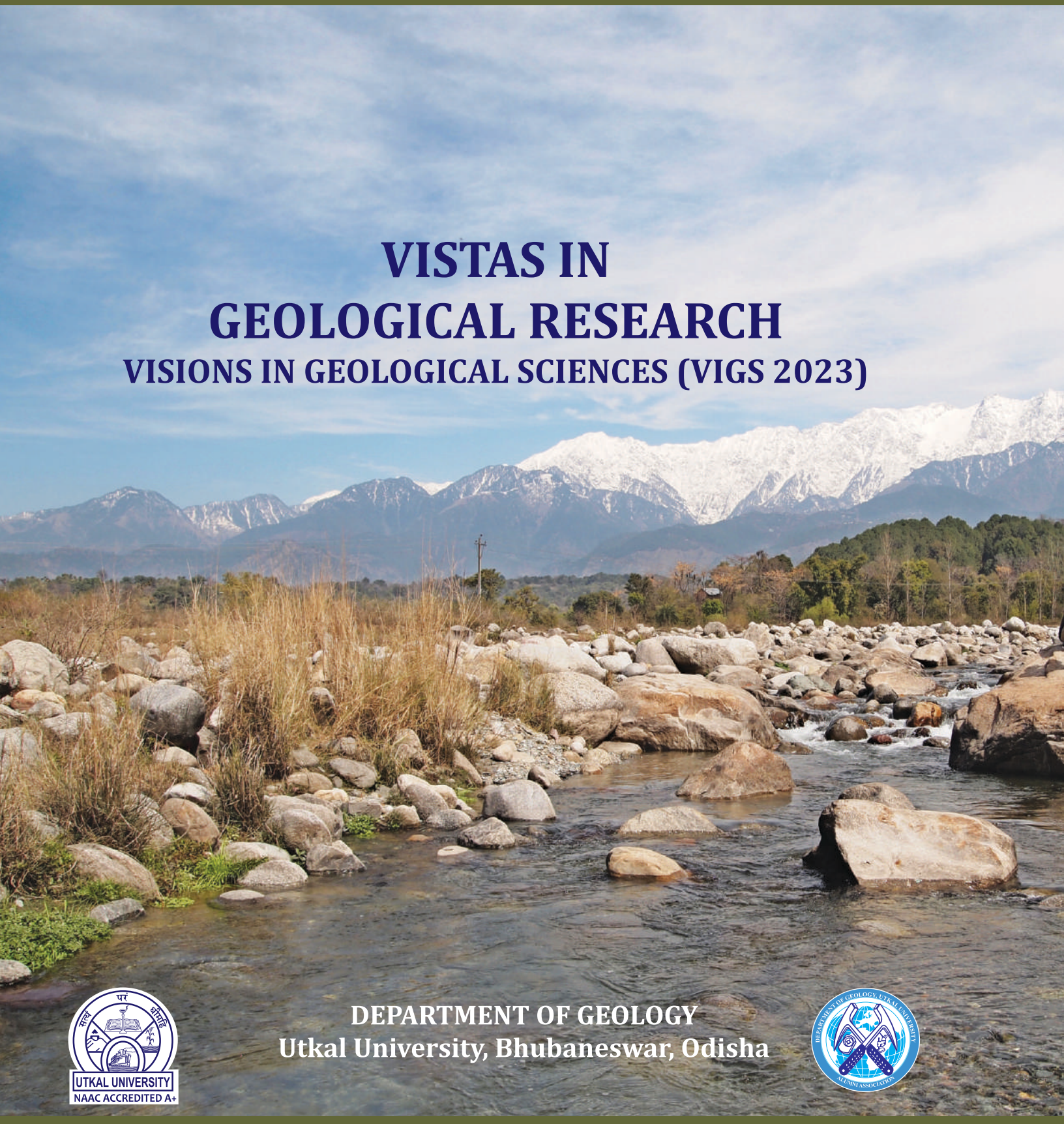

DEPARTMENT OF GEOLOGY
Utkal University, Bhubaneswar, Odisha

Special Publication in Geology (Vol-19)

VISTAS IN GEOLOGICAL RESEARCH

VISIONS IN GEOLOGICAL SCIENCES 2023

P.G. Department of Geology,
Utkal University, Bhubaneswar
Odisha

ISBN 978-93-5813-109-3

Published By:

Department of Geology Utkal University,
Bhubaneswar-751004 &
Alumni Association

Printed By:

Ankita Graphics, Bhubaneswar
Cell: 9437077337, E-mail: saroj77337@gmail.com

From the Editor's Desk

Education feeds the soul and nourishes the mind. Seminars are the festivals of learning. The Geology Department Alumni Association of Utkal University have planned a yeoman service to the geologist fraternity and mining industries by organizing a national seminar on geology and environment.

The national seminar "Vision in Geological Sciences 2023" is enriched with thirty nine research papers from various universities of India, however, a large number of papers are based on geology of Odisha. The recent happenings in Turkiye and Uttarakhand, Lithium finds in Reasi district of Jammu & Kashmir and apprehension due to land subsidence in Talcher are issues which may not be directly addressed in this seminar, but we hope to generate a deliberation which may educate our younger generation in the fundamentals of geoscience from a modern perspective to help us find answer to some of these questions.

It is not possible to write a few words on each paper in this volume but certainly by sampling a few we can appraise the reader the diversity of subjects covered by these research papers.

Petrography and microtextures of chromite ores of Asurabandha make a significant contribution to this volume (Ankita Behera,B.R.Nayak). Syn-sedimentary breccias in Iron Ore Group of rocks (P.K.Nayak) and the erosion-deposition of DID in Chamakpur (A.Parida) are relevant studies to understand various aspects of iron ore deposits of Keonjhar and Sundergarh districts of Odisha.

Seismic hazard assessment in and around Kangra valley (Ritu Mohapatra) and the paper on recent seismicity in Chenab Valley (Ahsan) deserve encouragement to carry forward their studies in an area which has become so relevant after the Joshimath and Turkiye's earthquake. The papers on hydrogeochemistry, groundwater, incursion of saline water in the coastal tract (SmrutipragyanParija) and the heavy metal pollution in the groundwater of Baliapal block (Pritam K. Barik) are significant contributions to society.Petrochemical analysis for evaluation of hydrocarbon potential in Tipam Formation of Assam (Sumani Das) makes an interesting study in hydrocarbon geology. Study of sand grain surface microtextures, under SEM, to unravel the depositional environment (P.C.Das) is a modern tool for sedimentological studies. Palaeofloral assemblage from a part of West Bokaro Coalfield (Soumyashree Nanda) and the effect of monsoonal variation on benthic foraminifera in Chilika Lagoon (K.R.Mallick) are some intriguing studies in palaeontology.

The organisers of this national seminar hope to achieve the objective of documenting the recent advances made in the researches in economic geology, physical geology, hydrogeochemistry, palaeontology and environmental science.

Editorial Board

VISTAS IN GEOLOGICAL RESEARCH

VISTAS IN GEOLOGICAL RESEARCH
Special Publication in Geology (19), March 2023, pp. 1-9

Random Reflectance Characteristics of Huminite, Vitrinite, Liptinite and Inertinite Maceral Groups for Coal Samples from the United States

ANUBHAV SHUKLA*, ANUP K. PRASAD AND ATUL K. VARMA

[a] Department of Applied Geology, Indian Institute of Technology (Indian School of Mines) Dhanbad-826004,Jharkhand, India
*E-mail: anubhavshukla123@gmail.com

Abstract: The heterogeneity of coal is visible in microscopic studies. The reflectance and fluorescence properties are widely used to distinguish constituents of coal (macerals and micro-lithotypes). Identification of macerals, a microscopic organic constituent of coal such as inertinite, vitrinite, and liptinite groups and sub-groups, is done based on their shape, size, colour, relief, reflectance, fluorescence, and spectroscopic properties under the microscope. The level of coalification and maturity of coal can be examined through the use of reflectance of the vitrinite segment in various coals. Nowadays, the standard framework for classifying coals by rank is predominantly based on their physical/chemical qualities. The relations of vitrinite reflectance in other coals can be utilized for proposed rank parameters. Vitrinite reflectance measurement on over approx. 400 coal samples were collected, in that almost 200 samples of different macerals were taken from North Slope Alaska (Nanushuk formation), and the rest were from Texas and Arkansas states of Gulf coast basin, Southern U.S. A. The significant level of maturity from the coalification process has been determined.

INTRODUCTION

Coal is a mixture of heterogeneous materials made of organic and inorganic substances. It is a Rock with no peculiar composition and crystal structure. The main vast source of land plant matter provides a favourable environment for major coal holds rise up at the late Carboniferous and Permian(Scott and Rex, 1985; Teichmüller, 1987). The measure of the coal reserves of these ages possesses around 56% of total world reserves. The second vital coal deposits formed in the Jurassic period, and the third formed in the Cretaceous and Tertiary periods. The thickest coal seam on the planet is found in the Tertiary period. Six nations hold more than 75% of proven recoverable reserves: the USA has 25%, the Russian Federation takes second place with 16%, and China, Australia, India, and Germany have 12%, 9%, 8%, and 7% separately (British Petroleum, 2021). Here, maceral composition is measured by optical microscopy which takes account of the original plant components visible in the coal sample and their early depositional conditions like oxidizing or reducing environments, and rank, which gives us an idea about the successive metamorphic account (Van Krevelen, Hermans and Schuyer, 1957). The percentage of Carbon (C) on earth is 0.36%. Dynamic carbon is responsible for all kinds of carbon deposits like coal, petroleum & natural gases, coal bed methane (CBM), and gas hydrates (Das, Saikia and Baruah, 2016; Varma et al., 2019; Saikia et al., 2021).

SOURCE OF DATA

The samples used in the present work were downloaded from multiple studies in a coalbed methane drilling project in Wainwright, Alaska, a coalbed methane study in Caldwell, Parish, Lousinana and a study evaluating coal rank and coalbed gas potential in Ashley and Bradley counties, Arakansas (Hackley et al., 2006) and a review of lignite resources of the Jackson Purchase Area of western Kentucky and western Tennessee (Hackely and Kolak, 2008). Organic petrographic analysis for vitrinite reflectance and maceral composition for all samples was completed at the U.S. Geological Survey Organic Petrology Laboratory in Reston, Virginia. Other organizations use different classifications for macerals in coal. (https://energy.usgs.gov/Coal/OrganicPetrology/PhotomicrographAtlas/OPTICCoalMaceralClassification.aspx).

METHODOLOGY

Maceral (optically microscopic, homogeneous, an organo-petrographic entity of coal) are originated from the plant remains and the results of the peatification and coalification process. In the peatification procedure, the plant remains have experienced biochemical change. After the burial of peat, the coalification process takes place. Macerals are named after the particular plant tissues commonly preserved in swamps as peat. Morphological identities and level of gelification also help in recognizing Macerals. Four groups of macerals can be found, i.e., Vitrinite (for hard coal), Huminite (for soft coal), Liptinite (previously known as Exinite), and Inertinite. Megascopic identification of coal was made on the basis of its physical properties like colour, hardness, fracture, specific gravity, density, and coal band analysis (lithotypes analysis). In microscopic studies (petrography of coal), macerals within the coal were characterized by their specific property under the transmitted or fluorescent light in the microscope, like size and shape of the material, reflectance fluorescence, and related structures. Vitrintie Random reflectance (Ro, %) is an important parameter for coal characterization. It is a common technique for estimating the coal's relative amount of coalification: rank, maturity or other organic substances. From this, it helps to identify the rank of the coal sample. It measures random orientations of vitrinite in nonpolarized white light. In general, the Ro value is the mean of 50 to 100 measurements. Ro random is the most common value employed in vitrinite reflectance measurements. In certain international coal classification schemes, reflectance measurements are utilised. The relationship between Ro, percent (%), and rank of a sample of coal is depicted in Table 1.

Table 1: Relationship between the random reflectance (Ro,%) and rank of coals (McCartney and Teichmüller, 1972; Hackely and Kolak, 2008).

Sl.	Rank of coal	Random Reflectance (Ro,%)
1.	Lignite	< 0.35
2.	Subbituminous	0.30-0.50
3.	High volatile bituminous	0.50-1.12
4.	Medium volatile bituminous	1.12-1.51
5.	Low volatile bituminous	1.51-1.92
6.	Semi-anthracite	1.92-2.50
7.	Anthracite	>2.50

HUMINITE

Huminite, also known as Brown coal, is a group of macerals whose colour is medium grey and soft compared to vitrinite, and reflectance (random, Ro) measured in oil is generally ≤ 0.5. Huminite is characterized by relatively low carbon and high oxygen content compared to the other maceral groups. It is the precursor of vitrinite and occurs in coal seams due to anaerobic preservation in peatlands/mires. Most of the tertiary coals have their major part of composition made up of huminitic substances (Sýkorová et al., 2005).

Maceral classification and Formation

The huminite group contains 3 sub-group and 6 macerals. (i) Telohuminite (made up of the lower part of tree-like woody tissues of the stem and root) appears in layered and sheet form. (ii) Detrohuminite (mainly consists of the strongly crushed upper part of a tree, i.e., branches, stem, and leaves) appear as groundmass of humic substance. (iii) Gelohuminite appears as a structureless filling of humic fluid in cell lumens, cracks or space within the coal. These subgroups are further subdivided into macerals like telohuminite is divided into two macerals Textinite, dirty yellow to brown made up of spherical to sub-spherical ungelified cell walls, and Ulminite, pale brown to dark brown woody type appearance (Fig. 1a). Detrohuminite is further subdivided into two macerals Attrinite, composed of strongly deteriorated loosely packed coarse grains, and Densinite, a fine-grained, well-packed gelified mixture of humic substances. Gelohuminite has two maceral types, i.e., Corpohuminite, which is a structureless, spherical to elongated humic cell filling, and Humicgelinite, which is structureless & compact (Levigelinite), spongy to porous type texture (Porigelinite) (Fig. 1b).

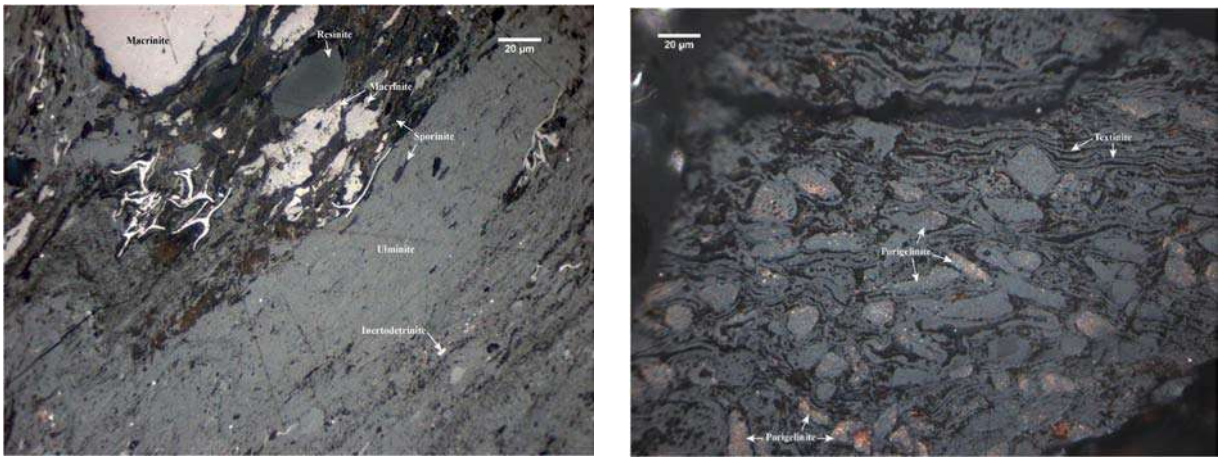

Fig. 1: Organic petrographs of (a) Ulminite,(b) Humic-gelinite (Source: USGS database).

VITRINITE

From the compaction of huminite, vitrinite is formed. Based on ICCP system, vitrinite defines a group of macerals whose colour is dark & hard, and reflectance (random, Ro) measured in oil is generally ≥ 0.5. The colour and reflectance of the vitrinite progressively change with rank, except in some places where the contact metamorphism causes coalification (Handbook, 1998). Vitrinite macerals are rich in carbon compared to other maceral groups (Paradise and Goswami, 2007; Mishra, Sharma, et al., 2016).

Maceral classification and Formation

The vitrinite group contains 3 sub-group and 6 macerals derived from humic matter. Sub-groups are Telovitrinite (derived from the lower part of trees, like woody tissues of the stem and root), Detrovitrinite (derived from strongly crushed branches, stem, and leaves), and Gelovitrinite (derived from humic gel solutions filled in empty spaces, voids, and cracks). Telovitrinite subdivided into Telinite and Collotelinite macerals, which show clearly visible cell walls and homogeneous distribution (Fig. 2a). Detrovitrinites are subdivided into Vitrodetrinite, made up of small vitrinitic material after the strong deterioration of woody tissues; when these small fragments are deposited in the layered form, that is called Collodetrinite (Fig. 2b). In gelovitrinite, when the humic solution is filled in empty cells, it is Corpogelinite. Similarly, when the solution is filled in empty cracks and voids, then it is Gelinite maceral. Vitrinite Random reflectance measured in oil ranges from 0.5-2.5% or higher depending upon the maturity of the coal. The Vitrinite group of macerals do not respond to fluorescent light and shows dark colours (Mishra, Bhowmick, et al., 2016; Zhou et al., 2017).

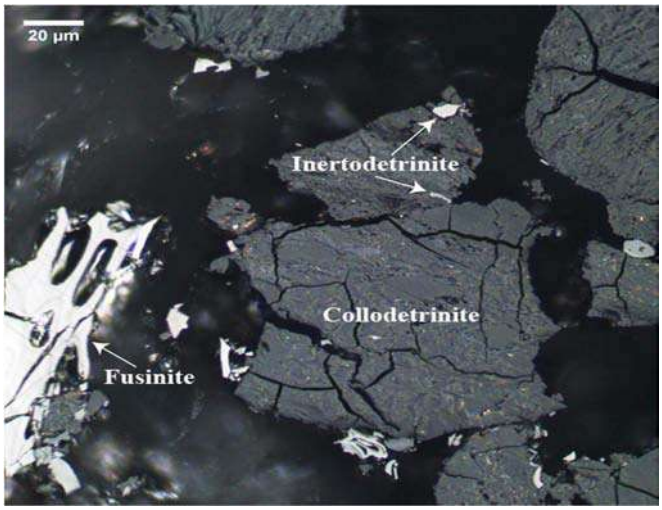

Fig. 2: Organic petrographs of (a) Telinite,(b) Collodetrinite (Source: USGS) database).

LIPTINITE

Liptinite is a group of macerals mainly made up of exine parts of the plant like spores, pollens, resins, and other fatty-rich tissues; because of this, it is also known as Exinite in the previous works of literature. (Pickel et al., 2017). This maceral group is rich in hydrogen content. These get volatilized to produce gases and oily tars; hence this maceral group has the greatest potential to produce oil and gas.

Maceral classification & Formation

In liptinites, primary macerals originate from the humic matter, but secondary macerals (such as bituminite and exsudatinite) are formed during the coalification process. Macerals of this group have a distinct morphology and colour variation under fluorescent light, dark grey to black under the reflected white light, depending upon the coal rank. Liptinites show very low reflectance compared to other maceral groups. Under the fluorescence light, it is easy to recognize because of the distinct colour, greenish-yellow in the UV extraction;

chlorophyllinite pigments show blood red colour under fluorescent light. Liptinite group contains nine maceral types i.e. Sporinite; derived from spores and pollens of the plant; Resinite, humic substance filled in cells or empty spaces in spherical to sub spherical shape and if it's in cracks then elongated; Cutinite, one side edge of leaves, strip type distribution, greenish yellow in fluorescent light (Fig. 3, a & b); Suberinite, one on one cell wall formation and lemon yellow under the fluorescence light; Alginite, derived from the algal matters at the time of coal formation, if its distributed in lens shape and internal structures is visible then its telalginite maceral variety, if distribution is linear then it is lamalginite maceral variety; Exsudatinite, formed after the coalification process, when liquid hydrocarbon of other liptinite macerals takes place in empty cell; Chlorophyllinite, derived from round shaped chlorophyll pigments; Liptodetrinite, fine grained fragment of other liptinite group macerals taken place as in thread type structure; Bituminite, degradation product of various organic matter, lamellar nature in distribution.

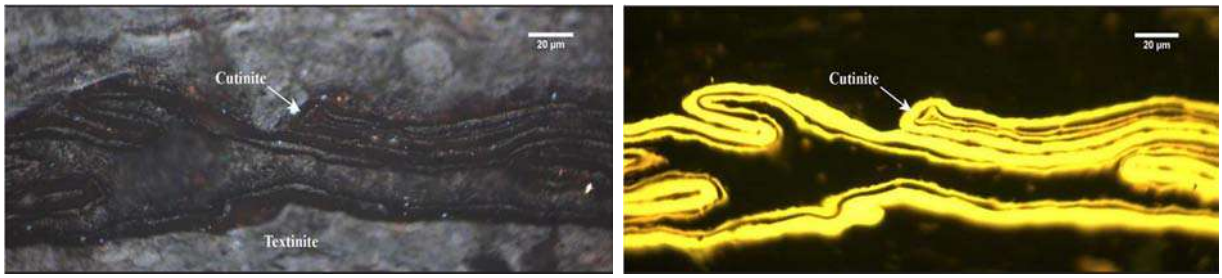

Fig. 3: Organic petrograph of Cutinite maceral of Liptinite group. (a) under reflected light, (b) under fluorescent light (Source: USGS database).

INERTINITE

Inertinite is common in most coals (Anon, 2001); based on the system, inertinite defines a group of macerals whose reflectance is generally higher in the comparison of vitrinite and liptinite maceral groups. Inertinites generally show high carbon and low hydrogen and oxygen contents because of their greater degree of aromatization and condensation (Taylor et al., 1998). The assemblage percentage of inertinite is higher in Gondwana coal compared to Mesozoic and Tertiary coal. The chemical and botanical precursors of inertinite are the same as vitrinite. However, significantly some changes are there because, during the time of coalification, vitrinite follows the vitrinization path, and inertinite follows the fusinization path. The interval in dehydration and oxidization forced vitrinite to change into inertinite.

Maceral classification and Formation

Constituents of this maceral group are generally inert/non-reactive compared to the other maceral groups because they will not react to temperature during the entire course of coalification and carbonization (D. Chandra and Singh, 2000). However, it is known that inertinite is not completely inert; micrinite and semifusinite react with temperature up to a limited extent. The group's constituents undergo the oxidization process during the time of coalification. The Inertinite group's macerals generally form due to dehydration and oxidization of vitrinitic macerals. Macerals of this group are Fusinite, grey to white in colour, and it shows well-preserved cell cavities and high reflectance; Semifusinite, same as fusinite but undeveloped cell walls, made up of leaves and stem tissue of a plant (Fig. 4a); Funginite, derived from fungal matter present in plants, visible fungal structure, dark in colour, does not

show fluorescence; Macrinite, oval to round shaped bodies, white to light grey in colour, the smallest size is >10 µm (Fig. 4b); Micrinite, fine-grained inertinite, if the size of Macrinite is smaller than 10 µm then it will be called as micrinite., size is < 2µm; Inertodetrinite, fragments of inertinite macerals deposited in threaded form, does not show fluorescence; Secretinite, pale yellow to yellowish-white, round, vesicles to non-vesicle, and equant to elongate bodies without general plant structure.

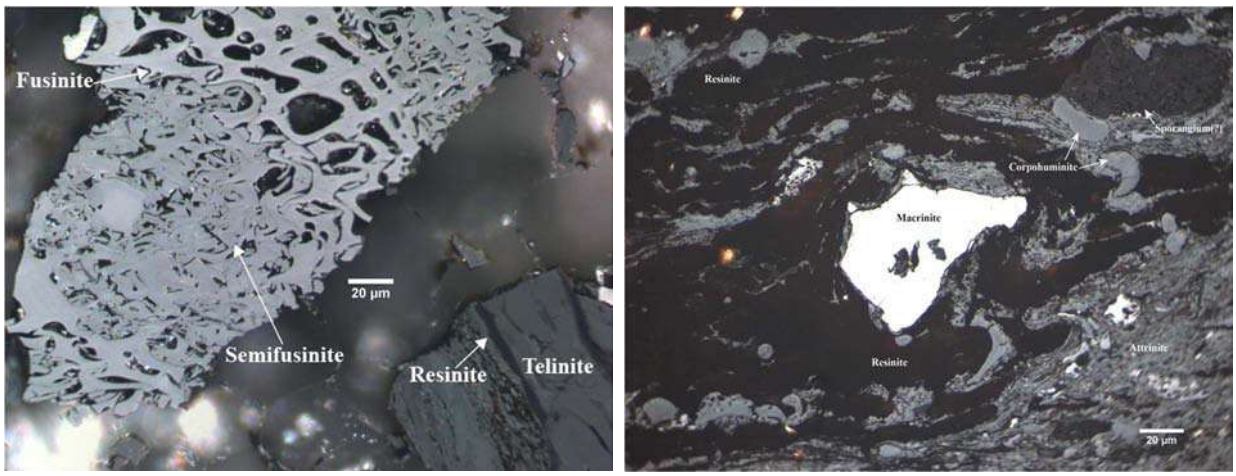

Fig. 4: Organic petrographs of (a) Semifusinite,(b) Macrinite (Source: USGS database).

RESULT AND DISCUSSION

Reflectance and fluorescence properties of Huminite

In the Huminite maceral group, random reflectance (Ro,%) varies from 0.31-0.54%, where Attrinite and Ulminite have the lowest reflectance and Humic Gelinite have a range bound Ro,% of 0.40-0.42% (Fig. 5). In peat, it attains a maximum limit of 0.26 Ro, % (Sýkorová et al., 2005), and under fluorescent light, it shows a yellow-brown to orange-brown colour best viewed in textinite A and ulminite A.

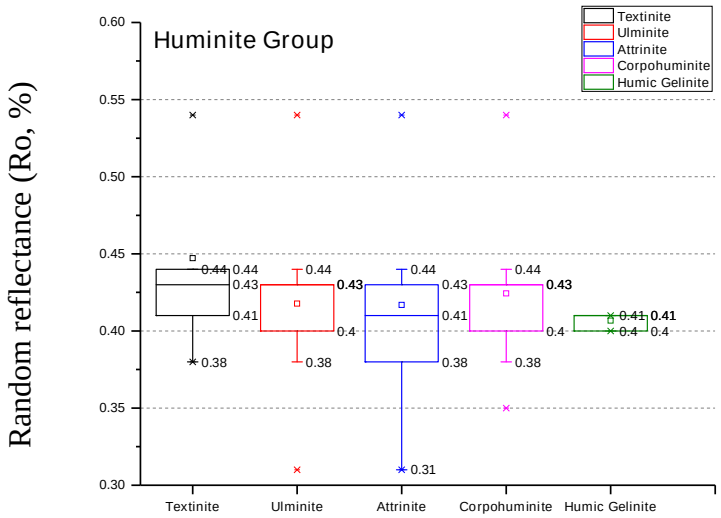

Fig. 5: Variation of random reflectance (Ro, %) in Huminite maceral group.

Reflectance and fluorescence properties of vitrinite

Vitrinite Random reflectance measured in oil begins at approximately 0.5% and attains its maximum intensity <2.0%. The present study ranges from 0.47-0.55%, with a mean of approximately 0.5 Ro %. Macerals of this group do not show fluorescence under fluorescent light; vitrinite maceral shows dark-brown to black colour. (Fig. 6).

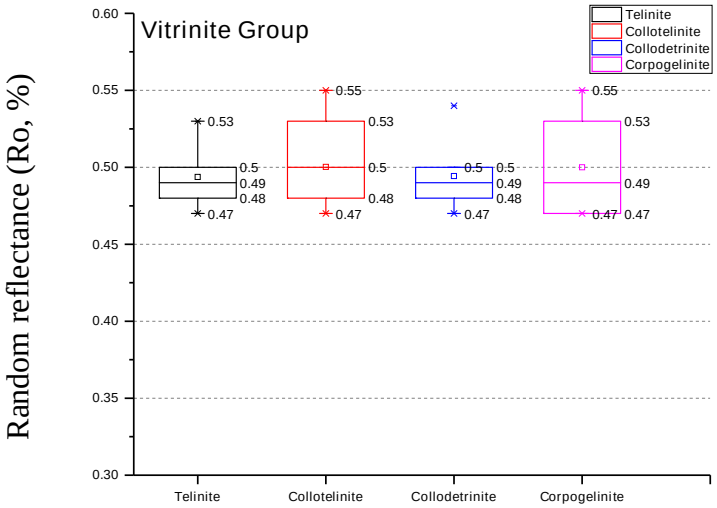

Fig. 6: Variation of random reflectance (Ro, %) in Vitrinite maceral group.

Reflectance and fluorescence properties of liptinite

In the present work, random reflectance (Ro,%) for cutinite, resinite and suberinite range between 0.37-0.54%, while sporinite has the lowest Ro,% value of 0.35%. Exsudatinite and Liptodetrinite ranged bound in betwenn 0.38-0.44% (Fig.7).

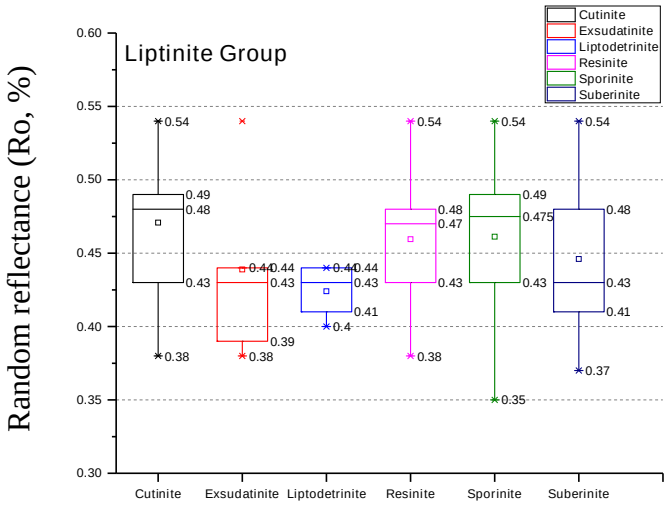

Fig.7: Variation of random reflectance (Ro, %) in Liptinite maceral group.

Reflectance and fluorescence properties of inertinite

Inertinite contains highly reflective components; reflectance is slightly higher than vitrinite, especially in anthracite. It shows no fluorescence and is dark grey to pale yellow under the

reflected light. The distribution of Ro, % for inertinite maceral is highest in the present study and varies from 0.35-0.54%, whereas Macrinite has the lowest variation from 0.38-0.44%, Ro (Fig 8).

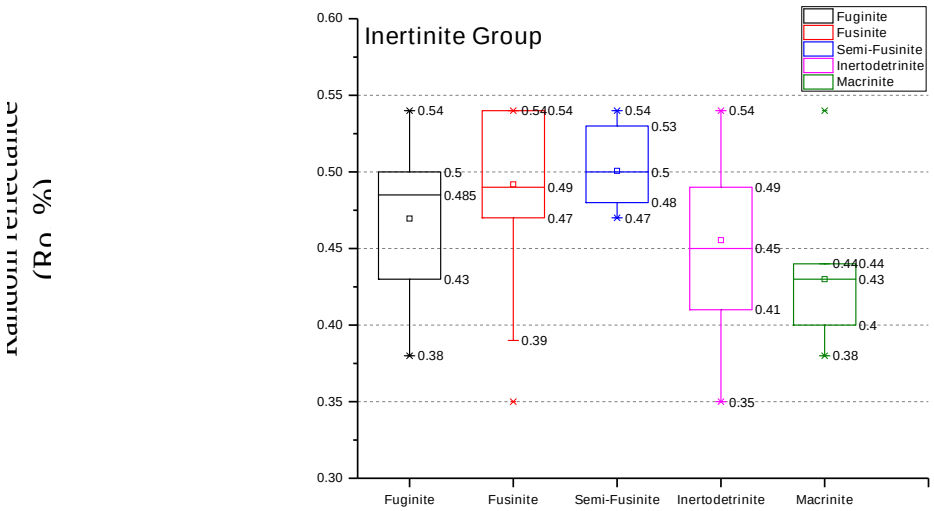

Fig 8Variation of random reflectance (Ro, %) in Inertinite maceral group.

CONCLUSION

In the present study, the authors estimated the variability of the random reflectance for the various maceral groups of US coal. Vitrinite random reflectance also depends upon the depth of the coal seam and the level of coalification. It is higher at greater depth as the maturity of coal increases. For the huminite maceral group, random reflectance ranges from 0.31-0.54% with a mean value of 0.42%, while for the vitrinite maceral group, it ranges between 0.47-0.55%, and the mean is 0.50%. Similarly, for the liptinite and inertinite group of macerals, the range of variation is 0.35-0.54%, Ro with a mean of approx. 0.48% and 0.47%, Ro respectively. With the help of random reflectance, the rank of coal used in this work is Sub-bituminous to High volatile bituminous.

REFERENCES

Anon (2001) ‘New inertinite classification (ICCP System 1994)’, Fuel, 80(4), pp. 459–471. doi: 10.1016/S0016-2361(00)00102-2.

British Petroleum (2021) Statistical Review of World Energy globally consistent data on world energy markets, BP Statistical Review of World Energy.

D. Chandra, R. M. S. and Singh, M. P. (2000) TEXT BOOK OF COAL (Indian context). Tara Book Agency.

Das, T., Saikia, B. K. and Baruah, B. P. (2016) ‘Formation of carbon nano-balls and carbon nano-tubes from northeast Indian Tertiary coal: Value added products from low grade coal’, Gondwana Research. International Association for Gondwana Research, 31, pp. 295–304. doi: 10.1016/j.gr.2015.01.012.

Hackely, P. C. and Kolak, J. J. (2008) ‘Petrographic and vitrinite reflectance analyses of a suite of high volatile bituminous coal samples from the United States and Venezuela U . S . Department of the Interior’, U S Geological Survey, Open-File, p. 36.

Hackley, B. P. C. et al. (2006) 'Reflectance Measurements of Well Cuttings from Ashley and Bradley Counties , Arkansas U . S . Department of the Interior'.

Handbook, I. (1998) 'The new vitrinite classification (ICCP System 1994)', Fuel, 77(5), pp. 349–358. doi: 10.1016/S0016-2361(98)80024-0.

Van Krevelen, D. W., Hermans, P. H. and Schuyer, J. (1957) Coal Science. Aspects of Coal Constitution. Elsevier publishing company.

McCartney, J. T. and Teichmüller, M. (1972) 'Classification of coals according to degree of coalification by reflectance of the vitrinite component', Fuel, 51(1), pp. 64–68. doi: 10.1016/0016-2361(72)90041-5.

Mishra, V., Sharma, M., et al. (2016) 'Changes in organic structure and mineral phases transformation of coal during heat treatment on laboratory scale', International Journal of Coal Science and Technology. China Coal Society, 3(4), pp. 418–428. doi: 10.1007/s40789-016-0153-y.

Mishra, V., Bhowmick, T., et al. (2016) 'Influence of coal quality on combustion behaviour and mineral phases transformations', Fuel. Elsevier Ltd, 186, pp. 443–455. doi: 10.1016/j.fuel.2016.08.092.

Paradise, M. and Goswami, T. (2007) 'Carbon nanotubes - Production and industrial applications', Materials and Design, 28(5), pp. 1477–1489. doi: 10.1016/j.matdes.2006.03.008.

Pickel, W. et al. (2017) 'International Journal of Coal Geology Classi fi cation of liptinite – ICCP System 1994', 169, pp. 40–61.

Saikia, B. K. et al. (2021) 'Geochemistry and petrology of coal and coal fly ash from a thermal power plant in India', Fuel. Elsevier Ltd, 291(January), p. 120122. doi: 10.1016/j.fuel.2020.120122.

Scott, A. C. and Rex, G. (1985) 'The formation and significance of Carboniferous coal balls', Philosophical Transactions of the Royal Society B, 311(October 1985), pp. 123–137. doi: 10.1098/rstb.1985.0144.

Sýkorová, I. et al. (2005) 'Classification of huminite - ICCP System 1994', International Journal of Coal Geology, 62(1-2 SPEC. ISS.), pp. 85–106. doi: 10.1016/j.coal.2004.06.006.

Taylor, G. H. et al. (1998) 'Organic petrology'.

Teichmüller, M. (1987) 'Recent advances in coalification studies and their application to geology', Geological Society Special Publication, 32, pp. 127–169. doi: 10.1144/GSL.SP.1987.032.01.09.

Varma, A. K. et al. (2019) 'Petrographic controls of coal from Ib valley Basin for carbon nano-products formation', International Journal of Coal Geology. Elsevier, 211(February), p. 103211. doi: 10.1016/j.coal.2019.103211.

Zhou, S. et al. (2017) 'Effects of the coalification jump on the petrophysical properties of lignite, subbituminous and high-volatile bituminous coals', Fuel. Elsevier Ltd, 199, pp. 219–228. doi: 10.1016/j.fuel.2017.02.092.

VISTAS IN GEOLOGICAL RESEARCH
Special Publication in Geology (19), March 2023, pp. 10-15

Permian Floral Assemblage of a part of East Bokaro Coalfield, Jharkhand, India and its Implications

PARESH RANJAN DASH[1], SHREERUP GOSWAMI[2*], SANGHAMITRA PRADHAN[1], GYANA RANJAN PARIDA[2] AND DURYADHAN BEHERA[1]

[1]Department of Earth Sciences, Sambalpur University, Jyoti Vihar, Burla-768019
[2]Department of Geology, Utkal University, Vani Vihar, Bhubaneswar- 751004
*Corresponding author mail id: goswamishreerup@utkaluniversity.ac.in

Abstract: The East Bokaro Coalfield is one of the major coalfields in terms of coal potentiality amongst Indian coalfields. It covers an area of 237 sq. kms. in Hazaribagh and Bokara districts of Jharkhand and bounded by 23°44' and 23°49' N latitude and 85°42' and 86°04'30" E longitude. 'Bokaro Coalfield' the name is first coined by WILLIAMS (1846–1847) after the river Bokaro which flows for a distance of about 40 km in this region. The research work deals with floristic analysis of fossil bearing horizons to establish the palaeoclimate and palaeovegetation in the studied area. The floral remains are intensively searched in different shale and sandstone units of the coalfield and samples are collected from Karo Open Cast Project (OCP) of Bokaro & Kargali (B & K) area of East Bokaro Coalfield. The Permian megafloral assemblages are exclusively studied by means of species diversification and elementary morphology (apex, base, midrib, shape and mesh form) to reconstruct the palaeovegetation and palaeoclimate during the deposition of Lower Gondwana sediments in the studied area. The *Glossopteris* species of various size ranges from very small to very large are recovered from fine-grained carbonaceous shale units. *Glossopteris communis* and *G. vulgaris* dominate in the assemblage, while *G. tenuifolia* and *G. searsolensis* are sub-dominant in the collection. The floral composite depicts a lush green vegetation of arborescent deciduous trees with small herbs and shrubs during Artinskian-Kungurian age (deposition of Barakar Formation). These land plants are believed to be the major contributors of organic detritus for peat formation in the studied basin. The lanceolate shape, acute apices, acute cuneate bases, entire margins and narrow to broad mesh forms depict a cool to moderately warm climate with high humidity and adequate light intensity during late Artinskian- Kungurian age. Dominance of petiolate leaves in the assemblage suggests prevalence of wind speed in the Permian atmosphere. The formation of coal swamps during Barakar time clearly indicates the coexistence of terrestrial and marshy ecosystem, dense vegetation and sufficient rainfall in this area during Lower Permian period.

Keywords: Permian, Palaeoclimate, Palaeovegetation, *Glossopteris*, Barakar Formation

INTRODUCTION

A thick pile of late Palaeozoic sediments is well deposited in four major Gondwana basins of India namely Damodar, Son-Mahanadi, Godavari and Satpura basins. The various formations of these basins have yielded rich floral assemblages of Permian time. Megafloral assemblages play a vital role in palaeovegetational reconstruction, establishment of stratigraphic position

and depiction of palaeoclimate, palaeoenvironment and palaeobiodiversity in coal bearing formations (Chandra and Chandra, 1988; Goswami, 2004; 2006; 2007; Goswami and Singh, 2013; Goswami et al., 2018b). B & K area is one of the operational areas of the East Bokaro Coalfield located mainly in the Bokaro District and the Hazaribagh District of Jharkhand. The coalfield forms an east-west trending synclinal half-basin closing towards east (Raja Rao, 1987). The present work is a palaeobotanical approach to interpret biostratigraphy, palaeoclimate, palaeobiodiversity, palaeovegetation and palaeoecology during the deposition of coal bearing formations in B & K area. Six genera of order Glossopteridales including thirty-one species and 436 specimens are congregated from the studied location. The assemblage is dominated by *Glossopteris communis* followed by *G. vulgaris.*

GEOLOGICAL SETTINGS

The East Bokaro Coalfield occupies an area of 237 sq. kms. in Hazaribagh and Bokaro districts of Jharkhand and extends over 23°44' and 23° 49' N latitude to 85° 42' and 86° 04' 30" E longitude (Fig. 1). The Bokaro Coalfield can be recognised as an elongated strip of Gondwana sediments stretching over 64 km in EW direction and 12km in width. Lugu hill divides the coalfield and the eastern most part is known as East Bokaro Coalfield (Fox, 1934). A complete sequence of Gondwana sediments ranging from Talchir to Mahadeva Formation is deposited in the East Bokaro Basin. The Damuda group of sediments lie unconformably over the Precambrian metamorphics. The Talchir Formation is present in the form of patches which are barely of 2m- 3m thick. Thus, it has not recorded over the major part of the basin (Raja Rao, 1987). The Barakar Formation directly lies over the Precambrian basement and occupied a major part of the field, attains maximum thickness i.e. 900m amongst other formations. Nearly 500m thick Barren Measures Formation crops out along the axial region of the basin.

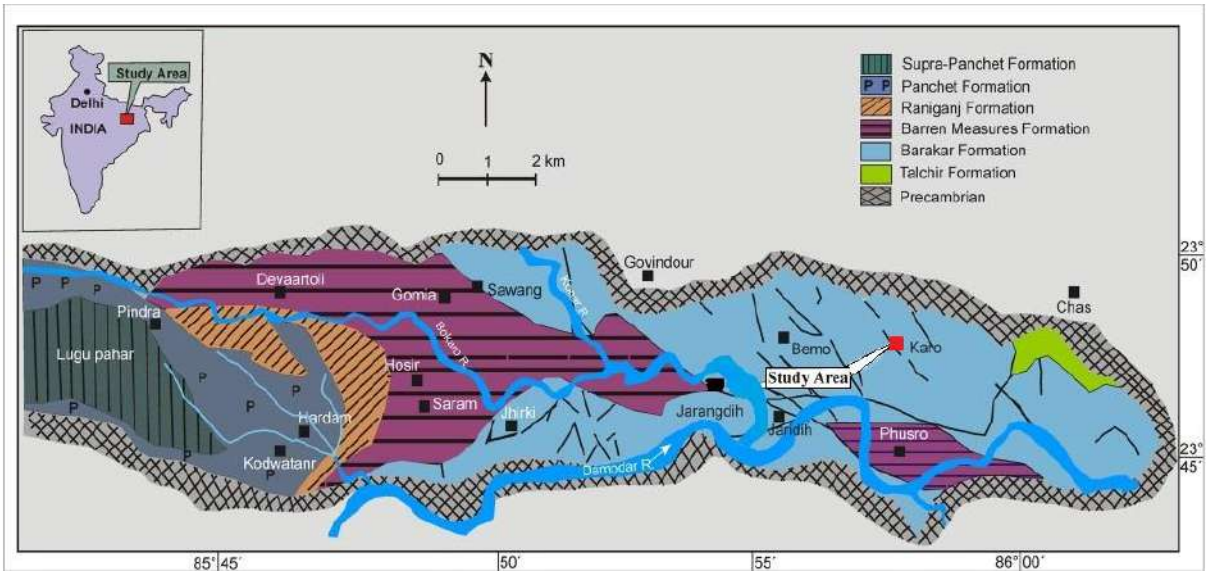

Fig. 1: Geological map of East Bokaro Coalfield area, Jharkhand showing various localities (after Raja Rao, 1987; Saxena *et. al,* 2020).

The younger Raniganj and Panchet strata are of 600m thick and superimposed by Supra-Panchet/Mahadeva (?) Formation (Raja Rao, 1987). The Gondwana formations of East Bokaro Coalfield are intruded by dolerites and lamprophyres of Lower Cretaceous age. The Barakar Formation accounts the maximum coal seams of the basin (Raja Rao, 1987). The stratigraphic succession of the coalfield is represented in Table 1.

Table 1: Geological succession of the East Bokaro Coalfield area, Jharkhand (Raja Rao, 1987; Saxena *et. al*, 2020)

Age	Formation	Lithology
Lower Cretaceous	Intrusive	Lamprophyre and dolerite dykes and sills
Upper Triassic	Supra-Panchet	Coarse-grained ferruginous sandstone, pebbly sandstone and red clay (600 m).
Unconformity		
Lower Triassic	Panchet	Greenish micaceous sandstone, buff fine-grained sandstone, red, and green shale (500–600 m).
Upper Permian	Raniganj	Medium to coarse–grained calcareous, sandstone, fine-grained greenish sandstone, grey shale, carbonaceous shale and thin coal seams (600 m).
Middle Permian	Barren Measures	Flaggy, fine-grained ferruginous sandstone micaceous sandy shale and black shale with siderite band (500 m).
Lower Permian	Barakar	Coarse-grained arkosic sandstone, fine-grained laminated sandstone, grey shale, carbonaceous shale and coal seams (900 m).
U-Carboniferous to L-Permian	Talchir	Tillite, greenish sandstones and needle shale
Pre-Cambrian	Pre-Cambrian	Granite gneisses, amphibolites, and Mica schist

METHODOLOGY

The coal bearing formations in the part of B & K area of East Bokaro Basin are exclusively searched to delineate fossiliferous horizons. A large number of floral imprints were recovered from fine grained carbonaceous shale layer of Karo Colliery of B & K area. The retrieved chunks containing fossil imprints are carefully brought to the laboratory. The samples are catalogued as KTR and specified by numbers and are kept in the repository of Department of Earth Sciences, Sambalpur University. Almost all specimens were further cleared by removing the superficial layers with the help of Palaeobotanical tools. The morphological features of the leaves like size, shape, apex, base, midrib and nature of veins were examined under Stereo-zoom Olympus microscope. The collection was then nomenclated and grouped systematically by following International Stratigraphic Code (Murphy and Salvador, 1999), Modern plant systematic (Novíkov and Barabaš- Krasni, 2015) and the International Code of Nomenclature (Turland et al., 2018). The specimens are photographed with DSLR-5300 digital camera.

RESULT AND DISCUSSION

The *Glossopteris* flora is well known from almost all the major Gondwana basins of India. An extensive exposition of a rich and well-preserved Glossopterid floral assemblage recovered from the Barakar Formation. The mega floral assemblage is dominated by the

order *Glossopteridales* recovered from the area includes six genera (*Glossopteris, Vertebraria, Eretmonia, Glossotheca, Partha and Venustostrobus*) and thirty- one species viz. *Glossopteris communis, G. barakarensis, G. bosei, G. browniana, G. decipiens, G. densinervis, G. giridihensis, G. indica, G. intermedia, G. intermittens, G. karharbariensis, G. linearis, G. maheswarii, G. major, G. mohudaensis, G. nakkarea, G. nautiyalii, G. pantii, G. raniganjensis, G. searsolensis, G. senii, G. stenoneura, G. taeniensis, G. tenuifolia, G. vulgaris, G. zeilleri, Vertebraria indica, Partha Spatulata, Venustostrobus indicus, Eretmonia utkalensis, Glossotheca orissiana and stem cast.* Both of the genera *Glossopteris* and *Vertebraria* are reported from the same bed in abundance. The fine-grained carbonaceous shale with good preservation of *Glossopteris* implies the deposition of sediments in low energy environment. Leaves are longer than broad in size and midribs were thick persistent. The meshes are narrow polygonal to pentagonal in nature. Broadly, the meshes are denser near the margin rather than that of near midrib. In the present megafloral assemblage, dominance of *Glossopteris* genus without the presence of lower Permian taxa (typical Karharbari flora) infers that the sediments belong to Barakar Formation i.e. late Artinskian-Kungurian age.

The maximum proliferation of plants during late Artinskian-Kungurian period indicates conducive climatic condition. The flora habits signified by narrow to medium mesh leaves of medium to large size, lanceolate shape, acute apices, acute cuneate bases with entire margins and narrow vein meshes during late Artinskian- Kungurian depict moderately warm climatic conditions with high humidity (Tiwari and Tripathi, 1988; Goswami et al., 2018b). The dominance of long narrow leaves with acute apices and acute cuneate bases suggests sufficient insolation during the deposition of Barakar Formation. The formation of coal swamps during Barakar time clearly indicates the presence dense vegetation and sufficient rainfall in this area during this period (Chandra and Chandra, 1988; Goswami, 2004; 2006; 2008; Goswami et al., 2006; Goswami and Singh, 2010; 2013; Goswami et al., 2018a, b; Patel et al., 2021, 2022a, b; Tripathy et al., 2021; 2022; Pradhan et al., 2022).

The dominance of *Glossopteris* in the collection illustrates the presence of terrestrial ecosystem. Singh and Maheswari (2000) and Saxena et al. (2020) reported the occurrence of Cordaitales and Filicales from the coalfield. Thus, the presence of marshy ecosystem can be depicted near the vicinity. The terrestrial elements can be the major source of organic detritus for the peat formation in swamps.

CONCLUSION

The present study concludes that the megafloral assemblage recovered from the fine-grained carbonaceous shale horizon of Karo Colliery of B & K area belongs to late Artinskian-Kungurian age. It also suggests that the forests were dense and swampy growing within low lying river valley. The vegetation is lush green subjugated by arborescent deciduous trees bearing *Glossopteris* foliage. The significant floral habits possessed by the assemblage depicts moderately warm high humid climate with sufficient rainfall and maximum insolation during the deposition of Barakar sediments in the studied locality. There were two

interrelated ecosystems i.e. terrestrial and marshy which might have provided conducive coal forming environment near the vicinity.

REFERENCES

Chandra, S. and Chandra, A. (1988) Vegetational changes and their climatic implications in coal-bearing Gondwana; Palaeobotanist v. 36 pp.74- 86.

Goswami, S. (2006) Record of Lower Gondwana megafloral assemblage from Lower Kamthi Formation of Ib River Coalfield, Mahanadi Basin, Orissa, India; J. Biosci. v. 31 pp. 115–128.

Goswami, S. (2008) Marine influence and incursion in the Gondwana basins of Orissa, India: A review; Palaeoworld, v 17(1) pp. 21-32.

Goswami, S. and Singh, K. J. (2010) Occurrences of gymnosperms from Lower Gondwana Formations of Ib River Coalfield, Orissa and their environmental significance; J. Palaeontol. Soc. India, v 55 pp. 121-135.

Goswami, S., Das, K., Sahoo, M., Bal, S., Pradhan, S., Singh, K. J. and Saxena, A. (2018b) Biostratigraphy and floristic evolution of coal swamp floras of a part of Talcher basin, India: a window on a Permian temperate ecosystem; Arab. J. Geosci. v. 11(17) 524.

Goswami, S., Saxena, A., Singh, K. J., Chandra, S. and Cleal, C. J. (2018a) An appraisal of the Permian palaeobiodiversity and geology of Ib River Basin, eastern coastal area, India; J. Asian Earth Sci. v 157 pp. 283–301.

Goswami, S., Singh, K. J. (2013) Floral diversity and geology of Talcher Basin, Orissa, India during the Permian-Triassic interval; Geol. J. v 48 pp. 39–56.

Goswami, S., Singh, K. J. and Chandra, S. (2006) Pteridophytes from Lower Gondwana Formations of Ib River Coalfield, Orissa, and their diversity and distribution in the Permian of India; J. Asian Earth Sci. v 28 pp. 234–250.

Goswami, S. (2004). Biodiversity in Indian Gondwana: A Kaleidoscopic Review. Minetech v 25 (6), pp. 23-36

Murphy, M. A. and Salvador, A. (1999) International stratigraphic guide—an abridged version; Epis. J. Int. Geosci. v. 22(4) pp. 255-271.

Novíkov, A. and Barabaš- Krasni, B. (2015) Modern plant systematics.

Patel, R., Goswami, S., Aggarwal, N. and Mathews, R. P. (2022a) Palaeofloristics of Lower Gondwana exposure in Hingula area, Talcher Basin, Odisha, India: an inclusive study on biomarkers, megafloral and palynofloral assemblages; Historical Biology v 34(9) pp. 1877-1893.

Patel, R., Goswami, S., Aggarwal, N. and Mathews, R. P. (2022b) Lower Gondwana megaflora, palynoflora, and biomarkers from Jagannath Colliery, Talcher Basin, Odisha, India, and its biostratigraphic significance; Geol. J v .57(3) pp. 986-1004.

Patel, R., Goswami, S., Sahoo, M., Pillai, S. S. K., Aggarwal, N., Mathews, R. P. and Singh, K. J. (2021). Biodiversity of a Permian temperate forest: a case study from Ustali area, Ib River Basin, Odisha, India; Geol. J v 56(2) pp. 903-933.

Pradhan, S., Goswami, S., Pradhan, S. S, Das. S. B. (2022) A study on morphotaxonomy and distribution of glossopterid scale leaves from the Barakar Formation, South Karanpura Coalfield, Jharkhand, India. J. Palaeontolo. Soc. India v 67(2) pp. 341-347

Raja Rao, C. S. (1987) Coalfields of India; Bull. Geol. Sur. India Ser. A v 45 pp. 336.

Saxena, A., Murthy, S., & Singh, K. J. (2020). Floral diversity and environment during the early Permian: a case study from Jarangdih Colliery, East Bokaro Coalfield, Damodar Basin, India. Palaeobiodiversity and Palaeoenvironments, v 100(1), pp. 33-50.

Singh, S. M. and Maheshwari, H. K. (2000) On the species of genus *Glossopteris* from Barakar Formation of Karanpura & Bokaro Coalfields, India; Palaeobotanist v 49(3) pp. 409-441.

Singh, S. M., & Maheshwari, H. K. (2000). On the species of genus Glossopteris from Barakar Formation of Karanpura and Bokaro coalfields, India.

Tiwari, R. S. and Tripathi, A. (1988) Palynological zones and their climatic inference in the coal- bearing Gondwana of Peninsular India; Palaeobotanist v 36 pp. 87-101.

Tripathy, G., Goswami, S. and Das, P. P. (2021) Late Permian species diversity of the genus Glossopteris in and around Himgir, Ib River Basin, Odisha, India, with a clue on palaeoclimate and palaeoenvironment; Arab. J. Geosci. v 14(8) pp. 1-22.

Turland, N. J., Wiersema, J. H., Barrie, F. R., Greuter, W., Hawksworth, D. L., and Herendeen, P. S. (2018) International Code of Nomenclature for algae, fungi, and plants (Shenzhen Code) adopted by the Nineteenth International Botanical Congress Shenzhen, China. Koeltz botanical books.

VISTAS IN GEOLOGICAL RESEARCH
Special Publication in Geology (19), March 2023, pp. 16-22

Seed Germination with Devotional Music: An Experiment with Mung Bean (*Vigna Radiata* L.)

SWAMI YUGAL SHARAN[1,2], SHREERUP GOSWAMI[3*], PRANAB KUMAR GHOSH[2], LALIT KUMAR BARIK[2] AND RAJDEEP KUMAR SAW[2]

[1]Department of Earth Sciences, Sambalpur University, Jyoti Vihar-768 019
[2]Braj Gopika Seva Mission, Tutumbarpalli, Pariorada, Tangi, Khurda, Odisha-752023
[3]Department of Geology, Utkal University, Vani Vihar, Bhubaneswar-751004
Email: goswamishreerup@utkaluniversity.ac.in

ORCID: Shreerup Goswami- https://orcid.org/0000-0002-2558-3623

Abstract: The environment is a dynamic interplay of numerous factors, and these factors influence the growth and development of life-forms in a direct or indirect ways. Seed germination and plant growth is affected by air, water, light and nutrients availability in the plant growth medium. Scientific research for the past few decades has shown a growing interest in the impact of sound or to say the vibrational energy on the life process; and has reported that sound especially the rhythmic sound, soft and natural sound, classical music, and chanting has a definite positive impact on plants. Experimentation with a devotional music on the seed germination of Mung bean (*Vigna radiata*) revealed that devotional music has a positive impact on germination percentage, germination index, and seed vigour index when administered for an optimum period with an optimum sound pressure level. Significant and the highest seed vigour index was observed when Mung bean seeds were exposed to devotional music at 90-100dB(A) for a duration of 2 hours per day. Seed vigour index improved by 110.48% in comparison to the control group not exposed to devotional music.

Keywords: Mung bean, seed germination, seed vigour index, devotional music

INTRODUCTION

The dynamism of the life and life-building process rest on the multitude of environmental factor. While the interaction of plants with the natural factors like Light, Temperature, Air, Water, Nutritional Elements, etc., has received much attention in the science and scientific communities, the study of Sound as naturally occurring stimuli remains undervalued (Mishra et al., 2016). With recent development in acoustic science studies of the acoustic impact on plants have gained rapid attention from plant and behavioural scientists in the last few decades (Gagliano, 2013b). Studies in the past have given a definite direction to the fact that sound as stimulation to plants has a definite impact on the growth and development of plants at physical, physiological, biochemical, molecular, and genetic levels (Mishra et al., 2016; Chowdhury et al., 2014). The sound impact on plants is both negative and positive in terms of the development of plants. The impact of sound has varied with the composition of sound, quality, strength, duration of exposure, and obviously the specific subject, the plants being studied.

The present study was directed to find the impact of devotional music as a sound stimulus for the germination of Mung bean Seeds. The rational for such a study was drawn from the review of past scientific research as well as the importance of devotional singing and the glorification of God's name as given in Indian spiritual scriptures. Srila Vrindavandas Thakur in Chaitany Bhagbatam proclaims that lower beings who can't chant by themselves are also benefited when exposed to loud chanting of god's name by human beings (Vrindavandas, 1995). Srila Krishnadas Kabiraj in Chaitany Charitamrita writes plants and creepers were exuberant with joy and ecstasy upon the presence of the divine personality of Sri Chaitany Mahaprabhu and by his melodious chanting of god's name (Kabiraj, 1993). Sri Kripaluji Maharaj in his book Glories of Divine Name explains Astapadi (a conclave of eight verses) composed by Sri Chaitanya Mahaprapbhu and writes that god's name is the very life of all transcendental knowledge. Every utterance of the divine name gives a full taste of its nectarine sweetness that swells in the heart of the chanter, like a surging ocean of everlasting Bliss and Peace (Maharaj, 2009). In Indian scripture it has been repeatedly pointed out that God's name is as powerful as God himself, God resides in each and every name of God, and Chanting God's name aloud is beneficial to all beings. Haid & Huprikar, reported that seed germination and growth of Seedlings were affected by watering them with meditative intents. Germination of pea seeds was significantly higher when watered with the intent of stimulation and germination of wheat seeds was significantly lower when watered with intent of inhibition. Biomass production of wheat seedlings on the tenth day was reported to be significantly lower when compared with untreated one. Thus, it was concluded that the meditative intent behind an action had an effect on the outcome of the action and human interaction via ceremony and rituals can affect the natural world (Haid & Huprikar, 2001).

To consolidate the statement of the spiritual scriptures and the scientific findings resulting from the development of acoustic science, it was believed that the impact of devotional music on plants may give footage for some novel findings. Thus it was planned to make an experimental research entitled "Seed germination with devotional music an experimental study with Mung bean. (Vigna radiata L.)

MATERIALS AND METHODS

The research was conducted in the serene spiritual atmosphere of Braj Gopika Seva Mission situated at Tetumberpalli, Khurda, Odisha, India in February 2022. The control condition for the experimental research was created with the construction of a polyhouse (20mt x 16mt) and ten numbers of specially designed acoustic growth chambers with an internal dimension of 40 x 40 x 72 inches. Acoustic growth chambers were fitted with speakers for audio output and connected to a control panel with music players. Acoustic growth chambers were so designed that all the treatments could be played simultaneously in a single polyhouse without any acoustic interference. Mung Bean seed germination test was conducted in petri dishes with 25 numbers of seeds in each petri-plates. PDM 139 (Samrat) Variety Mung bean was selected for the experiment for its availability and for the matters of an established variety for a long. Twenty-five numbers of seeds were arranged uniformly in a 5 x 5 layout on double layers of pre-soaked germination papers inside the sterilized petri-plates. Distilled water was

used to maintain the moisture condition of the petri-plates. Seed germination parameters were recorded at an interval of 12hrs i.e., twice daily once at 5 am in the morning and another at 5 pm in the evening till 48th hours from initiation of the germination test. The petri-plates were kept in dark beyond the treatment hours.

Six devotional songs were purposively selected from devotional compositions and practices of Sri Kripaluji Maharaj and soundtracks were prepared for a definite time period of 10 minutes, 20 minutes, and 30 minutes each. Thus constitute a combined exposure period of 1 hour, 2 hours, and 3 hours per day. Apart from being semi-classical in nature, the composition had a special attribute of contemplative mediation upon God's name, glories, and pastime. Soundtracks were combined as per the playing hours and single track consisting of two songs each were prepared and recorded on separate pen-drives. Details of the devotional songs used for soundtracks are presented in Table 1.

Soundtracks were played over three ranges of sound pressure levels (SPL) that is 70-80 dB(A), 80-90 dB(A) and 90-100 dB(A) and over three levels of the duration of exposure i.e., 1 hour, 2 hours, and 3 hours per day and thus constituted nine experimental groups. There was one group, which was not exposed to devotional music to form a control group, making a total of ten numbers of treatment levels. Details of the formulation of treatment levels are presented in Table 2. Treatments were executed thrice a day first in the early morning from 5:30 am to 6:30 am, second in the daytime from 8:00 am to 9:00 am, and third in the evening from 4:00 pm to 5:00 pm inside the acoustic growth chambers and from height of three feet from the base where petri-plates were placed.

Table 1: Details of devotional songs selected for the composition of devotional music.

Sl. No.	Title of devotional Song	Source /or written by	Music composed by	Lead Singer	Playing Time
1	Hare Ram Mahamantra	Upanishad	Sri Kripaluji Maharaj	Sri Kripaluji Maharaj	5:30 am-6:30 am
2	Radhe Govinda	Daina Madhuri: Radhe Govinda Geet; Sri Kripaluji Maharaj	Sri Kripaluji Maharaj	Rasheswari Deviji	
3	Radhe Govinda	Braj Dham Madhuri: Radhe Govinda Geet; Sri Kripaluji Maharaj	Sri Kripaluji Maharaj	Rasheswari Deviji	8:00 am - 9:00 am
4	Hare Ram Mahamantra	Upanishad	Rasheswari Deviji	Rasheswari Deviji	
5	Sri Radha Sharanam Sri Krishna Sharanam	Sankirtan Ras Madhuri, Sri Kripaluji Maharaj	Sri Kripaluji Maharaj	Rasheswari Deviji	4:00 pm - 5:00 pm
6	Gopijana Ballava Shyam	Sri Kripaluji Maharaj	Sri Kripaluji Maharaj	Rasheswari Deviji	

A completely Randomised Design (CRD) was employed to run the experiment with ten different levels of treatments with four replications in each. Seed germination data were recorded for each experimental unit on every 12 hours and continued for 48 hours for

germination. Length of Root and Shoot was also measured and recorded at 48 hours from the initiation of the germination test.

Table 2: Treatment Levels and specifications.

Sl. No.	Treatment Level Code (short)	Specification		Treatment Level Code (elaborate)
		SPL Range & Average (in dB(A))	DOE (in hours)	
1	T0 (C)	No Exposure (NE)	No Exposure (NE)	T0(Con)
2	T1	70-80 (75)	1	T1(75,1)
3	T2	70-80 (75)	2	T2(75,2)
4	T3	70-80 (75)	3	T3(75,3)
5	T4	80-90 (85)	1	T4(85,1)
6	T5	80-90 (85)	2	T5(85,2)
7	T6	80-90 (85)	3	T6(85,3)
8	T7	90-100 (95)	1	T7(95,1)
9	T8	90-100 (95)	2	T8(95,2)
10	T9	90-100 (95)	3	T9(95,3)

SPL: Sound Pressure Level; dB: Decibel, C: Control and Con: Control

Data measured were expressed in mean values with standard deviation (SD) or Standard Error (SE). Effects of ten levels of treatments on the Germination parameters were analysed with one-way analysis of variance (ANOVA) separately for each parameter at $p < 0.05$. ANOVA was followed by mean comparisons using Tukey's Honestly Significance Difference test (HSD) test at 5% level of significance.

RESULTS

One-way analysis of variance for final germination percentage of Mung bean seed under the treatment of devotional music (Table 3) after 48 hours of initiation of the germination test resulted with 'F' value of 2.44 and the same was significant at $p < 0.05$.

Table 3: One-way ANOVA for Final Germination Percentage (FGP), Germination Index (GI), and Seed Vigour Index (SVI).

Germination Parameters	Source of variance	Sum of Squares	df	Mean Square	F	p
FGP	Between	1349.89	9	149.99	2.44	0.03
	Within	1841.65	30	61.39	30	
GI	Between	32.07	9	3.56	2.19	0.05
	Within	48.73	30	1.62		
SVI	Between	420.46	9	46.72	4.72	< .001
	Within	297.15	30	9.9		

The final germination percentage in T2, T4, T5, T7, T8, and T9 was higher in comparison to the control group but not significant. The final germination percentage of T7 was

significantly higher than T1 at p <0.05 (Table 4). Table 3 presents that the difference in the germination index was significant with an F value of 2.19 and p ≤ 0.05. Germination index was highest in T7 and lowest in T1. The germination index of T2, T4, T5, T7, T8, and T9 was higher in comparison to the control group but not statistically significant (Table 4).

Table 4: Effect of Devotional Music on Final Germination Percentage (FGP) and Germination Index (GI), and Seed Vigour Index (SVI).

Treatment Levels	FGP			GI			SVI		
	Mean	SE	Sig.	Mean	SE	Sig.	Mean	SE	Sig.
T0(CON)	82.00	5.29	ab	11.54	0.66	ab	10.21	1.45	c
T1(75,1)	75.00	1.91	b	10.88	0.38	b	13.05	1.21	bc
T2(75,2)	83.00	2.52	ab	12.46	0.73	ab	19.05	1.79	ab
T3(75,3)	80.00	2.31	ab	11.21	0.46	ab	18.32	1.81	ab
T4(85,1)	86.00	5.77	ab	12.71	1.00	ab	19.03	2.74	ab
T5(85,2)	89.00	4.43	ab	12.79	0.52	ab	15.24	1.06	abc
T6(85,3)	82.00	4.76	ab	11.50	0.63	ab	17.62	1.28	abc
T7(95,1)	96.00	2.83	a	14.12	0.31	a	19.09	1.37	ab
T8(95,2)	84.00	4.32	ab	12.21	0.92	ab	21.49	1.13	a
T9(95,3)	85.00	1.91	ab	12.17	0.35	ab	19.45	1.15	ab

Mean, Standard Error (SE) column is followed by Significance of Difference (Sig.) represented by different letters as per Tukey's HSD Test at P < 0.05.

Differences in seed vigour index (SVI) among the treatment levels were found to be highly significant with an F ratio of 4.72 and p < .001 (Table 3). Seed Vigour Index for all the experimental groups (T1, T2, T3, T4, T5, T6, T7, T8, and T9) were found to be higher in comparison to the control group and the variations were statistically significant for T3, T4, T7, T8, and T9. The highest SVI was observed in T8 with a difference of 110.48% in comparison to the control group (Table 4 & Fig 1).

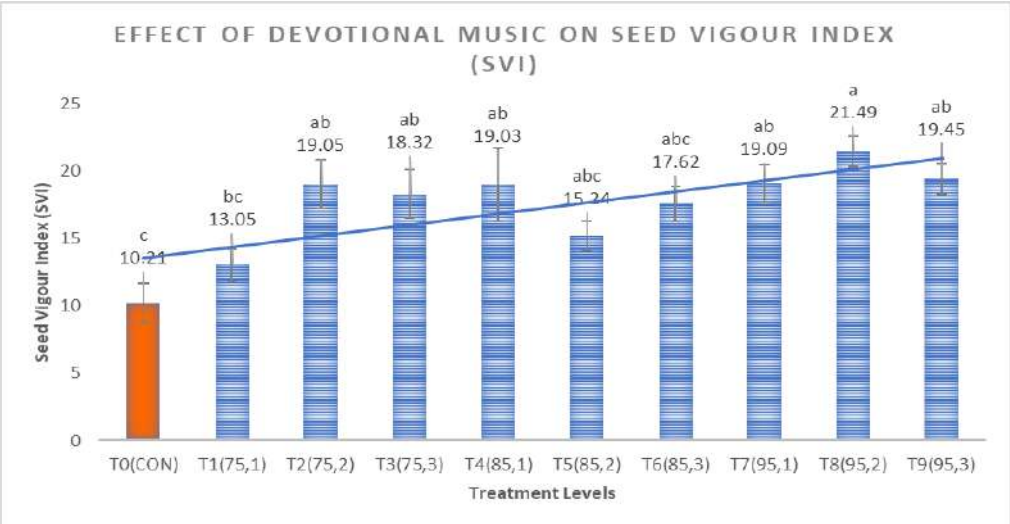

Fig. 1: Mean Seed vigour index 48 hours after seed germination test under nine experimental groups and one control group (n=4). Different letters on each bar represent the significance of the difference in comparison to the other treatment groups at P < 0.05.

DISCUSSION

Results revealed that devotional music had a definite and promising effect on seed germination. The final germination percentage of Mung bean seed was higher in most groups exposed to one or other levels of devotional music. The final germination percentage was highest in the group exposed to devotional music at 90-100 dB(A) for a duration of one hour per day. Creath & Schwartz, (2004) reported that musical sound had a statistically significant effect on the numbers of okra and zucchini seed sprouted compared to untreated control as well as noise. Healing energy also had a significant effect on seed germination compared to untreated control. But no significant difference was reported between seeds exposed to noise and untreated control. Munasinghe et al., (2018) reported that a significant difference in the germination of rice was observed when seeds were treated with sound rhythm treatment at 55-60 dB(A) for 7 days in comparison to control and out of two sound rhythms used i.e., Buddhist Pirith chanting and Pop music, germination percentage was higher in Pirith treatment.

Earlier Cai et al., (2014) reported that an audible sound with an intensity of around 90 dB(A) and frequency of around 2000 Hz reduced the germination period of Mung Bean as well as improved its growth. The most relevant findings in the present study were obtained for radical development and overall seed vigour index. Most groups exposed to devotional music had significantly higher radicle growth which resulted in a higher seed vigour index in comparison to the control groups. Exposure of Mung bean seeds to devotional music at 90-100 dB(A) for 2 hours per day resulted in the highest and most significant increase in overall seed vigour index. Chowdhury & Gupta, (2015) in their germination experiment on Cicer arietinum (chickpea) exposed to Light Indian Music, found that throughout the period of germination and development of the saplings, the ones exposed to Indian Light Music were having higher germinated seedlings and seedlings were blooming better compared to the control saplings. They also stated that soft rhythmic audible frequencies (that is music) must have affected the absorption of nutrients and formation of metabolites in the plants and thus expediting the germination of seeds, growth, and development of plants.

It may be concluded that exposure of Mung bean seeds to devotional music resulted in a higher final germination percentage and germination index in comparison to the control group. An exposure of Mung bean seeds to devotional music with a sound pressure level of 90-100 dB(A) for 2 hours duration resulted in the highest and most significant improvement in seed vigour index in comparison to the control group not exposed to devotional music. Seed vigour index of germinated Mung bean seeds were measured to be 110.48% higher in comparison to the control group when recorded at the 48^{th} hours of germination test. In general, it may be stated that Mung beans seed preferred a high sound pressure level of 90-100 dB(A) and an exposure of 1 to 2 hours per day to bring about significant improvement in the germination parameter like final germination percentage, germination index, and overall seed vigour index.

ACKNOWLEDGMENT

The authors would like to express their gratitude to all the ashramites of Braj Gopika Seva Mission for their unwavering support at all levels for executing this work.

REFERENCES

Cai, W., He, H., Zhu, S., & Wang, N. (2014). Biological Effect of Audible Sound Control on Mung Bean (*Vigna radiate*) Sprout. *BioMed Research International*, *2014*, 1–6. https://doi.org/10.1155/2014/931740

Chandrakala, Y., & Trivedi, L. (2019). Role of music on seed germination: A mini review. *International Journal of Agriculture and Plant Science*, *1*(2), 01–03.

Chowdhury, M. E. K., Lim, H.-S., & Bae, H. (2014). Update on the Effects of Sound Wave on Plants. *Research in Plant Disease*, *20*(1), 1–7. https://doi.org/10.5423/RPD.2014.20.1.001

Creath, K., & Schwartz, G. E. (2004). Measuring Effects of Music, Noise, and Healing Energy Using a Seed Germination Bioassay. *The Journal of Alternative and Complementary Medicine*, *10*(1), 113–122. https://doi.org/10.1089/107555304322849039

Gagliano, M. (2013). The flowering of plant bioacoustics: How and why. *Behavioral Ecology*, *24*(4), 800–801. https://doi.org/10.1093/beheco/art021

Haid, M., & Huprikar, S. (2001). Modulation of Germination and Growth of Plants by Meditation. *The American Journal of Chinese Medicine*, *29*(03n04), 393–401. https://doi.org/10.1142/S0192415X01000411

Kripaluji Maharaj. (2009). In *Bhagavannama Mahatmya: The Glories of the Divine Name* (First 2009; Second 2018, p. Preface, 1-7). Radha Govinda Samiti, New Delhi;

Krishnadas Kabiraj. (1993). In *Sri Sri Chaitany Charitamrita* (1st 1993, 2nd 2006, p. Madhya Lila page 225, Verse 45; page 231, Verse 200.). Nabadweep Sri Chaitanya-Saraswat Math.

Mishra, R. C., Ghosh, R., & Bae, H. (2016). Plant acoustics: In the search of a sound mechanism for sound signaling in plants. *Journal of Experimental Botany*, *67*(15), 4483–4494. https://doi.org/10.1093/jxb/erw235

Munasinghe, S., Liyanage, K., Weerakoon, S., Somaratne, S., & Dissanayake, D. (2018). A preliminary study on effect of buddhist pirith chanting and pop music on the growth and yield performance in rice (Oryza sativa L.). *Sri Lankan Journal of Biology*, *3*, 44. https://doi.org/10.4038/sljb.v3i1.17

Roy Chowdhury, A., & Gupta, A. (2015). Effect of Music on Plants – An Overview. *International Journal of Integrative Sciences, Innovation and Technology (IJIIT)*, *4*(6), 30–34.

Thakur Vrindavandas. (1995). In *Shri Shri Chaitanya Bhagwat* (1st 1995, p. Adikhanda page 104 verses 280 & 286). Nabadweep Sri Chaitanya-Saraswat Math.

VISTAS IN GEOLOGICAL RESEARCH
Special Publication in Geology (19), March 2023, pp. 23-32

Seismic Hazard Assessment in and Around Kangra Valley, India

[1]RITU MOHAPATRA, [1*]SANTISWARUP SAHOO AND [2]MADAN MOHAN ROUT

[1]*Department of Geology, Utkal University, Bhubaneswar 751004, India.*
[1, *]*Corresponding author. e-mail: sahoosantiswarup@gmail.com*
[2] Former *Scientist-C, Institute of Seismological Research, Gujarat 382009, India*

Abstract: The huge Alpine-Himalayan convergent tectonic band, of which the Himalayan arc is a part, continues to be the host for active seismic activity. It is essential to update knowledge of seismic hazard to include the most recent information on earthquake occurrence and attenuation process given in its active seismic status and ongoing development operations in mountainous states. The current study uses the Probabilistic Seismic Hazard Assessment (PSHA) approach to estimate Peak Ground Acceleration (PGA) for the Kangra valley and surrounding regions. The 1905 Kangra Earthquake (Mw7.8), which caused the most damage at the study site, as well as the recently identified Kangra Valley Fault (KVF), (Malik et al.,2015), have both been considered in this study. Improved procedures for PSHA have been adopted for this study and PGA values have been estimated for 10% and 2% likelihood of exceedance in 50 years. The PGA values range from 0.06 to 0.14g and 0.16 to 0.3g, respectively, when taking into account b-value. When necessary, the strong ground motion calculated at the firm rock level has been used to estimate ground motion at the surface by factoring in the site amplification factor. The data derived from this will be helpful in engineering planning and microzoning work.

Keywords: 1905 Kangra Earthquake; PSHA; PGA; Kangra Valley Fault (KVF); exceedance factor.

INTRODUCTION

One of the seismically active regions of the world is considered to be the Himalayan region. The strain energy that is being stored in the Himalayas as a result of the continuous collision and convergence of the Indian and Eurasian plates is released as earthquakes. The great Himalayan arc has witnessed several moderate to large scale earthquakes during the geologic past, including the1905 Kangra Earthquake (Mw 7.8). Taking into the consideration about the ongoing seismicity and based on varying earthquake damage levels, the Himalayan region has been assigned as seismic zone IV and V in the seismic zonation map of India (BIS 2002). Due to the area's seismicity and the current complex collisional tectonic setup, which includes the major thrust segments, namely the Main Central Thrust (MCT) and the Main Boundary Thrust (MBT) as well as numerous other tectonic faults, it is very crucial to conduct a seismic hazard assessment (SHA).

Probabilistic Seismic Hazard Assessment (PSHA) estimates have been made by a number of authors for the Indian Subcontinent and for the Himalayan regions but considering the one of the most devastating earthquakes, the need of SHA in the research area was made clean by the 1905 Kangra earthquake and the recently identified fault system, known as Kangra Valley Fault (KVF). Using the improved magnitude conversion techniques, updated attenuation

relations and adopted procedures, we delineated 9 seismogenic zones based on the examination of earthquake sites and as well as the most recent knowledge of the local geology and tectonics.

Seismic hazard parameters in terms of Peak Ground Acceleration (PGA) have been calculated for this research taking into account the estimated b-values for each seismogenic source zone, when taking into account the whole earthquake catalogue. For 475 years return period, in the region the PGA values vary from 0.06 to 0.14g, respectively. For 2500 years return period, the PGA varies between 0.16 to 0.3g. Major significant structures in the source area had their peak spectral and ground accelerations determined, and a seismic hazard curve was created by calculating both of these.

The data from the seismic hazard study of the Kangra valley and its surrounding areas will be useful for planning and implementing certain preventive measures to lessen the number of fatalities and economic losses that are likely to result from earthquake disaster in particular.

GEOLOGY AND TECTONICS

As the Indian and Eurasian plates continue to converge in the Himalayan orogenic belt, several zones of tectonic deformation have resulted in crustal shortening, especially along the notable boundary faults (Philip, Suresh and Bhakuni,2014). These crustal-scale major structural divisions (from north to south) are: (1) Indus-Tsangpo Suture Zone (ITSZ), which marks the zone of collision in the course of the northward drift of Indian plate during the Palaeogene (2) the Main Central Thrust (MCT), ductile thrust fault that separates the Greater Himalaya in the hanging wall from the Lesser Himalaya in the footwall,(3) the Main Boundary Thrust(MBT), which defines the faulted contact between the Lesser Himalaya and the Siwaliks (4) the Himalayan Frontal Thrust (HFT) or Himalayan Frontal Fault (HFF), which marks the boundary between the Siwalik front of the Himalayan province with the alluvial expanse of the Indo-Gangetic plain . These major thrust systems i.e., MCT, MBT and HFT from north to south which indicates foreland propagation in-sequence thrusting. It suggests that the southernmost part of the Himalaya represents the youngest deforming front (Valdiya,2003; Mukul,2000; Malik and Mohanty 2007; Paul and Bhakuni 2019).

The Kangra reentrant is one of the most distinguished structural features in the NW Himalaya. The MBT acts as an important belt which separates the two main tectonic features i.e., the Main Himalayan Belt and the Frontal Belt. The Kangra reentrant is shown by series of thrust faults and folded ranges spreading over a 100km wide zone marked by several imbricated thrust faults between HFT and MCT. The area is shown by combination of frontal and oblique thrust ramp, marked by sinuous pattern within the reentrant due to the change in the strike of MBT known as Kangra Recess. The study area is characterized by some major fault systems which are the part of MBT and HFT systems. The faults like Soan Thrust, Nalagarh Thrust, Jwalamukhi Thrust and Palampur Thrust show great importance in shaping the present complex landscape of the region.

The Kangra valley is confined between the JMT to its south and the PaT to the north. Several new active fault traces were identified considering the prominent active fault topographic features. Kangra Valley Fault (KVF), also known as the recognized active fault traces striking WNW-ESE and NW-SE, runs through the Kangra valley and Sihunta valley in the northwest. The entire fault track along the KVF is discontinuous and stretches over 60 km between the villages of Patka in the northwest and Tanda in the southeast. Taking into consideration the parameters of active fault trace along KVF, it is suggested that this fault is capable of producing earthquake of magnitude around Mw 7.7 (Sahoo and Malik ,2017).

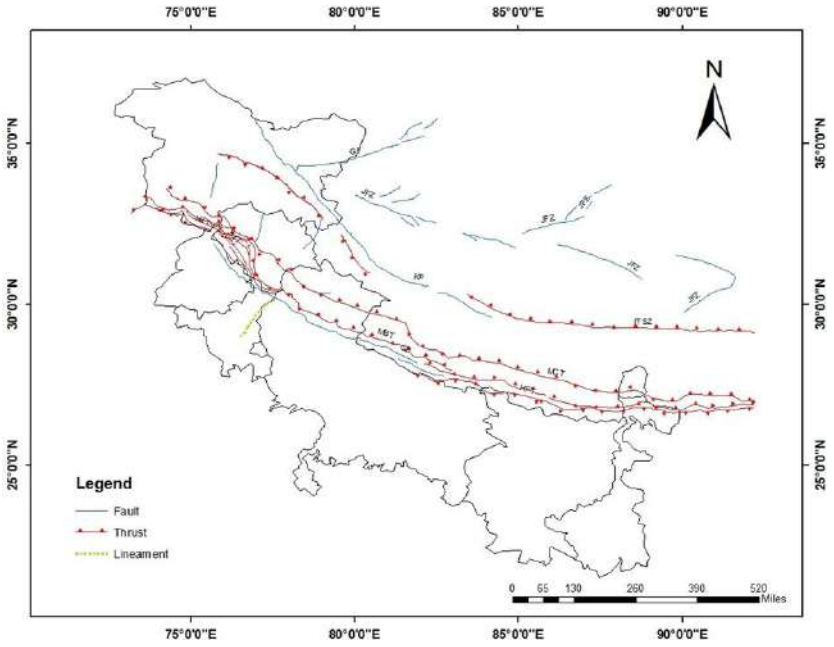

Fig 1: Tectonic features present in and around NW Himalaya. KKFKarakoram Fault, MCT-Main Central Thrust, MBT-Main Boundary Thrust, ITSZ-Indus Suture Zone, KFS-Kaurik Fault System, AF-Alaknanda Fault, JMT-Jwalamukhi Thrust, PaT- Palampur Thrust, MFT-Main Frontal Thrust, JF-Jhelum Fault, KF Kishtwar Fault, SNF-Sunder Nagar Fault KVF-Kangra Valley Fault

METHODOLOGY

Probabilistic Seismic Hazard Assessment (PSHA) is one of the best suitable methodologies referred for seismic hazard assessment through the estimation of ground motion parameters. PSHA methodology takes into account all the uncertainties involved in the seismogenic zone, size and rate of occurrences of earthquakes that were neglected in DSHA. The basic key steps in PSHA study are:

(a) Homogenization of the catalogue: Data on earthquake from three agencies were used in this study i.e., NDMA report 2011- catalogue up to 2008, Nath et al. (2017)-catalogue from 2009-2014, NCS and USGS-catalogue from 2015-2020. Based on the local correlations of moment magnitude with other magnitude scales, earthquake data gathered from multiple agencies was homogenized (Sitharam and Sil 2014). In particular, the regional relations for Himalayan region for conversion of body wave magnitude to

moment magnitude (Das et al. 2013) have been used and the equation is given as: $\mathbf{M_w = 1.17 m_{b,\,obs} - 0.74}$ **----------(1).**

(b) Declustering: The major shocks, aftershocks, and foreshocks included in the earthquake data gathered from multiple agencies can result in biased analysis. Declustering sometimes referred to as removing foreshocks and aftershocks from the collection, entails removing dependent events from independent events (Rout 2014; Das 2014). For this study, the Uhrhammer 1986 approach has been used considering specified time space windows. Using Z map, a MATLAB tool, the homogenized catalogue's declustering was accomplished.

(c) Estimation of seismic hazard parameters: The seismicity parameters were estimated after the completeness analysis of the catalogue. The minimum magnitude of completeness (Mc), Gutenberg-Richter (G-R) recurrence parameters (b and a) and maximum magnitude (M_{max}) values have been estimated for each seismogenic zone from the homogenized earthquake catalogue (table 1). The lowest magnitude over which it is deemed that the earthquake recording is complete is known as the minimum magnitude of completeness (Mc). Magnitudes that are smaller are not identified; they are too small to be recorded on sufficient stations in an aftershock sequence. In this research Mc is calculated using Maximum Curvature Method (MAXC) by Wiener and Wyss (2000). The relationship between the yearly rate of exceedance logarithm and earthquake magnitude is known as the (Gutenberg-Ritcher 1944). Regression analysis was used to estimate the parameters "a" and "b," and the relationship is represented by the following expression: $\mathbf{\log \lambda_m = a - bm}$**----------(2).** Where $\boldsymbol{\lambda_m}$is the mean annual rate of exceedance of magnitude ***m***, ***a*** is the general level earthquake activity in a given area during the study period and depends on seismicity of the region, ***b*** the slope describes the relative likelihood of large to small earthquakes. In the present study, ZMAP software has been used to compute seismic hazard parameters.

Table 1: Seismic hazard parameters considering the earthquake catalogue.

ZONE	Mc	a	b	β =2.303*b	b error	beta coeff	λm
1	4.2	4.26	1.01	2.32	0.09	0.20727	1.042317
2	4.4	3.05	0.76	1.75	0.1	0.2303	0.508159
3	4.5	2.29	0.74	1.70	0.2	0.4606	0.09506
4	4.3	1.89	0.77	1.76	0.1	0.2303	0.039464
5	4.3	2.74	0.80	1.84	0.1	0.2303	0.199526
6	4.4	3.46	0.96	2.20	0.2	0.4606	0.17394
7	4.1	2.25	0.73	1.67	0.1	0.2303	0.189452
8	4.5	2.72	0.72	1.67	0.09	0.20727	0.289734

The maximum magnitude M_{max} is defined as the upper limit of magnitude for a given seismogenic zone. No earthquakes are to be expected with magnitude exceeding $M_{max.}$ For calculating the maximum regional earthquake magnitude in this study. The Non-parametric Gaussian (N-P-G) best estimator equation presented by Kernel method was employed. Data were computed using the MATLAB, both historical and instrumental seismicity data has been used to determine M_{max} (table 2).

Table 2: Seismic zones and the corresponding observed and maximum magnitudes.

ZONES	$M_{obs\ max}$	M_{max}
1	7.3	7.61±0.31
2	6.8	7.14±0.34
3	7.0	7.31±0.31
4	8.0	8.21±0.21
5	7.0	7.47±0.47
6	7.0	8.05±0.75
7	6.7	6.91±0.21
8	6.5	6.59±0.09

GROUND MOTION PREDICTION EQUATIONS AND SEISMIC HAZARD ESTIMATION

The choice of an appropriate ground motion attenuation relationship is one of the most crucial elements in a seismic hazard analysis. The data, function, and approach that were used to derive these connections all affect how accurate they are. It is crucial for hazard estimation since it directly affects how strong ground motion is estimated. For the estimation of ground motion, region-specific attenuation relationships are typically preferable. Two GMPEs equations i.e., Campbell and Bozorgnia (2014) and Chiou and Youngs (2014) have been considered to estimate Peak Ground Acceleration (PGA) and Peak Spectral Acceleration (PSA). Due to the fact that we considered two equations, there may be some uncertainties, for this reason, we weighted both values equally to achieve better results.

The maximal ground motion was calculated at the B-C boundary in the current work because the shear wave velocity (V_{s30}) was assumed to be 760m/s, which means peak ground motion was computed at firm rock level. The probabilistic seismic hazard estimation software CRISIS-2012 developed by Ordaz et al. (2012) has been used.

DISCUSSION AND RESULTS

Based on the analysis of earthquake locations and focal mechanisms, as well as the most recent knowledge of the local geology and tectonics, a seismic source characterization has been defined. For the goal of understanding and knowing the impact of zone size and

geometry, the study area covering the NW Himalaya has been divided into 9 seismogenic zones based on the region's seismotectonic features. The procedure involves handling the earthquake database and estimating the seismicity parameters for the various zones. Peak Ground Accelerations (PGA) and Peak Spectral Accelerations (PSA) have been estimated for various probability of exceedance for 10% and 2% for all the sets in the grid at time periods of 0.01,0.05,0.1,0.2,0.5,1,2,4,5, and 10 seconds. However, in the instance of the Kangra region taken into consideration for this research work, zoning may be done logically as there is a fair amount of knowledge on seismogenic zones that is now available.

Seismogenic zone 1 encompasses portions of Jammu and Kashmir and the most notable regional features of the zones include MBT, MCT, HFT, and ITSZ, Transverse faults like SNF and KF, have an impact on this belt. Parts of Uttarakhand, Punjab and Himachal Pradesh are included in zone 2,3,5,6,7 and 8, which is characterized by the MBT, MCT, HFT, and Alakananda fault. The Kaurik fault system, which caused the Kinnaur earthquake, is also part of this zone. The research area and some areas of Himachal Pradesh are primarily in Zone 4, and the most extensive tectonic features include MBT, MCT, HFT, JMT and PaT. This zone also contains KVF, which triggered the Kangra Earthquake in 1905. Zone 9 is not taken into account because, according to its poor seismogeny, it will have little to no effect on the source.

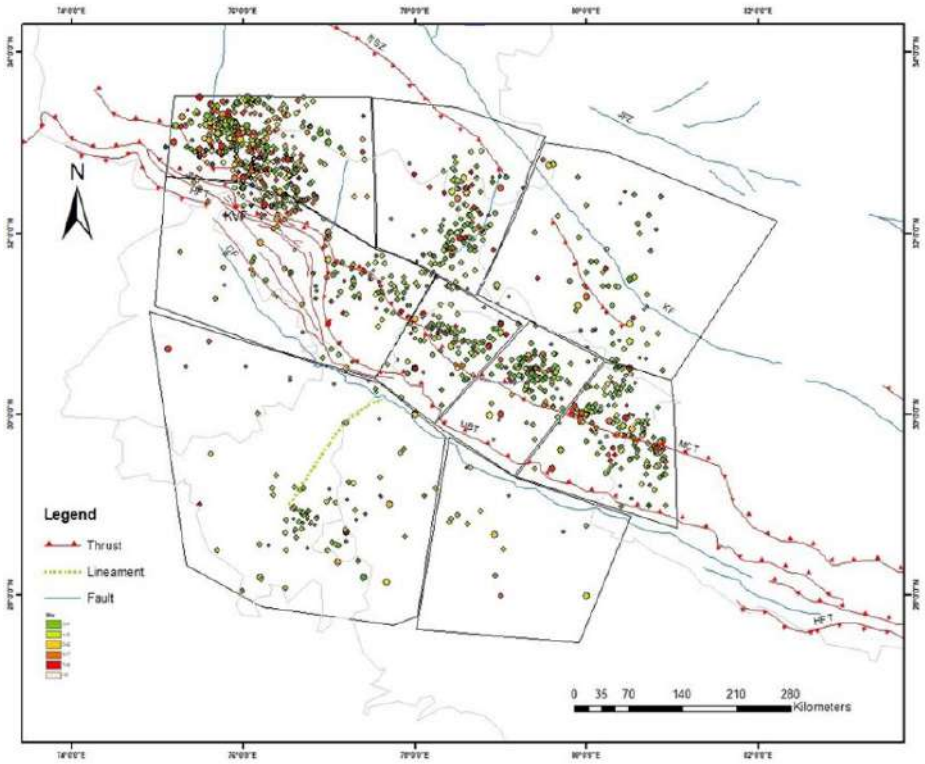

Fig. 2: Demarcation of seismogenic zones based on source-site characterization.

The research area between latitude 32°05′52.1" and longitude 76°16'10.65" is divided into tiny grids of size 0.05°*0.05° in order to estimate PSHA. In this method, the CRISIS (2015) programme receives input parameters like a, b, mc, mmax, and attenuation models, and output parameters like PGA and PSA are produced. Ground motion distribution is shown in the form of zones while taking into account variable b-values for each zone. PGA has been

computed at the center of all grid points for return periods of 475 years and 2500 years (i.e., 10% and 2% probability of exceedance in 50 years). For a 10% Probability of exceeding in 50 years (a return period of 475 years), the PGA values for the research area range from 0.06 to 0.14 g. However, the 2% probability of exceedance in 50 years (return period of 2500 years), the PGA values vary from 0.16 to 0.30 g for the study region.

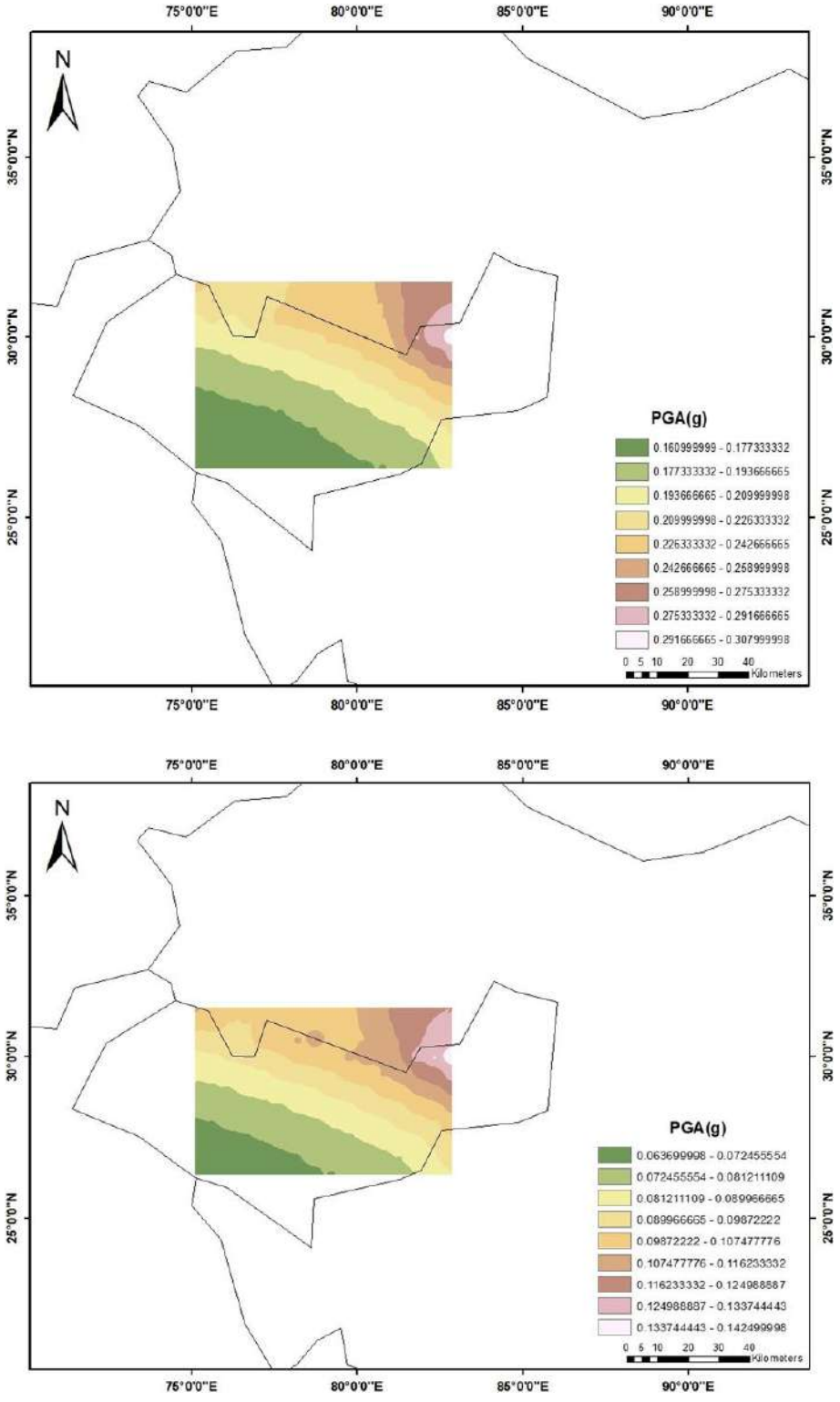

Fig. 3: Peak ground acceleration for 2% and 10% probability of exceedance in 50 years.

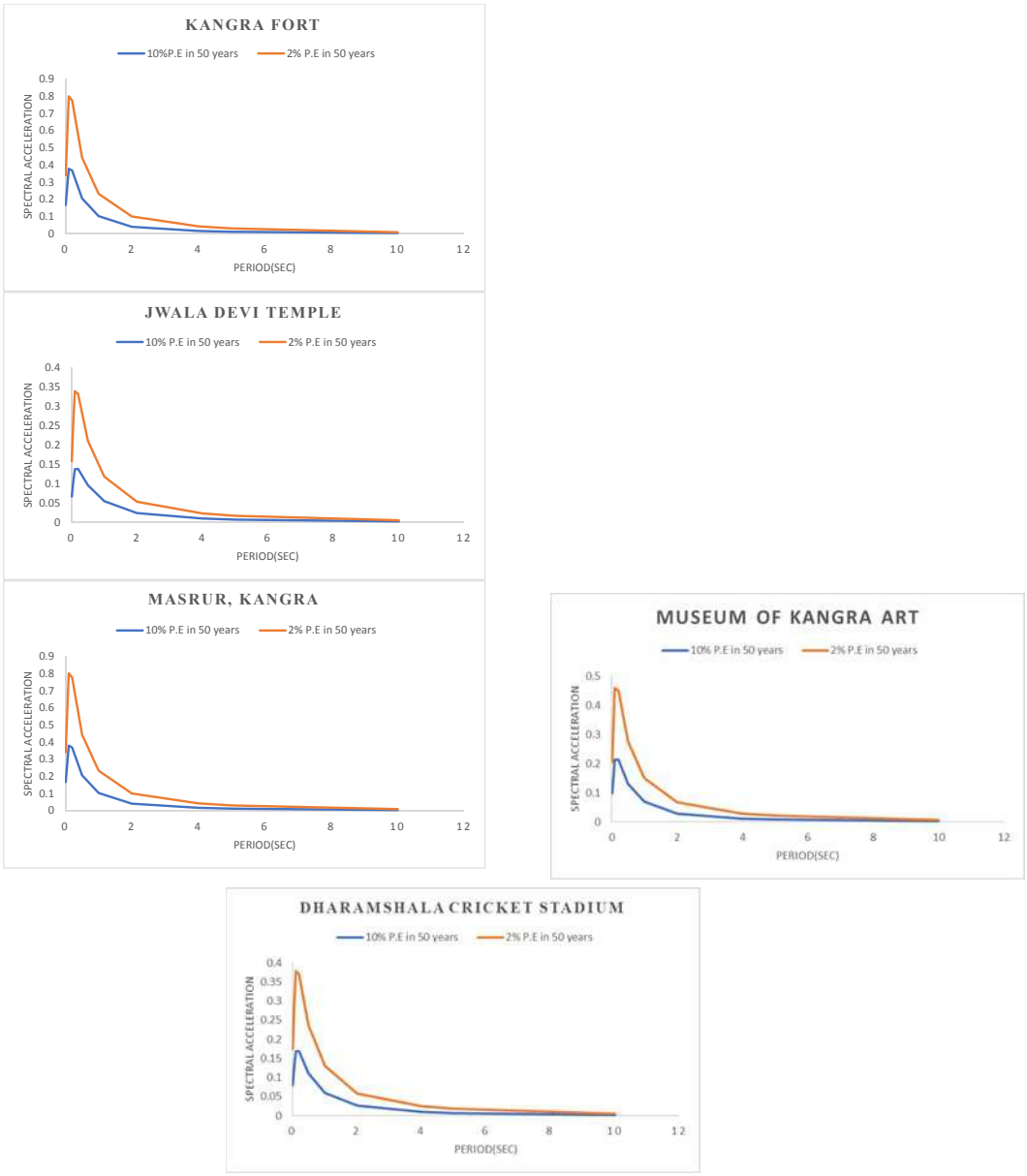

Fig 4: The seismic hazard curves for selected structures computed PGA and PSA at 10% and 2% exceedance.

CONCLUSIONS

The Himalayan region is still undertaking development projects. In addition to urbanisation, additional infrastructure projects are ongoing. Knowing the expected ground motion at a site as well as the return period is crucial for the engineering design of structures with seismic input. The knowledge of seismic hazard assessment has greater significance given the fact that we're dealing with an area that is located in the midst of a tectonically produced young Himalayan Mountain belt with a high level of seismicity and regional scale thrusts.

This study has been carried out to give next generation PSHA information for the source region in order to address the existing challenges. The updated attenuation relations,

improved magnitude conversion techniques, and various hazard computation techniques were used to create the new hazard map. The following broad conclusions could be drawn from the study, for 475 years return period, in the region enclosed by state boundary, the PGA values vary from 0.06 to 0.14 g, respectively. For 2500 years return period, the PGA varies between0.16 to 0.3g. The ground motion distribution pattern, as evidenced by the contours higher PGA values are observed in the South-West region of the state. Major significant structures in the source area had their peak spectral and ground accelerations determined, and a seismic hazard curve was created by calculating both of these accelerations.

REFERENCES

BIS Code 1893 2002 Earthquake hazard zoning map of India; www.bis.org.in.

Campbell, K. W. and Bozorgnia, Y. (2008), NGA Ground motion model for geometric mean horizontal component of PGA, PGV, PGD and 5% damped linear elastic response spectra for periods ranging from 0.01 to 10s, *Earthquake Spectra*, 24(1*), 139-171.*

Chiou B S J and Youngs R R 2008 Empirical ground motion model for the average horizontal component of peak acceleration and pseudo-spectral acceleration for spectral periods of 0.01 to 10s; *Earthquake spectra* 24(S1*)173-216.*

Development of probabilistic seismic hazard map of India 2011 Technical Report, National Disaster Management Authority (NDMA), Government of India, New Delhi.

GSI 2000 *Seismotectonic Atlas of India and its Environs;* Geological Survey of India.

Gupta I D 2006 Delineation of probable seismic sources in India and neighbourhood by a comprehensive analysis of seismotectonic characteristics of the region; Soil Dynamic Earthquake Eng. 267 766-790.

Kijko A 2004 Estimation of the maximum earthquake 681 magnitude, M_{max}; *Pure Appl. Geophys.* 161 1655-1681.

Mahajan A K, Thakur V C, Sharma M L and Chauhan M 2010 Probabilistic seismic hazard map of NW Himalaya and its adjoining area, India; *Nat. Hazards*53 443-457.

Nath S K and Thingbaijam K K S 2012 Probabilistic seismic hazard assessment of India; *Seismol. Res. Lett*. 83 135-149.

Nath S K and Thingbaijam K K S 2011 Peak ground motion predictions in India: An appraisal for rock sites; *J.seismol*15 295-315.

Rout, M. M., Das, J. D, Kumar A, Patil N. (2014), "Probabilistic seismic hazard assessment of Himachal Pradesh and adjoining region", Journal of Earth System science.

Sahoo S and Malik J N (2017), Active fault topography along Kangra Valley Fault in the epicentral zone of 1905 Mw 7.8 earthquake NW Himalaya, India, Quaternary International 462 90 -108.

Thakur, V. C., V. Sriram, and A. K. Mundepi (2000). Seismotectonics of the great 1905 Kangra earthquake meizoseismal region in Kangra- Chamba, NW Himalaya, Tectonophysics 326, 289-298.

Valdiya K S 1980 Geology of Kumaun Lesser Himalaya; Wadia Institute of Himalayan Geology, Dehradun, pp- 290-291.

Woessner J and Wienner S 2005 Assessing the quality of earthquakes catalogues: Estimating the magnitude of completeness and its uncertainty; *Bull, Seismol. Soc. Am.*95(2) 684-698.

Yeats. R. S., K. Sieh, and C.R. Allen (1997). *Geology of Earthquakes*, Oxford University Press, New York, 568 pp.

VISTAS IN GEOLOGICAL RESEARCH
Special Publication in Geology (19), March 2023, pp. 33-42

Vulnerability Assessment of Groundwater Contamination through Climate Variability in the Hard Rock Terrain of Nuapada District, Odisha, India

MADHUSMITAOJHA[1], CHANDRAKANTA OJHA[2], SHREERUP GOSWAMI[3] AND PRAMOD CHANDRA SAHU[1]

[1)]Maharaja Sriram Chandra BhanjaDeo University University, Odisha, India, 757003
[2)]Indian Institute of Science Education and Research Mohali, Punjab, India, 140306
[3)]Utkal University, Bhubaneswar, Odisha, India, 768019

madhusmita.hello@gmail.com, chandrakanta@iisermohali.ac.in
goswamishreerup@gmail.com, pcsahugeol@gmail.com
Corresponding Author:*madhusmita.hello@gmail.com*

Abstract: Assessment of the risk of groundwater contamination and its causes due to climate variability was studied in the western hard rock terrain of the northern Nuapada region of Odisha, India using hydro-geochemical, geospatial and statistical analysis. Result shows comparatively in pre monsoon season high fluoride (3.398mg/l), nitrate (257.62mg/l) and Iron (1.546mg/l) values exist than post-monsoon season respectively in the study area indicates the contaminated regions. Continuous rock-water interaction and leaching of iron oxides and fluoride-bearing minerals such as apatite, fluorite, mica, and amphibole from the country rocks increase the iron and fluoride concentration. Post-monsoon period is more responsible for the contamination of F^- , Fe^{2+} and NO_3^- because the surface water mixes with the groundwater. Regular practices of using fertilizers and poultry manure in the agricultural field has the key role in the nitrate enhancement. Among various causes, climate change extremities has the key role in assessing the vulnerability assessment of contamination of groundwater. It can be measured by predicting precipitation, humidity, and temperature pattern variance. With these advancements, risk assessment for groundwater contamination can be calculated as well as further groundwater development and management can be done in the study area.

Keywords: Groundwater contamination, hydro-geochemical analysis, Geospatial tool, Statistical analysis, Climate Variability

INTRODUCTION

Water is one among the precious natural resources and groundwater is an integral part of water resource which has worldwide importance. The socioeconomic condition of a country depends upon the quantity and quality of groundwater (Malik, M. S., & Shukla, J. P. 2019). The major controlling factors of the quality of groundwater in an area are natural geological processes, agricultural production, industrialization, urbanization and climate change inputs such as precipitation, temperature etc. (Shahnaz Sargazi et al., 2020; World Health

Organization, 2017). Currently, major problems of groundwater contamination are caused by extreme climate change and various anthropogenic activities such as land use pattern, urbanization, improper disposal of municipal and domestic sewage and intensive agricultural activities etc. (Kalhor, K., & Emaminejad, N. 2019). The current research focused on one of the western district of Odisha, India i.e. the Nuapada district comprising two blocks, Nuapada and Komna. The Groundwater of this region has been contaminated with fluoride, iron, nitrate and other toxic elements such as Pb, Cd, Hg and As. Further contamination may emerge due to changes in the climatic factors such as annual and diurnal temperature change, evapotranspiration, annual precipitation pattern variance and humidity variance etc. Most prominent effect has been seen during post monsoon period in the deterioration of groundwater quality as surface water mixed with groundwater. Therefore, this study has been conducted to assess the risk for groundwater contamination.

MATERIALS AND METHODS

Study Area

Nuapada is a western most district of the eastern Indian state Odisha. The study area includes two administrative blocks such as Nuapada and Komna blocks extending around 2068 km² bounded by 20°22’19’’-21°5’2’’ North latitude and 82°21’10’’-82°38’35’’East longitude. The study region is covered by consolidated basement terrain of hard crystalline and metamorphosed Precambrian formations such as granite, granite gneisses, khondalite and quartzite with little quaternary unconsolidated alluvial formations (Groundwater Information Booklet, Ministry of Water resources, Central Groundwater Board, SER, 2013). According to the climatic data (Groundwater Information Booklet, Ministry of Water resources, Central Groundwater Board, SER, 2013) this area experiences hot summer as well as cold winter ranges from 16.6°C to 45.2°C with fluctuated annual average precipitation ranges from 84.08mm to 148mm over ten year data analysis (2011-2020) (www. srcodisha.nic.in).

Sampling method

79 water samples were collected with GPS recorded coordinates from different sources in Pre-monsoon and Post-monsoon period in the year 2021following APHA (1998) standard procedures. Physical parameters such as pH, EC, TDS, Salinity, Turbidity, and Temperature were measured immediately in the field with the help of a multi-parameter handled sampling box. Later, samples were taken for major ion analysis in the laboratory. Few elements such as TH, TA, Ca^{2+} , Mg^{2+} , Cl^{-} , SO_4^{2-} are analysed through titration method and some are such as Na^{+} , K^{+} , F^{-} , Fe^{2+} ,NO_3^{-} with instruments. To show the contaminated as well as susceptible to contamination parts of the study area, isoconcentration maps of certain parameters such as F^{-} , Fe^{2+} ,NO_3^{-} above permissible limit were generated in ArcGIS 10.8 software. For qualitative analysis of groundwater contamination statistical analyses were done using SPSS software.

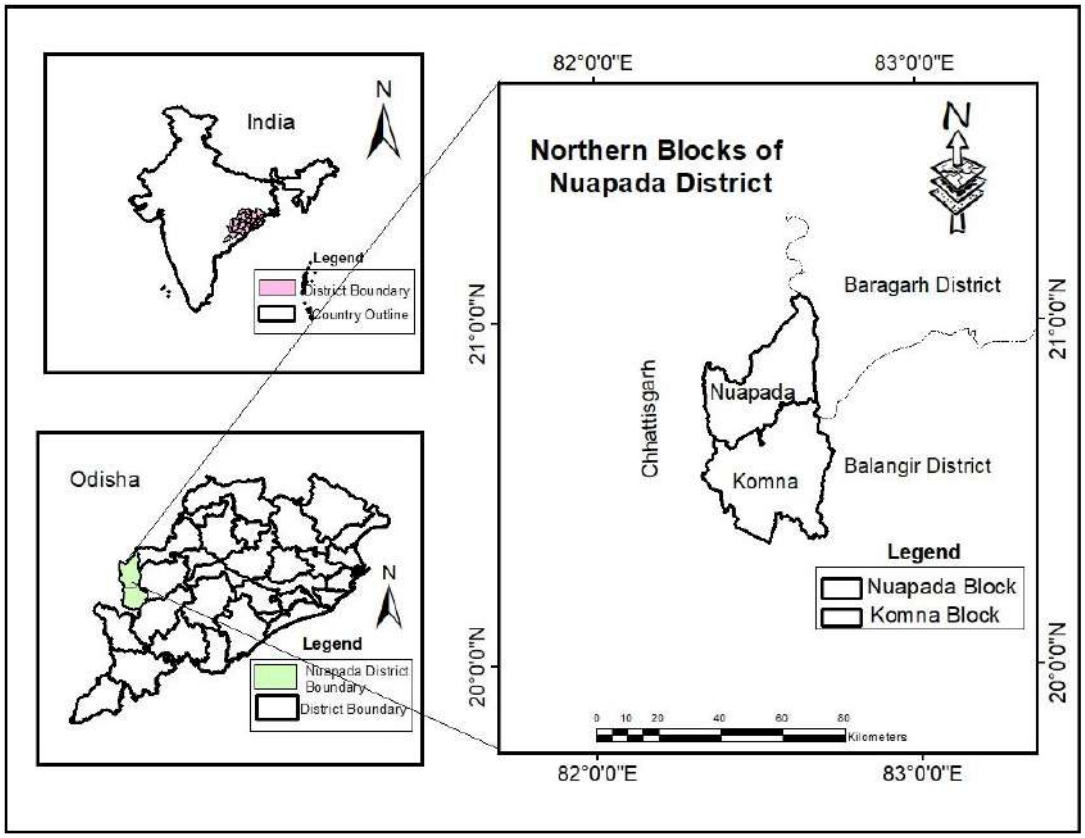

Fig. 1: Location Map of the study area showing two northern blocks of Nuapada district, Odisha interpolated within the Odisha and India.

RESULTS AND DISCUSSION

Hydrogeochemical data

To assess the groundwater contamination certain physical and chemical parameters such as pH, EC, TDS, TH, TA, major cations and anions such as Na^+ , K^+ , Ca^{2+} , Mg^{2+} , F^- , Cl^- , SO_4^{2-} , NO_3^- were taken into consideration to check the water chemistry and categorised in to above permissible limit those have higher values than the WHO (World Health Organisation, 2006) standard values. Among all analysed parameters fluoride, iron and nitrate concentrations of different regions over the study area are above the permissible limit. Nitrate concentration is above the permissible limit over entire study area. Fe^{2+} concentrations of the water samples in both seasons are slightly higher than the permissible limit. Nitrate concentrations are observed higher than the acceptable limit in both seasons almost in all regions. It may be due to the intermixing of agricultural, pesticides and anthropogenic sources inputs with the groundwater (Sunkari, E. D., Abu, M., &Zango, M. S. (2021). Fluoride concentration in the water samples is within the WHO acceptable limit except in some regions in both the season. It is believed to be from the weathering of the fluoride-bearing micaceous rocks such as granite, granite gneisses (Sunkari, E. D., Abu, M., &Zango, M. S. (2021).

a)

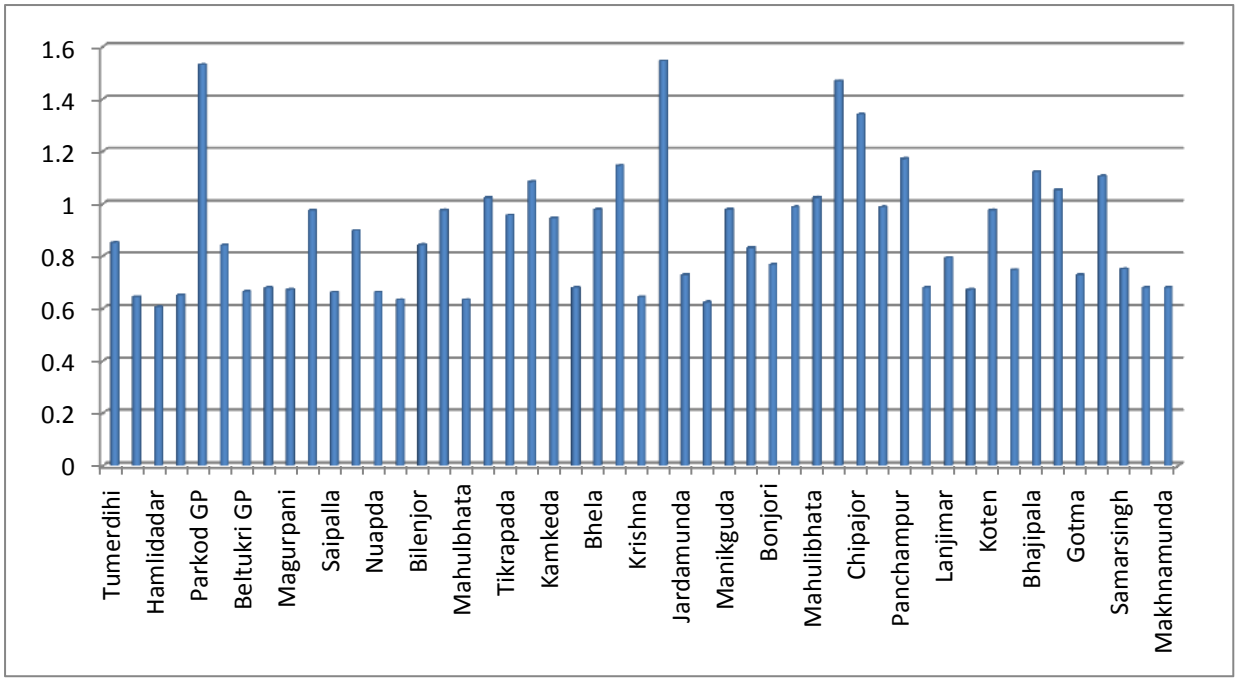

b)

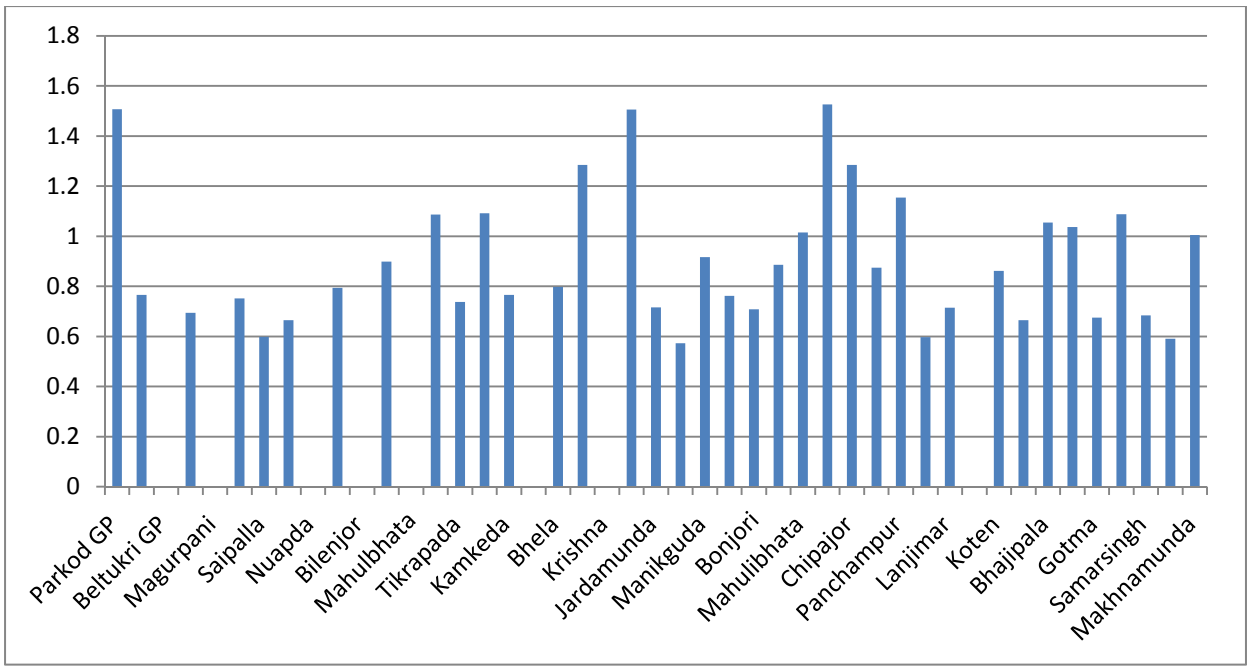

Distribution of Iron concentration above permissible limit of WHO of a) Pre and b) Post monsoon seasons respectively over different regions of the study region

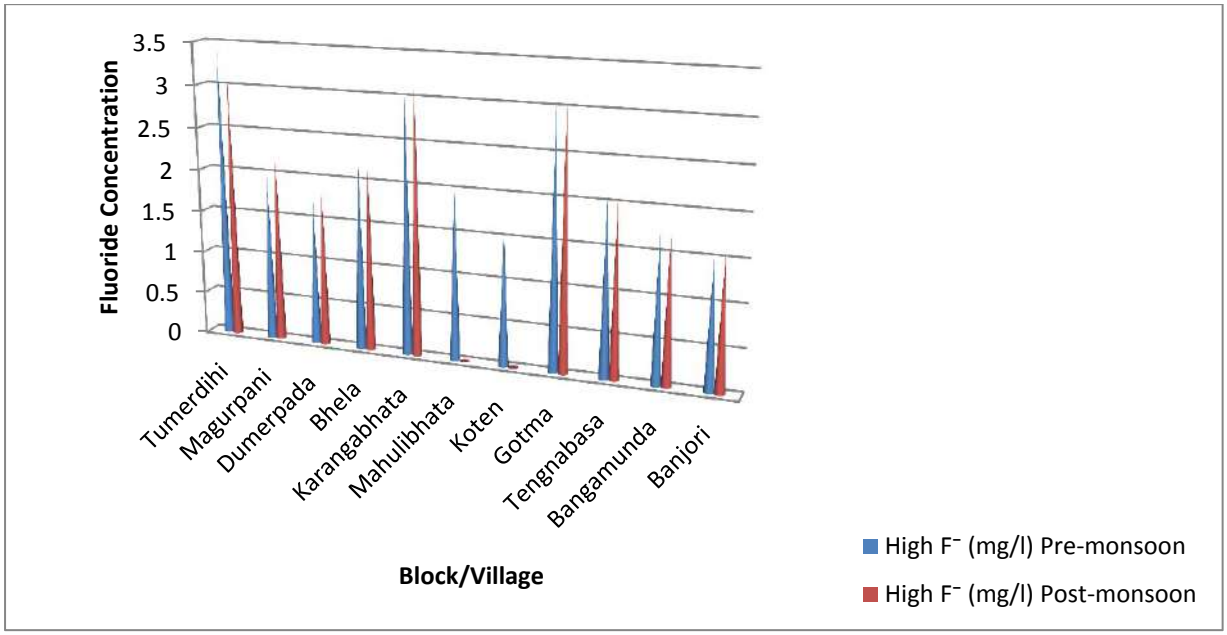

Distribution of Fluoride concentration above the permissible limit of WHO of both Pre and Post monsoon seasons over different regions of the study blocks

Statistical Estimation

Univariate Analysis

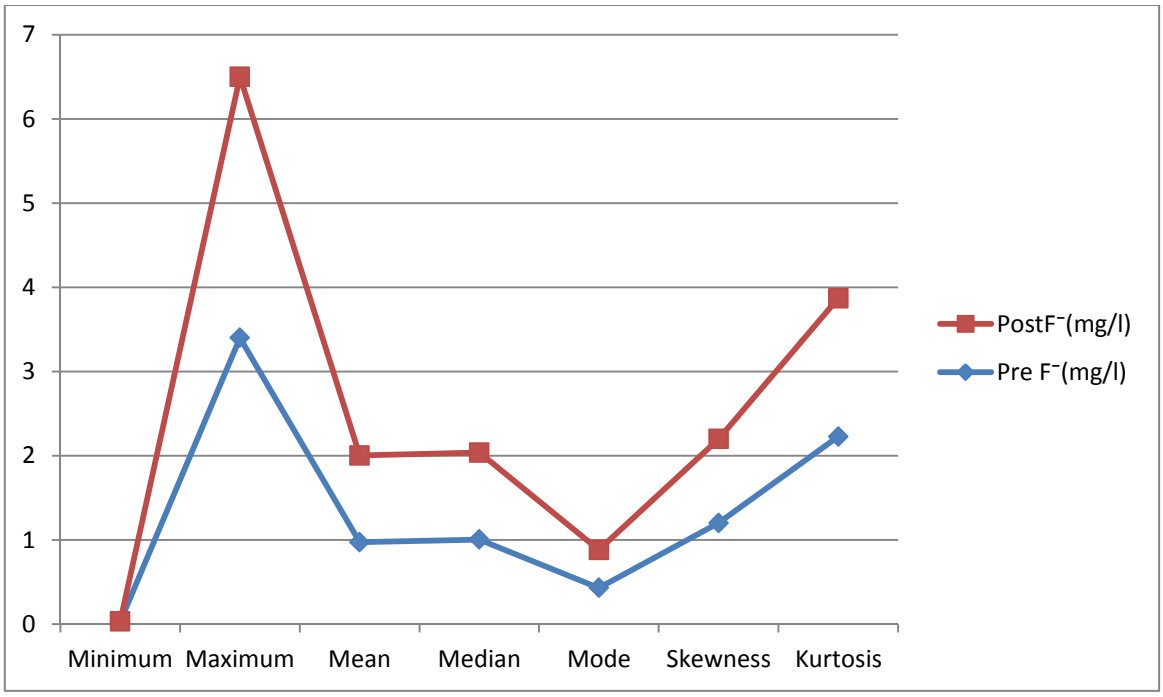

Univariate distribution of fluoride in both Pre and Post monsoon seasons over the study area

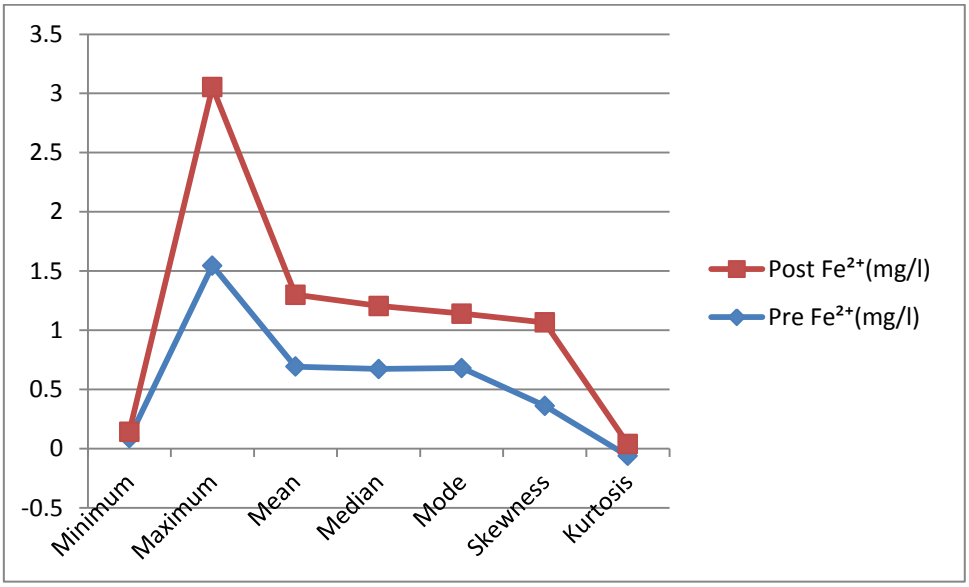

Univariate distribution of iron of both pre and post monsoon seasons over the study area

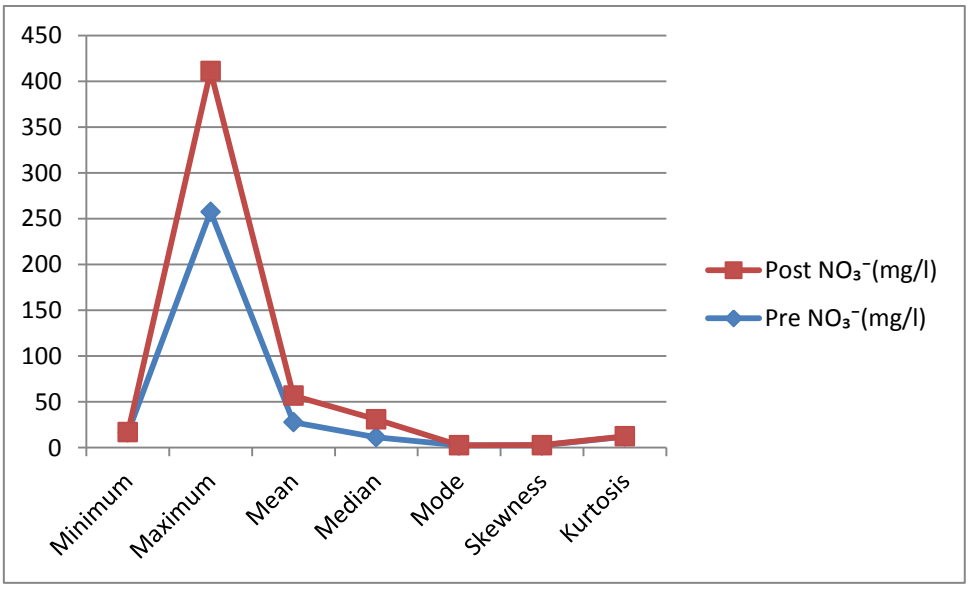

Univariate distribution of nitrate of both pre and post monsoon seasons over the study area

Multivariate Analysis

Multiple Regressions

Pre-monsoon TDS = 279.438 + 6.310Ca^{2+} + 7.920Mg^{2+} + 3.358Na^{+} - 14.196K^{+} + 42.863Fe^{2+} + 53.808HCO_3^- - 5.037SO_4^{2-} - 5.716Cl^- + 1.268NO_3^- + 35.806F^-

Post-monsoon TDS = -89.567 – 0.788Ca^{2+} - 3.875Mg^{2+} - 0.538Na^{+} - 2.170K^{+} - 78.720Fe^{2+} + 66.384HCO_3^- + 4.996SO_4^{2-} +1.206Cl^- + 1.640NO_3^- - 12.445F^-

Principal Component Analysis

Pre-monsoon Samples

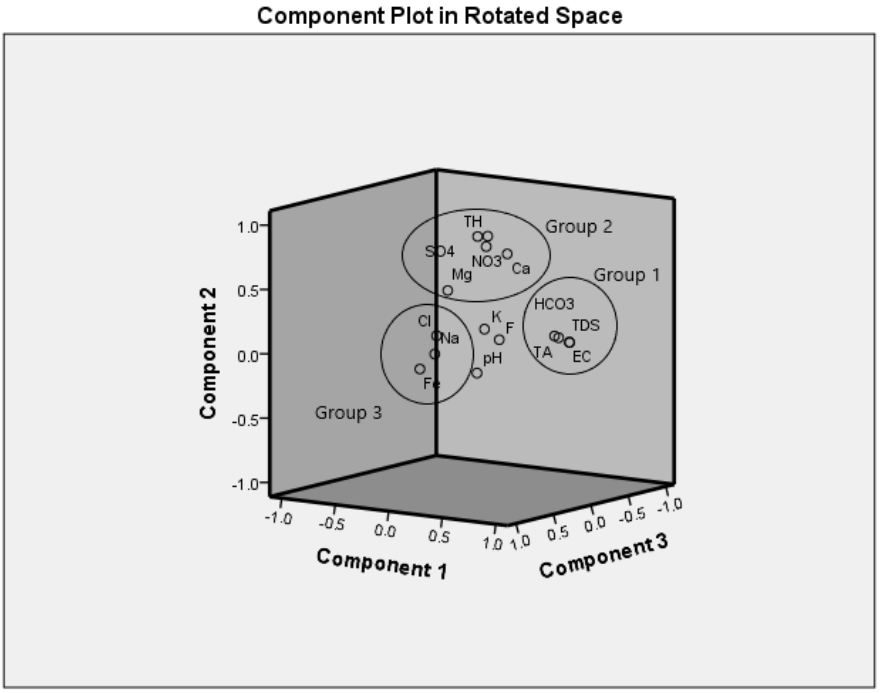

Distribution of extracted principal components into different groups

Post-monsoon Samples

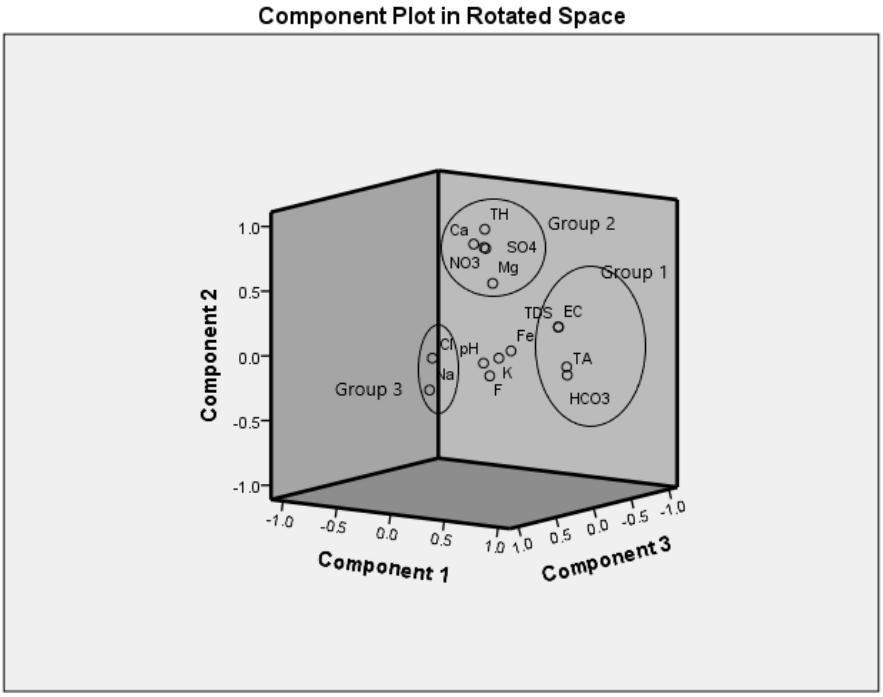

Distribution of extracted principal components into different groups

Source determination

Suspected sources of contamination of groundwater are properly determined by the Gibbs plot (Gibbs, 1907). The major natural factors responsible for contamination are aquifer rock types and their interaction with water (Sunkari, E. D., Abu, M., &Zango, M. S. (2021). Current study shows that the chemical composition of groundwater is varied by rock-water interaction and evaporation in both seasons. The increased concentration of iron in the study area mayhave been derived from the leaching of iron oxide. NO_3^- enrichment in groundwater may be due to major anthropogenic sources such as fertilizer, cattle and poultry manure. Fluoride influence in the groundwater may be from the weathering of the fluoride-bearing micaceous rocks and fluoride bearing minerals such as fluorite, apatite etc. It mayalso be due to partial or complete alteration of gneissic country rocks associated with alkaline type of water.

Impact of Climate Variability

The groundwater chemistry of the concerned area is more influenced by the climatic factors such as varied temperature, evaporation and precipitation etc. From source determination it is evident that most of the contamination is due to maximum evaporation and rock-water interaction. Maximum evaporation occurs during summer in a year and the annual average temperature has been recorded over ten year (2011-2020) data analysis. A variation in annual and diurnal temperatures is responsible for mechanical weathering process and leaching of elements into the groundwater. During post monsoon period surface water throughout its coursecarriessediments containing undesired elements mixes with groundwater as well as continuous reaction of water with the aquifer formation dissolves the substances making the groundwater more vulnerable to contamination.

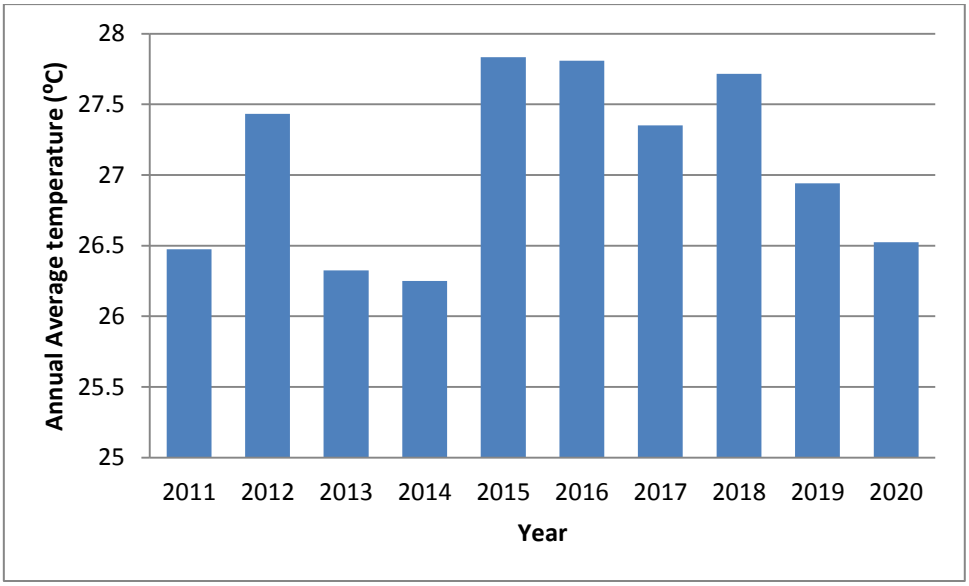

Annual average temperature of ten year (2011-2020) in the study area of Nuapada and Komna block of Nuapada district, Odisha

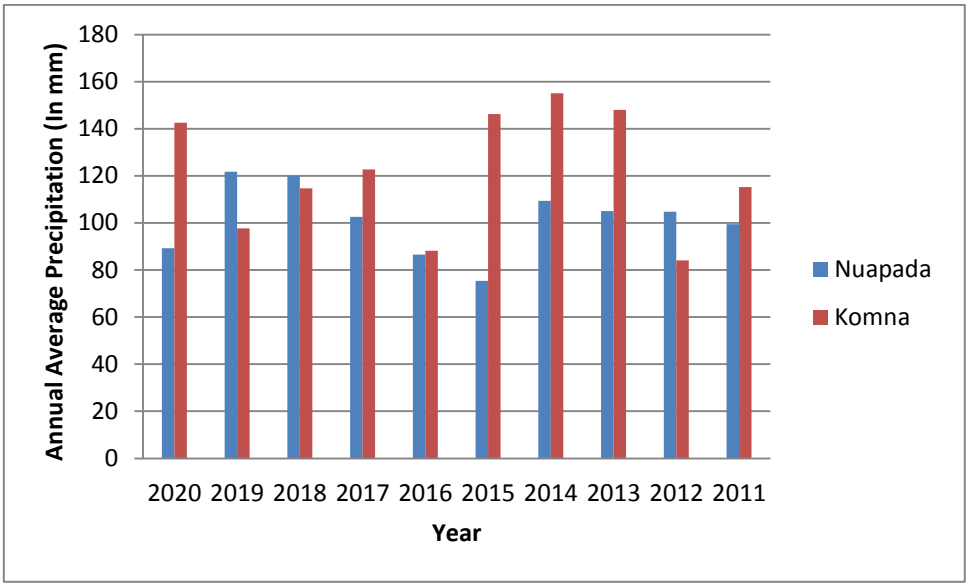

Annual average precipitation pattern of ten year (2011-2020) in the study area of Nuapada and Komna block of Nuapada district, Odisha

CONCLUSION

Climate change is an extreme phenomenon which has greater impact upon environmental factors such as air, water, soil etc. Major climatic factors such as temperature and precipitation variation bring dynamic changes in the water quality. Hydrgeochemical and geospatial and statistical tools were used to show qualitatively the contaminated portions of groundwater in the study region whereas climate variability in terms of temperature and precipitation have greater impact for the contamination as well as the susceptiblity to contamination of groundwater in the study region. The increased evaporation and chemical weathering of the surrounding rock with groundwater creates the vulnerable zones for contamination.

REFERENCES

APHA (1998) Standard Methods for the Examination of Water and Wastewater. 20th Edition, American Public Health Association, American Water Works Association and Water Environmental Federation, Washington DC.

Groundwater Information Booklet, Ministry of Water resources, Central Groundwater Board, SER, 2013

Kalhor, K., and Emaminejad, N. (2019) Sustainable development in cities: Studying the relationship between groundwater level and urbanization using remote sensing data. *Groundwater for Sustainable Development*, *9*, 100243.

Malik, M. S., and Shukla, J. P. (2019) GIS modeling approach for assessment of groundwater vulnerability in parts of Tawa river catchment area, Hoshangabad, Madhya Pradesh, India. *Groundwater for Sustainable Development*, *9*, 100249.

Sargazi, Shahnaz.,Mokhtari, Mahdi., Ehrampoush, Mohammad Hassan., Almodaresi, Seyed Ali., Sargazi, Hossein., Sarhadi, Masome. (2020) The application of Geographical Information System (GIS) approach for assessment of groundwater quality of Zahedan city, Sistan and Baluchestan Province, Iran

Sunkari, E. D., Abu, M., and Zango, M. S. (2021) Geochemical evolution and tracing of groundwater salinization using different ionic ratios, multivariate statistical and geochemical modeling approaches in a typical semi-arid basin. *Journal of Contaminant Hydrology*, *236*, 103742.

World Health Organization. (2017) *Global diffusion of eHealth: making universal health coverage achievable: report of the third global survey on eHealth*. World Health Organization.

VISTAS IN GEOLOGICAL RESEARCH
Special Publication in Geology (19), March 2023, pp. 43-56

Statistical Evaluation of Major Ion Chemistry of Premonsoon Groundwater of Kantapara Block, Cuttack District, Odisha

MADHUSMITA NAYAK[1] AND RABINDRA NATH HOTA[2]

[1]P.G.Department of Geology, Utkal University, Bhubaneswar – 751 004, Odisha
[2]P.G.Department of Geology, Fakir Mohan University, Nuapadhi, Balasore – 756089, Odisha
[*]Corresponding author e-mail: madhusmita_0000@yahoo.co.in

Abstract: The present study pertains to the application of statistical methods like bivariate correlation and multivariate factor, cluster and multiple regression analyses to interpret the processes influencing the major ion chemistry of the premonsoon groundwater of Kantapara block, Cuttack district, Odisha. The groundwater is alkaline and hard but suitable for drinking. Most of the parameters show significant positive correlations with each other. First three significant factors extracted by varimax rotation process explain 68.147% of the variance and can be used to evaluate the prominent hydrochemical processes in operation. The first factor with strong loadings on total dissolved solids (TDS), Mg^{2+}, Na^{+} and Cl^{-} with eigenvalue of 3.880 explains 38.804% of the variance. The second factor with prominent loadings on TDS, Ca^{2+}, HCO_3^{-} and F^{-} with eigenvalue of 1.757 explains 17.569% of the variance. These two factors incorporating TDS can be merged as one accounting for 56.373% of the variance. It is mostly geogenic in nature as most of the ions are derived by weathering of basement rocks. The third factor with loadings on K^{+}, $SO_4^{2-}$and NO_3^{-} is anthropogenic as these ions are derived from compost and fertilizers used by people to increase crop production. The cluster analysis segregates the constituent ions into two clusters. The dominant one includes TDS, Ca^{2+}, Mg^{2+}, Na^{+}, HCO_3^{-}, Cl^{-} and F^{-}, which belong to first two factors. The subsidiary cluster comprises K^{+} and SO_4^{2-}, while NO_3^{-} remains as residue and can be regarded as a cluster by itself. The multiple regression analysis suggests that Ca^{2+}, Mg^{2+}, Na^{+}, K^{+}, HCO_3^{-}, Cl^{-}, SO_4^{2-} and NO_3^{-} contribute significantly to the total dissolved solids (TDS) of the groundwater. The chemical constituents of the groundwater may be attributed to the effects of weathering, mineral dissolution, drainage wastes, septic tank leakage, irrigation-return-flows, chemical fertilizers and / or increase or decrease in chemical variables due to dissolution, precipitation, ion exchange and ionic concentration etc. The study demonstrates the usefulness of statistical methods as effectual tools for interpretation of the controlling processes of groundwater chemistry.

Keywords: Groundwater, Correlation analysis, Factor analysis, Cluster analysis, Multiple regression analysis

INTRODUCTION

Water is the most essential commodity for sustenance of life. Water is the main component for sustenance of life in the universe, without which any form of life would cease to exist. At present, water has a critical importance in the economic growth of all the modern societies. Therefore, water resource assessment and its sustainability are most important. Increasing population along with rapid urbanization during the recent decades has lead to focus on the utilization of groundwater. Its judicious usage and conservation are of fundamental

importance for mankind and economic growth.Groundwater meets about 80% of the need for different purposes including drinking, agriculture and industry in developing countries like India (Subba Rao et al. 2014). Use of water in different fields warrants stringent criteria in terms of quality and gross chemical composition (WHO, 2017). Since water is a universal solvent, it gathers several elements from the materials with which it comes in contact. As a result, the water becomes a mixture of several elements at different places. Multivariate statistics seems to be an appropriate tool for the effective study and interpretation of this multi-component system.

Factor, principal component and cluster analyses are the most important statistical tools which are being extensively used for the evaluation of the processes controlling groundwater chemistry and spatial distribution of pollutants (Hegeu and Kshetrimayum 2019; Ravish et al. 2020; Subba Rao et al. 2014, Naidu et al., 2021; Natesan et al. 2022 etc.). In the present study, in addition to correlation, factor and cluster analyses, the multiple regression analysis has also been used to evaluate the contribution of individual ions to the gross chemical composition of groundwater.

STUDY AREA

Location

The study area is bounded by east longitudes 85° 57' 30″ to 86° 03' 40" and north latitudes 20° 12' 30" to 20° 21' 30" and falls in the survey of India toposheets F45T15, F45T16, F45U3 and F45U4 in 1:50,000 scale covering an area of about 119.13 Sq Km (Fig.1). The area enjoys a warm humid climate with average rainfall about 1500 mm per year. The annual average temperature varies from 20° to 40° C.

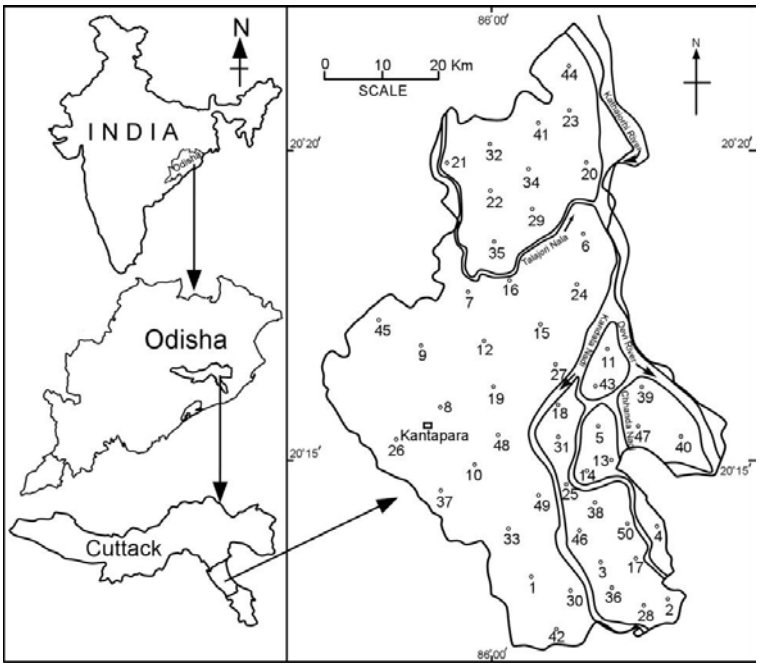

Fig. 1: Location map of Kantapara block showing groundwater sample locations.

Geology

Reddish and black soils are found in the Kantapara block, which come under the inceptisol and entisol categories respectively. The inceptisol is more abundant than entisol. The Eastern Ghats Supergroup, belonging to the Proterozoic Eon is the basement rock overlain by Tertiary sediments and alluvial soil of the Recent age. The alluvial soil consists of fine gravel, sand, silt and clay in different proportions. The area is characterized by moderate slope towards south.

Hydrogeology

The important rivers are Devi, Kandala and Chhanda which flow in the eastern part of the study area. The Talajori nala, a tributary of Kathjodi river flows from north and takes a northeasterly sinuous course in north-central part of the study area (Fig.1). Groundwater occurring under phreatic condition is extracted mostly through shallow tube wells. The premonsoon depth to water level ranges from 2 to 5 m below ground level. Irrigation practice is long term and intensive. Application of soil amendments and fertilizers are common for higher crop yield.

METHODOLOGY

Groundwater Sampling and Analysis

Since most of the dug wells in the Kantapara block of Odisha are not in use and many are abandoned, fifty groundwater samples were collected from tube wells fitted with hand pump during May (premonsoon season) 2018 in 500 ml capacity polyethylene bottles. These bottles were cleaned with dilute hydrochloric acid, washed thrice with distilled water and thoroughly rinsed with the groundwater before collection of water samples. Electrical conductivity (EC) and pH of the water samples were measured by water analysis kit (Systronics model no.371) in the field immediately after sampling. The concentrations of major cations (Ca^{2+}, Mg^{2+}, Na^{+} and K^{+}) and anions (HCO_3^{-}, Cl^{-}, SO_4^{2-}, NO^{3-} and F^{-}) of the water samples were estimated following the standard analytical procedures (APHA, 2012). The titration method was applied to estimate Calcium (Ca^{2+}) with standard EDTA solution. Chloride (Cl^{-}) and bicarbonate (HCO_3^{-}) were estimated by argentometric and sulphuric acid titrations respectively. Na^{+} and K^{+} concentrations were analysed by flame photometer (Systronics model no. 128). SO_4^{2-}, NO^{3-} and F^{-} were determined by UV- visible spectrophotometer (Systronics model no. 2701). Total dissolved solids (TDS) were estimated by multiplying 0.65 with the electrical conductance in μS/cm (Subba Rao, 2017). Mg^{2+} was calculated by employing standard equation. The ionic balance error (IBE, in percentage) was calculated to check the accuracy of the chemical analyses of groundwater samples using the equation proposed by Subba Rao (2017).

$$\text{IBE} = \frac{\sum \text{TCC} - \sum \text{TCA}}{\sum \text{TCC} + \sum \text{TCA}} \times 100$$

Where, ΣTCC and ΣTCA are the total concentrations of cations and anions in meq/l respectively. The ionic balance errors were about ±10% for all the groundwater samples suggesting reasonably accuracy of analyses.

Statistical Analysis

The data set of ten chemical variables (TDS, Ca^{2+}, Mg^{2+}, Na^{+}, K^{+}, HCO_3^{-}, Cl, SO_4^{2-}, NO_3^{-} and F^{-}) measured for fifty groundwater samples was used for correlation, factor, cluster and multiple regression analyses using IBM SPSS (version 23) and Statistica (version 7) softwares. The data were standardized to reduce the dimensionality and effects of outliers for correlation, factor and cluster analyses using equation proposed by Siddha and Sahu (2020).

$$Z_i = \frac{X_i - \overline{X}}{S}$$

where, Z_i = standardized value of sample 'i', X_i = ion concentration of the sample 'i', $\overline{X}$ = arithmetic average, and S = standard deviation.

However, the raw data was used for multiple regression analysis. Varimax rotation option was applied in factor analyses utilizing Kaiser's criterion (Kaiser 1958). The factor loadings help to look into the relative contribution of chemical variables on groundwater quality (Najafabadi et al. 2014). Cluster analysis classifies the variables into a set of more or less discrete groups. Correlation coefficient (r) and Euclidean distance (d_{ij}) are two well-known techniques for cluster analysis. In the present work, the correlation coefficient method was followed to group the pre-monsoon groundwater parameters. Pearson's bivariate correlation coefficients between different pairs of groundwater parameters were utilized for the preparation of the dendrogram in hierarchical cluster analysis (Davis 2002). Hierarchical clustering joins similar observations and then successively connects the next similar observations to the earlier ones. Ward's method (Ward 1963) was used for linking the water chemistry data in the present study. The cophenetic correlation between the actual correlation coefficients and apparent correlation coefficients extracted from the dendrogram was calculated. In multiple regression analysis, an attempt has been made to express the total dissolved solids (TDS, dependent variable) as a function of the concentrations of cations and anions (independent variables). The statistical significance of the equation and the contributions of different ions to the TDS were estimated by analysis of variance (ANOVA).

RESULTS AND DISCUSSION

Major Ion Chemistry

The statistical summary of the groundwater chemistry is presented in Table 1. Total dissolved solids (TDS) ranges from 216.58 to 550.4 mg/L with an average value of 317.88 mg/L and relatively high standard deviation of 63.62 mg/L. The concentrations (mg/L) of Ca^{2+}, Mg^{2+}, Na^{+}, K^{+}, HCO_3^{-}, Cl^{-}, SO_4^{2-}, NO_3^{-} and F^{-} vary from 30 to 90, 0.64 to 36.5, 11.98 to 37.66, 0.82 to 23.36, 0.16 to 2.45, 91.5 to 280.6, 20 to 60, 0.1 to 65.3, 3.59 to 32.71, and 0.18 to 0.49 with average values of 44.6, 12.4, 21.02, 4.97, 0.70, 156.4, 32.4, 11.47, 16.57 and 0.28 respectively (Table 1).

Table 1: Statistical summary of the groundwater chemistry.

Chemical variable	Min.	Max.	Avg.	S.D.
TDS	216.58	550.4	317.88	63.62
Ca^{2+}	30.0	90.0	44.6	10.50
Mg^{2+}	0.64	36.5	12.4	9.06
Na^{+}	11.98	37.66	21.02	6.85
K^{+}	0.82	23.36	4.97	4.19
Fe^{2+}	0.16	2.45	0.70	0.50
HCO_3^{-}	91.5	280.6	156.4	36.3
Cl^{-}	20.0	60.0	32.4	11.0
SO_4^{2-}	0.10	65.3	11.47	14.04
NO_3^{-}	3.59	32.71	16.57	4.93
F^{-}	0.18	0.49	0.28	0.07

* Units of all parameters are mg/L

The box and whisker plots (Fig.2) display the lower and upper quartile (rectangle), median (line within the rectangle), lowest-highest range (a vertical line with top and bottom lines) of ten chemical variables (TDS, Ca^{2+}, Mg^{2+}, Na^{+}, K^{+}, HCO_3^{-}, Cl^{-}, SO_4^{2-}, NO_3^{-} and F^{-}) for easy visualization of their relative variation. The upper limiting values of TDS, Ca^{2+}, Mg^{2+}, Na^{+}, K^{+}, Cl^{-}, HCO_3^{-}, SO_4^{2-}, NO_3^{-} and F^{-} are less than the permissible limits prescribed by WHO (2017). Hence the groundwater of the Kantapara block is safe for drinking purpose.

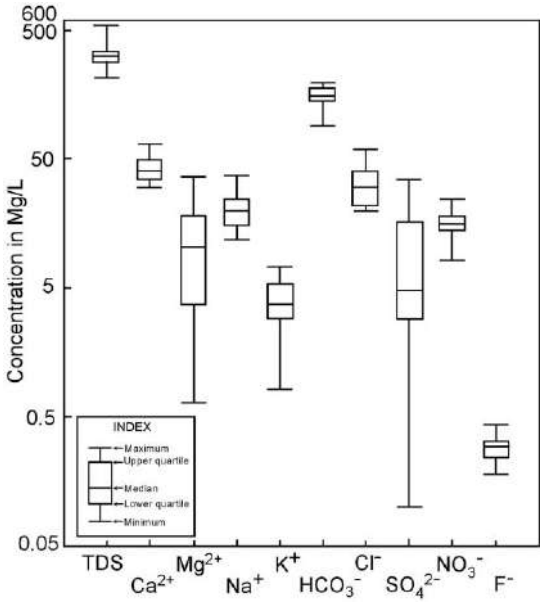

Fig. 2: Box and whisker plot of groundwater parameters of the study area.

Bivariate Correlation Analysis

Significant positive correlation of TDS with Ca^{2+} (r = 0.604), Mg^{2+} (r = 0.584), Na^{+} (r = 0.704), HCO_3^{-} (r = 0.861), Cl^{-} (r = 0.610), SO_4^{2-} (r = 0.510) and F^{-} (0.306) suggest that the

TDS is mostly controlled by these ions, which are derived from weathering and dissolution of minerals as well as anthropogenic activities (Subba Rao et al., 2022). The basement rocks are rich in plagioclase, pyroxenes, amphiboles and micas (Nanda et al. 2022), which by weathering release substantial amounts of Na^+, Ca^{2+}, Mg^{2+} and F^- (Subba Rao, 2021a). Cl^- is derived from non-lithological sources like domestic wastes, septic tank leakage and irrigation return flows (Subba Rao et al, 2021b). K^+, SO_4^{2-} and NO_3^- are derived mostly from fertilizers. HCO_3^- is mostly derived from interaction of CO_2 with H_2O. Its high correlation with TDS points to the possible water type in the study area. Contributions from alluvial soil also contribute substantial amounts of ions to the groundwater.

Significant positive correlation of Ca^{2+} with HCO_3^- (r = 0.701) and F^- (r = 0.411) may be due to their geogenic origin. Mg^{2+} shows good positive correlation with Na^+(r = 0.472), HCO_3^- (r = 0.416) Cl^- (r = 0.510), and low positive correlation with SO_4^{2-} (r = 0.307). Na^+ has positive correlation with HCO_3^- (0.326). K^+ shows positive correlation with SO_4^{2-} (r = 0.326). Significant positive correlations between HCO_3^- and F^- may be due to the effects of mineral dissolution, chemical fertilizers, mixing of fresh groundwater with surface contaminated water, and / or increase or decrease in chemical variables based on precipitation, ion exchange etc. (Brindha et al., 2017; Subba Rao et al. 2017; Badana et al., 2018 and Subba Rao et al., 2022).

Table 2: Actual correlations (above diagonal) and apparent correlations (below diagonal) extracted from the dendrogram (Fig.7).

	TDS	Ca^{2+}	Mg^{2+}	Na^+	K^+	HCO_3^-	Cl^-	SO_4^{2-}	NO_3^-	F^-
TDS		0.604**	0.584**	0.704**	0.140	0.861**	0.610**	0.510**	- 0.100	0.306*
Ca^{2+}	0.746		- 0.142	0.233	- 0.064	0.701**	0.124	0.190	-0.197	0.411**
Mg^{2+}	0.248	0.248		0.472**	0.011	0.416**	0.510**	0.307*	- 0.142	0.040
Na^+	0.759	0.746	0.248		0.099	0.416**	0.914**	0.323*	- 0.024	0.159
K^+	0.105	0.105	0.105	0.105		- 0.035	0.155	0.326*	0.014	- 0.013
HCO_3^-	0.861	0.746	0.248	0.759	0.105		0.300*	0.147	- 0.217	0.374**
Cl^-	0.759	0.746	0.248	0.914	0.105	0.759		0.245	- 0.014	0.068
SO_4^{2-}	0.105	0.105	0.105	0.105	0.326	0.105	0.105			0.024
NO_3^-	-0.051	-0.051	-0.051	-0.051	-0.051	-0.051	-0.051	-0.051		- 0.124
F^-	0.319	0.319	0.248	0.319	0.105	0.319	0.319	0.105	-0.051	

Factor Analysis

Though the factor analysis extracts same number of factors as the number of variables under consideration, on the basis of Kaiser criterion, only three of them are found to be statistically significant (Table-3). First three factors with eigenvalues of 3.880, 1.757 and 1.177 account for 38.804%, 17.569 % and 11.773% of variances respectively cumulating to 68.147 (Table-3). These three factors can be used to evaluate the dominant hydrochemical processes in operation in the study area without losing any significant information.

The factor loadings are listed in Table 3 and displayed in three-dimensional rotated space in Fig.3. The first factor has positive loadings on TDS (0.694), Mg^{2+} (0.814), Na^{+} (0.864) and Cl^{-} (0.882). The second factor is significantly loaded on TDS (0.639), Ca^{2+} (0.913), HCO_3^{-} (0.803) and F^{-} (0.656). Since both these factors have TDS as one of their component, they can be merged into one (Fig.3). Since it includes ions like Ca^{2+}, Mg^{2+}, Na^{+}, HCO_3^{-} and F^{-} (0.656), it may be regarded as geogenic. Factor – 3 has positive loadings on K^{+} (0.803), SO_4^{2-} (0.725) and NO_3^{-} (0.321). Since these ions are present in fertilizers used by people to increase the crop production this factor may be regarded as anthropogenic.

Table 3: Matrix of three factors and ten groundwater parameters with their eigenvalues, percentage of variance and factor loadings.

Groundwater parameters	Factor -1	Factor -2	Factor -3
TDS	**0.694**	**0.639**	0.249
Ca^{2+}	- 0.002	**0.913**	0.075
Mg^{2+}	**0.814**	- 0.014	- 0.052
Na^{+}	**0.864**	0.187	0.141
K^{+}	0.012	- 0.051	**0.803**
HCO_3^{-}	0.421	**0.803**	- 0.059
Cl^{-}	**0.882**	0.042	0.127
SO_4^{2-}	0.308	0.157	**0.725**
NO_3^{-}	- 0.071	- 0.319	**0.321**
F^{-}	- 0.020	**0.656**	- 0.034
Eigenvalues	3.880	1.757	1.177
Percentage of total variance	38.804	17.569	11.773
Cumulative percentage of total variance	38.804	56.373	68.147

Extraction Method: Principal component analysis; Rotation Method: Varimax with Kaiser normalization. Highest positive values are shown in bold numbers.

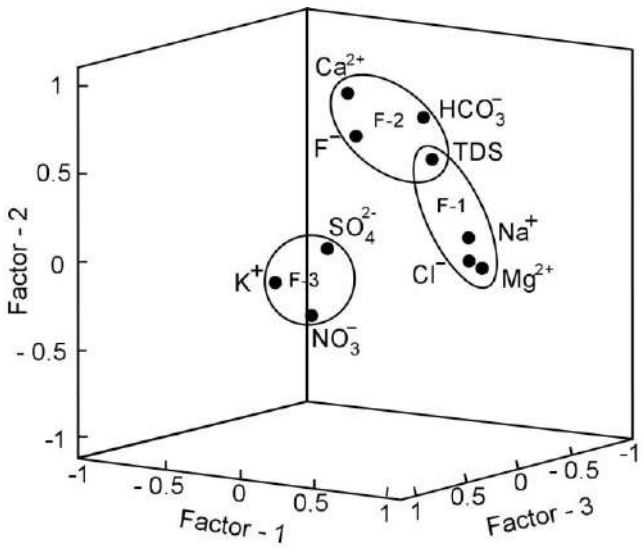

Fig. 3: Three dimensional plot of Factors 1, 2 and 3 showing distribution of groundwater parameters.

The factor scores of the above three factors are given in Table - 4 and their spatial variation diagrams are presented in Figs.4 – 6. Factor – 1 is pronounced in localities 15, 19, 24, 27, 28, 30, 31, 33, 38, 39, 43, 45 and 50 (Fig. 4). Factor – 2 is important around localities 9, 11, 12, 20, 21, 22, 24, 25, 26, 31, 34, 39, 41 and 47 (Fig. 5). Factor – 3 is well marked in localities 2, 9, 10, 26, 28, 31, 36, 37, 38, 45 and 47 (Fig. 6).

Table 4: Location-wise factor scores (scores > 0.5 are indicated by bold numbers).

Locality	Factor-1	Factor-2	Factor-3	Locality	Factor-1	Factor-2	Factor-3
1	-0.060	-1.259	0.316	26	-1.395	**0.719**	**2.476**
2	-0.250	-1.175	**1.237**	27	**1.209**	-0.358	-0.919
3	-1.246	-0.911	-0.003	28	**0.923**	-1.417	**1.152**
4	-0.413	-0.439	0.265	29	0.265	0.391	-0.676
5	-0.123	-0.446	-0.142	30	**0.883**	-0.295	-1.250
6	-0.010	-0.262	-0.476	31	**2.238**	**1.985**	**1.540**
7	-0.925	0.249	-0.657	32	-0.244	-0.338	-0.675
8	0.406	-0.933	-0.193	33	**1.163**	0.169	-0.558
9	-0.093	0.575	**0.507**	34	-0.508	**0.684**	-0.910
10	-0.412	-0.779	**1.517**	35	-1.305	-0.668	-0.412
11	-0.460	0.975	-0.511	36	-0.164	-1.096	**1.457**
12	-1.481	**1.362**	-0.342	37	-0.859	-0.222	**0.739**
13	-0.166	-0.791	-0.551	38	**2.110**	0.098	**2.101**
14	0.211	-0.714	-0.483	39	**1.468**	**3.493**	-0.011
15	**1.640**	-0.678	-0.644	40	0.107	-1.125	0.041
16	-0.414	-0.142	-0.332	41	-0.281	**0.607**	-0.824
17	-1.115	-0.860	-0.091	42	-1.211	0.416	-0.113
18	-0.918	-1.034	-0.520	43	**1.250**	-1.089	-0.935
19	**0.750**	0.193	-0.954	44	-1.071	0.190	-0.081
20	-0.381	**1.980**	-0.889	45	**1.745**	-0.663	**0.754**
21	-0.749	**2.224**	-0.563	46	-1.171	0.082	0.411
22	-0.298	0.671	-0.763	47	-0.464	**0.772**	**3.629**
23	-0.575	-0.734	-0.578	48	-0.368	-0.072	-0.306
24	**0.586**	0.577	0.491	49	0.276	0.309	-0.321
25	**-0.594**	0.552	-0.956	50	**2.493**	-0.770	-0.997

Cluster Analysis

The result of cluster analysis of groundwater parameters is shown as a dendrogram in Fig.7. The cophenetic correlation coefficient of 0.759 suggests higher degree of accuracy of the cluster analysis. The phenom line at r = 0.2 segregates the parameters into three clusters. Cluster – 1 comprises TDS, Ca^{2+}, Mg^{2+}, Na^{+}, HCO_3^{-} , Cl^{-} and F^{-}. Cluster – 2 includes K^{+} and SO_4^{2-}. NO_3^{-} remains as a separate entity and can be regarded as the residue or cluster – 3. The results of the cluster analysis closely match with the outcome of factor analysis. Constituents of cluster – 1 are those of factors 1 and 2 and may be regarded as geogenic, mostly derived from rock weathering. The members of clusters 2 and 3 (K^{+}, SO_4^{2-} and NO_3^{-}) are those of factor 3 and may be regarded as anthropogenic.

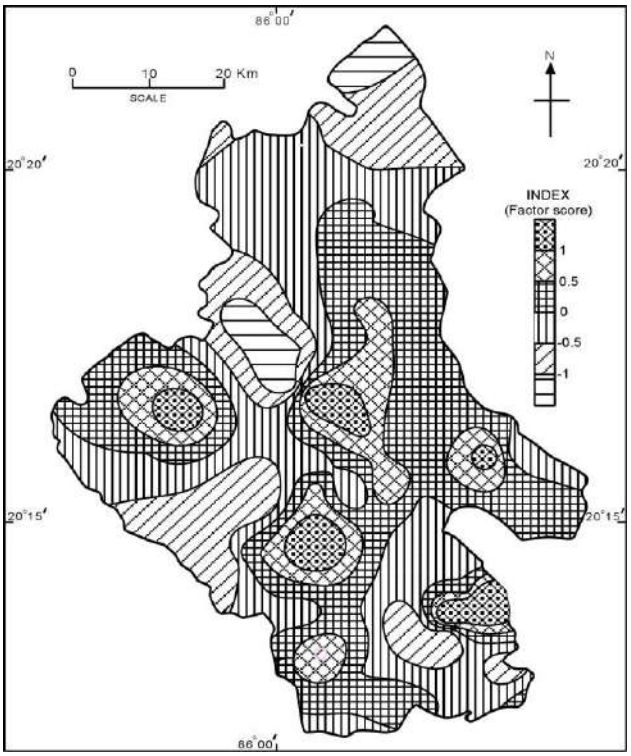

Fig. 4: Spatial influence of factor 1.

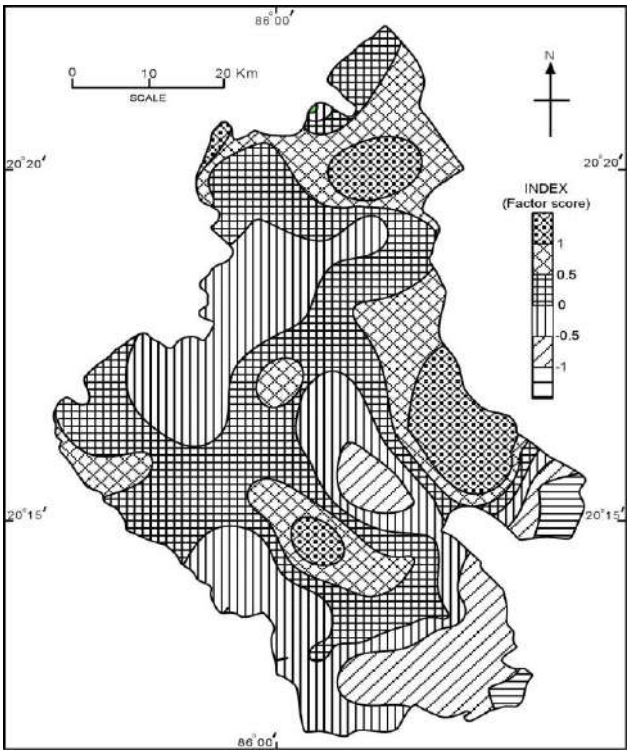

Fig. 5: Spatial influence of factor 2.

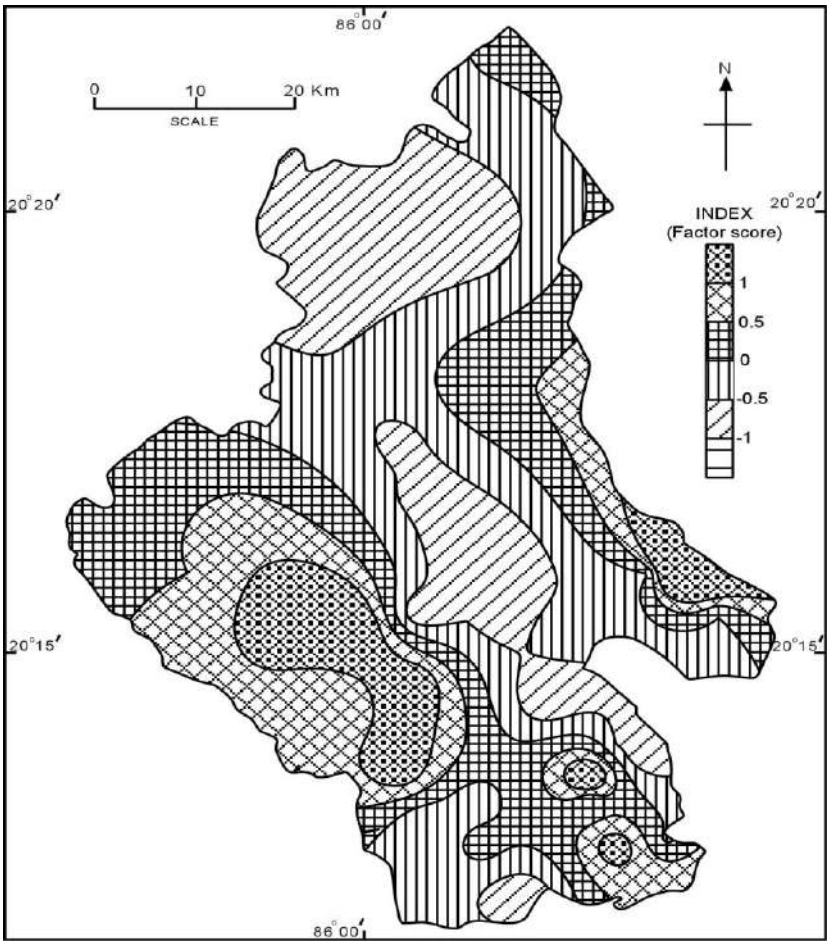

Fig. 6: Spatial influence of factor 3

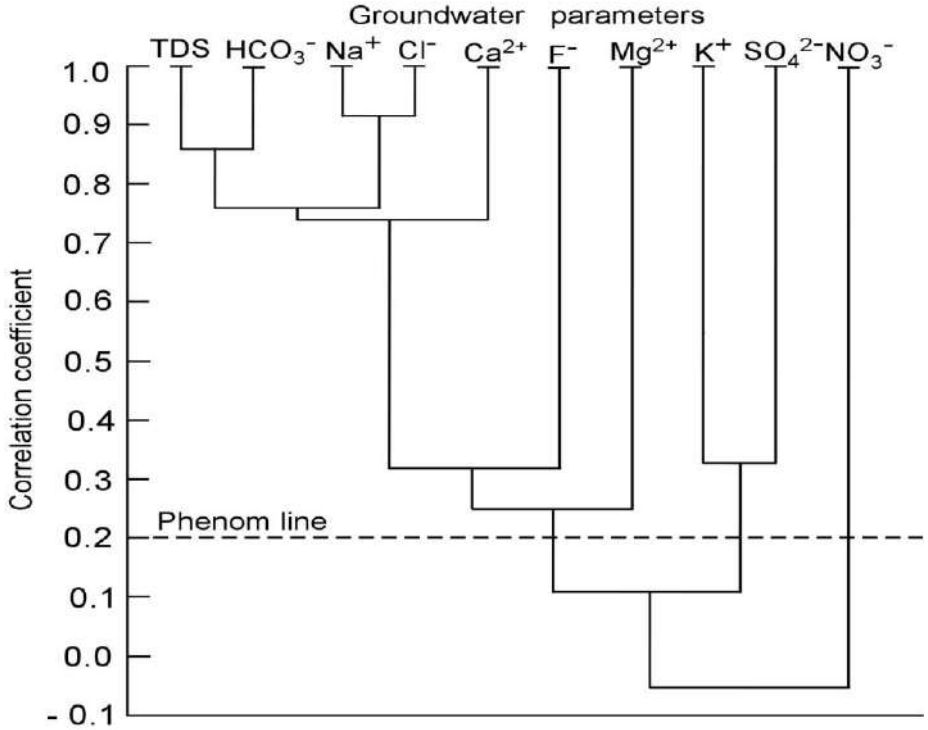

Fig. 7: Dendrogram showing clusters of groundwater ions

Multiple Regression Analysis

Though both factor and cluster analyses depict indirect contribution of ions to TDS, the multiple regression analysis expresses the TDS as a liner function of ions. In the present study the equation is " TDS = 23.972 + 0.925 Ca^{2+} + 1.172 Mg^{2+} + 1.496 Na^{+} + 0.790 K^{+} + 0.986 Cl^{-} + 0.714 HCO_3^{-}+ 1.104 SO_4^{2-} + 0.850 NO_3^{-} - 4.773 F^{-} with 95% confidence interval of ±14.074 mg/L. The analysis of variance (ANOVA) is presented in Table - 5. The computed value of 'F' (337.472) for the regression equation is greater than the critical value (4.02) at 0.001 significance level which confirms the best fitting of the equation. The computed values of 'F's for Ca^{2+} (84.442), Mg^{2+} (62.360), Na^{+} (35.707), K^{+} (13.331), HCO_3^{-} (1001.950), Cl^{-} (92.569), SO_4^{2-} (149.926) and NO_3^{-} (18.488) exceed the critical value (12.6) at 0.001 significance level. These ions contribute significantly to the TDS. When the relative values of 'F's are taken into consideration, it seems, Ca^{2+} among the cations and HCO_3^{-} among the anions mostly account for the groundwater composition of the Kantapara block and the dominant groundwater type is likely to be Ca-HCO_3 type. This matches well with the plotting of ionic data in Piper trilinear diagram (Fig.8).

Table 5: ANOVA for testing the significance of regression equation and individual ions.

Source of variation	Sum of squares	Degrees of freedom	Mean squares	F
Regression	195759.835	9	21751.093	337.472**
Ca^{2+}	5442.527	1	5442.527	84.442*
Mg^{2+}	4019.313	1	4019.313	62.360*
Na^{+}	2301.439	1	2301.439	35.707*
K^{+}	859.2134	1	859.213	13.331*
HCO_3^{-}	64578.700	1	64578.700	1001.950*
Cl^{-}	5966.320	1	5966.320	92.569*
SO_4^{2-}	9663.192	1	9663.192	149.926*
NO_3^{-}	1191.619	1	1191.619	18.488*
F^{-}	0.228	1	0.228	0.004
Deviation	2578.121	40	64.453	---------
Total variation	198337.956	49	----------	----------

** $F_{\upsilon_1 = 9, \upsilon_2 = 40, \alpha = 0.001} = 4.02$ * $F_{\upsilon_1 = 1, \upsilon_2 = 40, \alpha = 0.001} = 12.6$

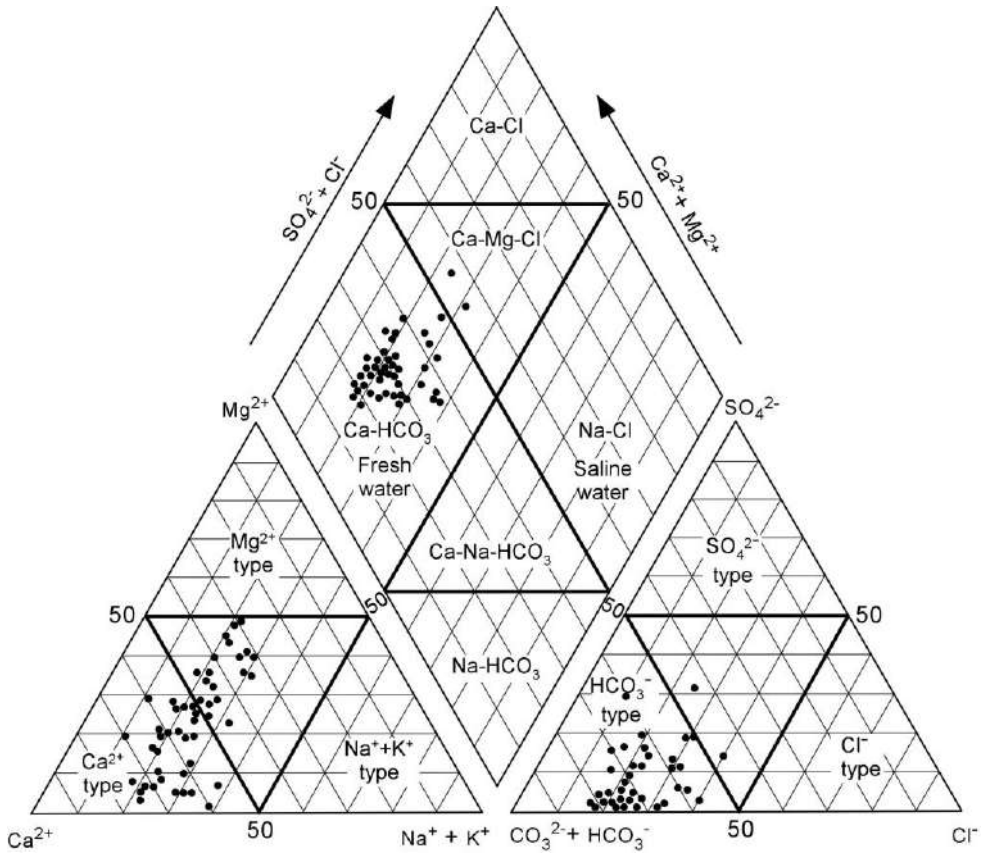

Fig. 8: Piper trilinear diagram of the groundwater data of Kantapara block.

CONCLUSIONS

The groundwater samples of the Kantapara block of Odisha state were studied by statistical methods like correlation, factor, cluster and multiple regression analyses with a view to decipher factors controlling the groundwater chemistry. All the groundwater parameters are within the permissible limits enunciated by WHO (2017) and are suitable for drinking. Following conclusions have been drawn from the present study.

(i) First three factors extracted by varimax rotation process have eigenvalues greater than 1 and thus are statistically significant.

(ii) These three factors explain 68.147% of the total variance and can be used to evaluate the prominent hydrochemical processes in operation. The first factor with eigenvalue of 3.880 explains 38.804% of the variance with strong loadings on total dissolved solids (TDS), Mg^{2+}, Na^{+} and Cl^{-}. The second factor with prominent loadings on TDS, Ca^{2+}, HCO_3^{-} and F^{-} with eigenvalue of 1.757 explains 17.569% of the variance. These two factors including TDS can be merged into one accounting for 56.373% of the variance. The ions excluding Cl^{-}, can be derived by weathering of basement rocks and thus may be regarded as geogenic. The third factor with loadings on K^{+}, $SO_4^{2-}$and NO_3^{-} is anthropogenic as these ions are present in compost and fertilizers used by people to increase crop production.

(iii) The cluster analysis segregates the constituent ions into two clusters. The dominant one includes TDS, Ca^{2+}, Mg^{2+}, Na^{+}, HCO_3^{-}, Cl^{-} and F^{-}, which belong to first two factors. The subsidiary cluster comprises K^{+} and SO_4^{2-}while NO_3^{-} remains as the residue or can be regarded as a cluster by itself. These three ions are incorporated in third factor.

(iv) The multiple regression analysis suggests that Ca^{2+}, Mg^{2+}, Na^{+}, K^{+}, HCO_3^{-}, Cl^{-}, SO_4^{2-} and NO_3^{-} contribute significantly to the total dissolved solids (TDS) of the groundwater. Quantitative values of 'F's suggest that the predominant water is likely to be Ca-HCO_3 type, which has been confirmed by the Piper trilinear diagram.

(v) The chemical constituents of the groundwater may be attributed to the effects of weathering, mineral dissolution, drainage wastes, septic tank leakage, irrigation-return-flows, chemical fertilizers and / or increase or decrease in chemical variables due to dissolution, precipitation, ion exchange etc.

(vi) The study reveals the usefulness of statistical methods as effective tools for interpretation of the controlling processes of groundwater chemistry.

REFERENCES

APHA (2012) Standard methods for the examination of water and wastewater. American Public Health Association, Washington DC.

Badana, N., Vetrimurugan, E. and Rajmohan, N. (2018) Coastal aquifer contamination and geochemical processes evaluation in Tugela catchment, South Africa-Geochemical and Statistical approaches. Water, v.10, pp.687.

Brindha, K., Pavelic, P., Sotoukee, T., Douangsavanh, S. and Elango, L. (2017) Geochemical characteristics and groundwater quality in the Vientiane Plain, Laos Expo Health, v.9, pp.89–104.

Davis, J. C. (2002) Statistics and data analysis in Geology. John Wiley & Sons, New Delhi.638p.

District, Telangana State, India. Arch. Environ. Contam. Toxicol., v.80, pp.11-30.

Hegeu, H. and Kshetrimayum, K. S. (2019) Hydrochemical characterization of groundwater in geomorphic units using graphical and multivariate statistical methods in Dimapur valley, Northest India. Groundwater for sustainable development, v.8, pp.484-500.

Hussain, M., Ahmad, S. M., and Abderrahman, W. (2008) Cluster analysis and quality assessment of logged water in an irrigation project, eastern Saudi Arabia. Jour. Environ. Management, v.86, pp.297-307.

Kaiser, H. F. (1958) The varimax criterion for analytic rotation in factor analysis. Psychometrika, v.23, pp.187-200.

Naidu, S., Gupta, G., Singh, R., Tahama, K. and Erram, V. C. (2021) Hydrogeochemical processes regulating the groundwater quality and its suitability for drinking and irrigation purpose in parts of coastal Sindhudurg district, Maharashtra. Jour. Geol. Soc. India, v.97, pp.173-185.

Najafabadi, Z. P., Khan, I. A. and Ghazifard, A. (2014) Statistical approach to groundwater quality assessment: An example from Zarinshahr city, Central Iran. Gond. Geol. Mag., v.29, pp.123-133.

Nanda, J. K., Mohanty, M. and Mahapatro, S. N. (2022) Geology of Odisha, Geol. Soc. India, 410p.

Natesan, D., Sabarathinam, C., Kamaraj, P., Mathivanan, M., Haji, M., Viswanathan, P. M., Chandrasekaran, T. and Rajendran, T. (2022) Impact of monsoon shower on the hydrogeochemistry of groundwater along the lithological contact: a case study from South India. Applied Water Science, v.12, pp.1-20.

Ravish, S., Setia, B. and Deswal, S. (2020) Groundwater quality analysis of northeastern Haryana using multivariate statistical techniques. Jour. Geol. Soc. India, v.95, pp.407-416**.**

Siddha, S. and Sahu, P. (2020) A statistical approach to study the evolution of groundwater of Vishwamitri river basin (VRB), Gujarat. Jou.r Geol. Soc. India., v.95, pp.503-506**.**

Subba Rao, N. (2017) Hydrogeology - Problems with solutions. PHI Learning Pvt. Ltd., Delhi.265p.

Subba Rao, N., Dinakar, A. and Sun, L. (2022) Estimation of groundwater pollution levels and specific ionic sources in the groundwater, using a comprehensive approach of geochemical ratios, pollution index of groundwater, unmix model and land use/land cover – A case study. Jour. Cont. Hydro., v.248, pp.1-18.

Subba Rao, N., Dinakar, A., Karuna, B., Kumari Karunanidhi, D. and Kamalesh, T. (2021b) Groundwater Quality Vulnerable Zones of Yellareddygudem Watershed, Nalgonda

Subba Rao, N., Dinakar, A., Sravanthi, M. and Kumari. B. K. (2021a) Geochemical characteristics and quality of groundwater evaluation for drinking, irrigation, and industrial purposes from a part of hard rock aquifer of South India. Env. Sci. and Poll. Res., v.28, pp.31941–31961.

Subba Rao, N., Surya Rao, P., Dinakar, A., Nageswara Rao, P. V. and Deepali, M. (2017) Fluoride occurrence in the groundwater in a coastal region of Andhra Pradesh, India. Appl. Water Sci. v.7, pp.1467–1478.

Subba Rao, N., Vidyasagar, G., Rao, P. S. and Bhanumurthy, P. (2014) Assessment of hydrogeochemical process in a coastal region: Application of multivariate statistical model. Jour. Geol. Soc. India, v.84, pp.494-500.

Ward, J. H. (1963) Hierarchical grouping to optimize an objective function. Jour American Statl. Asso., v.58, pp.236–244.

WHO (2017) Guidelines for Drinking Water Quality, 4th edn. Including the first addendum, World Health Organization, Geneva.541p.

VISTAS IN GEOLOGICAL RESEARCH
Special Publication in Geology (19), March 2023, pp. 57-68

Sedimentary Structures and Landforms in the Islands of Langkawi, Malaysia

SANDEEP N. KUNDU

Department of Geology, Ravenshaw University, Cuttack 753003
Email: sandeepkundu@ravenshawuniversity.ac.in

Abstract: Langkawi is located in the far north-western corner of Peninsular Malaysia, in the state of Kedah. It comprises of 99 islands with mesmerizing scenic and colourful natural landscapes which reflect the geo-diversity and complex geological history of the islands. The geological landscapes of Langkawi islands are shaped by long depositional history under varying *palaeo-environmental* condition, by *tectonic and magmatic events* and by *surface processes*. This makes it an ideal site for a sedimentological study. The exposures of sedimentary sequences, consisting of both clastic and carbonates, can be studied to understand the changes in depositional environment and the paleoenvironment. The effects weathering of the different rocks types of the island, which have eroded to form the many heterogeneous beaches across the island, can also be observed. Peculiar landscapes like formation of a freshwater lake surrounded by the saline are seen in the area of study. In this paper, an overview of the geology of Langkawi and the sedimentary processes that shaped the sediments of various beaches are presented with supporting field photographs.

Keywords: Fieldtrip, Stratigraphy, Beach Sediments

INTRODUCTION

Langkawi is located in the far north-western corner of Peninsular Malaysia, in the state of Kedah. It comprises of 99 islands with mesmerizing scenic and colourful natural landscapes which reflect the geo-diversity and complex geological history of the islands. Langkawi Islands can be reached by both air and water routes. By air, it is connected to Kuala Lumpur and from Taipei, London and Osaka. Langkawi has also regular port which receives many cruise ships. Through water, it is connected from other Malaysian places like Kuala Kedah, Kuala Perlis, and Penang and from Satun in Thailand.

The geological landscapes of Langkawi islands are shaped by long depositional history under varying palaeo-environmental condition, by tectonic and magmatic events and by surface processes. This makes it an ideal site for a sedimentological field discourse with multiple educational objectives. Sedimentary sequences, consisting of both clastic and carbonates can be observed and their environment of deposition can be inferred from field evidences. The effects weathering on different rocks types of the island can be studied from erosional landforms and the various beach deposits across the island. Peculiar landscapes like formation of a freshwater lake surrounded by the saline sea can be observed. In this paper, an overview of the geology of Langkawi and observations on sedimentary processes forming various beaches of heterogeneous sand is presented with supporting field photographs taken

during a field led by the author in 2016. Location map of Langkawi Island and the sites described in this paper is provided in .

Geologic Setting & History

The Cambrian rocks were deposited in the shallow shelf portion of what was previously known as the Yunnan-Malayan Geosyncline, a basin that extends from south China in the north to the Malay Peninsula in the south over a distance in excess of 2000 km (Lee, 2006). The rocks within this belt are exposed in a series of large folds which are roughly north–south trending anticlines with granitic core (Jones 1973). The Machinchang Anticline is one such feature that has brought resistant sedimentary rocks and granite to the surface to form the Langkawi Islands. The Machinchang Anticline can be traced northwards into Tarutao Island located approximately five kilometres across the border into Thailand and the Machinchang Formation consists of three members (Lee 2005). These formations of late Cambrian to Precambrian in age lie unconformably below a thrust faulted mylonite zone in the northern coastal Machinchang area (Lee, 2006).

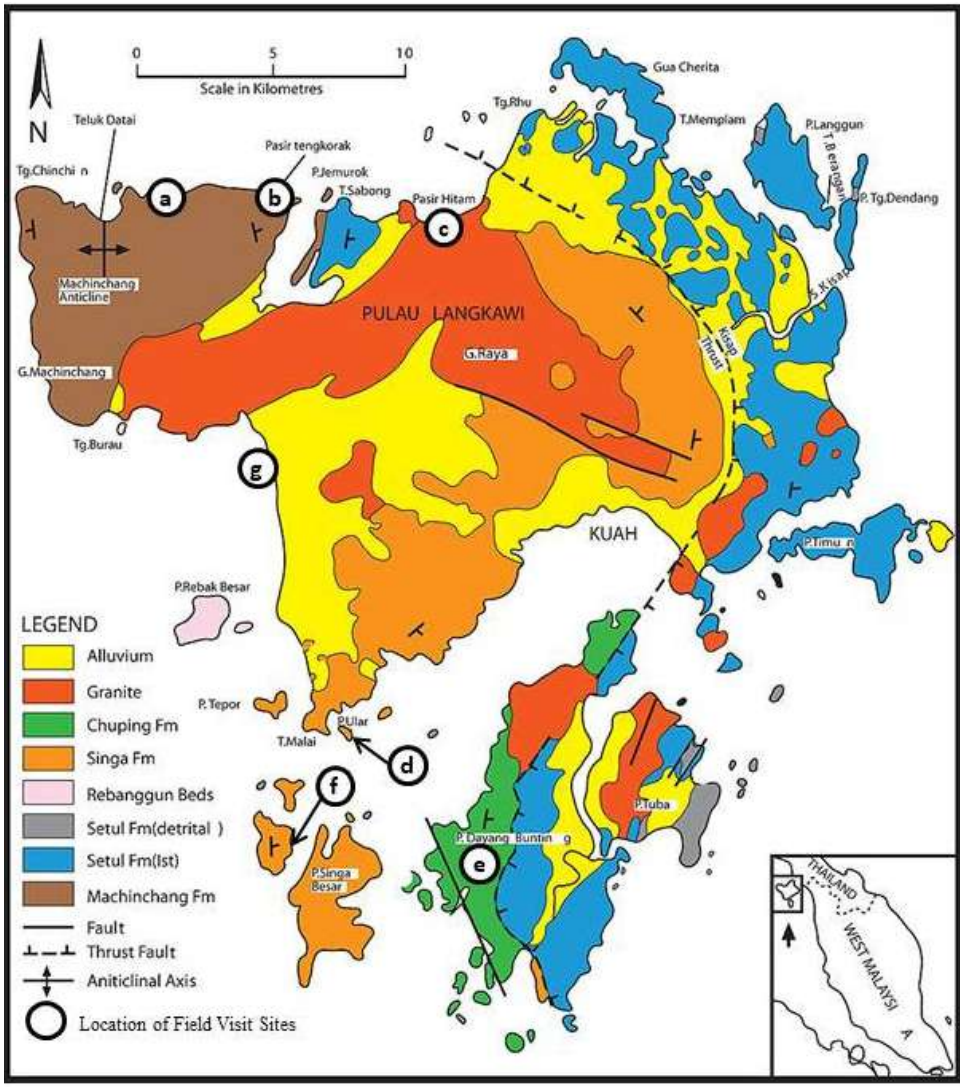

Fig. 1: Location and Geological Map of Langkawi and the sites described (adapted from Jones, 1981).

At the beginning of the ice age around 2 m.a., the sea had receded below 100m of the levels recorded about 2000 years ago. The Langkawi Islands were connected to the mainland at the peak of this ice age after which the sea rapidly rose and the coastal plain was drowned isolating the several islands of Langkawi. Thus Langkawi became a group of islands separated by shallow seas. The drowned enclosed basin at Dayang Bunting became isolated from the sea, making it a rain-fed fresh water lake. The base of the lake is well below the current sea level. The shoreline advanced along the west coast during the last 6,000 years giving rise to the Cenang plain and other events which are recorded on the surface, in the sediments and along the coasts of Langkawi (Tjia 2013).

Stratigraphy

The Palaeozoic sedimentary rocks in Langkawi had been placed under four Formations (Lee, 2014), which are the Machinchang, Setul, Singa and Chuping Formations (and

). These are mostly shallow marine shelf type deposits which form part of a belt that extends from South China all the way down through Burma, Thailand, and Northwest Peninsular Malaysia to North Sumatra.

a) Machinchang Formation

Machinchang Formation occurs as a serrated quartzite ridge of five peaks and consists of a thick succession of predominantly arenaceous rocks with minor interbeds of conglomerates, phyllitic slates and tuffs. The oldest part of the Formation is pelitic and exposed in the core of the Machinchang Anticline whereas the top of the formation has several thin calcareous horizons on which the succeeding Setul Formation limestone is unconformably deposited. Poorly preserved fragments of trilobites and brachiopods in the Formation, give it an age between late Cambrian to early Ordovician. Trace fossils and sedimentary structures such as various types of cross-beddings, convolute bedding and load casts can be seen in the upper parts of the Formation at Pasir Tengkorak and Pulau Jemurok. Palaeocurrent on the cross-beddings found in the Formation indicate a westward down current direction indicating the dominance of beach-barrier shoreline processes at that time. The overall depositional environment that can be deduced from the facies is that of a high-destructive, wave-dominated delta over an offshore shelf deposit.

b) Setul Formation

The Setul Formation is made up of predominantly dark coloured shelfal limestone with minor black detrital bands of early Ordovician to early Devonian age. Although largely metamorphosed, some fossiliferous outcrops are seen in the vicinity of Pulau Langgun. A rich fauna of both larger fossils such as gastropods, bivalves, nautiloids, brachiopods, trilobites and graptolites as well as microfossils such as conodonts, ostracods and tentaculitids are found in the Formation. The top of the Formation is represented by the arenaceous Upper Detrital Band with minor argillaceous beds at Pulau Langgun. The Setul Formation has been estimated to be about 1500 m thick.

c) Singa Formation

The Singa Formation consists of a clastic unit which has laminated, dark grey, poorly sorted mudstones. It has several dropstone horizons where the size of the dropstones ranges between granules to boulders of sandstone with subordinate limestone, vein quartz, granitic, volcanic and metamorphic rocks. This is indicative of a glacial environment, which is derived from some palaeo-Gondwana margin in the Carboniferous age. Fossils are uncommon but burrows and soft sediment deformation structures are observed. Some brachiopods found in the dropstone horizons at Kilim, Batu Asah and Pulau Singa Besar are "cold-water" forms of Permian age. Sandstone beds are few and mostly calcareous. The south-western part of Langkawi has the best exposure of Singa formation which has a basal contact with the unexposed Rebanggun Beds. The top of the Singa Formation grades into the overlying limestones of Chuping Formation which are exposed on Pulau (island) Singa Besar.

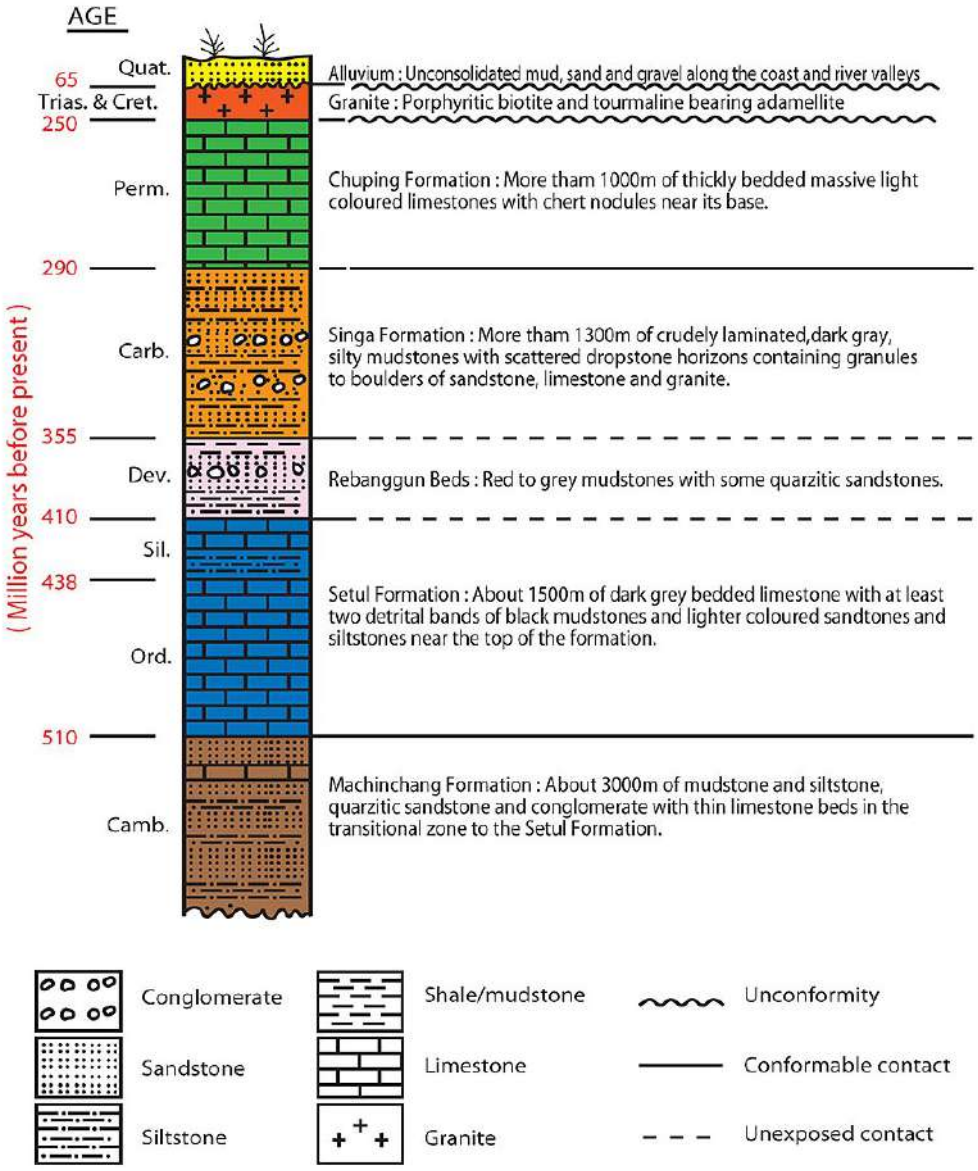

Fig. 2: Stratigraphy of Langkawi (Lee, 2014).

d) Chuping Formation

The Chuping Formation consists of a unit of thickly bedded to massive, light coloured limestones which can be easily distinguished from the dark coloured Setul limestone. The Chuping Formation is fossiliferous in its basal part which consists of fusulines, brachiopods, bivalves, gastropods, corals, bryozoans and algae that give it an age of early Middle Permian. Basal chert nodules occur at the base of Chuping formation which is exposed at Pulau Singa. The famous Langkawi marble is a white saccharoidal ornamental stone quarried from south-eastern Langkawi and Dayang Bunting Island. The marble resulted from contact metamorphism of limestones of Chuping Formation. The lake of Dayang Bunting is the best known geomorphic feature of this Formation. The floor of this freshwater lake amid the sea had been cored and the shells collected for radiocarbon dating. Dolomitic marble was once quarried along the north shore of Dayang Bunting with Italian craftsmen employed before the Second World War and the quarry was revived in 1962 to supply marble tiles for the National Mosque in Kuala Lumpur.

e) Langkawi Granites

Two granitic bodies, namely the Raya and Tuba granites cover about 113 sq. km of the islands. The Raya is the largest massif which rises to 878 m forming a peak in the main island. The age of the Raya is late Cretaceous whereas the Tuba Granite belongs to late Triassic. The two granites are petrographically similar and difficult to distinguish from field observations as both are porphyritic biotite granites with tourmaline clots and veins and have large K-feldspar phenocrysts and spherical quartz phenocrysts. Minor acid volcanic tuffs, which occur as thin, fine grained, pale green layers in the Machinchang Formation, are indicative of acid volcanism during Cambrian times.

1. Sedimentary Structures and Landforms

The landforms and sedimentary structures were studied to infer the sedimentary processes and environments. The landforms and structures were observed and documented at their exposures (marked ‘a’ to ‘g’ in) and their sedimentary significance are presented below.

a) Temurun Waterfall & Pebble Beach

The Temurun waterfall is located at the Machinchang Nature Park at latitude (6°26’3.13” N, 99°42’28.88” E) and longitude (6°26'6.68"N, 99°42'31.29"E). It cascades from the northern incline of the 850 m high Machinchang Hills and is one of the tallest and a three-step natural waterfall. Temurun Bed, a higher unit of the Chinchin Member of Machingchang Formation, consisting of wavy quartzitic sandstones, is exposed at this waterfall.

The sandstones have perpendicular sets of joints occupied by quartz veins. The waterfall cuts through and weathers the jointed quartzitic sandstone and the stream erodes it to form a pebbly beach, which consists of equant pebbles of size greater than an inch ().

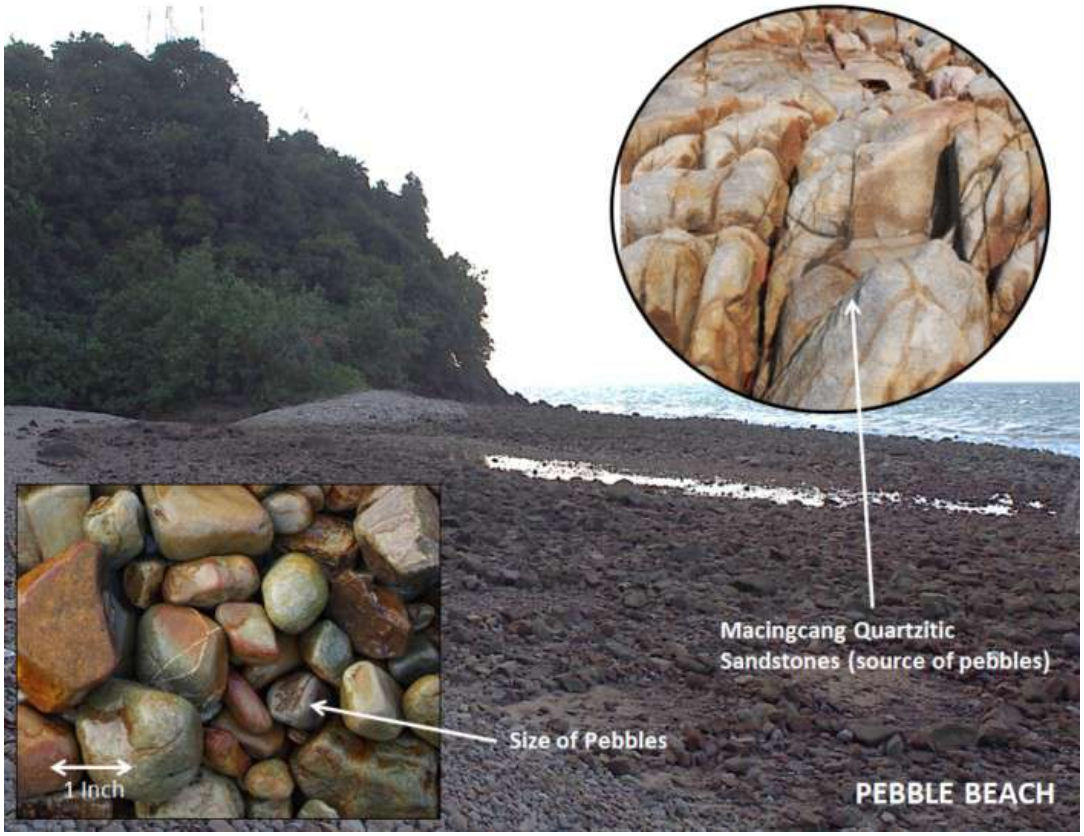

Fig. 3: Pebble Beach and (inset) the jointed sandstone provenance of the pebbles.

b) Tengkorak Beach

Tengkorak beach is located at latitude (6°25'50.74"N) and longitude (99°43'36.22"E). Ripple marked sandstone with slumped bedding and load casts interbedded with thinner beds of mudstone and siltstone and rare fine grained tuffaceous mudstones, belonging to the Tengkorak Bed of the Chinchin member of Machinchang Formation, are exposed here. Closely spaced jointing with thin quartz veins is found which weather to form honeycomb structures. Observed sedimentary structures are provided in Fig. 4. One can look northwards across the sea to view the island of Tarutao in Thailand, across which the rocks extend.

To the north-eastern tip of the area, the uppermost member of the Machinchang Formation is exposed, which consists of thin to thick bedded fine grained sandstone and siltstone inter-bedded with dark grey mudstone. The rocks transit through thinly inter-bedded siltstones and limestone bands to the limestones of the overlying Setul Formation. Low angle and hummocky cross bedding, horizontal trace fossils and fragmentary trilobite and brachiopod coquina have been reported in the area but the exposures were highly vegetated obscuring both accessibility and view.

The bedding characteristics, sedimentary structures and lithologies of the Tengkorak Bed change in bed thickness and grain size from the underlying unit. The sedimentary depositional settings of the various members of the Formation provide a sound understanding of the changing paleoenvironment.

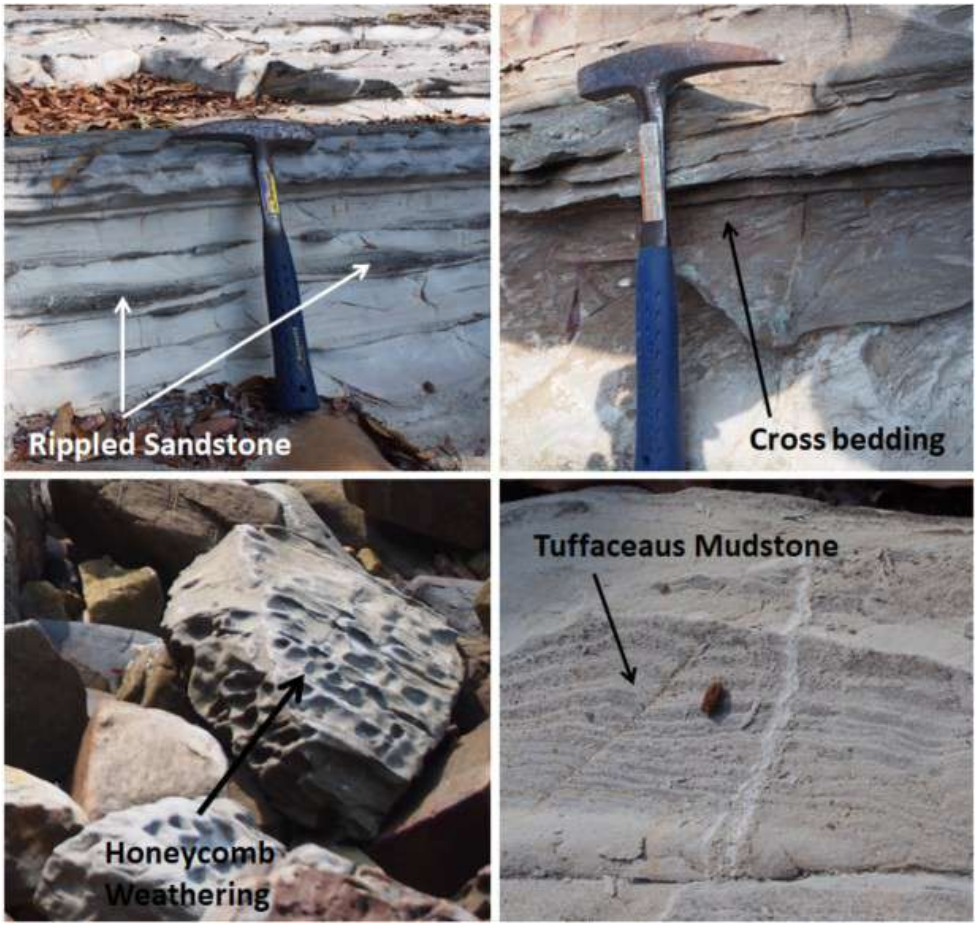

Fig. 4: Sedimentary structures of the different members of Machingchang formation at Tengkorak Beach.

c) Pasir Hitam (or Black Sand Beach)

Pasir Hitam, located at latitude (6°25'36.27"N) and longitude (99°47'40.03"E), is named after the black placer sands which are composed of mostly tourmaline with minor amounts of ilmenite and zircon. The sand minerals are products of weathering of the Raya granite, which is eroded hydrologically to this beach. Beach processes, mostly driven by waves, winnow the lighter minerals like quartz and mica and in the process the heavier tourmaline, ilmenite and zircon are concentrated which impart black colour to the beach. The grain size and the horizontal and vertical banding of dark (tourmaline, Ilmenite and zircon) and light coloured (Quartz) grains on the beach (and inset) were studied. The energy of the waves and diurnal tide were found to be responsible for the sorting of the coloured sediments both in the horizontal and vertical space. It was observed that the dark minerals were of smaller grain size as compared to quartz (). As quartz has a specific gravity lower than the dark minerals, similar amount of energy was needed to displace them. Although most beach sands consist of quartz, at Pasir Hitam the sand consisted of several lesser stable dark minerals. This was because the provenance of the tourmaline, ilmenite and zircon sands was the nearby Raya Granite, and with a small distance of transportation, complete breakdown of these less stable minerals was not possible.

Fig. 5: Sand types, size and stratification at Hitam Beach

d) Ular Island

Located at latitude (6°15'30.35"N) and longitude (99°44'30.72"E), this small island can be assessed by a motor boat from the Awana Portabello Resort. The island is made up of weathered yellow coloured Singa Formation sandstones and mudstones and a wave cut platform can be seen on the island (and inset). Trace fossils and pebbly mudstone horizons and slumped horizons are seen on the island.

Fig. 6: The site visit team in front of the strata of Singa formation and (inset) a wave cut platform.

The Singa formation consist of poorly sorted sandstone which grade into siltstone and mudstone towards the top. This swallowing upward sequence is typical of regressive shallow marine depositional environment. Trace fossils and pebbly mudstone horizons and slumped horizons are seen in the finer sediments but the lower older sandstones are devoid of fossils owing to a colder (glacial) environment of deposition.

e) Dayang Bunting Island

Located at latitude (6°12'27.24"N) and longitude (99°47'4.27"E), this island is named Dayang Bunting as it resembles that of a pregnant lady lying on her back from a distance. This island hosts the freshwater lake called Tasik Dayang Bunting (or the Lake of the Pregnant Maiden) at its south-western coast (Fig. 7). The lake surrounded by steep sided karstic limestones of Chuping Formation has resulted from the collapse of a sinkhole. The eastern part of the island is occupied by Setul Limestone that has been thrusted against the Chuping Limestone. The Permian Chuping Limestone is exposed on this island and can be differentiated from its lighter colour as compared to the darker Setul limestone. The Chuping limestone is dolomitized and exhibits typical 'elephant skin' weathered surfaces (Fig. 7 inset).The presence of coral forms in the limestone indicates that the limestones are of reef origin.

Fig. 7: Dayang Bunting Island and lake and (inset) Elephant skin texture of Setul limestone

f) Beras Basah Island

A 10 minute ferry from the Dayang Bunting Island is one of Langkawi's uninhabited islands, called Beras Basah Island (latitude - 6°13'18.11"N, longitude - 99°43'18.97"E). The island is known for its white sand beach and blue waters. Pulau Beras Basah is known for white-sand

beaches. The glaring white beaches consist of calcareous sand which results from the weathering and breakdown of reefs (

and inset). As the island has no fluvial system, clastic inputs like quartz sand were absent. The abundance of tropical reef islands around the area has contributed to the carbonate sands at the beach.

Fig. 8: Calcareous sand beach at Beras Basah Island and (inset) coral fragments found on the beach.

g) Pantai Cenang

Pantai Cenang, latitude (6°17'43.54"N) and longitude (99°43'22.27"E), is at the western side of Langkawi island. Across the beach is the famous underwater world of Langkawi. The beach has several exposures of rocks belonging to the Singa Formation. The rocks are hardened due to the contact metamorphism from the granitic intrusions but isolated dropstones of quartzite and granite, embedded in typical dark coloured silty mudstone () can be seen at several places. Slump folds are visible especially at the southern end of this coastal outcrop.

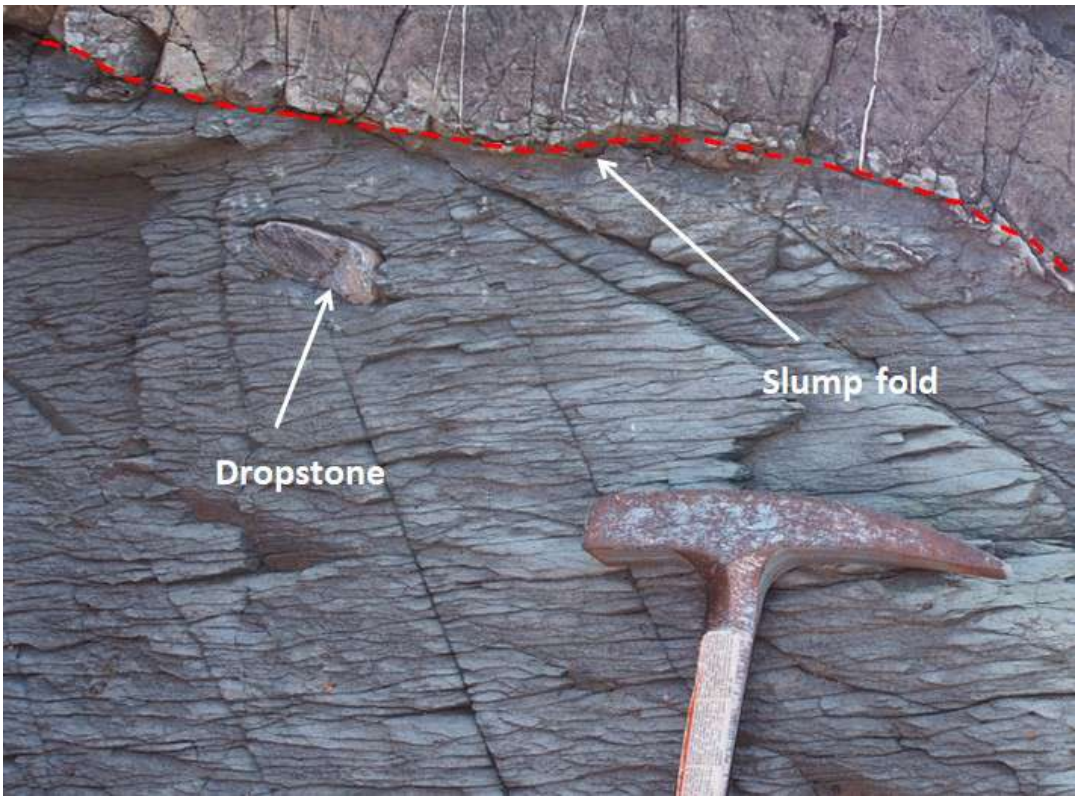

Fig. 9: A dropstone in the hardened silty mudstone of Singa formation at Pantai Cenang

Dropstones are isolated fragments of rock found within finer-grained lake-deposited. They ranged in size from small pebbles to boulders and are carried to the glacial lacustrine environment buy melting icebergs.

DISCUSSION

The islands of Langkawi preserved the rich history of rocks dating from Cambrian to Recent, which presents a wonderful place for conducting geological studies. One can observe evidences of contact metamorphism, igneous intrusions and various sediments deposited in a wide variety of depositional environments. Once can witness evidences of glacial environment from the dropstones in Singa formation and the various rippled and current bed structured in Machingchang formation representing a fluvial and shallow marine environment. From a geomorphic point of view, the topography of the main island and the prevailing hydrologic setting has resulted in formation of contrasting beach sediments across the island. From a sedimentological perspective, black sand beach of Hitam, white sand (calcareous) beach of Beras Basah island and the freshwater lake resulting from a collapsed sinkhole at Dayang Bunting are geological wonders.

REFERENCES

Lee, C.P., (2005). The Cambrian of Malaysia (abstract). Acta Micropalaeontol. Sinica 22 (Supplement), 88–90.

Lee, C. P. (2006). The Cambrian of Malaysia, Palaeoworld, 15(3-4), 242-255.

Lee, C. P. (2014). Geological Field Guide to Langkawi, Bulletin of the Geological Society of Malaysia (retrieved online at https://gsmpubl.wordpress.com/2014/09/02/geological-field-guide-to-langkawi/ on 12 January 2023)

Jones, C.R. (1973). Lower Palaeozoic, In: Gobett, D.J., Hutchison, C.S. (Eds.), Geology of the Malay Peninsula. John Wiley-Interscience, New York, pp. 25–60.

Jones, C.R. (1981). Geology and mineral resources of Perlis, North Kedah and the Langkawi Islands, Geological Survey Malaysia District Memoir 17, 275 pages.

Tjia, H. D. (2013). Evidence of Holocene and historical changes of sea level in the Langkawi Islands. Bulletin of the Geological Society of Malaysia, 59.

VISTAS IN GEOLOGICAL RESEARCH
Special Publication in Geology (18), March 2023, pp. 69-76

Understanding Some Trends and Relationships from Statistical Analysis of Historical Ground Water Quality Data of Odisha

TANKADHAR BEHERA, GARGI SINGH AND SANDEEP KUNDU*

Ravenshaw University, Cuttack 753003
Email: sandeepkundu@ravenshawuniversity.ac.in

Abstract: Groundwater is an important resource which is used for both domestic and industrial needs. It is a replenishable resource, which plays a key role in the agrarian economy of Odisha for mitigating the intermittent paucity of rain-fed water systems during extreme climatic events. However, growing population, urban sprawl and indiscriminate use of groundwater has led to both the depletion of ground water and degradation of its quality. The Central Ground Water Board (CGWB), South Eastern Region, Bhubaneswar has established more than1600 National Hydrograph Network Stations (NHNS) (open / dug wells) and piezometers in the state to monitor groundwater. Apart from measuring the water levels, chemical analysis is done on water samples to check its quality. The findings are reported annually by CGWB through its "Groundwater Year Book" each year, year on year comparisons are presented on the parameters measured. So far 9 such reports from 2013 -14 to 2021-22 have been published and are available online. Process-based models with data-driven methods improve predictive capability and understanding of water resources systems. Hence to understand the relationship of the various parameters of ground water quality, data science methods make use of statistical analysis of historical groundwater quality data. In this study, historical ground water quality data from past CGWB Groundwater Yearbooks were used to compute the correlation of various ground water quality parameters. Such analysis establishes the intricate relationship of various parameters and facilitates a cause-effect analysis. This short study found that various groundwater quality parameters are intricately related.

1. INTRODUCTION

Groundwater is an essential resource for mankind. It is vital for drinking water, food production and sustaining river flows and wetlands and as such, it needs to be protected. One important aspect is its quality, which can be affected by both human activities and naturally occurring contaminants. Today, global groundwater resources are under unprecedented pressure from a wide range of factors, all of which can potentially deteriorate its quality. To identify these factors in any study area, it is important to make use of data science techniques where historical water quality data is available.

In Odisha, around 90% of rural and more than 50% of the urban households depend on ground water (Chaudhuri and Roy, 2017). Hence monitoring of quality of ground water is essential. The Central Ground Water Board (CGWB), South Eastern Region, Bhubaneswar has established more than 1600 National Hydrograph Network Stations (NHNS) (open / dug wells) and piezometers in the state to monitor groundwater (CGWB 2014, 2015, 2016, 2017,

2018, 2019, 2020, 2021, 2022). Apart from measuring the water levels, chemical analysis are done on water samples to check its quality. The findings are reported annually by CGWB through its "Groundwater Year Book " each year, year on year comparisons are presented on the parameters measured. Of the 9 Groundwater Year Books available online from year 2013-14 to 2021-22, 7 contain groundwater quality data on 12 or more ground water chemical parameters which influence its quality. In this study, these historical data were extracted and their statistical analysis was performed to deduce the bivariate relationship between parameters to set the stage for a cause-effect analysis.

1.1 Factors affecting groundwater quality

The physical and chemical quality of ground water is important in deciding its suitability of use for various purposes. Bureau of Indian Standards (BIS) vide its document IS: 10500:2012, has recommended the quality standards for water on the basis of which ground water of India has been categorized as acceptable, permissible and unfit for human consumption. Although aquifers are inherently more susceptible to contamination owing to their geological characteristics and climate change, there are anthropogenic factors which impact groundwater quality. These are commonly identified as:

- Urban sprawl
- Indiscriminate pumping at coastal areas
- Indiscriminate usage of ground water

Industrialization also introduces broad groups of contaminants into groundwater and this is an emerging concern as they pose a direct threat to groundwater quality and human health. Monitoring of groundwater quality for these contaminants is now receiving more attention as many of them are still unregulated by law. Industries and products which belong to this category include the likes of pharmaceuticals, personal care products, plasticisers, biocides and micro plastics.

Ground water quality in an area is a function of physico-chemical parameters influenced by natural and anthropogenic processes (Barbecot et al. 2000). Ground water is mostly rain fed and therefore the chemistry of rainwater influences its quality. As the atmosphere is composed of several gases and some gaseous pollutants, it is natural for rainwater to take some proportion of these into solution before it reaches the ground. These make rainwater slightly acidic but its EC generally remains below 50µ S/cm. However, as rainwater flows on the surface, its chemistry becomes highly variable due to its interaction with soil and rocks. It has been observed that surface water or runoff mostly has high concentrations of Na and HCO_3. Percolation of surface water to become groundwater is an even more heterogeneous process where it interacts with rocks and unconsolidated sediments. The surface water, which is rich in carbonic acid, reacts with minerals in soil and rock, releasing several cations and anions like chlorine, fluorine, sulphates, bicarbonates, nitrate, sodium, potassium, calcium, magnesium, iron, arsenic etc. forms TDS in ground water and increases its EC.

Thus the chemical parameters like TDS, chloride, fluoride, iron, arsenic and nitrate etc. are main constituents defining the quality of ground water in unconfined aquifers (CGWB, 2010), which also influence the EC and the pH of water. These parameters are monitored periodically to evaluate its suitability for drinking, irrigation and industrial uses.

2 DATA AND METHODS

2.1 Groundwater Monitoring Data

In order to manage groundwater resources and mitigate threats to water supplies,an improved understanding of groundwater quality threats from both widely regulated and monitored contaminants is needed. To do this,it is needed to improve surveillance of water-quality threats and understanding of their links to human activities and health outcomes, including those from emerging hazardous contaminant and improve the visibility and sharing of groundwater-quality datasets.

Central Ground Water Board (CGWB), South Eastern Region, Bhubaneswar has established more than1600 National Hydrograph Network Stations (NHNS) (open / dug wells) and piezometers in the state to monitor groundwater. Apart from measuring the water levels, chemical analysis are done on water samples to check its quality. The findings are reported annually by CGWB through its “Groundwater Year Book " each year, Year on year comparisons are presented on the parameters measured. These reports are available online for download and use for the general public, especially data scientists who can extract the quality data for their analytics.

Seven CGWB Groundwater Year Books, 2015 to 2022 contains water chemistry data analysed from water samples collected from dug wells at the various NHNS sites in Odisha. The data was presented as tables in the appendices of the report. A total of 7734 records for the years, from 2015 to 2022, were extracted and merged into a single worksheet for exploratory analysis. The information from the report were organised under the following fields:

- Year
- District, Block, Village/Site
- EC, pH and TDS
- Cl, F and Na

2.2 Methodology

Data-driven methodologies have gained popularity in groundwater hydrology in recent years due to the advancement of analytical algorithms and increasing data accessibility. Sophisticated machine learning algorithms which capture and translate data patterns into actionable evidence could be applied. The core of these methodologies is statistical methods for data exploration and analysis which support the gathering, reviewing, analysing and deducing conclusions from appropriate variables. Statistical methods help in understanding

the relationships between parameters and their trends from historical data which lead to an increasingly accurate identification and enumeration of ground water quality trends. At the same time, insightful inter-relationships and potential cause-effect relationship interpretations can also be inferred.

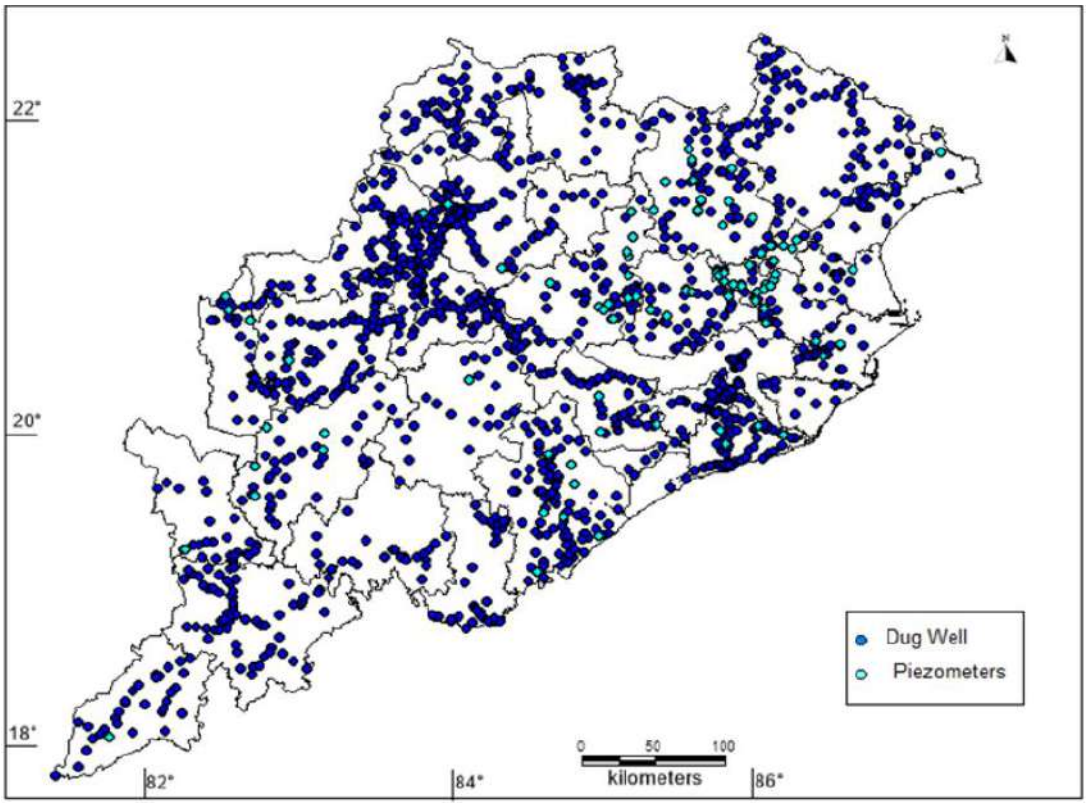

Fig. 1: National Hydrographical stations for groundwater quality monitoring (Source: Ground Water Year Book 2019-2020).

2.2.1 Summary Statistics & Trends

Summary statistics summarize and provide information about the sample data. Multivariate statistical methods and inverse geochemical modeling have been used to define the variation and the genetic origin of chemical parameters of groundwater (Belkhiri et al, 2010). Statistical analysis reveals information from the values in the dataset from its distribution. Statistical values like the minimum, maximum, mean, standard deviation etc. are important elements of summary statistics, which are helpful in spotting human errors in data that could originate from human and instrumentation errors. In the current study, summary statistics was helpful in detecting some errors in the CGWB published data where some values were out of range which adversely influenced the summary statistics. These errors were fixed based on the nearest most probable values from data from preceding and succeeding years.

Trend analysis is the practice that gives us the ability to look at data over time for monitoring changes. Statistical trends can be derived using histograms or line diagrams. In this study trends on pH, EC and TDS over time were calculated.

2.2.2 Cross plots and Correlation

Correlation is one of the statistical analyses where the relationship between two variables is computed and visualised using cross plots. This helps in testing simple hypotheses of association although conclusive cause-effect cannot be guaranteed. Correlation can help in determining to what extent it could be easier to estimate or predict the value of a variable when the value of the other variable is known.

Cross plots were generated for pairs of groundwater quality parameters with an aim to determine the degree of correlation. This is achieved through plots between pairs of parameters. From the commonly understood processes of the hydrologic cycle, expected association like TDS with EC, could be verified. At the same time, it was important to test the association of specific cations and anions with TDS and EC.

3 RESULTS AND DISCUSSION

3.1 TDS and EC

A fast, inexpensive and reliable way of measuring the ionic content in a solution is by measuring EC of ground water. Water is a poor conductor but its EC increases when it contains dissolved salts which serve as electrolytes. The amount of dissolved electrolytes can also be determined by measuring the TDS of ground water. Salinity is variable in ground water and is mostly influenced by the geology of the aquifer and the pathways for its recharge. In coastal areas, indiscriminate pumping of ground water for irrigation too results in sea water ingression which increases the EC of ground water.

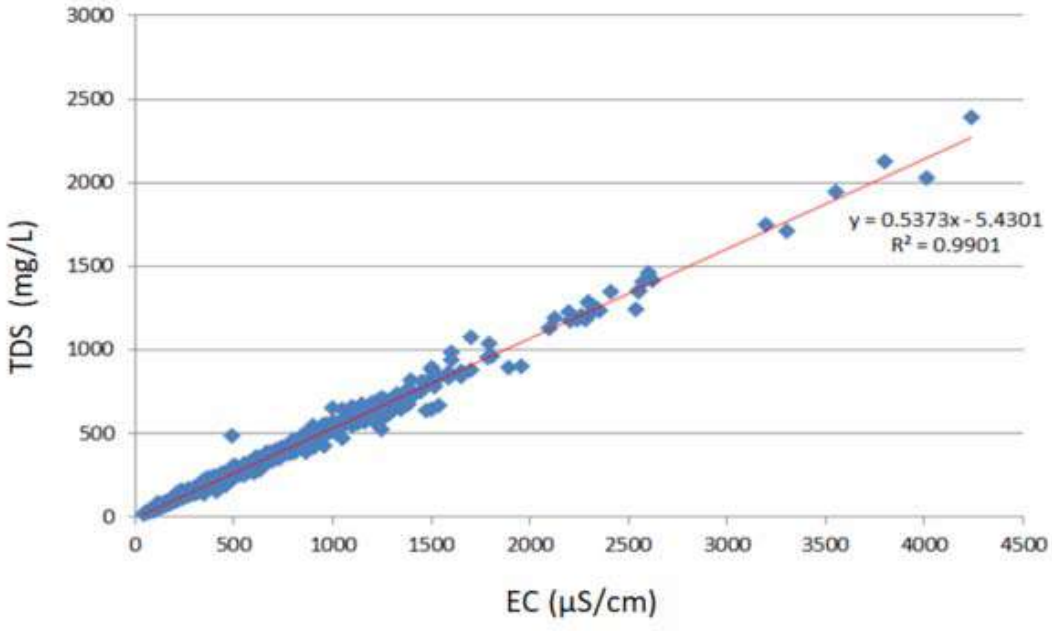

Fig. 2 : Cross plot between EC and TDS

Figure 2 is a cross plot between EC and TDS for all the data points since 2015 which clearly establishes the strong correlation between the two quality parameters. In the year books, several sites with anomalously high TDS and EC have been reported from some districts and these data points can be identified in this cross as the data points having TDS above 1500 mg/L and EC more than 3000 µS/cm.

3.2 Relating EC with Na, Cl, Fl and pH

Cross plots between EC Vs Na and EC Vs Cl revealed that there is a strong positive correlation (Figure 3, a & b). This means that NaCl is the major contributor to increased EC in the groundwater of Odisha. However, it remains to be investigated whether it is the same for just the coastal states or for all states. Influence of F on EC was not established (Figure 3, c) which indicates that salts are not the source of fluoride in ground water. This makes the processes of weathering and erosion of fluoride bearing minerals to be the most likely source of fluoride in the state of Odisha. However, such cross plots for smaller clusters of data confined districts or even blocks need to be extracted for further investigation. It was also found out that EC does not influence pH of groundwater in Odisha (Figure 3, d).

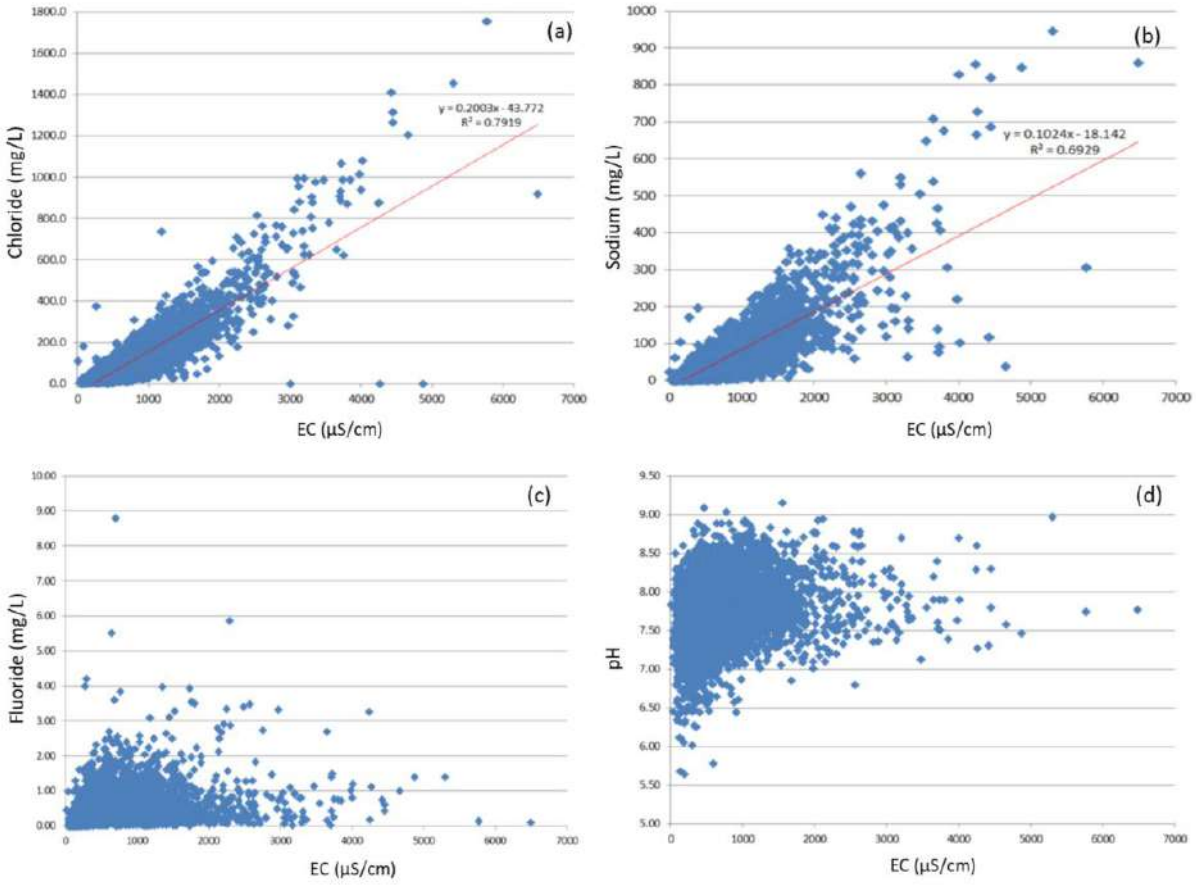

Fig. 3: Cross plots between (a) Chloride and EC, (b) Sodium and EC, (c) Fluoride and EC and (d) pH and EC.

3.3 TDS and EC Trends

Trends of EC and TDS provide a general understanding of the mineral content in groundwater. The trend of TDS and EC for the whole state since 2015 shows an increasing

trend although the rate of increase is different for consecutive years (Figure 4 left). There was a sharp increase in both TDS and EC between 2016-17 and 2017-18 and this is likely due to a reduction in precipitation in this period. A study by Pattanayak et al. (2018) on spatial and temporal variability of rainfall in Khordha district revealed various trends and rainfall patterns. Reduction in precipitation leads to lowering of ground water table and this increased the concentration of dissolved electrolytes. This phenomenon is revealed by water quality measurements during the pre-monsoon and post monsoon periods for the same dug wells.

When TDS and EC data for Khordha (the district belonging to block Bhubaneswar which is the state capital) was studied, it was found that the levels of TDS and EC was much lower in the district (Figure 4 b) as compared to the data for the whole state (Figure 4 c). But, contrary to the trend of TDS and EC for the whole state, Khordha district has displayed a steady increase since 2015. When the data for the block of Bhubaneswar, the most rapidly urbanizing part of the state, was studied, the rise of TDS and EC was steeper since 2018 (Figure 4 c). This steep increase is most likely due to the urban sprawl in the block of Bhubaneswar which needs to be investigated further.

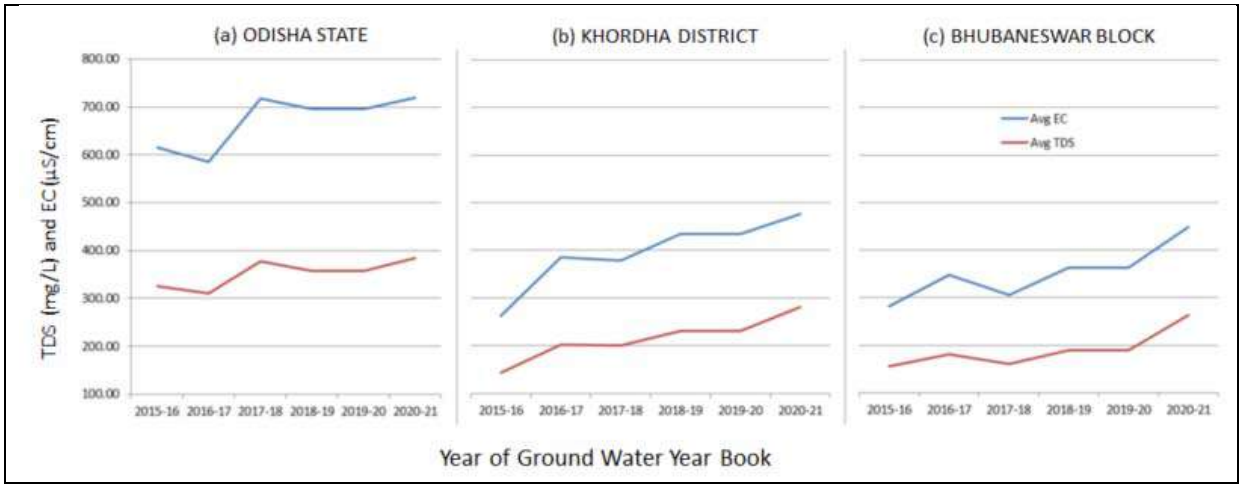

Fig. 4: Trends of TDS and EC for the whole state of Odisha (a), Khordha district (b) and for the block of Bhubaneswar in Khordha district (c)

CONCLUSION

Historical data analysis of groundwater quality is an important means to identify the trends and to establish the inter-relationships between the various ground water parameters. Such analyses identify deterioration of water quality which need to be addressed and corrective measures to be mitigate them. Statistical analyses, which forms the core of data science, has been established as an important tool to detect the relationships and trends, can be performed on any data available for any area for similar studies

In the current study, the trends and relationships of a few ground water quality parameters were studied from which it was clearly identified that the rapidly urbanizing region of Khordha district is witnessing a steep increase in TDS and EC. The reasons for this steep increase could result from urban sprawl, increased vehicular pollution and industrialization.

This calls for an in-depth investigation to establish the influence of urbanization, vehicular pollution and industrialization and to understand the potential pathways of contamination of ground water from the emerging pollution sources.

REFERENCES

Barbecot, F., Marlin, C., Gibert, E., & Dever, L. (2000). Hydrochemical and isotopic characterisation of the Bathonian and Bajocian coastal aquifer of the Caen area (northern France). Applied Geochemistry, 15(6), 791-805.

Belkhiri, L., Boudoukha, A., Mouni, L., & Baouz, T. (2010). Application of multivariate statistical methods and inverse geochemical modeling for characterization of groundwater—A case study: Ain Azel plain (Algeria). Geoderma, 159(3-4), 390-398.

CGWB (2010). Ground water quality in shallow aquifers of India. Ministry of water resources, Government of India.

CGWB (2014). GROUND WATER YEAR BOOK 2013-2014, Ministry of water resources, Government of India., South East Region, Bhubaneswar.

CGWB (2015). GROUND WATER YEAR BOOK 2014-2015, Ministry of water resources, Government of India., South East Region, Bhubaneswar

CGWB (2016). GROUND WATER YEAR BOOK 2015-2016, Ministry of water resources, Government of India., South East Region, Bhubaneswar

CGWB (2017). GROUND WATER YEAR BOOK 2016-2017, Ministry of water resources, Government of India., South East Region, Bhubaneswar

CGWB (2018). GROUND WATER YEAR BOOK 2017-2018, Ministry of water resources, Government of India., South East Region, Bhubaneswar

CGWB (2019). GROUND WATER YEAR BOOK 2018-2019, Ministry of water resources, Government of India., South East Region, Bhubaneswar

CGWB (2020). GROUND WATER YEAR BOOK 2019-2020, Ministry of water resources, Government of India., South East Region, Bhubaneswar

CGWB (2021). GROUND WATER YEAR BOOK 2020-2021, Ministry of water resources, Government of India., South East Region, Bhubaneswar

CGWB (2022). GROUND WATER YEAR BOOK 2021-2022, Ministry of water resources, Government of India., South East Region, Bhubaneswar

Chaudhuri, S., & Roy, M. (2017). Drinking water sources in India: how safe is safe? Current Science, 393-402.

Pattanayak, S., Rath, B. S., Pasupalak, S., Baliarsingh, A., Mohapatra, A. K. B., Nanda, A., & Panigrahi, G. S. (2018). Spatial and temporal variability of rainfall in Khordha district of Odisha. The Pharma Innovation Journal, 7(10),716-722.

VISTAS IN GEOLOGICAL RESEARCH
Special Publication in Geology (18), March 2023, pp. 77-86

Petrophysical Analysis – A Tool for Evaluation of Hydrocarbon Potential: A Case Study from Tipam Formation, Upper Assam Basin, India

SUMANI DAS AND DURGA SHANKAR PATTANAIK

Department of Geology, Utkal University, Bhubaneswar

Abstract: The Miocene to Early Pliocene 500m thick four interesting zones, namely (TS-40, TS-2, TS-3, TS-4) in upper Assam is identified on logs at depths of 3400m to 3900m. Although it is in the vicinity of existing producing oil and gas fields, detailed depositional environment studies and petrophysical analysis were carried out to understand the heterogeneity nature of the Tipam reservoirs. The study area which is in close proximity to Naga Thrust has undergone multiple stages of tectonic subsidence and sedimentation influenced by the movements of Indian, Eurasian and Burmese plates. Tipam fluvial sandstone was deposited under variable energy conditions in the peripheral foreland basin. Three distinct facies types, i.e., prograding sandy facies in the bottom (TS-4), followed by aggrading thick sandy facies with minor shale bands in the middle (TS-2 and TS-3) and finally retrograding sand-shale sequence at the top (Girujan and TS-40) were identified. Advanced petrophysical study has been carried out by qualitative and quantitative analysis. The Gamma ray and Neutron-Density log is used to determine the lithology, depositional environment and calculation of volume of shale present in the sand reservoir. With the help of Gamma ray signatures, side wall core and drill-cutting descriptions, the Tipam sands are classified into different depositional facies. The interesting zones represent resistivity of 13-17 Ω-m in TS-40, 15-35 Ω-m in TS-2, TS-3 and 14-20 Ω-m in TS-4, Resistivity of water 0.47Ω-m (tested). Effective porosity is 10-20% and permeability is moderate to low. The low permeability streaks in the reservoir packs may be attributed to the dispersed clay present within the sands.

Key words: Petrophysical analysis, Hydrocarbon potential, Tipam Formation

INTRODUCTION

The study area is in the northern most part of Assam Shelf in Assam-Arakan Basin (**Fig. 1**). It is bounded in the North by Eastern Himalayas, in the NE by Mishmi Hills, in the South by the Naga-Patkai hills and in the SW by Mikir hills and Shillong Plateau. Major fields in the upper Assam Shelf are Nahorkatiya, Tengakhat, Moran, Lakwa, Rudrasagar, Geleki etc. The area has undergone multiple stages of tectonic subsidence and sedimentation influenced by the movements of Indian, Eurasian and Burmese plates.

A total of 3 wells (Well-1, 2 & 3) (Fig. **2**) were drilled and encountered multiple oil/gas/condensate bearing zones in Tipam Group (Miocene age). The area is surrounded by several discovered oil and gas fields e.g., Digboi, Dumduma and Nahorkatiya. There is possible upside in deeper zones in the field as one well showed indications of oil in

Surma/Tipam Group (Miocene age). The well-1 was drilled in the seismic high of Dumduma, primarily to explore the Tipam hydrocarbon prospects and discovered gas and condensate in the 3,565 m Tipam T-40 sand. Surma sands were also tested in this well, but it flowed water with only minor traces of oil. The T-40 sand produced gas at a rate of 1.465 MMSCF/day and condensate at a rate of 125.8 BOPD.

Based on the result of well-1, well-2 was drilled in the vicinity and Barail Main Sand (BMS) and Tipam sands were tested. On testing, BMS flowed formation water while Tipam sands produced water with minor traces of oil of 35.8°API.

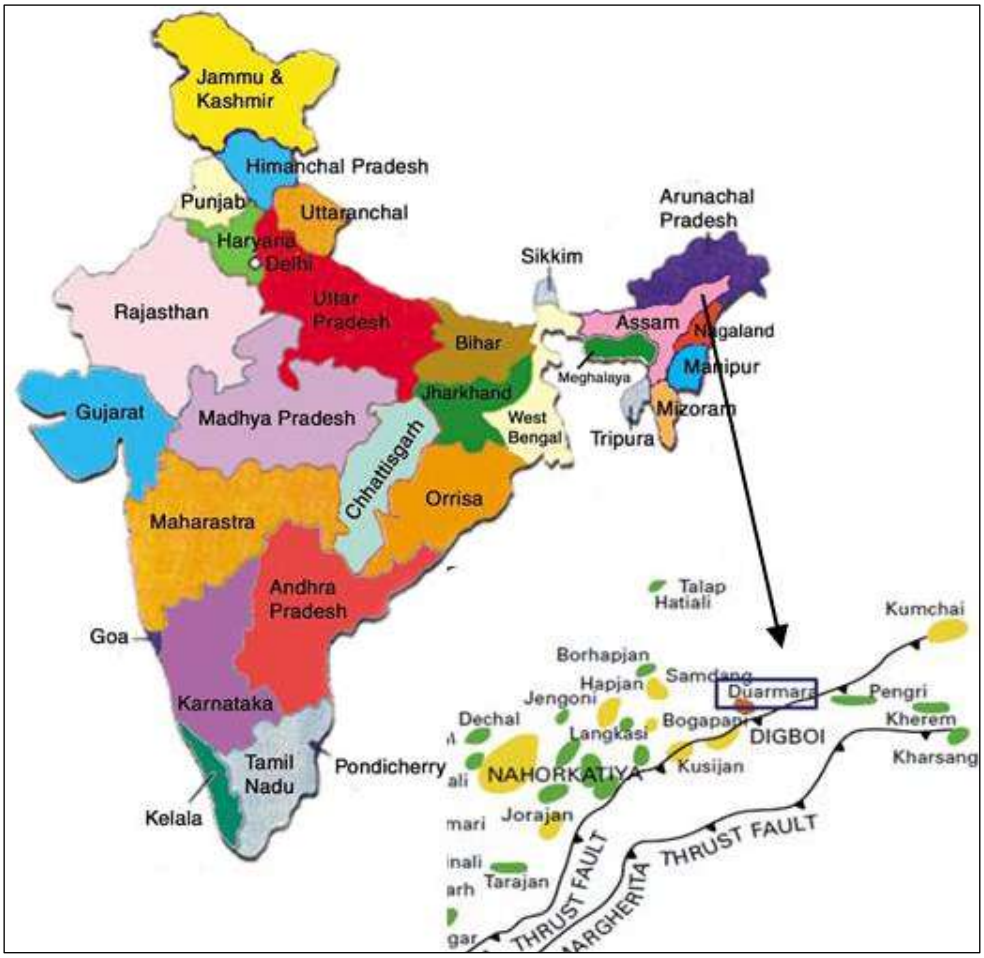

Fig. 1: Location map of the study area.

Generalised Stratigraphy

The stratigraphic record of the Assam Shelf is controlled by three variables: eustasy, tectonic subsidence and sediment supply. The sediment supply feeds the foreland basin either from NW side of Himalayan mountains or from SE side of overriding thrust belt. The basin is a Tertiary basin containing sediments from Palaeocene to Recent (Fig. **3**).

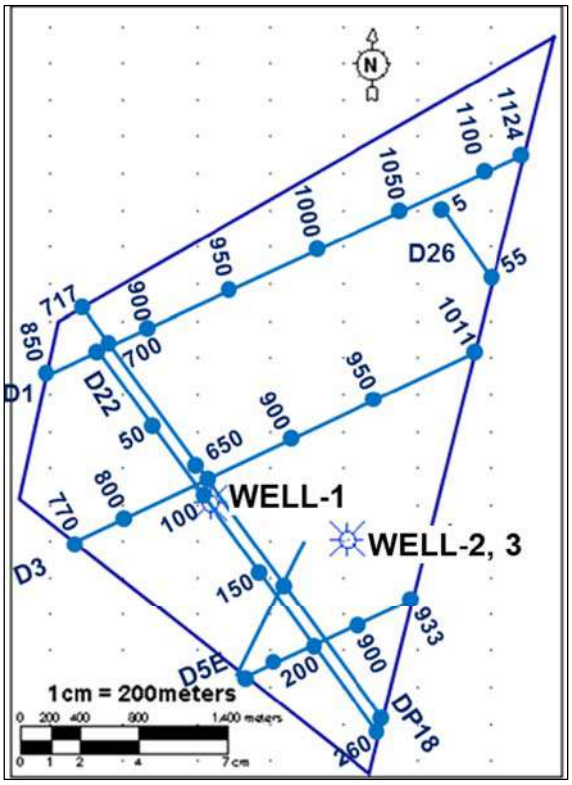

Fig. 2: Base map of the study area with 3 wells.

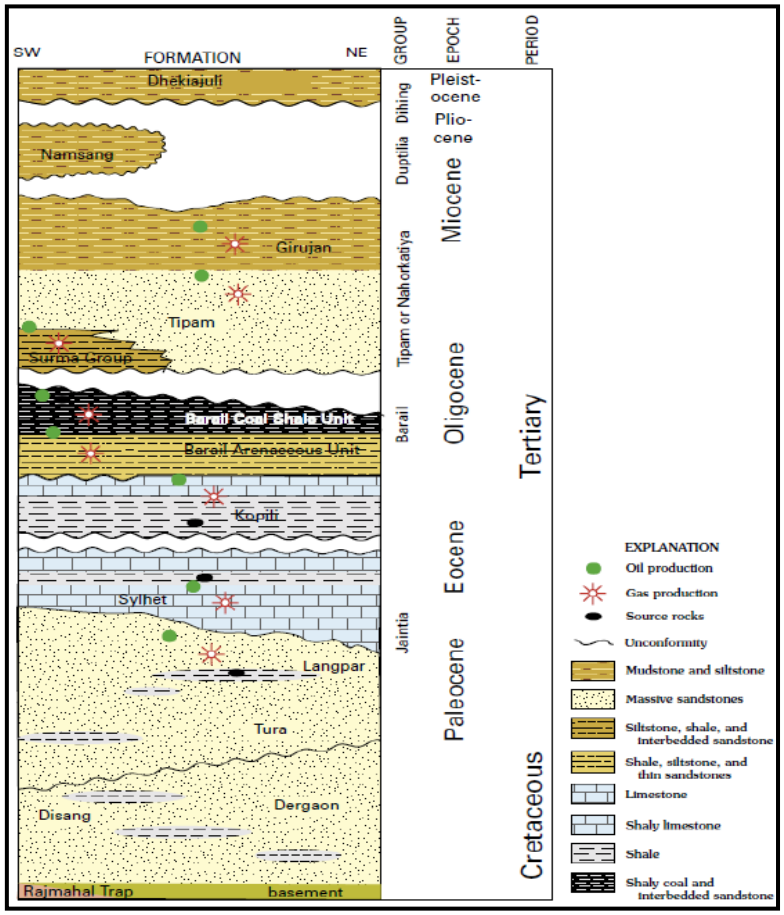

Fig. 3: Generalised Stratigraphy of the study area.

Tertiary sediments lie non-conformably over basement. Tertiary sedimentation in the area began because of transgression when Basal Sandstone was deposited in paralic – marine environment. As a result of gradual submergence of basin and minor supply of terrigenous clastics, Sylhet Limestone in the form of fossiliferous carbonates was deposited in shallow open marine condition. Regression began by the end of Middle Eocene when Kopili Formation was deposited and is characterized dominantly by argillaceous clastics and continued up to Upper Eocene period (Ishwar et. al 2013).

Due to differential adjustment in the basin during Upper Eocene – Oligocene, further regressive phase advanced in the area when fine grained sand and shale alternations gave way to lagoonal coal-shale alternations of Barail Group. After deposition of Rudrasagar Formation there was a prominent eustatic fall in the Lower Miocene due to which the younger units of Barail Group are eroded to form an unconformity surface.

In the shelf area, a major hiatus is observed after deposition of the Barails because of block adjustment in the Assam basin. Hiatus continued till the end of Lower Miocene. During Upper Miocene–Lower Pliocene, Tipam Group was deposited under high energy conditions as interlaced braided channel deposits when the shelf area was tilted because of upliftment in the Arakan-Chin axial belt. A major transgression over the entire basin led to deposition of the Girujan Clay. Lacustrine to fluvial deposits of Namsang and Dhekiajuli Formations continued being deposited because of episodic tectono-sedimentary events related to plate movement during post Tipam age.

Methodology for Petrophysical Analysis

A thorough understanding of the subsurface is made possible by geophysical logging, which provides a chance to ascertain the composition, variability, and petrophysical characteristics of the rocks near the borewell . The raw data was in LAS file format and well top in notepad file format. The following suit of well logs were processed using the computer application Decision Space Petrophysics software (**Table 1**) for well No- 1, 2 & 3:

Table 1: Wireline Logs available in well-1, 2 & 3.

LOGS	WELL-1	WELL-2	WELL-3
Caliper	1164- 4249	4001- 4469	3390- 3949
SP	1164- 4248	3382- 4469	2325- 3954
GR	-	1450- 4432	3390- 3949
RXO	2133- 4261	-	2325- 3954
RT	2133- 4261	-	2325- 3954
LLD	-	3382- 4469	-
LLS	-	3382- 4469	-
RHOB	-	4000- 4434	3390- 3949
NPHI	-	4000- 4434	3390- 3949
DT	121- 4248	135- 4419	-

The logs were processed to remove any ambiguities and to make them reliable for interpretation and estimation of petrophysical parameters. The log data were conditioned over bad hole sections. Missing P-wave Sonic and Density logs were synthesized. During the raw log processing Multi-linear Regression, Normalisation, Depth Matching and Quality Control (QC) of conditioned logs steps were carried out. Post processing of logs include estimation of V_{shale} using Gamma Ray (GR), Neutron and Neutron-Density logs. Total Porosity was calculated for the wells using Neutron and Density logs. Water saturation was estimated from the processed Resistivity and Porosity logs using Picket Cross-plot method.

RESULTS AND DISCUSSIONS

Bivariate analysis of well logs such as Resistivity vs GR and RHOB vs NPHI shows some outliers present in the data (Fig. **4**), which are removed in the conditioned log to optimise the result. As GR and Neutron-Density logs were either over-estimating or under-estimating the sand volumes in the reservoirs (possibly due to the presence of hot sands), final V_{shale} values were taken from Neutron logs. On the other hand, V_{shale} for well-1 was estimated from resistivity logs due to unavailability of GR, Neutron and Density logs for the well.

The Girujan thickness is seen to be gradually increasing from west to east towards the study area. In Tipam Group, thickness is almost uniform from west to east. The Tipam-30 is shaly across the region. Development of Basal Sandstone is seen all along the southern and south-eastern part of the basin. The development of this facies towards the south and south-eastern part near and below the thrust belt areas may be of significance as it might develop as another possible play in unexplored areas (this is already a producing reservoir in Jorajan area). The limit of this facies, however, is possibly controlled by bounding faults of Jorajan, Kusijan and Duarmara structures towards north and north-west. The Eocene sequence is more or less of similar thickness with gradual dipping towards east (Fig. **5**).

The formation lithology in the well is interpreted using the natural gamma ray, which is used for differentiating between clean sands formations and shale formations. The more impermeable zones show shale intervals with a high value of the concentration of clay minerals which decrease the permeability and effective porosity. Permeable zones are expected to be one of the leading mineralogies (sandstone/limestone/dolomite), but in this research, sandstones are the only leading mineralogy in permeable portion (Mahbaz 2011; Olurotimi 2013).

Estimation of V_{shale} for well-2 and 3 was attempted using GR, Neutron and Neutron-Density logs. As GR and Neutron-Density logs were either over-estimating or under-estimating the sand volumes in the reservoirs (possibly due to the presence of hot sands), final V_{shale} values were taken from Neutron logs. On the other hand, V_{shale} for well DMR-1 was estimated from resistivity logs due to unavailability of GR, Neutron and Density logs for the well (Fig. **6**).

Vshale ≤ 20%: Clean Sand; 20% <Vshale< 40%:Silty Sand; Vshale≥ 40%: Shale

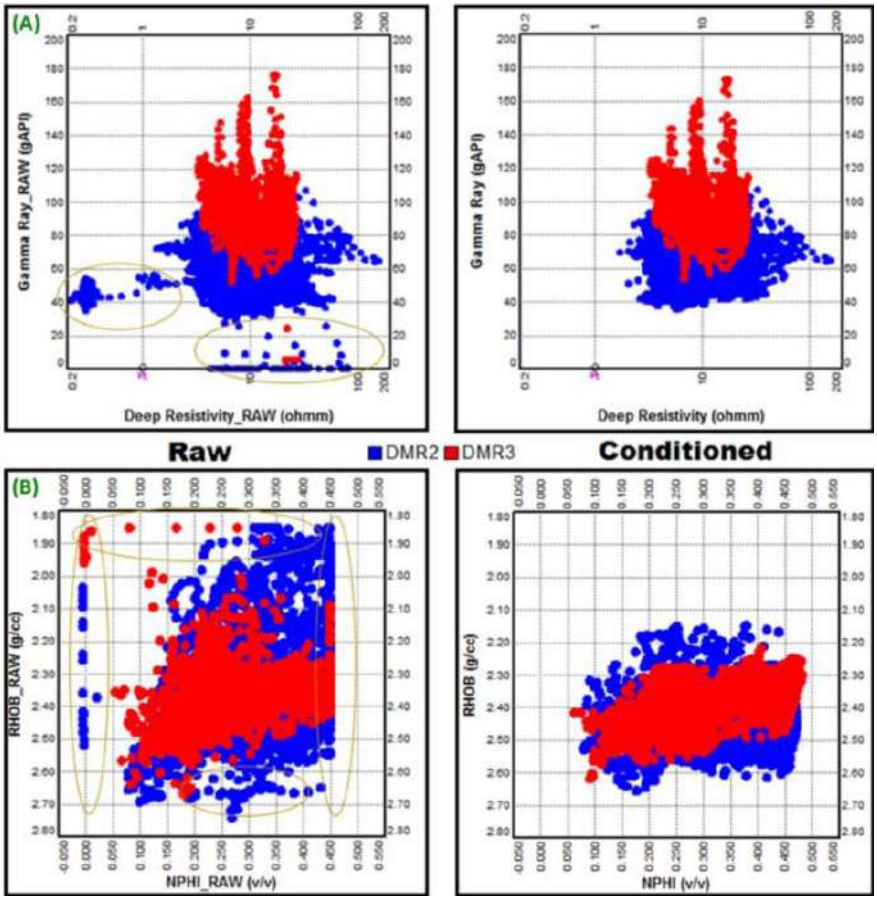

Fig. 4: Conditioning of the well logs.

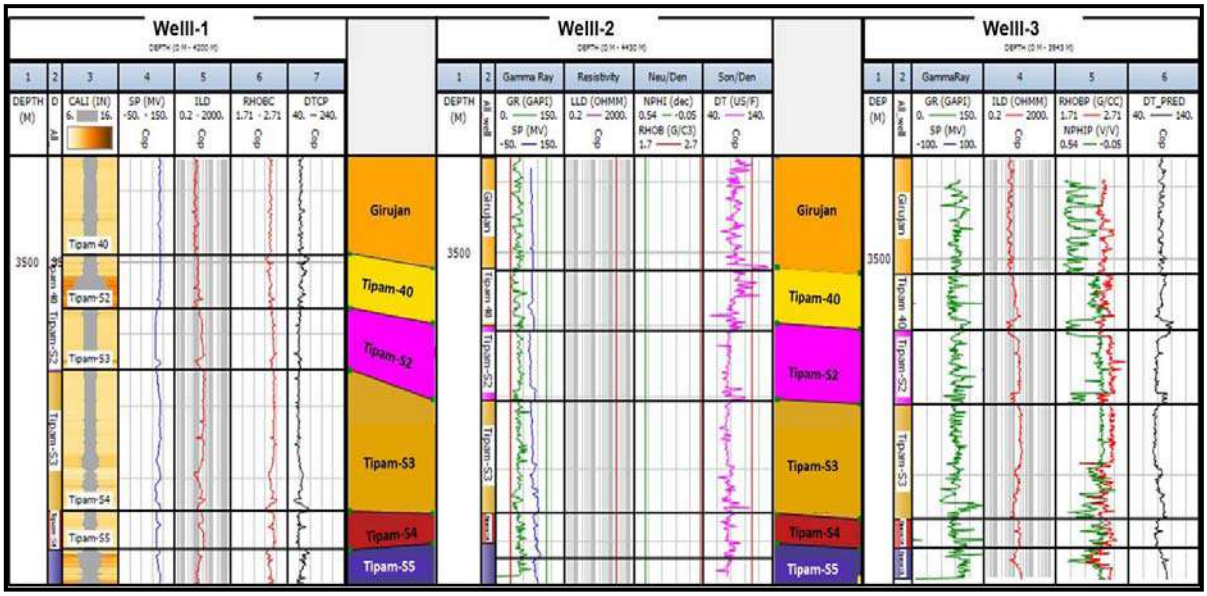

Fig. 5: Well log correlation for wells 1, 2 & 3.

Total Porosity was calculated for the wells using Neutron and Density logs. It was further calibrated with core data; the calibration resulted in good correlation between log and core data. Effective Porosity was estimated using the relation:

$PHIE = PHIT - V_{shale} * PHIT\_SH$

Where PHIE: Effective Porosity & PHIT: Total Porosity

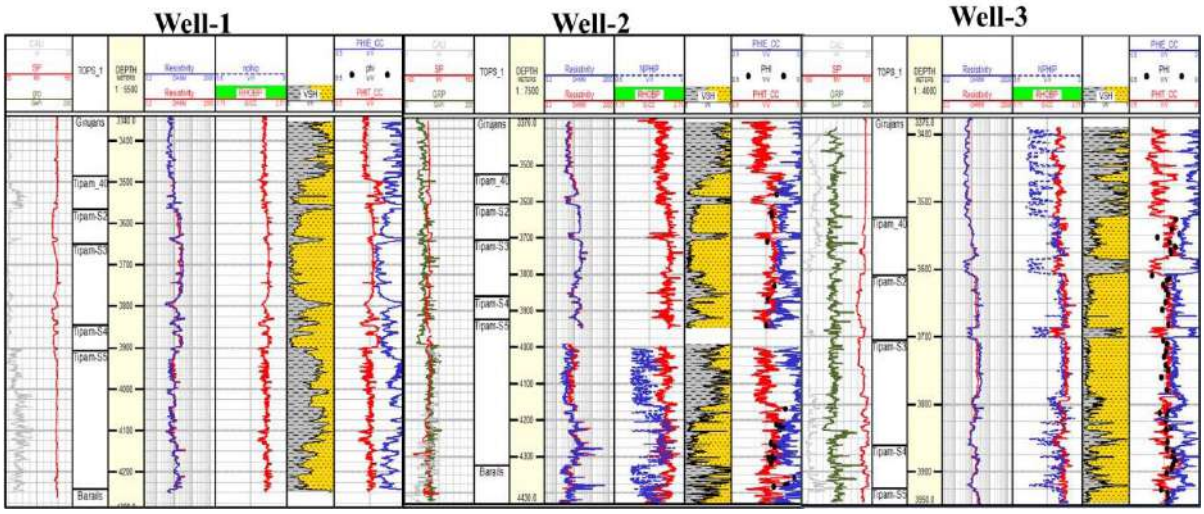

Fig. 6: Estimation of Vshale and Porosity.

The log and core data have shown a good match with the resulted porosity from deterministic approach. Water saturation was estimated from the processed Resistivity and Porosity logs using Picket Cross-plot (**Fig. 7**) and the following parameters:

Water Salinity = 4700 ppm and Temperature = 190 °F at 3967 m

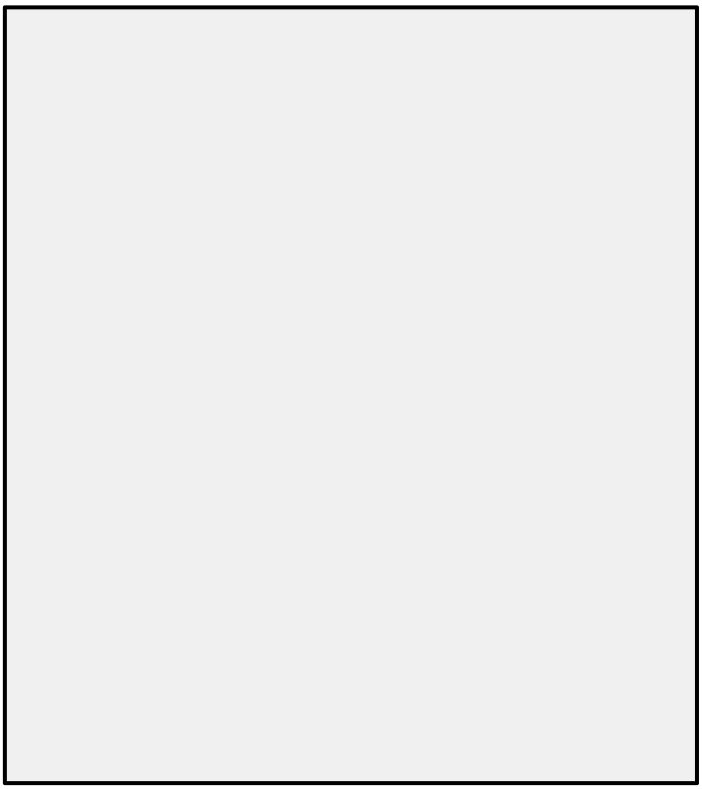

Fig. 7: Picket plot (Resistivity-Porosity Cross-plot)

From the cross-plot, it was estimated that Rw = 0.47 Ω-m and Archie's parameter 'm' = 1.5. The HC pay zones identified using the processed logs and calculated effective porosity, Vshale and water saturation.

Permeability was estimated using core data (porosity and permeability) from Tipam sands (Fig. **8**).

F = 1/(PHIe^1.5) and PERMf = (7.0*(10^6))/(F^4.5)

Where, F = Formation Factor (fractional)

PHIe = Effective porosity (fractional)

PERMf = calculated permeability (md)

PE – perm equation from analogue

PF- perm from formation factor

KH is in md-m

Formation Factor used to derive permeability based on log derived effective porosity

Quantitative evaluation for petrophysical characteristics, such as, effective porosity, facies, net to gross, permeability and fluid types were carried out to identify the prospectivity and upside potentials in the existing wells (Fig. **9**). Petrophysical properties for the delineated reservoir sand units have the porosity ranges from 15 to 20% and hydrocarbon saturation ranges from 60 to 80%. It favours for the significant amount of hydrocarbon presence in the reservoir.

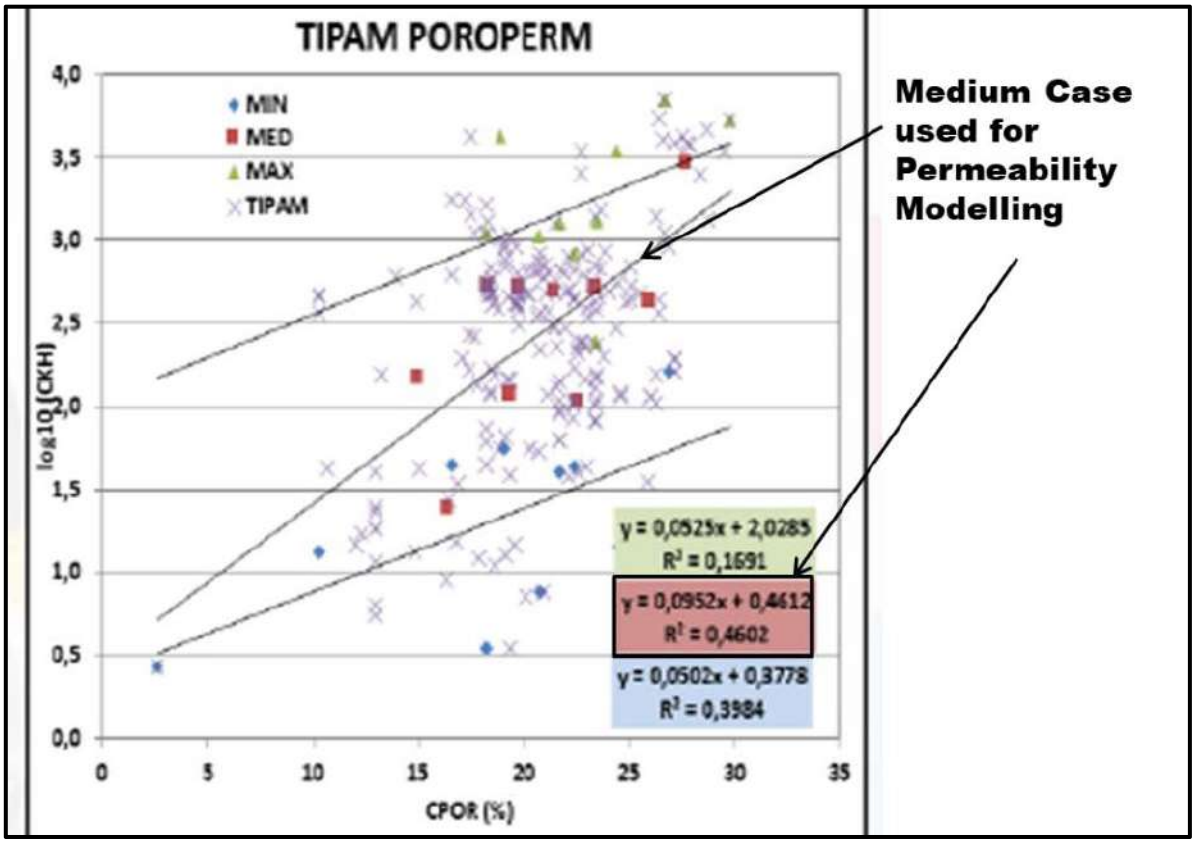

Fig. 8: Permeability modelling.

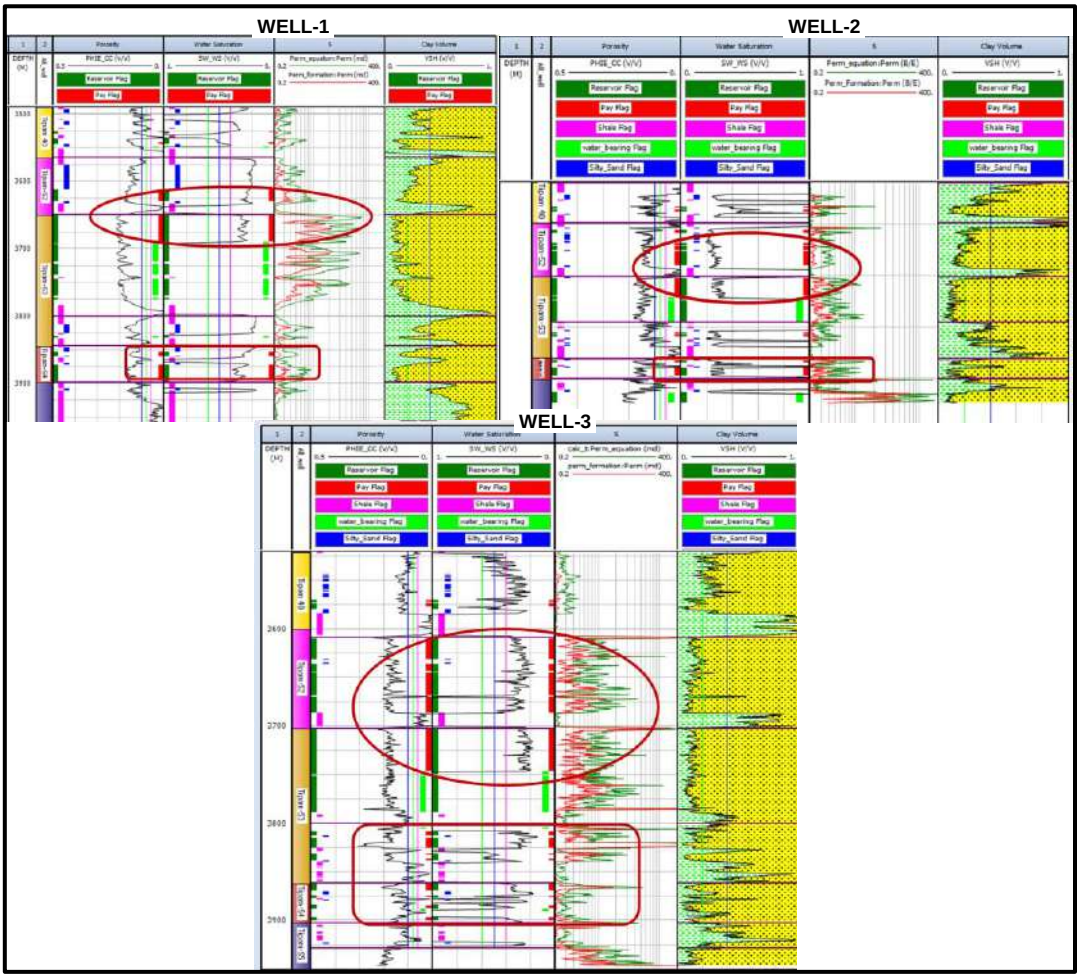

Fig. 9: Hydrocarbon potential zones in wells 1, 2 & 3.

CONCLUSIONS

On the basis of petrophysical analysis Tipam Group was divided into 6 zones viz. TS-40 gas, TS-2 gas, TS-3 gas, TS-3 oil, TS-4 oil and TS-5 oil. Logs recorded in the bad hole sections were corrected to optimise the results. For well-2 and 3 final V_{shale} values were taken from Neutron logs, possibly due to the presence of hot sands. On the other hand, V_{shale} for well DMR-1 was estimated from resistivity logs due to unavailability of GR, Neutron and Density logs. Further, V_{shale} was used to define the clean sand, silty sand and shale facies.

Based on the GR log responses in the wells, three major depositional patterns were recognised such as coarsening Upwards (shale to sand facies), blocky sands with good reservoir properties and thin, laminated sand-shale alternations. These patterns were used to infer the reservoir quality prior to determining the net reservoir pay zones. Water saturation was estimated from the processed Resistivity and Porosity logs using Picket Cross-plot, water salinity was considered as 4700ppm and temperature as 190 °F at 3967 m.

For the Tipam section (all 6 sands) in well-1, 2 & 3 permeability ranges from 6 to 80 md, 5 to 40md and 15-70 md respectively. Finally, lithology classification, net pay delineation and fluid contacts were marked in all the 6 reservoir levels in the Tipam level.

REFERENCES

Bhuyan, D., Borgohain, P. and Bezbaruah, D., 2022. Diagenesis and reservoir quality of Oligocene Barail Group of Upper Assam Shelf, Assam and Assam Arakan basin, India. *Journal of Asian Earth Sciences: X*, *7*, p.100100.

Gogoi, T. and Chatterjee, R., 2019. Estimation of petrophysical parameters using seismic inversion and neural network modelling in Upper Assam basin, India. *Geoscience Frontiers*, *10*(3), pp.1113-1124.

Ishwar, N.B. and Bhardwaj, A., 2013. Petrophysical well log analysis for hydrocarbon exploration in parts of Assam Arakan Basin, India. In *10th Biennial international conference and exposition, society of exploration geophysicists, Kochi, India* (Vol. 153).

Kumar, P., Solomon, R., Varun, T.R. and Samanta, A., 2009. An integrated approach to solve reverse resistivity contrast problem in fresh water shaly sand reservoir of Changmaigaon field. In *Assam India–A case Ssudy. 2nd SPWLA-India Symposium, November* (pp. 19-20).

Mahbaz, S., Sardar, H., Namjouyan, M. and Mirzaahmadian, Y., 2011. Optimization of reservoir cut-off parameters: a case study in SW Iran.

Rai, K., Yadav, L. and Haldiya, B.S., 2006. Validation of Shaly Sand Model using Electrical Core Measurements in Low Resistive Reservoirs of Upper Assam, India. In *6th International Conference & Exposisition on Petroleum Geophysics, Kolkata*.

Saikia, G. and Borgohain, P., Petrography and sandstone chemistry of oil bearing tipam sandstone formation in parts of Upper Assam shelf. *Journal of Earth Science*, pp.95-105.

VISTAS IN GEOLOGICAL RESEARCH
Special Publication in Geology (19), March 2023, pp. 88-91

Impact of Dem Correction on the Measures of Errors

KUMARI PREETY*, ANUP K. PRASAD AND ATUL K. VARMA

Photogeology and Image Processing Laboratory, Department of Applied Geology, Indian Institute of Technology (Indian School of Mines), Dhanbad 826004, India;

E-mail: preetygeol@gmail.com*; anup@iitism.ac.in; atul@iitism.ac.in

Abstract: Digital Elevation Models (DEM) are the fundamental data resources for many geoscience applications. Any geoscientific project's success, where DEMs are the basic input data, depends on the reliability and accuracy of these data sets in terms of vertical accuracy. DEM contains errors from a variety of sources such as steps of methodology, input data and tech-niques used in creation of DEM etc. The errors existing in DEMs can be reduced by various means. The algorithms derived from linear-regression can be used to reduce the vertical error. This paper presents the impact of linear-regression based correction applied to open source DEMs to reduce the error and enhance the vertical accuracy on the measures of error and bias.

Keywords: DEM, Vertical Accuracy, DGPS, Correction Error Bias

INTRODUCTION

Many geoscience applications require Digital Elevation models (DEM) as the prime input data such as geological, and hydrological mapping and modelling etc (Das & Lindenschmidt, 2021; Hsu et al., 2016; Jafarzadegan & Merwade, 2017; Li et al., 2020; Saksena & Merwade, 2015; Tsimi & Ganas, 2015; Wang et al., 2012). This paper presents the impact of linear-regression based DEM (Preety et al., 2022) correction on measures of error in terms of vertical accuracy.

STUDY AREA AND DATA

This study's geographical focus is the IIT(ISM) campus and adjacent areas with mostly flat hard rock topography (Preety et al., 2022). Six Digital Elevation Models with varying grid resolutions and freely accessible from various national and international web portals; ASTER GDEM v3, CartoSAT DEM v3R1, SRTM v3 each with 30 m and SRTM v4.1, TanDEM-X and MERIT DEM each with 90 m grid spacing were taken for the analysis.

METHODOLOGY

To achieve the goal of this study ground-observation data at 145 ground locations ie. ground control points (GCPs) and space-based DEMs from various web-portals for this area were collected. A ground survey was conducted using survey-grade GPS equipment; Leica CS14/GS15 DGPS (Differential Global Positioning System) system. In the GIS environment and using online libraries, processing of DEMs to make uniform projection and datum for

Impact of Dem Correction on the Measures of Errors

REFERENCES

Das, A., & Lindenschmidt, K.-E. (2021). Evaluation of the sensitivity of hydraulic model parameters, boundary conditions and digital elevation models on ice-jam flood delineation. *Cold Regions Science and Technology*, *183*, 103218. https://doi.org/10.1016/j.coldregions.2020.103218

Hsu, Y.-C., Prinsen, G., Bouaziz, L., Lin, Y.-J., & Dahm, R. (2016). An Investigation of DEM Resolution Influence on Flood Inundation Simulation. *Procedia Engineering*, *154*, 826–834. https://doi.org/10.1016/j.proeng.2016.07.435

Jafarzadegan, K., & Merwade, V. (2017). A DEM-based approach for large-scale floodplain mapping in ungauged watersheds. *Journal of Hydrology*, *550*, 650–662. https://doi.org/10.1016/j.jhydrol.2017.04.053

Li, J., Zhao, Y., Bates, P., Neal, J., Tooth, S., Hawker, L., & Maffei, C. (2020). Digital Elevation Models for topographic characterisation and flood flow modelling along low-gradient, terminal dryland rivers: A comparison of spaceborne datasets for the Río Colorado, Bolivia. *Journal of Hydrology*, *591*, 125617. https://doi.org/10.1016/j.jhydrol.2020.125617

Preety, K., Prasad, A. K., Varma, A. K., & El-Askary, H. (2022). Accuracy Assessment, Comparative Performance, and Enhancement of Public Domain Digital Elevation Models (ASTER 30 m, SRTM 30 m, CARTOSAT 30 m, SRTM 90 m, MERIT 90 m, and TanDEM-X 90 m) Using DGPS. *Remote Sensing*, *14*(6), 1334. https://doi.org/10.3390/rs14061334

Saksena, S., & Merwade, V. (2015). Incorporating the effect of DEM resolution and accuracy for improved flood inundation mapping. *Journal of Hydrology*, *530*, 180–194. https://doi.org/10.1016/j.jhydrol.2015.09.069

Tsimi, C., & Ganas, A. (2015). Using the ASTER global DEM to derive empirical relationships among triangular facet slope, facet height and slip rates along active normal faults. *Geomorphology*, *234*, 171–181. https://doi.org/10.1016/j.geomorph.2015.01.018

Wang, W., Yang, X., & Yao, T. (2012). Evaluation of ASTER GDEM and SRTM and their suitability in hydraulic modelling of a glacial lake outburst flood in southeast Tibet. *Hydrological Processes*, *26*(2), Article 2.

VISTAS IN GEOLOGICAL RESEARCH
Special Publication in Geology (19), March 2023, pp. 92-105

Land Use/Land Cover Change and its Impact on Land Surface Temperature: A Case Study of Bhubaneswar City, Odisha, India

[1]DEBABRATA NANDI*, [1]SUBHASMITA DAS,[1]HIMANI MISHRA,[1]CHINMAY KU. SAHOO, [1]SIDDHARTHA SAHOO AND [1]JYOTIPUSPA PUTHAL

[1] Department of Remote Sensing and GIS, MSCB University, Baripada, Mayurbhanj, Odisha,India, 757003
*Corresponding Author Email:debabrata.gis@gmail.com

Abstract: Urbanization produces substantial land use changes by causing the construction of different urban infrastructures in the city region for habitation, transportation, industry, and other reasons. As a result, it has a significant impact on Land Surface Temperature (LST) by disrupting the surface energy balance. The objective of this paper is to assess the impact of land-use/land-cover (LU/LC) dynamics on urban land surface temperature (LST) of Bhubaneswar City in Eastern India during years (2016–2021) using Landsat data (TM, ETM , and OLI/TIRS) . The finding reveals that the mean LST over the entire study domain grows significantly between 2016 and, 2021due to urbanization (b coefficient 0.07, and 0.06 in 2016-2021, and loss of green space (b coefficient - 0.125 and - 0.065 in 2016 and 2021. The highest class recorded for agricultural land (49.60 $km^{2,}$ accounting for 33.94% of the total land area), followed by vegetation (41.27 km^2, 28.19% of the total land area), and built-up land (27.59 km^2, 18.84% of the total land area). The sharp decline of vegetation cover continued until 2021 due to increasing built-up areas. Built-up land (62.60 km^2, accounting for 42.76% of the total land area, an increase of 35.01 km^2) as the highest class followed by water bodies (21.57%, 32.60 km^2 of the land area), and agricultural land (31.57 km^2, 21.57% of the land area) in 2021. Remote sensing techniques proved to be an important tool to urban planners and policymakers to take adequate steps to promote sustainable development and minimize urbanization influence on LST. Urban green space (UGS) can help improve the overall liveability and environmental sustainability of Bhubaneswar city.

Keywords: RS&GIS, LULC, NDVI, NDLI, NDBI, LST.

INTRODUCTION

Land surface temperature (LST) is one of the major components in the physical processes of surface energy balance as well as water balance at both local and global scales (Imran et al., 2021; Hussain & Karuppannan 2021; Imran et al.,2019; Hereher 2017; Karakuş 2019;). Land surface data extracted from the satellite thermal infrared (TIR) imagery is a vital data as it is mainly employed for modelling the surface energy fluxes, measuring urban heat island (UHI) effect (Kustas & Anderson, 2009; Feizizadeh & Blaschke, 2012; Sekertekin & Bonafoni, 2020; Naughton & McDonald,2019). The land surface temperature (LST) is the temperature of the earth's surface (Liu et al.,2020; Barkhordarian et al., 2019; Mutiibwa et al.,2015; Ghouri, 2022) The LST varies with Land Use Land Cover (LULC) type. It is a result of the

energy and water balance of the earth's surface at the global and regional levels. It gives information about the surface energy changes with time. This is an important parameter for monitoring vegetation, global warming and changes in built-up area (Yeh & Li, 1997; WENG, 2001). Currently, the LST is a significant environmental issue. The temperature is increasing across the world daily because of the greenhouse gas effect and the ozone hole etc. The first remotely sensed thermal images were obtained in 1960 from the NOAA satellite TIROS II with a very low resolution. In 1984, NASA launched the first operational satellite mission with a thermal camera (Landsat 4 TM), which covered the 10.5–12.5 μm spectrum with a resolution of 60–120 m. In 2013, NASA launched Landsat 8, with an enhanced thermal infrared (TIRS) camera. This had two bands (bands 10 and 11), covering the thermal spectrum (10.6–12.5 μm). Atmospheric correction was carried out using the split-window technique. Landsat is still the only mission with more than 30 years of archived imagery, including thermal infrared imagery. Kustas & Anderson, 2009 utilized thermal infrared remote sensing to model land surfaces. Heat islands are formed in the air above urban areas due to the heat absorbed and discharged by buildings, concrete structures and other impervious surfaces, which act as inactive vaults. It plays a key role in the physics of the land surface processes. The LST and vegetation are strongly related. Temperature–vegetation plots reveal the chronological trajectory of pixels from low temperature– high-vegetation conditions to high temperature–low vegetation conditions (Amiri et al. 2009). A study carried out in an urban area showed that an increase in the built-up area was accompanied by a decrease in vegetation, resulting in urban microclimatic changes. Both the LST and surface imperviousness (SI) can be derived from satellite imagery. The temperatures of non-urban areas are lower than those of urban areas. In this study, we attempted to calculate changes in the LST using thermal remote sensing and GIS. As we all know, the use of remote sensing and GIS is a powerful technique for acquiring temporal and spatial information within a narrow time span. This methodology allows to detect LULC change. Two major urban patches and a suburban-rural area were studied. The primary objectives of this study were (1) to extract and calculate the LST of the present study area during three timespans and (2) to analyse the LULC changes in relation to the changes in the LST.

This study begins with an overview of increased urbanisation and LULC Change in the context of the world. This follows the description of the location of the study area and the methods employed for the study. The significant objective of this research paper is-Land use Land cover change over the period of pre and post developments as a Smart city. Determine the Dynamic changes of urban sprawl in Bhubaneswar City. Land Surface Temperature change over the period of 2016-2021.

STUDY AREA

The study area is located in Bhubaneswar city, the capital of Odisha, in the eastern part of India. Bhubaneswar with a total area of 146.39km^2 and a population of 881988 extends from $20^0$12'N to $20^0$25'N latitudes and $85^0$44'E to $85^0$55'E longitudes. The study area is undergoing at the accelerated growth rate in one of Eastern India's agglomeration, economic development, and urban expansion. Bhubaneswar has a tropical Savana climate according to

the koppen climate classification. The annual mean temperature is 27.4^0c monthly mean temperature are 22 to 32^0 C. Summers are hot and humid with the low temperature of 30^0C and the high temperature often touches 40^0C. May is the hottest month, when daily temperature range form 32-42^0C. January is the coldest month has temperature varying from15-28^0C.

MATERIAL AND METHODS

In our present study, both the primary and secondary data were collected from various sources. The primary data like the topographical sheets of 1:50,000 scale and cloud free multispectral Landsat satellite imagery data of three dates available in the past three decades for the related region were collected from Survey of India (SOI) and earth explorer (USGS) respectively. The Table-1 shows the sources of collected satellite imagery data. Here, true colour Google satellite image of study area, 73 H/15 And 73H/16 topographical sheets from Survey of India and different time municipal boundary map of the study area from Bhubaneswar municipal office are also collected. The secondary data were collected including the demographic information from the primary census data of the study area for 2016 & 2021, from the Directorate of Census Bureau (Census of India).

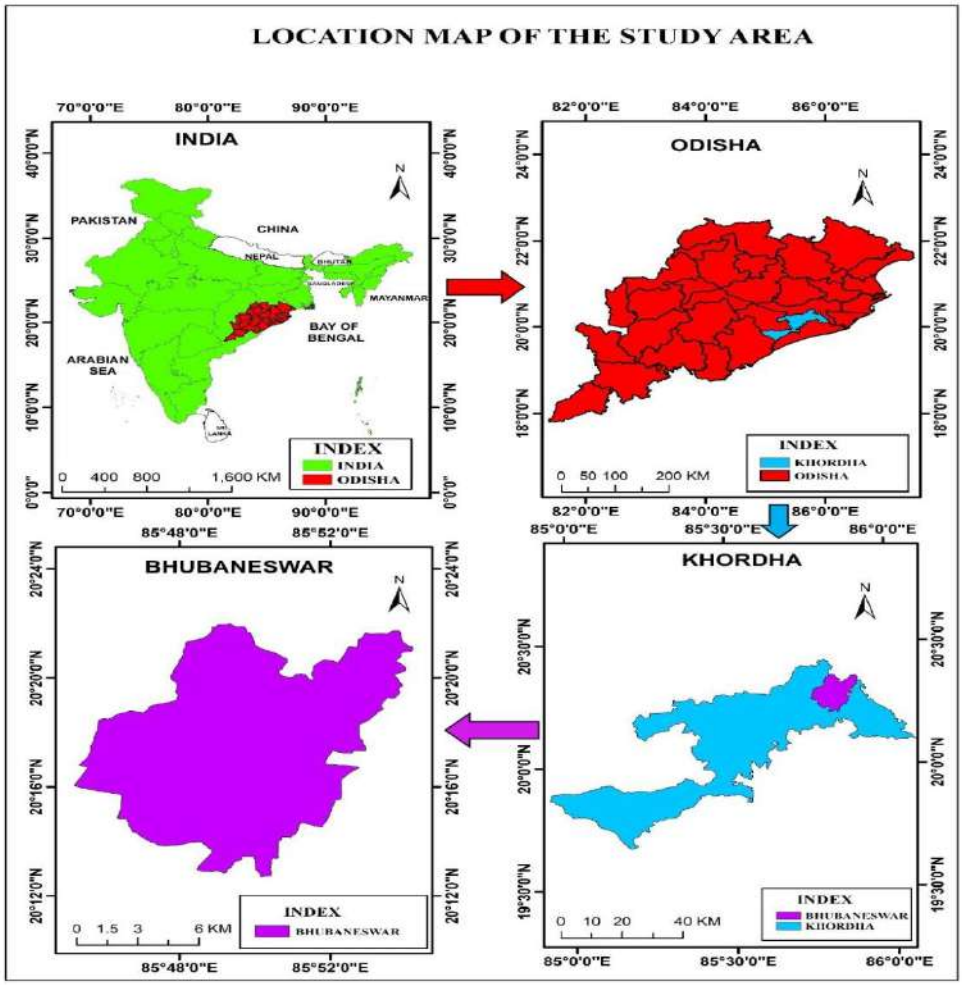

Fig. 1: Location map of the study area.

NO	DATE OF IMAGE	SATELLITE/SENSOR	REFERENCE SYSTEM/ PATH/ROW
1	2016	Landsate8	WRS-2 / 140 / 46
2	2021	Landsate8	WRS-2 / 140 / 46

In laboratory different techniques were performed with the help of ERDAS IMAGINE-2015 and ArcGIS10.8 software, using satellite images.

Image Processing and Geo-referencing:

To get the composite images, different types of bands and stacking are performed of all the collected images content. Some image improvement techniques like data scaling and histogram equalization laboratory work are also performed on each image to improve the image quality. Then, satellite images were rectified with the help of pre-referenced topographical sheet by the image-to-image rectification process with geographic co-ordinate system (lat/long), spheroid – Everest and datum-WGS84, using ArcGIS 10.8 software.

Create AOI layer and Subset:

Extract of our study area is done with the help of clip tools in Arc GIS software. After creation of AOI, the study area is extracted by subset from main images. After creation of the AOI layer sub setting is done to extract the interested area.

IMAGE CLASSIFICATION

There is no doubt that human actions have extremely changed land use land cover in the Bhubaneswar municipality area throughout the last twenty years. The entire ecosystem of the land is comprised with water, soil and plant. Therefore, land is one of the most significant natural resources for human beings because the human society demands food, energy, water and other daily requirements for livelihood. Now it is very crucial to understand the temporal influence of the human activities on their natural resource base by observing the earth from space. In situations of quick and often unrecorded and undocumented changes in land use patterns, observations of the earth from space give intent information of human actions and use of the landscape. The classified images provide all the relevant information to understand the land use and land cover change of the study area. We have taken built-up area, vegetation, water bodies, waste land and agricultural land for land use land cover classification.

Table 1: Land use land cover Data of 2016.

Land Use Land Cover Data of 2016		
Land Use Type	**Area in km**	**Percentage (%)**
Built Up Area	47.03841598	32%
Vegetation	51.43813188	35%
Water	1.59447541	1%
barren Land	45.60480136	31%
Sand Dune	1.736531959	1%
Total area	147.4123566	100%

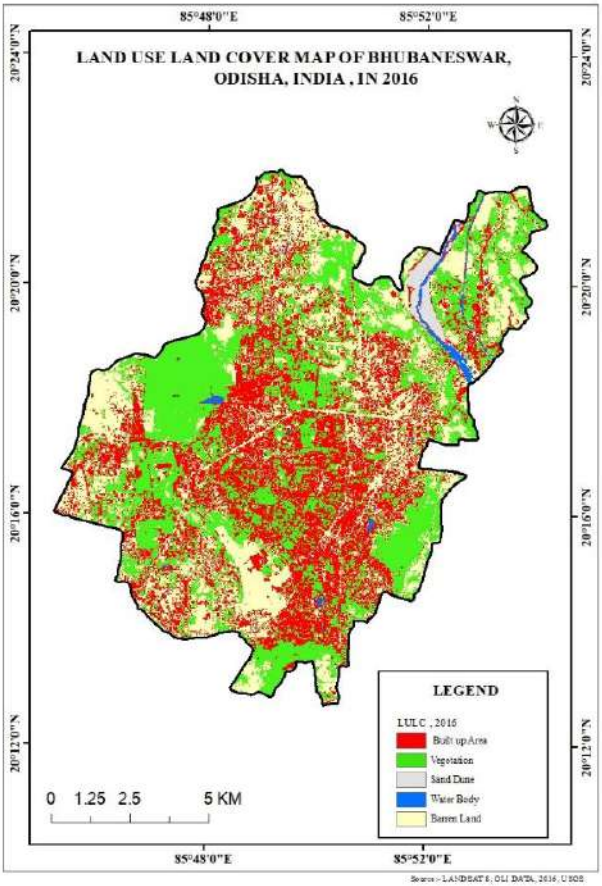

Fig. 3: LULC classification of Bhubaneswar in 2016.

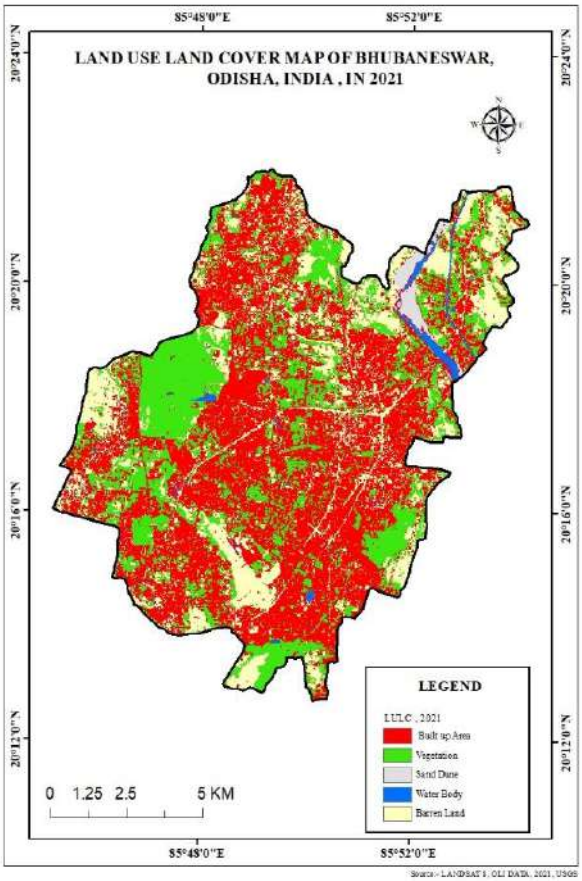

Fig. 2: LULC classification of Bhubaneswar in 2021.

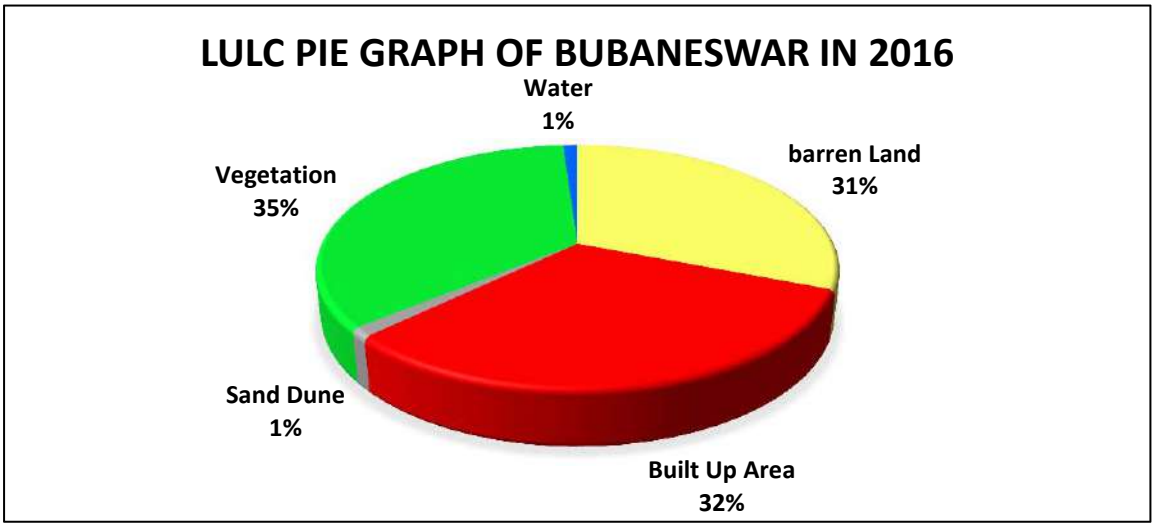

Fig. 4: LULC Pie diagram of Bhubaneswar in 2016.

Table 2: Land use land cover Data of 2021.

Land Use Land Cover Data of 2021		
Land Use Type	**Area in km**	**Percentage (%)**
Built Up Area	73.04987657	50%
Vegetation	39.74193917	27%
Water	2.157044533	1%
barren Land	30.69606236	21%
Sand Dune	1.78058784	1%
Total area	147.4255105	100%

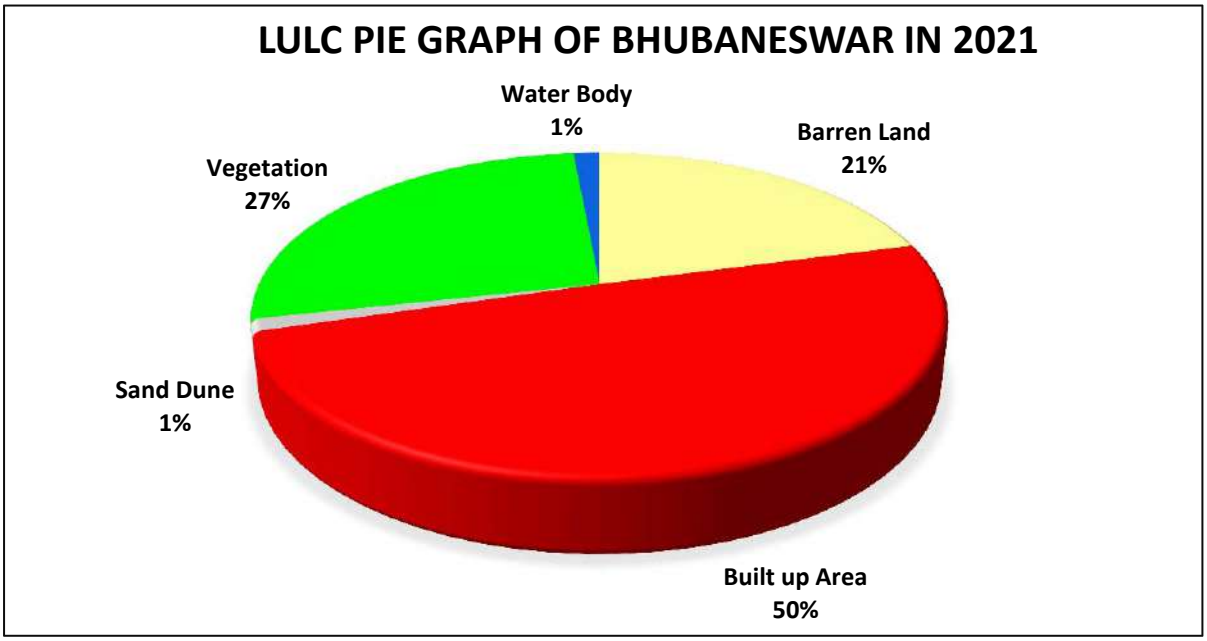

Fig. 5: LULC Pie diagram of Bhubaneswar in 2021.

RESULT AND DISCUSSION

LULC types (build up area, vegetation cover, water, and barren land) shows decreasing trends, and two LULC types (Built-up land and water body) show increasing trends. The statistical result indicates that the most land in BMC was covered by Built-up land (32% in 2016, 50% in 2021) followed by water body (1%in 2016, 1% in 2021), barren land (47.03% in 2016, 30.69% in 2021) and vegetation (35% in 2016, 27% in 2021) and sand dunes (1.74% in 2016, 1.78% in 2021)

The greatest decline was found for vegetation; a total number of 91.18 km^2 vegetation cover loss was observed in BMC during the study period (2016–2021), is11.7 km^2. Barren land also showed an obvious decreasing trend with a total loss of 76.29km^2 during 2016–2021, decreasing at a rate of 14.91 km^2

The remote sensing techniques are utilized to monitor and analysis of environmental issues at the global, national, and regional level. The purpose of change detection is to analyse the variability in the images related to a specific area that is captured over a distinct period of times.

This paper reports the urban change analysis which is based on the statistical data extracted from the three different land use and land cover maps of Bhubaneswar city. It clearly shows with diagrammatic representation (Pie Diagram) the changes of land use and land cover of 2016-2021 period. The built-up area as well as vegetation cover area has been significantly changed from 2016 to 2021. Built-up area has been increased by 32% (26sq.km), vegetation decreased by 8%(11.7sq.km) and water body has been decreased by 0.5(sq.km).

There are so many reasons behind the expansion of built-up area. Bhubaneswar City is one of the important centres for educational institutions and health facilities of surrounding people in eastern India. Therefore, the pressures of daily and seasonal migrated people are gradually increased day by day. The eutrophication phenomena in all the water bodies of the study area were found to occur due to the deposition of sediments and haphazard dumping of solid waste.

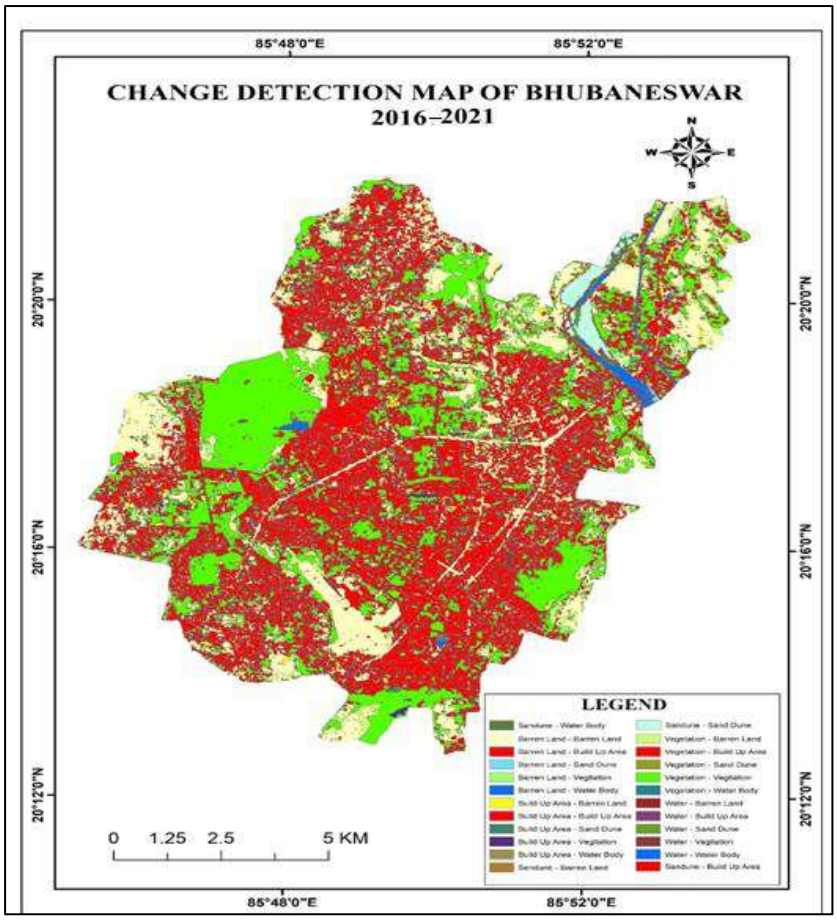

Fig. 6: Change Detection map of Bhubaneswar 2016-2021.

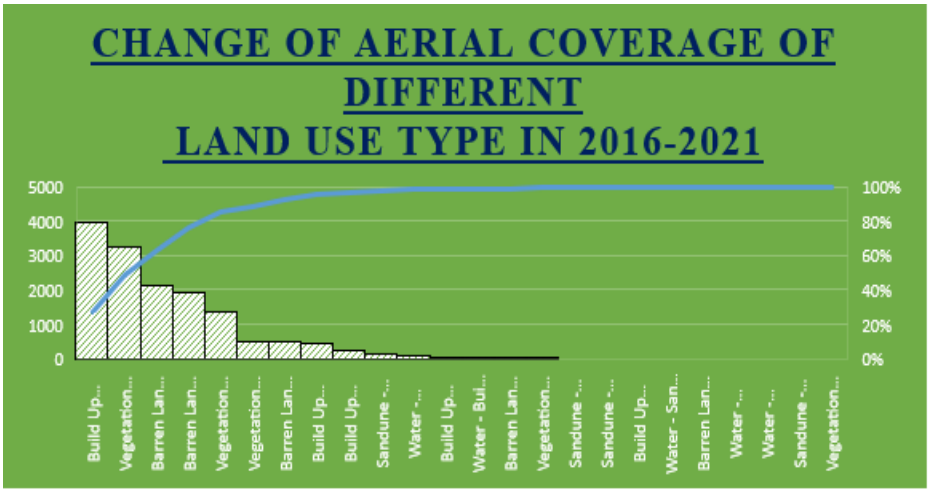

Fig. 7: Bar Diagram of Change of Aerial cover of Different Land use type.

Normalized Different Vegetation Index (NDVI)

The normalized different vegetation index (NDVI) is the most extensively used vegetation index in urban heat island (UHI). And is computed with the red and near-infrared band in multispectral satellite image.

$$\mathbf{NDVI} = \frac{(\mathbf{NIR} - \mathbf{RED})}{(\mathbf{NIR} + \mathbf{RED})}$$

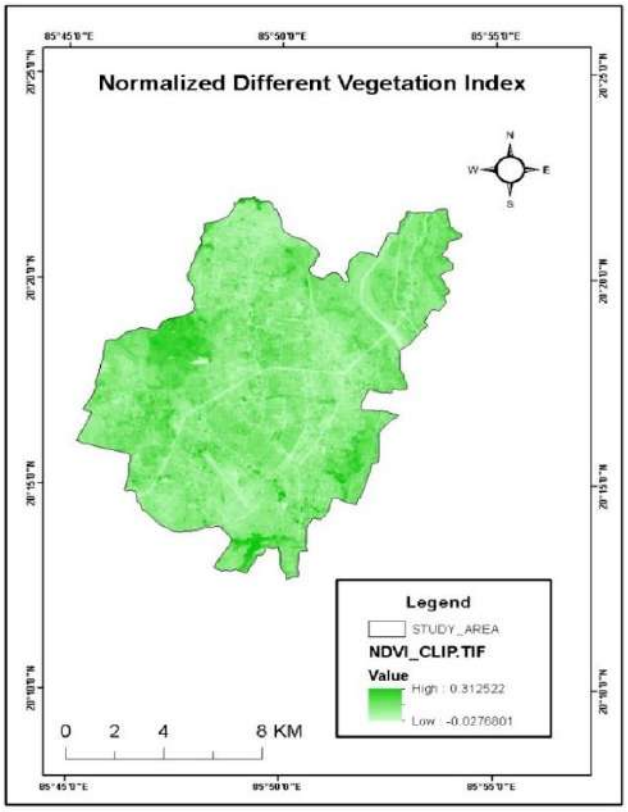

Fig. 9: NDVI Map of 2016 of Bhubaneswar

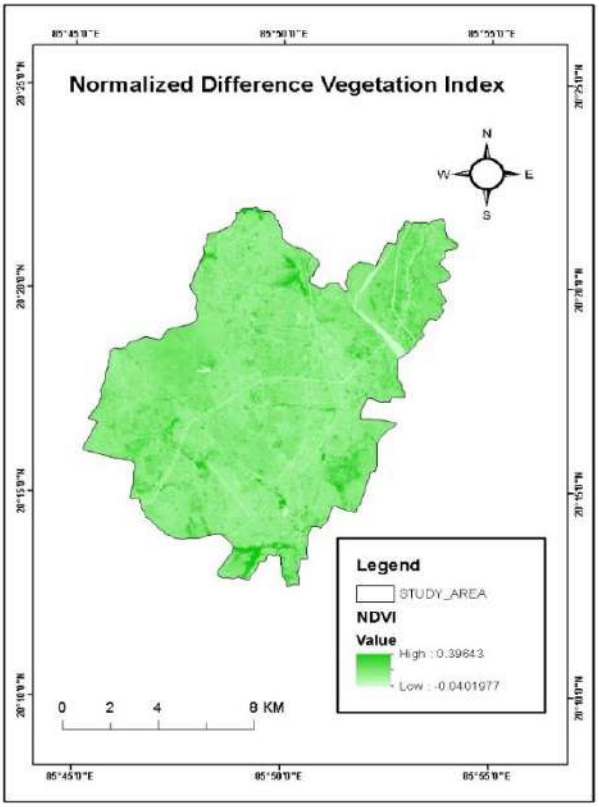

Fig. 8: NDVI Map of 2021 of Bhubaneswar

N

For the mapping of urban constructed areas or impervious surface, normalized difference build-up index (NDBI) is extremely helpful.

$$\mathbf{NDBI} = \frac{(\mathbf{SWIR} - \mathbf{NIR})}{(\mathbf{SWIR} + \mathbf{NIR})}$$

Normalized Difference Water Index:

The Normalized difference water index (NDWI) is used to highlight open water features in a satellite image, allowing a water body to "stand out" against the soil and vegetation. The NDVI index was proposed by McFeatters in 1996. Its primary use today is to detect and monitor slight changes in water content of the water bodies.

$$\text{NDWI}=\frac{(\boldsymbol{GREEN-NIR})}{(\boldsymbol{GREEN+NIR})}$$

Normalized Difference Latent Heat Index:

The normalized difference latent heat index (NDLI) is the most accurate and reliable index for determining the properties of water content in various land cover types. The Landsat image is used to develop the index (NDLI) which is defined as

$$\mathbf{NDLI}=\frac{(\boldsymbol{GREEN-RED})}{(\boldsymbol{GREEN+RED+SWIR})}$$

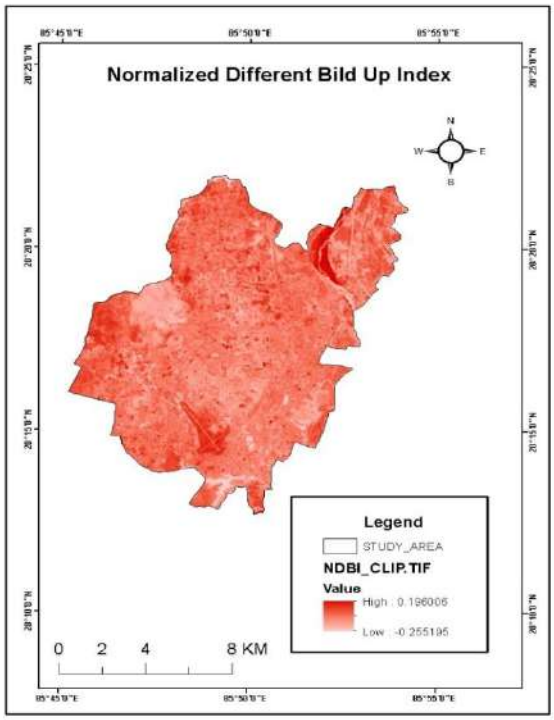

Fig. 10: NDBI of Bhubaneswar 2016.

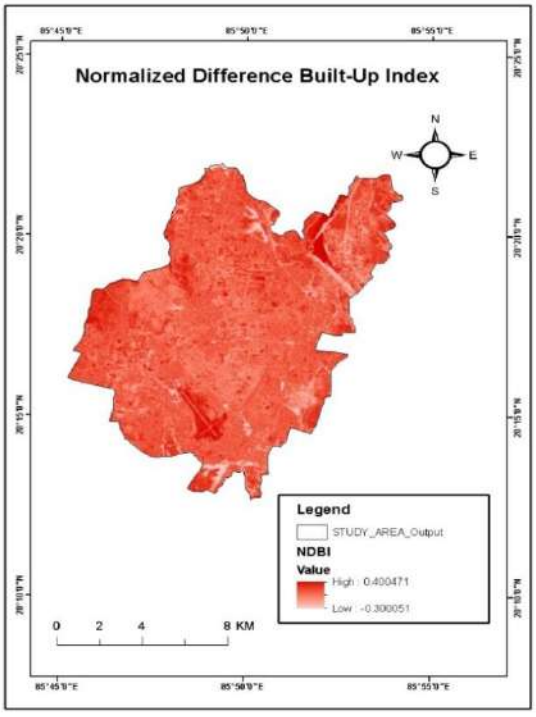

Fig. 11: NDBI of Bhubaneswar 2021.

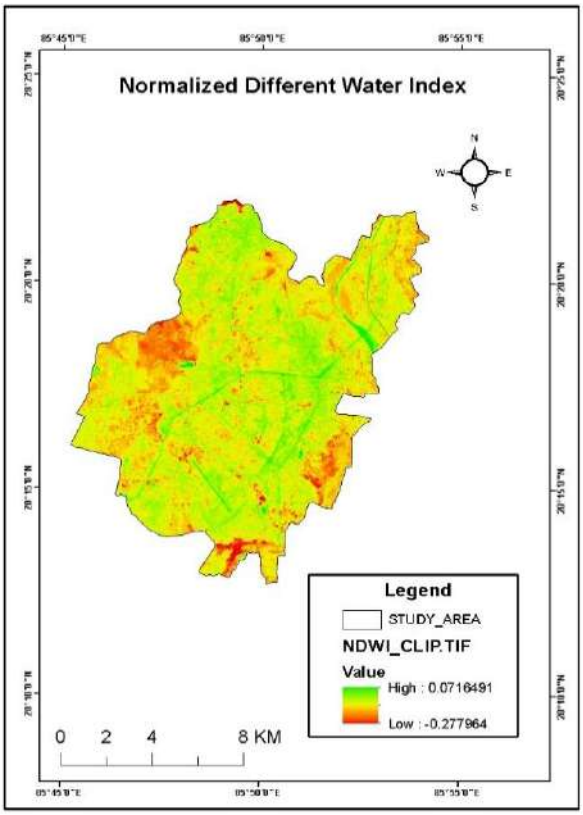

Fig. 12: NDWI of Bhubaneswar 2016.

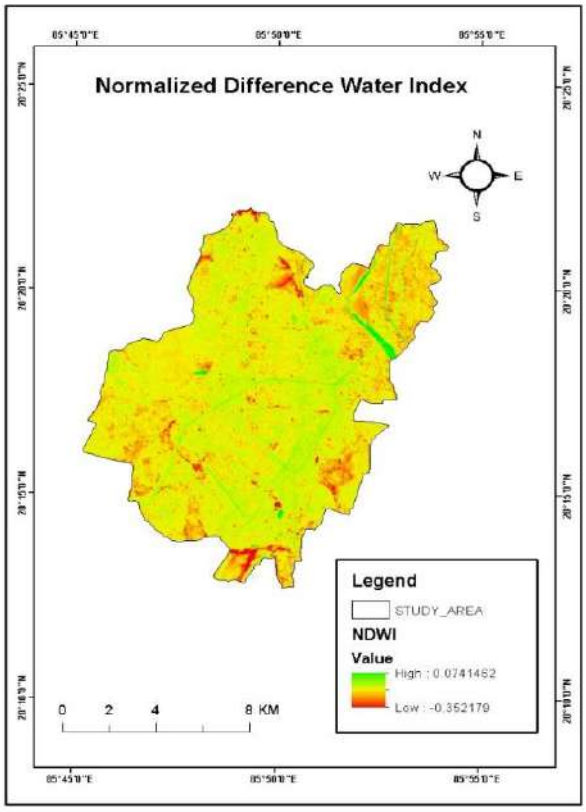

Fig. 11: NDWI of Bhubaneswar 2021.

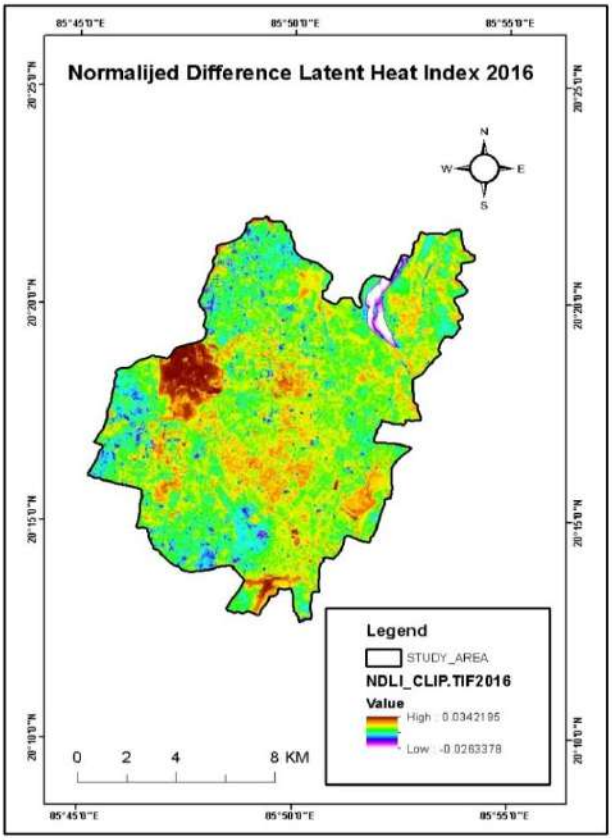

Fig. 14: NDLI of Bhubaneswar 2016.

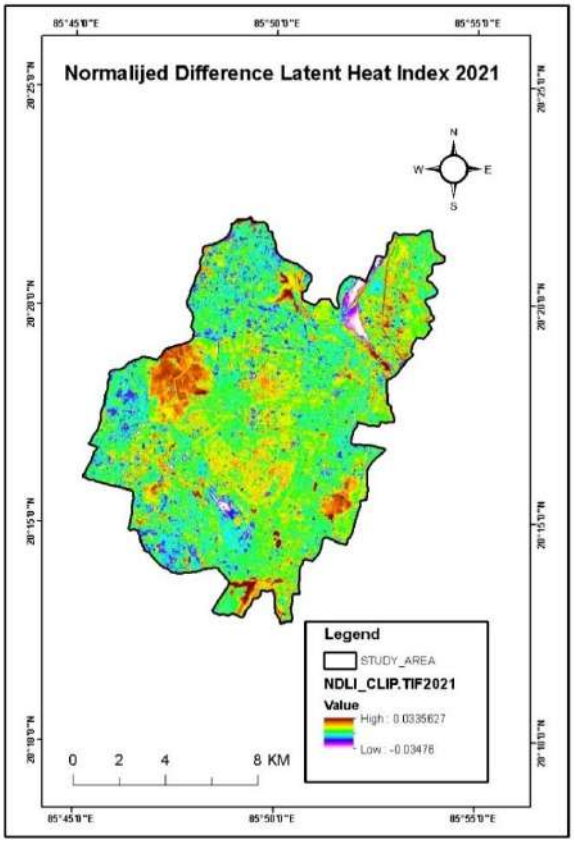

Fig. 13: NDLI of Bhubaneswar 2021.

Retrieval of Land Surface Temperature: To calculate land surface temperature (LST), raw thermal band data (band 6 in Landsat 5 (TM) and Landsat 7 (ETM ?), and band 10 in Landsat 8 (TIRS) were converted into spectral radiance using the following formula

$$L_\lambda = M_L * Q_{CAL} + A_L$$

Where Lλ is the top of atmospheric spectral radiance is the band-specific multiplicative rescaling factors form the metadata, And A_L is the band-specific additive rescaling factor form the metadata.

To obtain at sensor temperature (brightness) was evaluated by Equation-

$$BT = \frac{K_2}{Ln\left(\frac{K_1}{L_\lambda} + 1\right)} - 273.15$$

Where BT is at-satellite Brightness Temperature is TOA Spectral Radiance, K_1 is calibration constant, And k_2 is calibration. For LANDSAT-5 TM value of K_1 for band 6 is 607.76 and k_2 for band 6 is 1260.56 respectively. For LANDSAT 8 TIRS values of k_1 for band 10 and 11 are 774.8853 and 480.8883 respectively and k_2 for band 10 and 11 are 1321.0789 and 1201.1442 respectively.

$$P_V = \left[\frac{NDVI - NDVI_{Min}}{NDVI_{Max} - NDVI_{Min}}\right]^2$$

One of the most key considerations for determining vegetation cover is the normalized difference vegetation index (NDVI). Since the index is calculated through a normalization procedure, the NDVI value range is 0 to 1, with a resilient response to green vegetation even in areas with little vegetation NDVI was calculated from the red and near-infrared bands. where NIR means near-infrared band and R means red band. The proportion of Vegetation (PV) is derived by the following format:

Where p_V is the proportion of vegetation. Finally land surface temperature (LST) was estimated by the following format

$$LST = \frac{BT}{1 + \left(\frac{W_\lambda * BT}{\rho}\right) * Ln(E)} - 273.1$$

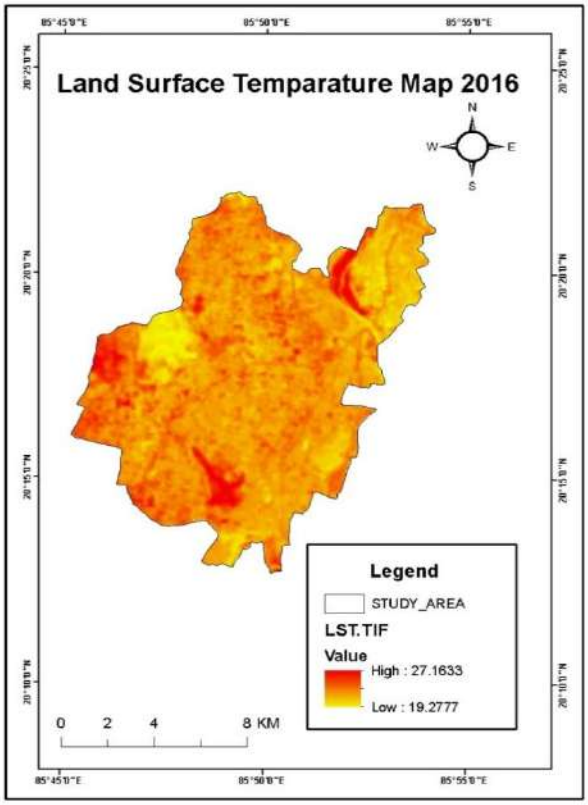

Fig. 15: LST map of Bhubaneswar 2016.

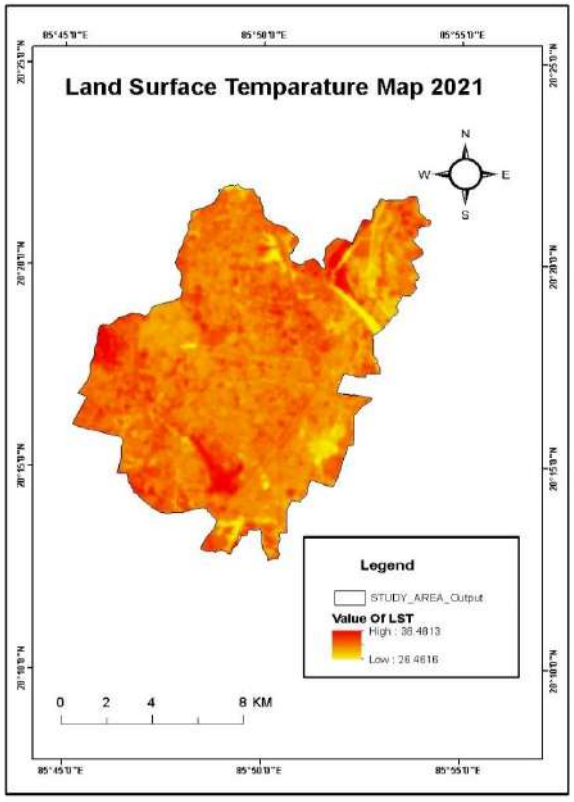

Fig. 16: LST map of Bhubaneswar 2021.

The special distribution of surface temperature of 2016 to 2021 are estimated using Landsat TM satellite image. In the year of 2016 the range between highest and lowest value of temperature is 27.16 to 19.27, in the year of 2021 its range is 38.48 to 26.46.

According to the study we known that the maximum surface temperature is cover by build-up area and also minimum surface temperature are followed by water land and surrounding area. From this image report we can easily say that the temperature of land surface of Bhubaneswar city has increased day by day from the year 2016 to 2021.

CONCLUSIONS

Remote sensing techniques were used in this study to identify the spatio-temporal pattern of the LULC change and how this pattern impacts the LST in the Bhubaneswar city. It was found that the city area experienced significant changes between 2016 and 2021. The research area was classified into Five categories: Agriculture, Fallow, Sand, Settlement, Vegetation, Water Body. The area under this category grew particularly in the periphery of Bhubaneswar City through the conversion of High-density built-up area, agricultural fallow, fallow land, etc. The extent of the industrial area and fallow land has also increased through the transformation of agricultural fallow land. There is a strong relationship between the LULC and LST. This study found that the LST value varies depending on the LULC category. The radiant temperature in fallow land, sand and built-up areas has increased. The temperatures were higher not only in settlement or built-up areas but also in industrial areas

and on riverside sand. From 2000 to 2020, the mean LST of the whole study area increased remarkably. This increasing trend of the LST can be explained by the growth of the built-up area, especially in the regions around Bhubaneswar city.

REFERENCE

Imran, H. M., Hossain, A., Islam, A. K. M. S., Rahman, A., Bhuiyan, M. A. E., Paul, S., & Alam, A. (2021). Impact of Land Cover Changes on Land Surface Temperature and Human Thermal Comfort in Dhaka City of Bangladesh. Earth Systems and Environment, 5(3), 667–693. https://doi.org/10.1007/s41748-021-00243-4

Hussain, S., & Karuppannan, S. (2021). Land use/land cover changes and their impact on land surface temperature using remote sensing technique in district Khanewal, Punjab Pakistan. Geology, Ecology, and Landscapes, 1–13. https://doi.org/10.1080/24749508.2021.1923272

Imran, H. M., Kala, J., Ng, A. W. M., & Muthukumaran, S. (2019). Impacts of future urban expansion on urban heat island effects during heatwave events in the city of Melbourne in southeast Australia. Quarterly Journal of the Royal Meteorological Society, 145(723), 2586–2602. https://doi.org/10.1002/qj.3580

Hereher, M. E. (2017). Effect of land use/cover change on land surface temperatures - The Nile Delta, Egypt. Journal of African Earth Sciences, 126, 75–83. https://doi.org/10.1016/j.jafrearsci.2016.11.027.

Karakuş, C. B. (2019). The Impact of Land Use/Land Cover (LULC) Changes on Land Surface Temperature in Sivas City Center and Its Surroundings and Assessment of Urban Heat Island. Asia-Pacific Journal of Atmospheric Sciences, 55(4), 669–684. https://doi.org/10.1007/s13143-019-00109-w

Kustas, W., & Anderson, M. (2009). Advances in thermal infrared remote sensing for land surface modeling. Agricultural and Forest Meteorology, 149(12), 2071–2081. https://doi.org/10.1016/j.agrformet.2009.05.016

Feizizadeh, B., & Blaschke, T. (2012). Thermal remote sensing for land surface temperature monitoring: Maraqeh County, Iran. 2012 IEEE International Geoscience and Remote Sensing Symposium. https://doi.org/10.1109/igarss.2012.6350808

Sekertekin, A., & Bonafoni, S. (2020). Land Surface Temperature Retrieval from Landsat 5, 7, and 8 over Rural Areas: Assessment of Different Retrieval Algorithms and Emissivity Models and Toolbox Implementation. Remote Sensing, 12(2), 294. https://doi.org/10.3390/rs12020294

Naughton, J., & McDonald, W. (2019). Evaluating the Variability of Urban Land Surface Temperatures Using Drone Observations. Remote Sensing, 11(14), 1722. https://doi.org/10.3390/rs11141722

Liu, J., Hagan, D. F. T., & Liu, Y. (2020). Global Land Surface Temperature Change (2003–2017) and Its Relationship with Climate Drivers: AIRS, MODIS, and ERA5-Land Based Analysis. Remote Sensing, 13(1), 44. https://doi.org/10.3390/rs13010044

Barkhordarian, A., Saatchi, S. S., Behrangi, A., Loikith, P. C., & Mechoso, C. R. (2019). A Recent Systematic Increase in Vapor Pressure Deficit over Tropical South America. Scientific Reports, 9(1). https://doi.org/10.1038/s41598-019-51857-8

Mutiibwa, D., Strachan, S., & Albright, T. (2015). Land Surface Temperature and Surface Air Temperature in Complex Terrain. IEEE Journal of Selected Topics in Applied Earth Observations and Remote Sensing, 8(10), 4762–4774. https://doi.org/10.1109/jstars.2015.2468594

Ghouri AY, Khan A (2022) Monitoring the Land Surface Temperature and Its Correlation with NDVI of Chiniot by Using GIS Technology and Remote Sensing. J Earth Sci Clim Change, 13: 621. DOI: 10.4172/2157-7617.1000621

Yeh, A. G., & Li, X. (1997). An integrated remote sensing and GIS approach in the monitoring and evaluation of rapid urban growth for sustainable development in the Pearl River Delta, China. International Planning Studies, 2(2), 193–210. https://doi.org/10.1080/13563479708721678

WENG, Q. (2001). Modelling Urban Growth Effects on Surface Runoff with the Integration of Remote Sensing and GIS. Environmental Management, 28(6), 737–748. https://doi.org/10.1007/s002670010258

VISTAS IN GEOLOGICAL RESEARCH
Special Publication in Geology (19), March 2023, pp. 105-110

Recent Foraminiferal Diversity, Distribution and Abundance In and Around Chandipur Area, Odisha, India

JUMEE DOWARI[1*] AND URBASHI SARKAR[1]

[1]Department of Earth Science, Assam University, Silchar - 788011
[*] Corresponding author: jdowari92@gmail.com

Abstract: Foraminifera, a group of single-cell shelled organisms, are excellent indicators of water quality and the state of the coastal environment. The coastal region of Chandipur, Odisha is very suitable for studying about the behavioural variability of foraminifera since the area consists of different sub-environments like beach, tidal flat, estuary, bar, marsh and creek. In this study, a set of thirty-eight (<10cm) sediment samples, collected from Chandipur area, were studied and the patterns of distribution, diversity and abundance of recent benthic foraminifera were analysed. Different physicochemical parameters from this area were measured and found to be almost similar: temperature varies from 28°c to 32°c, salinity varies from 23ppt to 30ppt, pH varies from 7 to 8 and DO varies from 5mg/l to 7mg/l. Calcareous foraminifera (*Ammonia* sp., *Asterotalia* sp., *Haynesina* sp., *Elphidium* sp., *Hemirotalia* sp., *Pararotalia* sp., *Discorbis* sp., *Bolivina* sp.) dominate over porcelaneous (*Quinqueloculina* sp. and *Triloculina* sp.) foraminifera. Higher foraminiferal abundance and diversity are found in areas with muddy sediment and mixed sand to muddy substrate as compared to other sub-environments. This may be because the area has a low energy, which allows for the accumulation of these species. The study found that substrate parameters and environment conditions seem to play a significant role in distribution, diversity and abundance of foraminifera.

Keywords: Benthic foraminifera, Beach, Tidal flat, Estuary, Back bar, *Ammonia beccarii*, *Asterotalia tripinosa*, Chandipur coast.

INTRODUCTION

Benthic foraminifers are among the richest and most numerous in marine sediments. It is widespread and has ecological adaptability. The coastal region around Chandipur is near the Budhabalanga River confluence. The different processes that take place in rivers, the ocean and the air contribute to the creation of different environments (Das *et al*., 2019 and Mondal and Sarkar, 2021). Foraminiferal assemblage is largely controlled by physical factors (such as water current, depth as well as the bottom sediments), chemical factors (such as temperature, salinity, pH and Dissolve Oxygen) and biological factors {such as food supply, predators etc. (Elakkiya and Manivannan,2012)}. In this study, we have investigated the diversity, distribution and abundance of foraminifers in different sub-environments of Chandipur coastal area.

STUDY AREA AND METHODS

The study was conducted on the coast of Chandipur (21°27'45" N, 87 ° 00'12" E to 21 ° 26'04" N to 87 ° 01'08" E) lying on the eastern coast of India (fig: 1). Thirty-eight sediment samples (table 1) were collected from various sub-environments (beach, tidal flat, estuary and back bar) at depth of <10cm by hand-dredging or scraping following standard procedure. At the time of collection of samples, each sample was soaked in Rose Bengal solution which helps in distinguishing living species from the dead one. Samples were processed following the standard procedure. Foraminiferal specimens were hand-picked under a LEICA EZ4 stereo zoom microscope at the department of Earth Science, Assam University, Silchar and kept on micropaleontological slides. Along with collection of samples, physico-chemical parameters like temperature, pH, salinity and DO were measured with the help of portable kit (HANNA).

Fig 1: Map showing Chandipur coastal area with location of sample sites, Odisha, India.

RESULTS AND DISCUSSIONS

From the samples, collected from all the stations, benthic foraminifera were picked and studied. Total 23 species belonging to 12 genera were identified. Identified foraminiferal species from the area include; *Ammonia becarii, Ammonia bellaria, Ammonia tepida, Ammonia inflata, Ammonia parkinsoniana, Ammonia dentata, Asterotalia tripinosa, Haynesina germanica, Haynesina depressula, Hemirotalia foraminulosa, Pararotalia* sp., *Elphidium advenum, Elphidium clavatum, Elphidium excavatum, Quinqueloculina seminulum, Quinqueloculina* sp., *Triloculina* sp., *Discorbis* sp., *Rosalina* sp., *Bolivina striatula, Bolivina* sp., *Nonion* sp., and *Elphidium* sp. Calcareous foraminifera accounts for 10 genera and porcelaneous foraminifera accounts for 2 genera whereas agglutinated foraminifera was not found to be present from the studied samples.

Table 1: Table showing number of samples w.r.t. sub-environments.

SAMPLE NO.	SUB-ENVIRONMENT
3	BEACH
5	
9	
19	
20	
1	ESTUARY
2	
4	
6	TIDAL FLAT
12	
13	
14	
15	
16	
17	
18	
21	
22	
23	
27	
28	
29	
30	
32	
33	
34	
35	
36	
8	BACK BAR
11	
24	
25	
26	
31	
37	
38	

Out of all the specimens *Ammonia becarii, Asterotalia tripinosa, Ammonia dentata, Hemirotalia foraminulosa* and *pararotalia* sp., were found to be evenly distributed in the fine-grained sediments of different sub-environments. However, their abundance increases in medium to fine grained sandy sediments of the beach. *Haynesina germanica* were found to dominate in the mixed sediment zone of tidal flat, estuary and back bar with a rare occurrence of *Haynesina depressula, Ammonia tepida, Ammonia inflata, Elphidium excavatum, Elphidium advenum, Rosalina* sp., *Bolivina* sp. and *Elphidium clavatum.* Tidal flat and back bar region shows the highest abundance and diversity of foraminifera which includes; *Ammonia becarii, Ammonia bellaria, Ammonia tepida, Ammonia inflata, Ammonia parkinsoniana, Ammonia dentata, Haynesina germanica, Haynesina depressula, Hemirotalia foraminulosa, Pararotalia* sp., *Elphidium advenum, Elphidium clavatum, Elphidium excavatum, Quinqueloculina seminulum, Quinqueloculina* sp., *Discorbis* sp., *Bolivina striatula, Bolivina* sp., *Nonion* sp., and *Elphidium* sp. Estuary region shows lower abudance and medium to lower diversity as compare to other sub-environments and it includes; *Ammonia becarii, Ammonia dentata, Hemirotalia foraminulosa, Haynesina germanica, Elphidium advenum,* and *Haynesina depressula* with a rare occurrence of *Ammonia tepida, Ammonia inflata, Ammonia tepida, Elphidium excavatum, Elphidum clavatum, Triloculina* sp., and *Quinqueloculina* sp. Physico- chemical parameters didn't show much in variation in the area (temperature varies from 28°c to 32 °c, salinity varies from 23ppt to 30ppt, pH varies from 7 to 8 and DO varies from 5mg/l to 7mg/l). The species diversity index (fig: 2) for the concerned foraminiferal assemblage is found to have low to medium diversity, indicating that there are a few but distinct species present. Alpha (α) value for beach foraminiferal assemblage varies from α =< 1 to > 2 where for tidal flat it varies from α = <1 to 3. For back bar region it varies in between α= 1 and 2. On the other hand, estuary samples occur in the field α=< 1 to2. Overall, the alpha diversity indicates a shallow coastal region where the maximum alpha value is attained the tidal flat area indicating a more open marine condition there.

The Murray's ternary diagram (fig: 3) plot shows the variation in different types of foraminiferal test (agglutinated, calcareous porcelaneous and calcareous hyaline). Tidal flat region specimens bloom well in hyposaline marshes and hyposaline lagoons. Specimens from estuary and back bar blooms well mostly in hyposaline marshes, hyposaline lagoons and hypersaline lagoons. Specimens from beach region were seen under hyposaline lagoons. The overall study reveals higher variation in abundance, distribution and diversity of foraminifera in muddy and mixed sand to muddy substrate as compare to sandy substrate. Most found species are; *Ammonia beccarii, Asterotalia tripinosa, Haynesina germanica, Hemirotalia foraminulosa, Pararotalia* sp., and *Elphidium advenum.* The distribution of these species shows that they were found in all of the samples studied, indicating that they have a lot of tolerance to adapt in their environment. The lower abundance of *Quinqueloculina seminulum, Quinqueloculina* sp. and *Triloculina s*p. suggests that the area is shallow marine, with a moderate to high fluvial influence. The low abundance of milioliid groups (*Quinqueloculina seminulum, Quinqueloculina* sp. and *Triloculina* sp.) suggests that the water is high in turbidity, which suggests that the assemblage is likely near to river outlets (Rossi *et al*., 2008, Massari *et al*., 2004, Das *et al*., 2019).

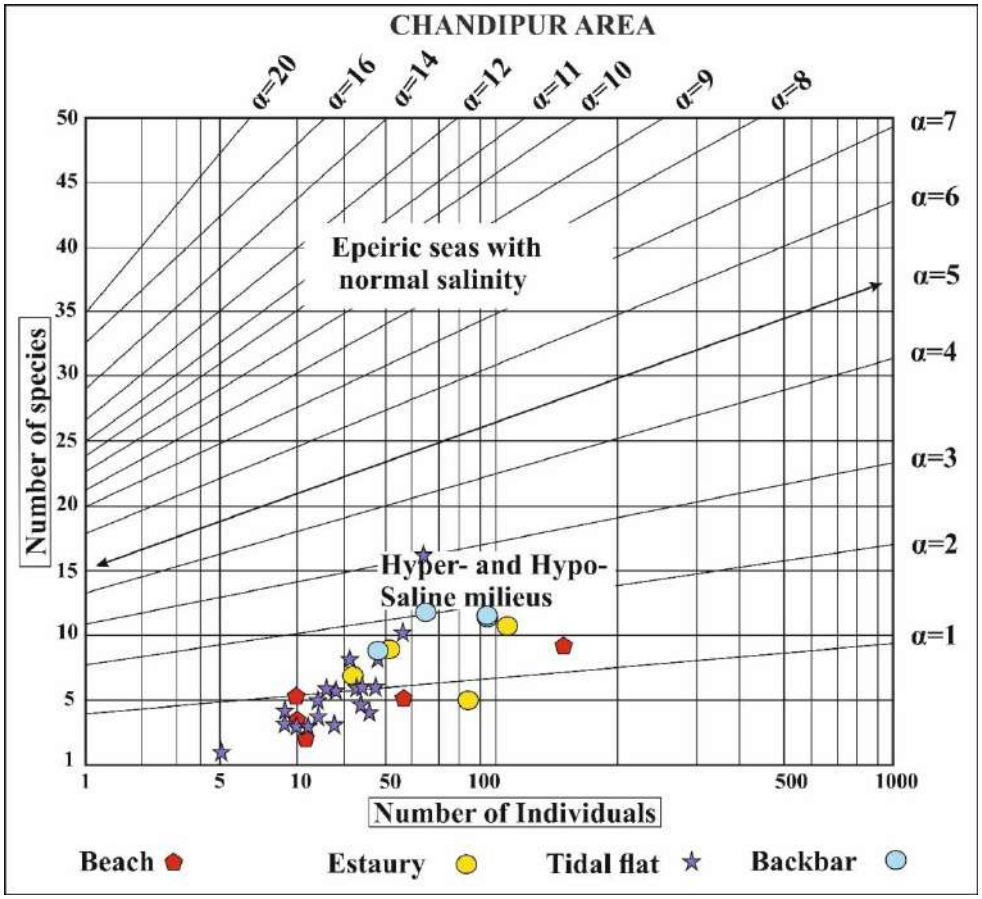

Fig. 2: Species diversity diagram showing fields defined by values of identified benthic foraminiferal assemblages (modified from Murray, 1974).

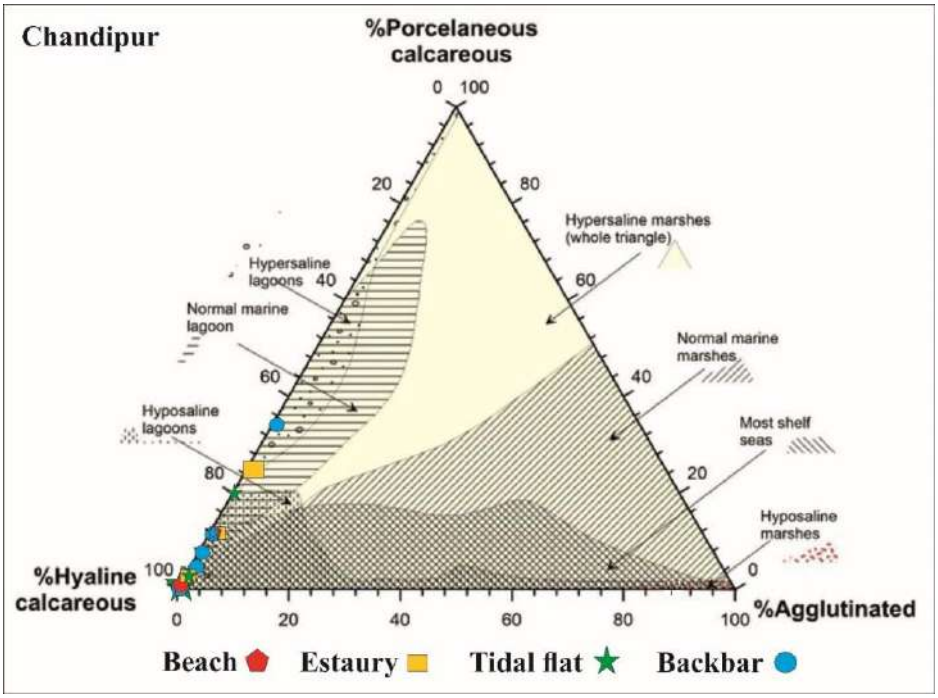

Fig. 3: Shell-type ternary diagram showing fields defined by identified benthic foraminifera assemblages of Chandipur area (modified from Murray, 1974).

CONCLUSIONS

This study shows that different environmental variables, substrate parameter and hydrodynamic condition play a major role in determining foraminifera distribution, diversity and abundance in different sub-environments. Twenty-three species were identified which include both calcareous and porcelaneous foraminifera. Benthic foraminifera of Chandipur coastal area mostly contain calcareous forms with rare occurrence of porcelaneous forms. Muddy and mixed sediment zone to muddy substrate contain the greater abundance and diversity of foraminifera as compare to sandy substrate. Physicochemical parameters were also measured but the variations among the data in the area are found to be very less.

ACKOWLEDGENMENTS

The authors are grateful to all faculty members, co-scholars and juniors of Department of Earth Science of Assam University for support and guidance during sample collections and laboratory works.

REFERENCE

Das, I., Ghosh, A., and Buragohain, D., 2019. A study of microhabitat of intertidal foraminifera from Chandipur, Odisha. Journal of the paleontological society of India, volume 64(1), June 30, 2019; 49-60.

Elakkiya, p., and Manivannam,V., 2013. Recent benthic foraminifera from off the coast of Arkattuhurai(near Nagapattinam), south east coast of India. Indian Journal of Geo-Marine Sciences; volume 42(7), November 2013, pp.877-887

Massari, F., Rio, D., Serandarei Barbero, R., Asioli, A., Capraio, L., Fornaciari, E., and Vargerio, P. P. 2004. The environment of Venice area in the past two million years. Palaeogeography, Paleoclimatology, Paleoecology, 202: 273-308.

Mondal, S., amd Sarkar, U. 2021. Predatory drilling traces of recent foraminifera from Chandipur coast, Odisha, Journal of Foraminiferal Research, Volume 51, no.4, p.286-293.

Murray, JW. 1973. Distribution and ecology of living benthic foraminiferids. London; Heinamen.

Rossi, V and Valani, S. C., 2008. Benthic foraminiferal evidence of sediment supply changes and fluvial drainage reorganization in Holocene deposits of the Po Delta. Marine Micropaleontology 69: 106-118.

.

VISTAS IN GEOLOGICAL RESEARCH
Special Publication in Geology (19), March 2023, pp. 111-116

Palaeofloral Assemblages from A Part of West Bokaro Coalfield, Damodar Valley Basin, Jharkhand, India

SOUMYASHREE NANDA[1,2], SANGHAMITRA PRADHAN[1] AND SHREERUP GOSWAMI[3]

[1]Department of Earth Sciences, Sambalpur University, Jyoti Vihar, Burla-768019
[2]Office of the Joint Director Geology, Zonal Survey, Sambalpur-768001
[3]Department of Geology, Utkal University, Vani Vihar, Bhubaneswar- 751004
*Corresponding author mail id: goswamishreerup@utkaluniversity.ac.in

Abstract: Fossiliferous carbonaceous shale samples were collected from the Parej East Open Cast Project of West Bokaro Coalfield to study the detailed morphological characters of plant megafossil impressions. The megafloral assemblages reported constitute Glossopteridales (leaf form, root form), Equisetales, and stem casts. Detailed study of the morphology of the megaflora demonstrates a warm temperate climate with abundant sunlight and sufficient water supply. The preservation of fossil leaves in fine-grained carbonaceous shale represents a low-energy environment for the deposition of sediments. Morphotaxonomy of the fossil floras and lithology of the investigated locality indicates that the sediments belong to Barakar Formation of Late Artinskian- Kungurian age (late lower Permian).

INTRODUCTION

The Lower Gondwana sediments in the Damodar Valley Basin occur in an East-West trending linear belt. Thick sequences of sediments of the Barakar Formation are well-developed in all the coalfields of the Damodar Valley Basin (Gupta, 1999). The West Bokaro Coalfield, a part of Damodar Basin, occupies an area of 207km. It is bounded by latitudes 23^0 41' and 23^0 52' N and longitudes 85^0 24' and 85^0 41' E (Tiwari et al., 2014). The Lugu hill separates West Bokaro Coalfield from East Bokaro Coalfield. The palaeofloristics of the area have been extensively studied by Surange et al., 1953; Lele, 1973; Navale et al., 1989; Khan & Tewari, 1991; Singh & Maheshwari, 2000; Singh, 2000a, 2000b, 2000c, 2000d; Bhattacharya et al., 2005; and Varma et al., 2014. In this research, an attempt has been made to carry out a detailed morpho-taxonomical study of the megafloral assemblages collected from the Parej East Open Cast Project.

Geological Setting

The West Bokaro Coalfield (Fig. 1), a broad half basin, has its closure on the west (Raja Rao, 1987; Equeenuddin et al., 2016). The basement for the complete sequence of Gondwana formation is Precambrian rocks like granitoids and amphibolites. In the northern part of the basin, an east-west trending set of faults marks the Gondwana- Precambrian boundary. The unevenness of the basement and the presence of faults result in local variations in dip and

strike. The regional strike of the Gondwana sediments is about East-West (Raja Rao, 1987). The stratigraphy of the sedimentary sequence comprises Talchir, Karharbari, Barakar, Barren Measures, Raniganj, Panchet, and Supra- Panchet formations ranging from early Permian to upper Triassic age (Raja Rao, 1987). The overall stratigraphic sequence of the West Bokaro Coalfield is given in Table 1.

The main coal-bearing Barakar Formation covering almost 125 sq. km contains a thick sequence of conglomerates, pebbly sandstones, very coarse to fine-grained sandstone, grey shale, carbonaceous shale, fire clay, and coal seams (Raja Rao, 1987). This Barakar Formation is mainly associated with Permian coal of bituminous rank (Equeenuddin et al., 2016). In general, it is reported that the rank of coal improves from east to west and from near the surface to depth (Tiwari et al., 2014). The intrusion of dolerite dyke, lamprophyre, and mica peridotite has also been found from this coalfield.

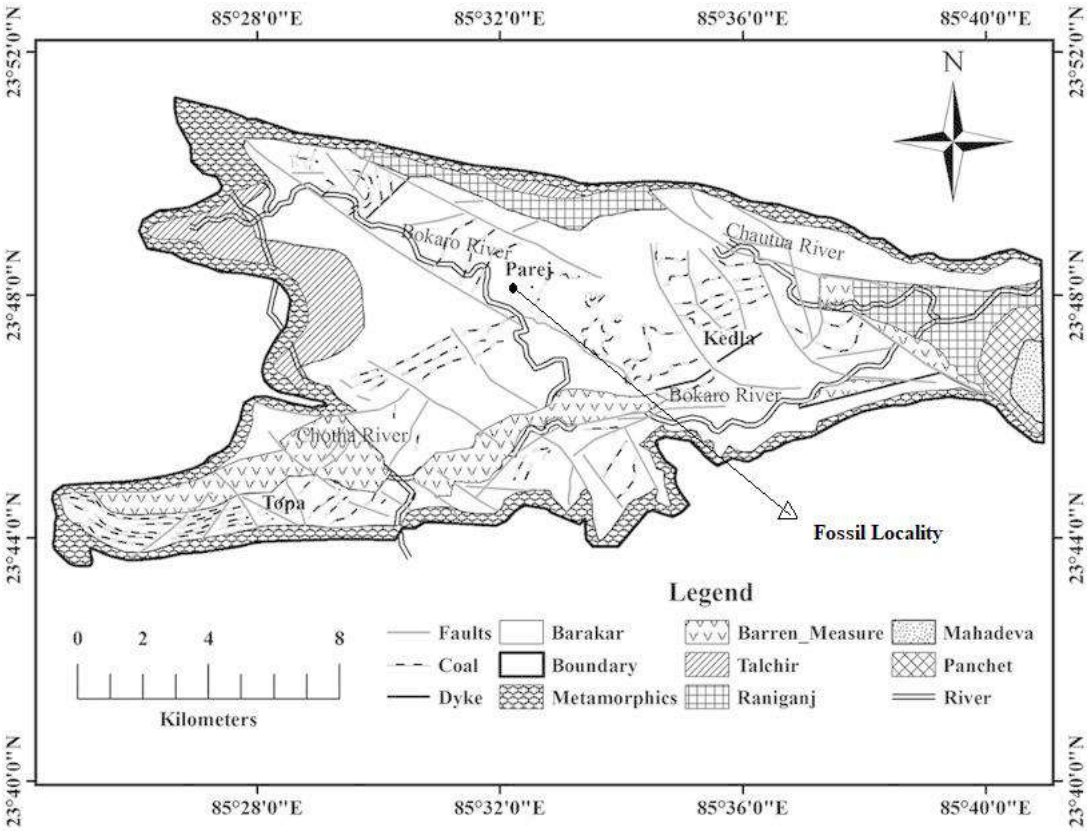

Fig. 1: Geological Map of West Bokaro Coalfield (after Raja Rao, 1987).

MATERIALS AND METHODS

A total of 369 nos. of fossil specimens including fossil leaves, stems and roots have been collected from carbonaceous shale samples below the Coal Seam III Top (Fig. 2) from the Parej East Open Cast Project (Lat: 23˚ 48' 24.3" N, long: 85˚ 32' 51.1" E) of West Bokaro Coalfield, Jharkhand. The fossil samples have been deposited in the museum of the

Department of Earth Sciences, Sambalpur University, and are registered as P. Morphological features like shape, size, presence or absence of mid-rib (if present, then type of midrib) and venation pattern of fossil specimens have been observed under a low power binocular microscope and grouped systematically following *International Code of Nomenclature for algae, fungi, and plants* (Turland et. al., 2018). Glossopteris species are identified using the methodology given by Chandra and Surange (1979). The list of studied taxa is given in Table 2.

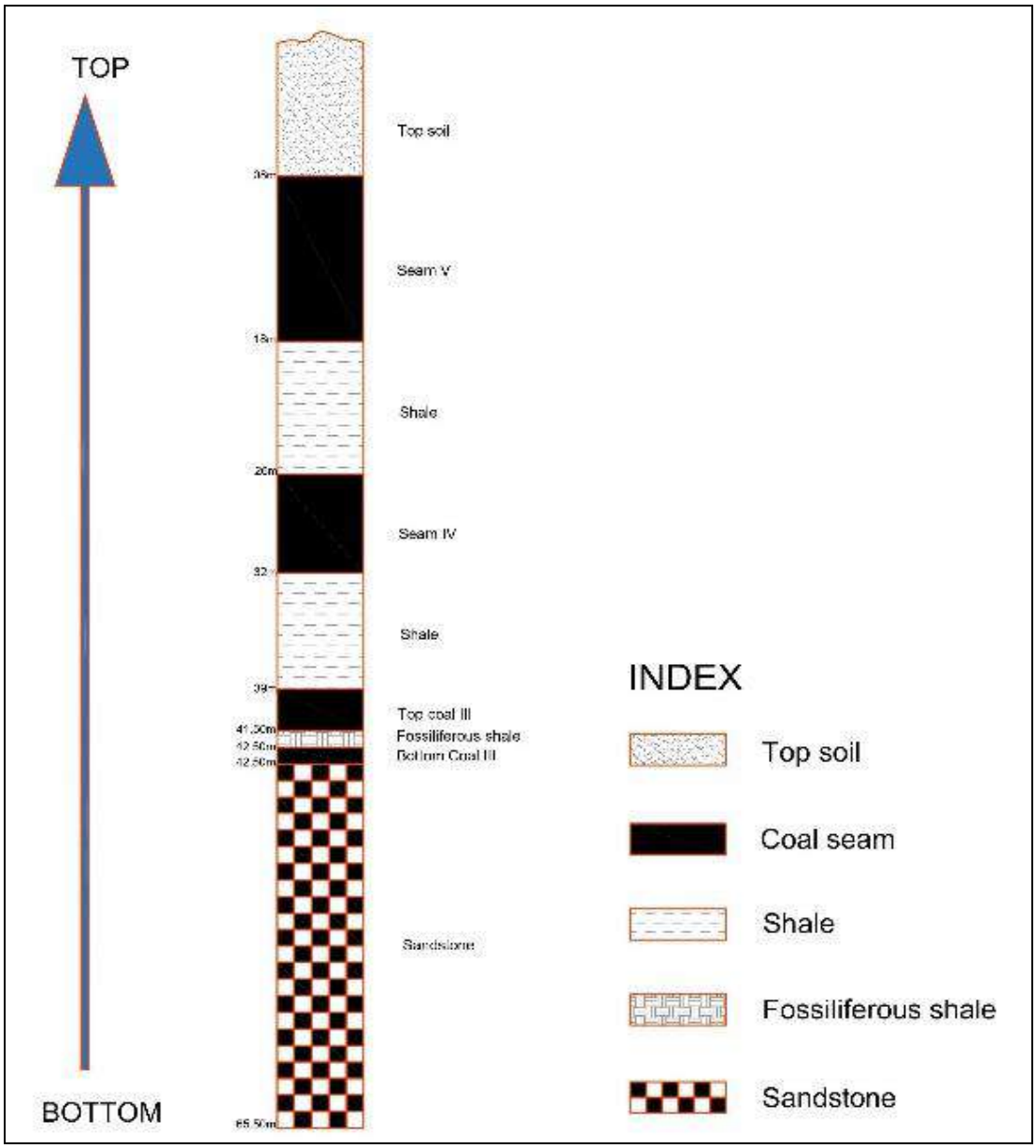

Fig. 2: Geological section along the investigated fossil locality.

Table 1: Stratigraphic Succession of West Bokaro Coalfield **(**Raja Rao, 1987**)**

Age	Formation	Lithology and Thickness in meter
Quaternary		Quaternary
Upper Triassic	Supra- Panchet (Mahadeva?)	Conglomerates, ferruginous sandstone, and siltstones; 600m
Lower Triassic	Panchet	Fine-grained sandstone, green shales, and red and chocolate coloured shale and clay; 450m
Upper Permian	Raniganj	Fine-grained sandstone, siltstone, carbonaceous and grey shales with thin coal seams; 550m
Middle Permian	Barren Measures	Carbonaceous shales, grey micaceous shales with ironstone; 300m
Lower Permian	Barakar	Conglomerates, pebbly sandstones, very coarse-grained to fine-grained sandstone, grey shale, carbonaceous shale, fire clay, and coal seams; 610m
	Karharbari	Conglomerate, very coarse-grained sandstone, carbonaceous at places, and thin coal seam; 40mto60m
	Talchir	Diamictite, fine to medium-grained greenish and buff coloured sandstones, shale, rhythmite, turbidite, etc.; 160m
~~Unconformity~~~~~~~~~~~~~~~~~~~~~~~~~~~~~~~~~~		
Precambrian	Granites, gneisses, amphibolites, quartzites, pegmatites, etc.	

DISCUSSION AND CONCLUSION

Megafloral assemblage of the area indicates that the area is rich in equisetales and glossoptereidales. Fossils are well preserved in fine-grained carbonaceous shale of the Barakar Formation. The leaves of *Glossopteris* of the present collection is variable from small (*Glossopteris angustifolia, G. linearis, G. stenoneura, G. zeilleri*) to big (*Glossopteris communis, G. karanpuraensis, G. taeniopteroides, G. raniganjensis*) having narrow (*Glossopteris angustifolia, G. linearis, G. vulgaris)* to broad lamina (*Glossopteris spatulata, G. karanpuraensis, G. raniganjensis, G. taeniopteroides*). Varieties of leaf morphology of *Glossopteris* depicts that some of the *Glossopteris* plants found in this area were perhaps very stunted forms, like bushy plants, attaining a height of a small shrub and some of the others attained the height of big trees. During this time, some of the *Glossopteris* plants were arborescent, having larger leaves providing shade to several herbaceous plants having smaller leaves. Again, *Glossopteris* formed a terrestrial ecosystem, which provided organic detritus for peat formation, whereas equisetalean plants growing in and around small lakes and ponds formed the marshy ecosystem.

The Glossopteris leaves reported are mainly from medium to large in size, lanceolate shape, acute apices, narrow tapering bases, and entire margins suggesting the availability of sufficient water supply. Acute apices and narrow tapering bases indicate the existence of enough sunlight during the deposition of the fossiliferous sediments (Goswami et.al., 2018).

Table 2: List of Glossopteris flora reported from the study area.

	Name of fossil taxa
Dominant (more than 5%)	Stem cast
	G. indica
	Vertebraria
	G. communis
	Stem axis
Subdominant (less than 5%)	*Glossopteris stenoneura*
	G. searsolensis
	G. browniana
	G. tenuifolia
	G. decipiens
	G. major
Rare (less than 1%)	*Equisetaceous stem*
	Glossopteris zeilleri
	G. nautiyalii
	G. raniganjensis
	G. intermittens
	G. spatulata
	G. densinervis
	G. vulgaris
	G. maculata
	G. lanceolatus
	G. karanpuraensis
	G. taeniopteroids
	G. linearis
	G. angustifolia

The preservation of megafossils in fine-grained carbonaceous shale suggests a low-energy depositional environment. Detailed morphological study of the fossil floras reveals a warm temperate climate. The deposition of a vast amount of coal in the investigated locality depicts the presence of dense vegetation and a sufficient amount of rainfall during the deposition of sediments. It is inferred that deposition of the coal measures took place primarily within alluvial settings dominated by large, low-sinuosity river systems with low-energy coal-forming environments The dominance of narrow and medium mesh form *Glossopteris* species and the lithology of the investigated locality indicate that the sediments belong to the Barakar Formation of Late Artinskian- Kungurian age (late lower Permian).

REFERENCES

Bhattacharya, H. N., Chakraborty, A., Bhattacharya, B. (2005) Significance of transition between Talchir Formation and Karharbari Formation in Lower Gondwana basin evolution—a study in West Bokaro Coal basin, Jharkhand, India. Journal of earth system science, v. 114(3), pp. 275-286.

Chandra, S., Surange, K. R. (1979) Revision of the Indian species of Glossopteris. Monograph 2, (Lucknow: Birbal Sahni Institute of Palaeobotany), pp. 1- 291.

Equeenuddin, S.K. Md., Tripathy S., Sahoo P. K., Ranjan A. (2016). Geochemical characteristics and mode of occurrence of trace elements in coal at West Bokaro coalfield. Int J Coal Sci Technol, v. 3(4), pp. 399–406.

Goswami, S., Saxena, A., Singh, K. J., Chandra, S. and Cleal, C. J. (2018) An appraisal of the Permian palaeobiodiversity and geology of the Ib-River Basin, eastern coastal area, India. Journal of Asian Earth Sciences, v. 157, pp. 283- 301.

Gupta, A. (1999) Early Permian Palaeoenvironment in Damodar Valley Coalfields, India: an Overview. Gondwana Research, v. 21, pp. 149-165.

Khan, Z.A., Tewari, R. C. (1991) Net subsidence and number of cycles; their interrelationship in different Permian Gondwana basins of peninsular India. Sedimentary Geology, v. 73, pp. 161-169.Lele, K. M. (1973) Studies in the Talchir flora of India-10. Early and Late Talchir microfloras from the West Bokaro Coalfield, Bihar.

Navale, G. K. B., Saxena R. (1989) An appraisal of coal petrographic facies in Lower Gondwana (Permian) coal seams of India. International Journal of Coal Geology, v. 12 (1- 4), pp. 553-588.

Raja Rao, C. S. (1987) Coalfields of India, Bull. Geol. Surv. India, Series A 45, pp. 61-122.Singh, S. M. (2000a) Glossopteris flora from the Early Permian of Karanpura & Bokaro Coalfields, India. Geophytology, v. 29 (1,2), pp. 69- 80.

Singh, S. M. (2000b) On the genera *Pantophyllum*, *Euryphyllum* & *Kawizophyllum* from Karanpura & Bokaro Coalfields, India. Palaeobotanist, v. 49, pp. 31- 42.Singh, S. M. (2000c). Taxonomy and diversity of the genus *Glossopteris*. Palaeobotanist, v. 49 (3), pp. 333- 352.

Singh, S. M. (2000d) On the species of genus *Glossopteris* from Barakar Formation of Karanpura and Bokaro Coalfields, India. Palaeobotanist, v. 49 (3), pp. 409- 441.

Singh, S.M., Maheshwari, H. K. (2000) On the species of genus *Glossopteris* from Barakar Formation of Karanpura & Bokaro Coalfields, India. Palaeobotanist, v. 49 (3), pp. 409- 441.

Surange, K. R., Singh, P., Srivastava, P. N. (1953) Megaspores from the West Bokaro Coalfield (Lower Gondwanas) of Bihar.

Tiwari, A. K., Singh, P. K., Mahato, M. K. (2014) GIS-Based Evaluation of Water Quality of Groundwater Resources in West Bokaro coalfield, India. Current World Environment, v. 9(3), pp. 843-850.

Turland, N. J., Wiersema, J. H., Barrie, F.R., Greuter, W., Hawksworth, D. L., Herendeen, P. S., Knapp, S., Kusber, W. H., Li, D. Z., Marhold, K. May, T. W. (2018) International Code of Nomenclature for algae, fungi, and plants (Shenzhen Code) adopted by the Nineteenth International Botanical Congress Shenzhen, China, July 2017. Koeltz Botanical Books.

Varma, A. K., Hazra, B., Samad, S. K., Panda, S. Mendhe, V. A. (2014) Methane sorption dynamics and hydrocarbon generation of shale samples from West Bokaro and Raniganj basins, India. Journal of Natural Gas Science and Engineering, v. 21, pp. 1138-1147.

VISTAS IN GEOLOGICAL RESEARCH
Special Publication in Geology (18), March 2023, pp. 117-125

Alteration in Ghutrigaon Chromite from the Singhbhum Craton

ASISH KUMAR DAS, SOMNATH KHAOASH, PATITAPABAN MISHRA AND BIRENDRA KUMAR MOHAPATRA

Ravenshaw University, Cuttack

Abstract: The Chromite occurrences of Ghutrigaon, Dhenkanal district of Odisha, shares a unique position in the mineral map of the country because of its sedimentary genealogy which is a significant departure from the well-established orthomagmatic deposits of the world. The Ghutrigaon chromite grains are usually homogenous and have distinct compositional range. However, some grains are found altered. Alteration is irregular, usually consisting of two optical zones (bright and dull). Mostly, the larger chromite grains exhibit a core of high reflectivity (brighter zone) encrusted by peripheral zone of low reflectivity (dull zone). The alteration in Ghutrigaon Chromite is in stark contrast to other chromiferous ores reported from different parts of the world where the chromite grain shows margins of higher reflectivity. These two zones are not uniformly developed, and show wavy to irregular outlines. Sometimes, the brighter zone appears skeletal, single or in multiple patches.

The altered chromite from Ghutrigaon is heterogeneous and demonstrates a different compositional trend. There is significant increase in Fe from the peripheral zone (avg. FeO ~19 %) to the core zone (avg. FeO ~24%). Cr also increases in the same order (avg. Cr_2O_3 ~52% in the periphery to 56% at the core). The alteration of chromite in the present set-up roughly indicates the results of compositional zoning. The zoned chromite shows aluminum trend where the concentration of Al, Mg, Mn and Co are the highest in the peripheral zone, while Cr and Fe are enriched in the core zone of the spinel.

From the difference in their composition, it is suggested that such zoning might have developed due to alteration of chromite through solid-state diffusion in which Mg-Al diffuse out of the core region and Fe ions diffuse into the core.

Keywords: Altered Chromite, Ghutrigaon, Singhbhum Craton

1. INTRODUCTION

The Singhbhum Craton in eastern India is one of the four significant cratonic nuclei in the Indian Shield (Radhakrishna and Naqvi, 1986; Saha, 1994), which contains several chromitite- bearing layered ultramafic bodies within the Archean greenstone belts (Acharya, 1993; Mondal et al., 2002). The Boula-Nuasahi Igneous Complex and the Sukinda Ultramafic Belt are the two main repositories of chromite in Odisha. Chromite deposits of Ghutrigaon, is unique of its kind for its sedimentary origin. The occurrence of chromite in Ghutrigaon was first brought to light in 1949 by the prospecting division of Tisco, presently known as Tata

Steel. Prasad Rao from Geological Survey of India carried out systematic mapping of the area during 1951-52. The study area forms a part of the Survey of India Toposheet No. F45N12 wherein Ghutrigaon (21^0 07'30''Latitude - 85^0 35'30'' Longitude) is a tiny village nestled amidst hills and forest in the Dhenkanal-Keonjhar district boundary of Odisha (Fig 1). It is situated within the Iron Ore Group in close proximity to the Rengali Province.

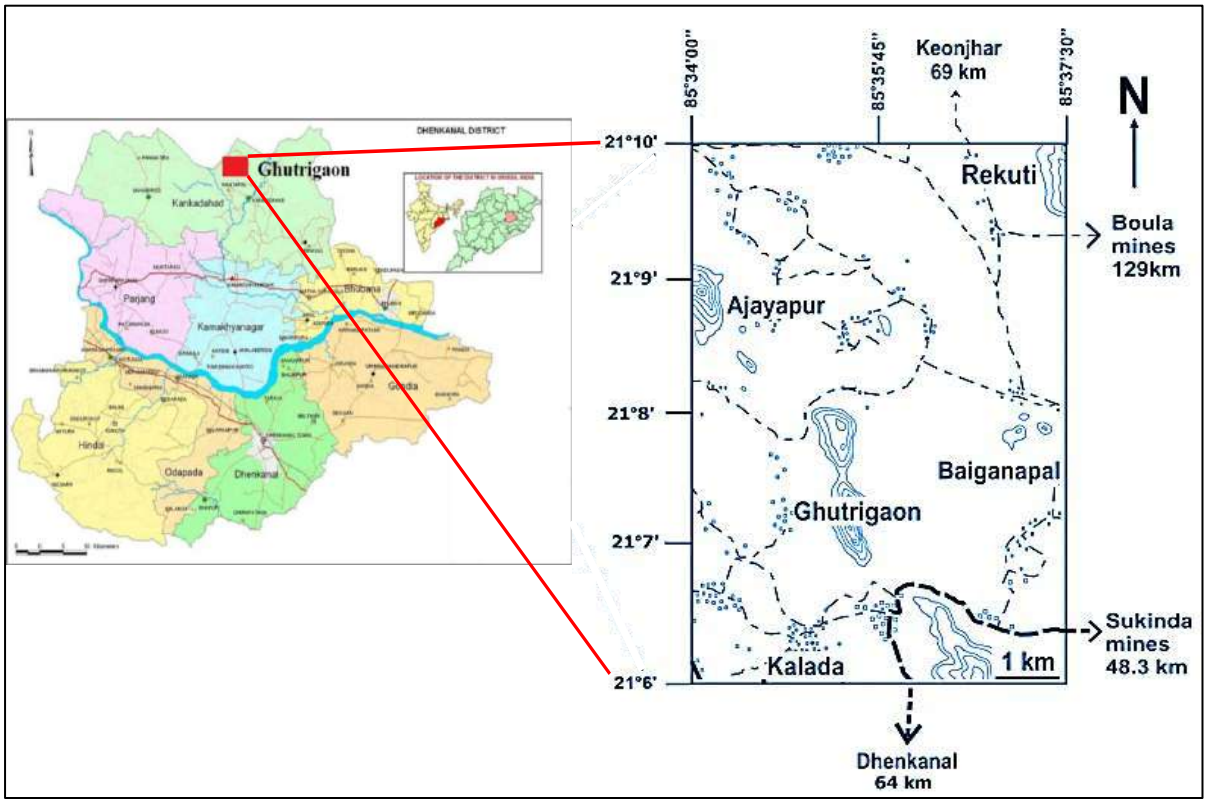

Fig. 1: Location map of Ghutrigaon, Dhenkanal district, Odisha, Eastern India. (Survey of India, Toposheet no F45N12).

Two major lithounits such as Chromite bearing Quartzite/ Fuchsite Quartzite and volcanic tuff, occupy a major part of the study area. Sporadic occurrence of chromite outcrop is observed, while a large part of the mineralization is covered under scree. Mostly, the chromite is associated with quartzite/ fuchsite quartzite and occurs as bands of variable thickness (Fig 2 A). Often some bands coalesce with other bands or peter out (Fig 2 B).

Nature of chromite mineralisation, petrographic characteristics, and mineral assemblages at Ghutrigaon was recently reported by Das et al. (2021). Chromite grains are in general, homogenous, irregular in shape with wavy outlines. However, some spinel show variation in its reflectivity from core to peripheral region. Nature of such variation, compositional difference if any and reason thereof are the major focus of the present research article. Alteration is only recorded under the reflected light microscope. Although few grains show alteration, the author examined the detailed petrography and microscopic study of such altered grain and attempted to establish the genesis of such alteration.

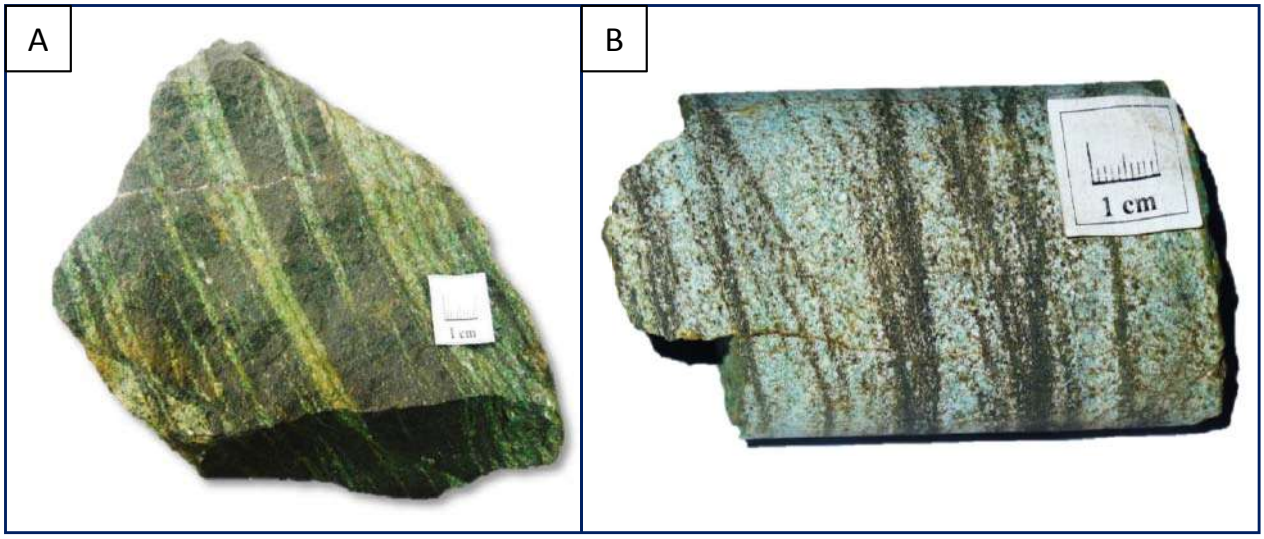

Fig. 2: Representative Ghutrigaon Chromite bearing rock
A. Surface sample **B**. Core Sample

2. NATURE OF ALTERATION

The alteration is revealed by chromite grains that show a core of high reflectivity (brighter zone) encrusted by a periphery of low reflectivity (dull zone). This is in stark contrast to other chromiferous ores reported from different parts of the world where the chromite shows margins of higher reflectivity, and core of low reflectivity. Some of the pioneer workers who reported the alteration behaviour of chromite are: Augustithis (1960), Irvin (1967), Hutchison (1972), Bliss and MacLean (1975), Barnes (2000). Variation in reflectivity in the core region is either confined to a localised area or appear in multiple areas as shown in Fig 3. Under high magnification (SEM), some of the bright core regions are found to be fractured.

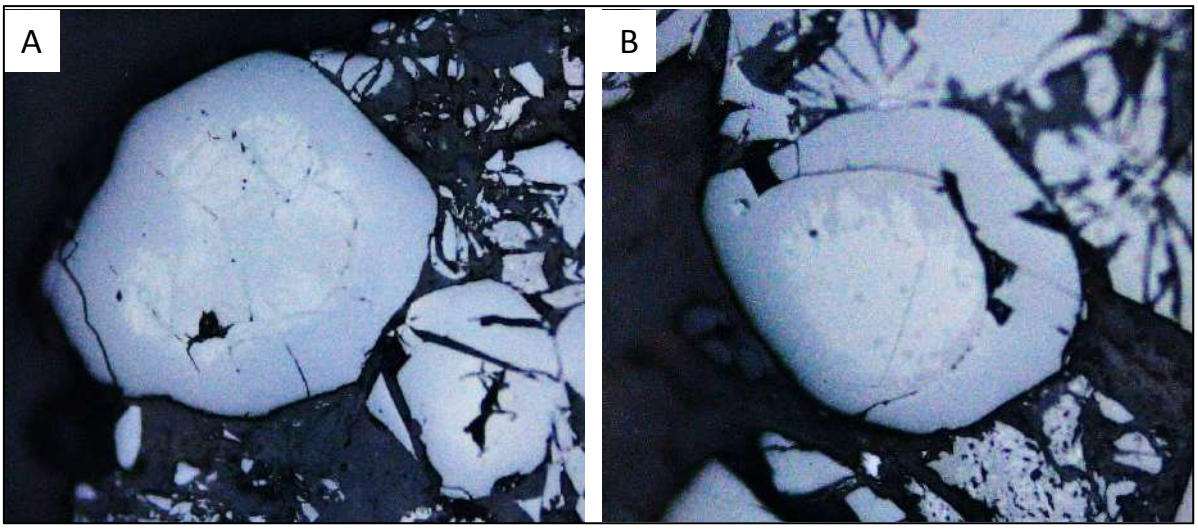

Fig. 3: Optical micrographs of zoning observed chromite.

3. PETROGRAPHY OF ALTERED CHROMITE GRAINS

Under reflected light microscope, alteration in some chromite grains is distinctly observed from optical zoning. Such grains are sub-rounded/ spheroidal/ irregular/ rectangular/ euhedral/ prismatic in shape and vary in size between 100 to 300 µm. The optical zoning is irregular, and consists of two zones (bright and dull). These two zones are not uniformly developed in all the samples. These zones are dissimilar in size and may be more complex (multiple bright zones) in some samples.

The periphery of the chromite grains is homogenous with uniform and low reflectance, grey in colour, whose boundaries with the bright zone is wavy and irregular. The core zone shows high reflectance. Often, a low reflectance host encloses an irregular shaped higher reflectance bleb. Irregular and patchy pattern of zoning is also observed. In some grains, the bright zone appears skeletal, single or in multiple patches. Some chromite core is fractured and the fracture is filled with low reflective zones.

4. PETROCHEMISTRY OF ALTERED CHROMITE GRAINS

The two zones observed in chromite grains are found to be compositionally different (Fig 4). Compositional difference between bright and dull zone as determined from in-situ EPMA analysis are given in Table 1 and their average values are presented graphically in histogram (Fig 5). Typically, the periphery of chromite is poor in Cr and Fe and enriched in Al, Mg and Mn with respect to the core that it surrounds (Fig 6).

The X-ray image map of typical chromite grains confirm difference between the two zones. Presence of two phases such as aluminous chromite and chromite are recorded and broadly the aluminous chromite is followed by ferrian chromite in the core showing higher reflectivity.

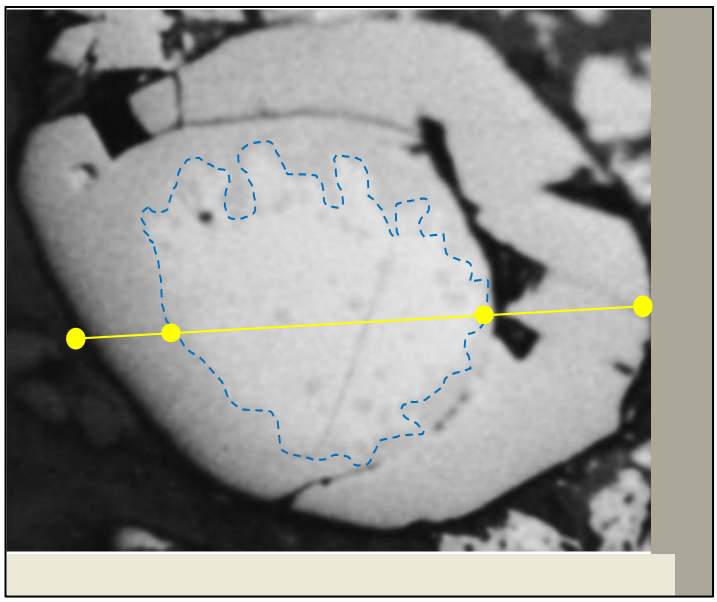

Fig 4: Line Scanning of Altered Chromite.

Table 1: In-situ EPMA results of bright and dull zones in altered chromite grain.

	Periphery (Darker zone 1)			Core (Brighter zone)				Periphery (Darker Zone 2)			Avg. Brighter Zone	Avg. Darker Zone
Points	**1**	**2**	**3**	**4**	**5**	**6**	**7**	**8**	**9**	**10**		
Cr_2O_3	51.82	53.31	52.92	56.62	56.25	56.4	57.55	53.84	52.67	53.62	56.71	53.03
FeO	19.34	21.64	21.89	26.54	26.64	25.04	23.28	19.46	20.54	18.91	25.38	20.30
Al_2O_3	12.11	11.19	10.74	7.98	8.84	9.18	10.54	11.68	12.46	11.27	9.14	11.58
MgO	8.32	6.87	6.58	1.36	2.68	2.62	3.98	7.51	7.46	8.23	2.66	7.50
MnO	2.63	2.67	2.32	0.84	0.88	1	0.11	2.45	2.11	2.36	0.71	2.42
CoO	0.18	0.17	0.13	0.09	0.08	0.06	0.07	0.15	0.17	0.14	0.08	0.16
NiO	0.03	0.15	0.25	0.17	0.47	0.32	0.46	0.19	0.24	0.21	0.36	0.18
V_2O_3	0.19	0.14	0.19	0.16	0.14	0.2	0.11	0.16	0.17	0.14	0.15	0.17

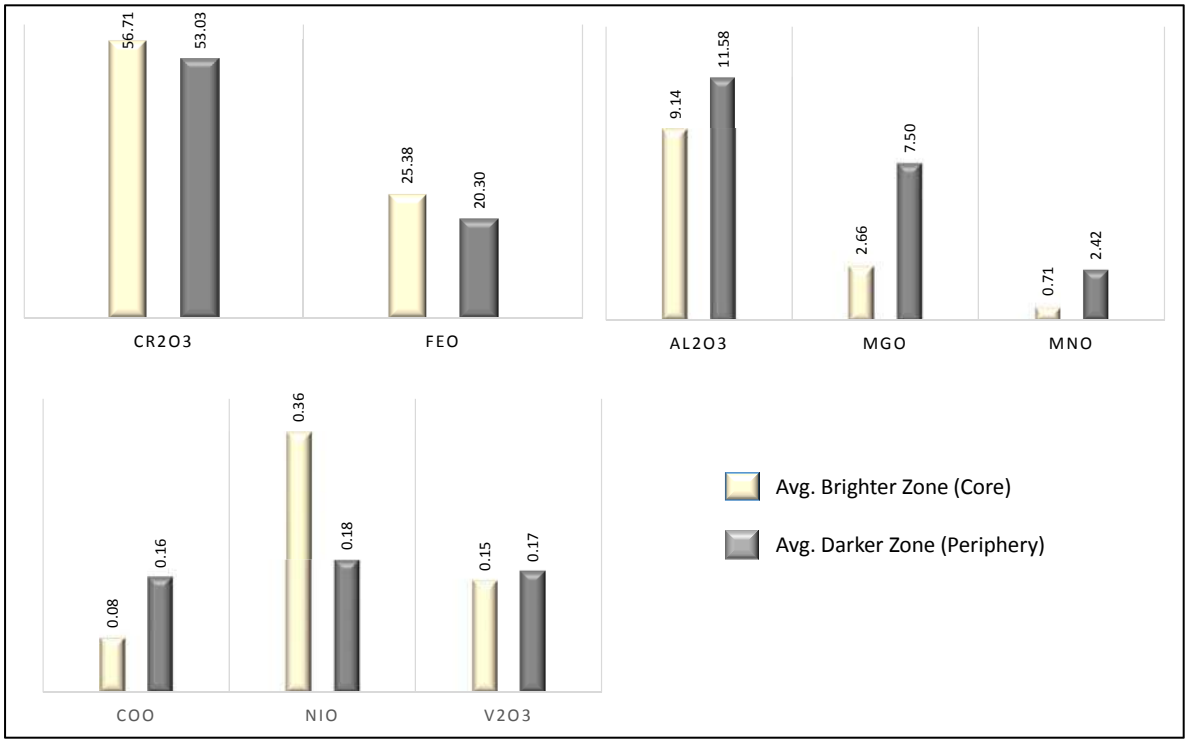

Fig. 5: Average compositional variation between core and periphery of altered chromite.

The behaviour of some selective elements in the two different zones are discussed below.

4.1 Nature of Cr & Fe: The two zones in chromite grains show distinct difference in Cr and Fe distribution. The increase in the reflectivity in the core region may be attributed to the increase in Cr-Fe content. Chemically, (i) there is a significant increase in Fe content from the peripheral zone of dull zone (avg. FeO ~20 %) to the core zone in high reflective phase (avg. FeO ~25%), (ii) Cr also increases in the same order (avg. Cr_2O_3 ~53% in the periphery to 56% in the core zone) (Fig 6).

4.2 Nature of Al & Mg: Appreciable aluminium (avg. ~11%) is recorded in the dull peripheral zone while it is relatively lower in concentration in the brighter core zone (avg. ~9%). Appreciable magnesium (avg. ~7%) is present in the peripheral zone, while its concentration is poor in the bright zone (avg. ~2%) (Fig 6). X-ray image map of Mg show the peripheral dull zone to be enriched in Mg while the reflective bright zone is almost devoid of it.

4.3 Nature of Mn & Co: A characteristic chemical feature of the zoned chromite grain is the appreciable variation in the Mn and Co between the dull zone and the bright zone (Table 1, Fig 5). The graphical image map of Mn and Co (Fig 6) confirms its confinement to the peripheral zone and its impoverishment in the core zone.

4.4 Nature of Ni & V: Ni and V show minor difference between the bright and dull zones (Table 1). Appreciable amount of Ni is observed to be confined to the Core (Fig 5) while V show more or less similar distribution in both the zones (Fig 6).

5. GENETIC EVOLUTION

The chromite grains in Ghutrigaon is usually homogenous but some show alteration and appear heterogeneous. Such heterogeneous grains show compositional zoning. According to Haggerty (1976), there are two kinds of zoning: it could be called as iron trend or the aluminium trend. The iron trend is common in ultramafites but the aluminium trend is found in granulite belt. The zoned chromite in Ghutrigaon shows aluminium trend where the Al, Mg, Mn and Co content are relatively higher in the peripheral zone, while Cr and Fe are enriched in the core zone of the crystal.

The paragenesis of such zoning appears to be uncertain. One can extrapolate the possibility of such zoning considering the proposed views put forth by different authors on zoning of orthomagmatic chromite. The zoning in chromite has been attributed to (i) serpentinization (Golding and Bayliss, 1968; Beeson and Jackson, 1969; Snetsinger, 1973); (ii) magmatic reaction (Rost. 1968, Cerny, 1986;); (iii) regional metamorphism (Engin and Aucott 1971, Mitra 1972); (iv) alteration product of original chromite, (solid state diffusion in which Mg^{2+} and Al^{3+} diffuse out while iron ions diffuse in) (Simpson and Chamberlain 1967, Panagos and Ottemann, 1966; Beeson and Jackson, 1969); (v) an overgrowth nucleated on top of the original chromite.

ASISH KUMAR DAS, SOMNATH KHAOASH, PATITAPABAN MISHRA,
BIRENDRA KUMAR MOHAPATRA

Alteration may occur through dissolution, ion exchange, and precipitation and / or recrystallisation process. In the present case the contact between bright and dull zone is irregular. The reflective core often occurs as skeletal relicts within the dull zone. The dull zone often appears at the fracture plane of brighter phase in chromite grain. Considering the nature of optical and chemical zoning it may be suggested that the zoning could have developed due to alteration of original chromite through solid state diffusion in which Mg^{2+} and Al^{3+} diffuse out as iron ions diffuse in

.

REFERENCE

AUGUSTITHIS, S. S., (1960)., Alterations of chromite Ore-microscopic observation on chromite-ores from Rodiani, Greece., Neues Jahrb. Mineral.

BARNES, S. J., (2000) Chromite in komatiites, II. Modification during greenschist to mid amphibolite facies metamorphism. Journal of Petrology, v. 41, pp. 387–409.

BEESON M.H., JACKSON, E.D., (1969) Chemical composition of altered chromites from the Stillwater complex, Montana. Amer. Mineral. v. 54, pp. 1084-1100.

BLISS, N.W., AND MCLEAN, W.H., (1975) The paragenesis of zoned chromite from central Manitoba. Geochim. Cosmochim. Acta, v.39, pp. 973 - 990.

CERNY, P., (1986) Mineralized pegmatitic granites at Red Sucker Lake, Manitoba. - Manitoba Minerals Div. Rept. Field Activities. pp. 184–190.

DAS, A. K., KHAOASH, S., MISHRA, P., MOHAPATRA, B. K., MOHNATY, J. K., (2021)., Chromite-bearing quartzite in the southern fringe of Singhbhum Craton around Ghutrigaon, Eastern India: Petrogenetic implication, Geological Journal, V 56, I-7, pp. 3472-3496.

ENGINE, T., and AUCOTT, J.W., (1971) A microprobe study of chromites from the Andizlik-Zimparalik area, S. W. Turkey. Min. Mag.. v. 38, pp.76-82.

GOLDING, H. G. and BAYLISS, P., (1968) Altered chrome ores from the Coolac serpentine belt, New South Wales, Australia.Amer.Mineral., v.51, pp.75-98.

HAGGERTY, D., (1976) Opaque mineral oxides in terrestrial igneous rocks in oxide minerals (D.Rumble III ed.) Mineral. Soc. Amer. Rev. Miner., v.3, pp 101-300.

HUTCHISON, C. S., (1972) Alpine-type chromite in north Borneo, with special reference to Darvel Bay. Am. Mineral., v. 37,pp. 835-56.

IRVINE, T. N., (1967) Chromian spinel as a petrogenetic indicator. Part 2, Petrologic applications. Canadian Journal of Earth Sciences, v. 4, pp. 71-102.

MITRA, S., (1972) Metamorphic rims in chromites from Sukinda, Orissa, India. N.Jb. Miner. Mh. v. 8, pp. 360-375.

PANAGOS, A. & OTTEMANN, J., (1966) Chemical differentiation of chromite grains in the nodular chromite from Rodiani(Greece).Minerallium Deposita, v.1, pp. 72-75.

ROST F. (1968) Uber die Fazieseinstufung orogenotyper Peridotite und ihre Bezichungen zur Peridofitschale des Erdmantels. Proc. XXIII Int. Geol. Congr., v. 1, pp.187-196.

SIMPSON P. R. and CHAMBERLAIN J. A. (1967) Nickel distribution in serpentinites from Puddy Lake, Ontario. Proc. Geol. Assoc. Can. v. 18, pp. 67-91.

SNETSINGER K. G., (1973) Chromian aluminian magnetite and two rhodium alloys in a platinum nugget from Goodnews Bay, Alaska. Amer. Mineral. v. 58, pp. 189-194.

RADHAKRISHNA, B.P., NAQVI, S.M. (1986) Precambrian continental crust of India and its evolution. Jour. Geol. v. 94, pp. 145-166.

SAHA, A.K., (1994) Crustal evolution of Singhbhum North Orissa Eastern India. Mem. Geol. Soc. India, no. v. 27, pp. 341.

ACHARYYA, S.K., (1993) Greenstones from Singhbhum Craton, their Archaean character, oceanic crustal affinity and tectonics. Proc.Natl. Acad. Sci. India 63 (A), pp. 211–222.

MONDAL, S.K., GLASCOCK, M.D., RIPLEY, E.M., (2002) Characteristics of Cr-spinel and whole rock geochemistry of the Nuasahi Igneous Complex, Orissa, India. In: Proceedings of the Ninth International Pt-Symposium, Billings, Montana, Abstract with program, pp. 317–320.

VISTAS IN GEOLOGICAL RESEARCH
Special Publication in Geology (19), March 2023, pp. 126-133

Appraisal of Nature of Groundwater in Parts of Kalahandi District of Odisha, India through Statistical Analysis

NANDITA MAHANTA*, MADHUSMITA OJHA, H.K. SAHOO AND S. GOSWAMI

Department of Geology, Utkal University, VaniVihar, Bhubaneswar-751004
*Corresponding Author, E-mail: nandita.mahanta12@gmail.com

Abstract: Nature of groundwater of a region depicts the behavior of dissolved substances, geological processes and resultant hydrofacies. The activities of these substances influence the quality, distribution and movement of groundwater. The current research work aimed at the assessment of nature of groundwater in two blocks namely Dharmagarh and Golamunda of Kalahandi district of Odisha using statistical analysis. The former research and current analysis show that high fluoride concentration has been found mainly in these two blocks for which the study area has been chosen. As the study areas of Kalahandi district lie in the western part of Odisha that mostly comprises hard crystalline formation of Easternghat Supergroup, the hydrogeological set up and the behavior of different quality controlling parameters will vary considerably. Also, the activities of parameters can be assessed significantly using statistical approaches. The parameters such as pH, TH, Ca, Mg, Cl, SO_4 of Dharmagarh, EC, TDS of Golamunda block and TA, F and HCO_3 of both block show negative kurtosis indicating flat peak distribution compared to normal distribution pattern. All parameters of both blocks except pH of Dharmagarh block have positive skewness reflecting higher valued distribution. Comparatively, Golamunda block has more significant correlating coefficients ($\rho > 0.5$) than Dharmagarh block. PCA displays the extraction of five main factors explaining cumulative % variance of 78.99% and 77.512% in Dharmagarh and Golamunda block respectively. Regression analysis shows the significant contribution towards TDS of Ca, K, SO_4, Cl in the Golamunda block whereas Ca, F, HCO_3 in Dharmagarh block. This advanced proposed work has significant effect in the quality determination of water in the study region.

Keywords: Nature of groundwater, Hydrogeochemical approach, Statistical estimation

INTRODUCTION

The purest and reliable form of water that exists in the subsurface region is the groundwater. The exponential increase in use of the groundwater occurred when it shows its wide area of utility in different sectors such as agriculture, industries and domestic purpose (Molekao, et al., 2019).The behavior of groundwater has been assessed before easily in the shallow aquifers for which it is essential to analyze in the deeper sections with some holistic approaches as quality is as important as the quantity (Molekao, et al., 2019). There are various natural as well as anthropogenic means such as weathering, mining, urban set up, population growth land use pattern etc. which are responsible for the deterioration in the quality of groundwater. The utility of groundwater for specific purpose needs the physical, chemical and biological characteristics of the dissolved constituents to be within certain

thresholds regarded as the permissible limits (Swain, S., Sahoo, S., and Taloor, A. K. 2022). Several parts of world have suffered from water quality deterioration and most of the western parts of Odisha show the quality as well as quantity degradations Current study focused to assess the behaviour of dissolved substances in the groundwater with a qualitative approach of statistics in two western most blocks Dharmagarh and Golamunda of Kalahandi district of Odisha, India.

STUDY AREA

Kalahandi district lies in the South western part of Odisha. The study region includes two blocks such as Dharmagarh and Golamunda located in the western margin of the district. Dharmagarh block stretches between 19°42’15’’ to 19°57’15’’ North latitudes and 82°37’15’’ to 82°52’02’’ East longitudes and Golamunda block extended between 19°54’ to 20°10’ North latitudes and82°44’ to 83°5’ East longitudes covering an area of about 382.45 km² and 595.99 km² respectively. It falls on the Survey of India toposheet nos. 65I9, 65I13, 65I14, 64P4, 65M1, 64L16 and 64L12. The Golamunda block is surrounded in the north by Balangir district and Bhawanipatna block, in the east by Bhawanipatna and Junagarh blocks, in the south by Dharmagarh block and parts of Chhattisgarh state and in the west by Nuapada district whereas Dharmagarh block is surrounded in the north by Golamunda block, in the east by Junagarh block, in the south by Jaypatna and Koksara blocks and in the west by Chhattisgarh state. (Groundwater Information Booklet, 2013).

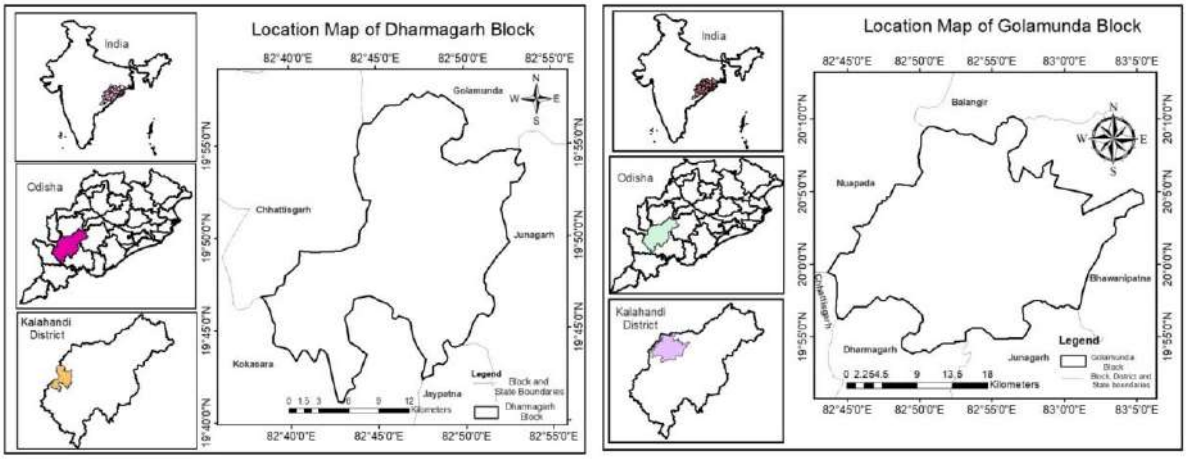

Fig.1: Location Map of Dharmagarh and Golamunda blocks of Kalahandi district, Odisha, India.

MATERIALS AND METHODS

Thirty four and thirty seven water samples were collected in the year 2020 with GPS recorded coordinates from different regions of Dharmagarh and Golamunda blocks respectively in Post-monsoon period following APHA, 1998 standard procedures. Physical parameters such as pH, EC, TDS and Temperature were measured in the field with the help of a multi-parameter water analysis kit. Total hardness in terms of calcium and magnesium hardness and total alkalinity in terms of carbonate and bicarbonate were determined through

the titration method. The Ca^{2+} and Mg^{2+} were analysed by titrating with standard EDTA. The Na^{+} and K^{+} were determined by flame photometer, and F^{-} was estimated by fluorimeter. Chloride was determined titrimetrically using standard $AgNO_3^{-}$ solution. SO_4^{2-} and NO_3^{-} were also determinedby titration method. For qualitative approach, the univariate, bivariate and multivariate statistical analyses were done. All statistical parameters were computed in SPSS software.

RESULTS

Hydro-parameter analysis

The nature of water depicts its characteristic through the behaviour of the dissolved constituents. In Dharmagarh and Golamunda blocks, pH values (mean; 6.8) of the samples indicate slightly less than the neutral value (BIS 2012, WHO 2017). Temperature of the water samples though have not so prominent effect still has minor physical and chemical impact such as change in the reaction rate. TDS and EC concentrations of the water samples indicate the concentrations of the dissolved substances in the water samples. The order of cation and anion concentrations within the water samples of Golamunda block are $Ca^{2+} > Na^{+} > Mg^{2+} > K^{+}$ and $HCO_3^{-} > SO_4^{2-} > Cl^{-} > NO_3^{-} > F^{-}$ and of Dharmagarh block are $Na^{+} > Ca^{2+} > Mg^{2+} > K^{+}$ and $HCO_3^{-} > Cl^{-} > SO_4^{2-} > NO_3^{-} > F^{-}$ respectively as shown in the fig.2.

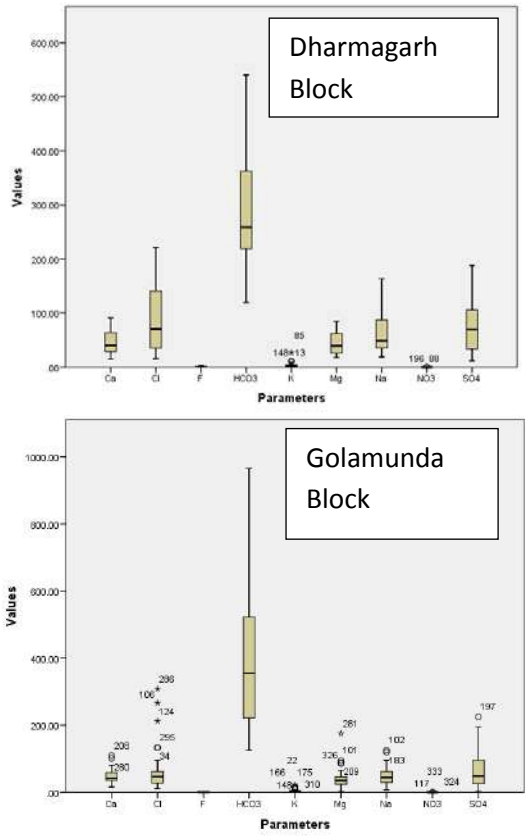

Fig. 2: Showing the order of distribution of cations and anions in the groundwater of Dharmagarh and Golamunda blocks, Odisha.

HYDROGEOCHEMISTRY

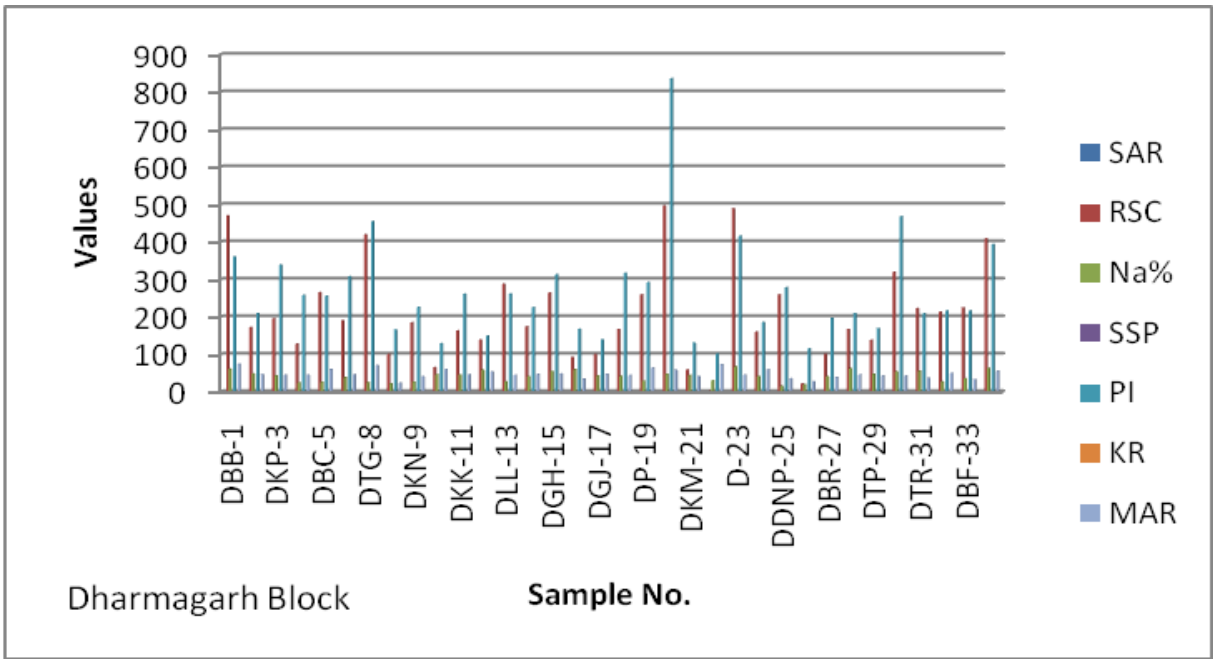

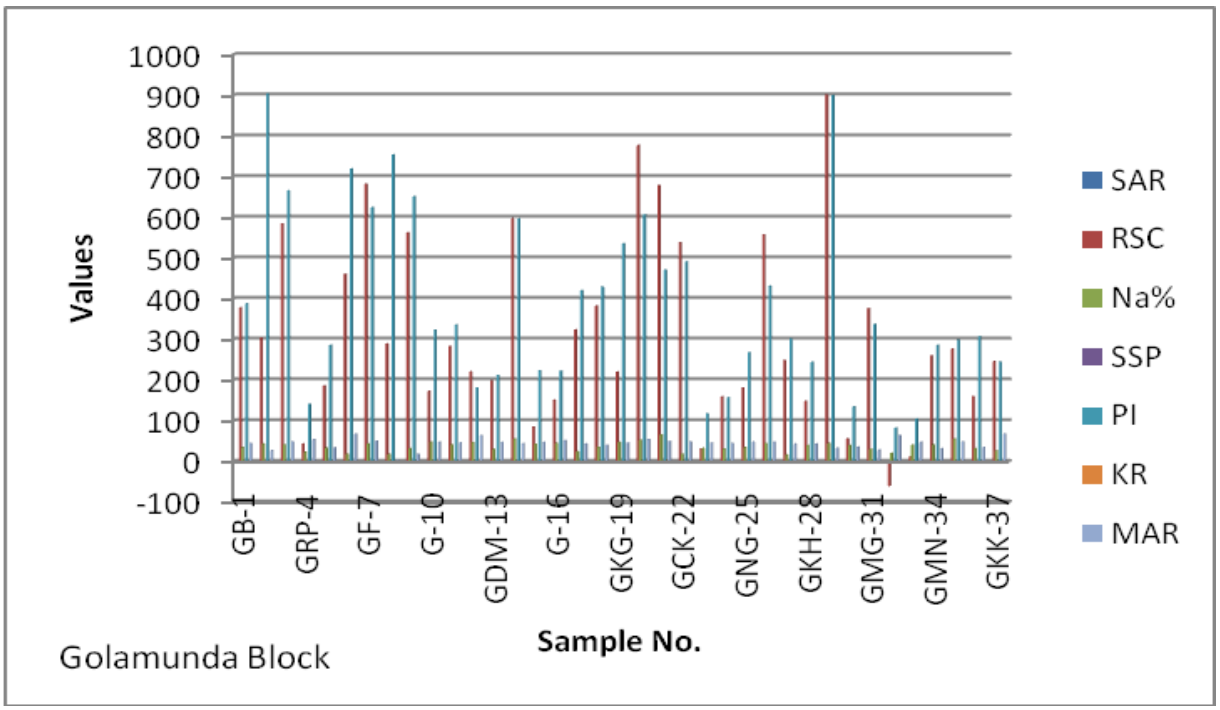

Fig. 3: showing distribution of different quality defining parameters for different purposes of Dharmagarh and Golamunda blocks.

STATISTICAL ANALYSIS

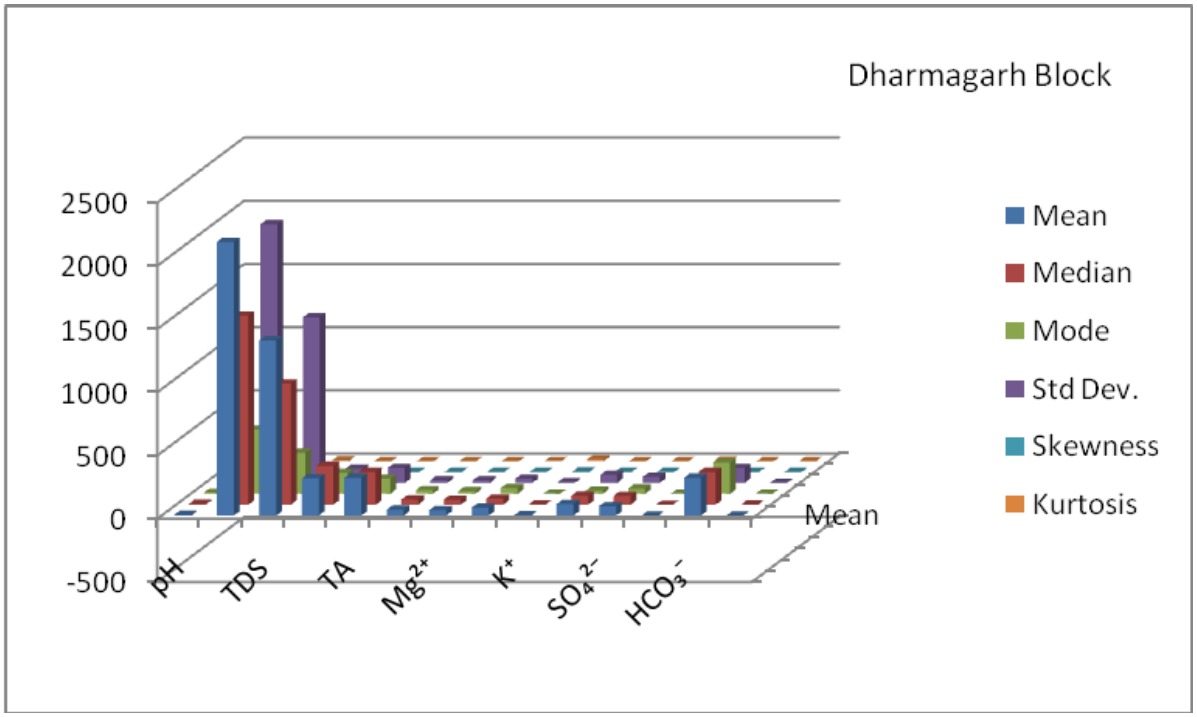

Fig. 4a: Univariate distribution of parameters in Dharmagarh Block.

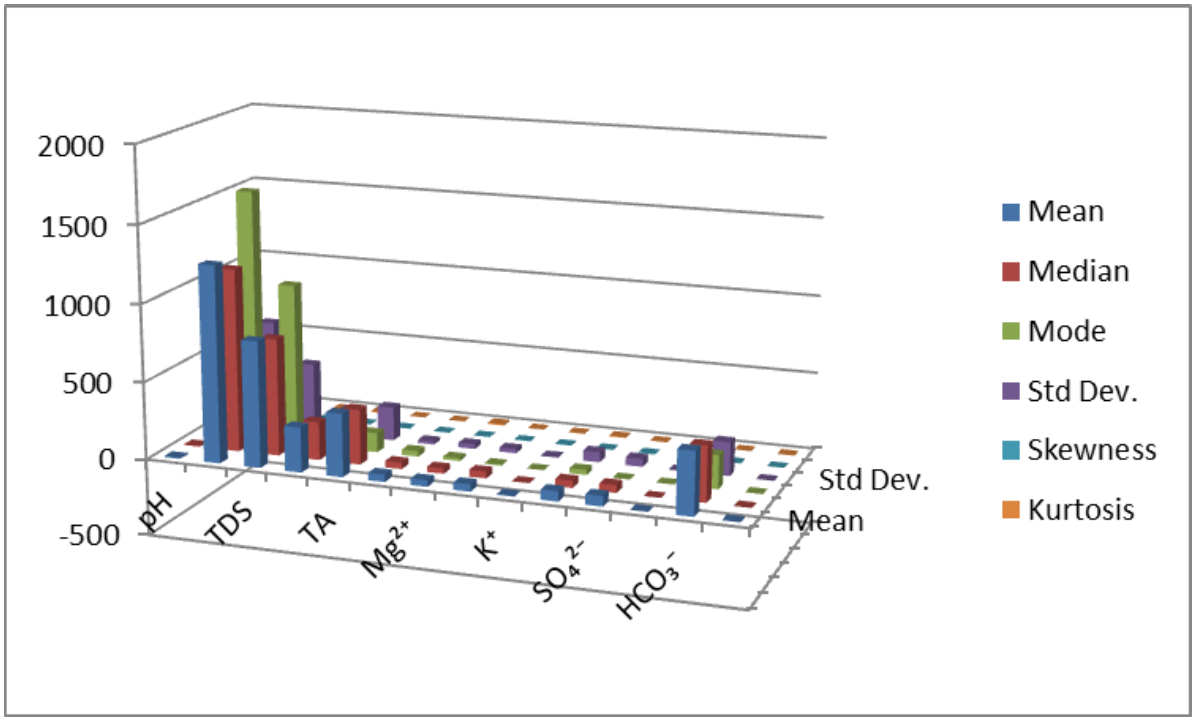

Fig. 4b: Univariate distribution of parameters in Golamunda Block.

a)	pH	EC	TDS	TH	TA	Ca^{2+}	Mg^{2+}	Na^{+}	K^{+}	Cl^{-}	SO_4^{2-}	NO_3^{-}	HCO_3^{-}	F^{-}
pH	1													
EC	**0.107**	1												
TDS	**0.107**	**1.000****	1											
TH	-0.247	-0.114	-0.114	1										
TA	-0.001	-0.184	-0.184	-0.096	1									
Ca^{2+}	-0.048	-0.234	-0.234	**.711****	-0.261	1								
Mg^{2+}	-0.303	-.002**	-0.002	**0.89**	**0.04**	**0.313**	1							
Na^{+}	**0.065**	**0.044**	**0.044**	**0.16**	**0.068**	**0.038**	**0.192**	1						
K^{+}	-0.319	**0.203**	**.203****	**0.368**	-0.218	**0.089**	**0.44**	**0.212**	1					
Cl^{-}	-0.241	-0.129	-0.129	**0.229**	-0.223	**0.33**	**0.095**	-0.113	**0.222**	1				
SO_4^{2-}	-0.56	-0.078	-0.078	**.079****	-0.221	**0.034**	**0.085**	-0.131	**0.158**	**0.148**	1			
NO_3^{-}	-0.545	**.048****	**0.048**	**0.278**	-0.386	**0.065**	**0.334**	-0.079	**0.516**	**0.355**	**0.742**	1		
HCO_3^{-}	-0.001	-0.184	-0.184	-0.096	**1**	-0.261	**0.04**	**0.068**	-0.218	-0.223	-0.221	-0.386	1	
F^{-}	**0.313**	**0.162**	**0.162**	**0.074**	**0.086**	**.000****	**.100****	**0.392**	-.104*	-0.217	-0.086	-0.2	**0.086**	1

Fig. 5a. Correlation Coefficient of different variables in the collected groundwater samples of Dharmagarh.

b)	pH	EC	TDS	TH	TA	Ca^{2+}	Mg^{2+}	Na^{+}	K^{+}	Cl^{-}	SO_4^{2-}	NO_3^{-}	HCO_3^{-}	F^{-}
pH	1													
EC	-.223	1												
TDS	-.223	**1.000****	1											
TH	**.241**	**.217**	**.217**	1										
TA	**.010**	-.010	-.010	-.145	1									
Ca^{2+}	**.312**	**.269**	**.269**	**.821****	-.109	1								
Mg^{2+}	**.187**	**.174**	**.174**	**.971****	-.144	**.662****	1							
Na^{+}	**.270**	**.146**	**.146**	**.462****	**.184**	**.368***	**.453**	1						
K^{+}	**.112**	**.127**	**.127**	-.098	**.130**	-.127	-.076	-.032	1					
Cl^{-}	**.012**	**.236**	**.236**	**.592****	-.082	**.246**	**.674**	**.426**	-.115	1				
SO_4^{2-}	**.110**	**.328***	**.328***	**.133**	**.013**	**.144**	**.115**	-.100*	-.121*	**.123**	1			
NO_3^{-}	**.257**	-.080	-.080	**.173****	-.042	**.086**	**.192****	-.050*	-.098	**.003**	**.110**	1		
HCO_3^{-}	**.010**	-.010	-.010**	-.145	**1.000**	-.109	-.144	**.184**	**.130****	-.082	**.013**	-.042	1	
F^{-}	**.347**	**.092****	**.092**	**.516**	**.224**	**.553**	**.447**	**.540****	-.117	**.042**	-.011	**.003**	**.224**	1

Fig. 5b. Correlation Coefficient of different variables in the collected groundwater samples of Golamunda.

**. Correlation is significant at the 0.01 level (2-tailed).
*. Correlation is significant at the 0.05 level (2-tailed).

Regression Analysis

TDS(Dharmagarh)=3146.314-17.155Ca^{2+} -.187Mg^{2+} -3.703Na^{+} +61.403K^{+} - 2.891HCO_3^- - 4.788SO_4^{2-} -2.074Cl^- +689.628 NO_3^- +440.303F^-

TDS (Golamunda) = 235.193 + 7.605 Ca^{2+} -5.415 Mg^{2+} + .620 Na^{+} + 19.753 K^{+} -.111 HCO_3^- + 2.759 SO_4^{2-} + 2.458 Cl^- -162.897 NO_3^- + 41.321 F^-

Principal Component Analysis

a)

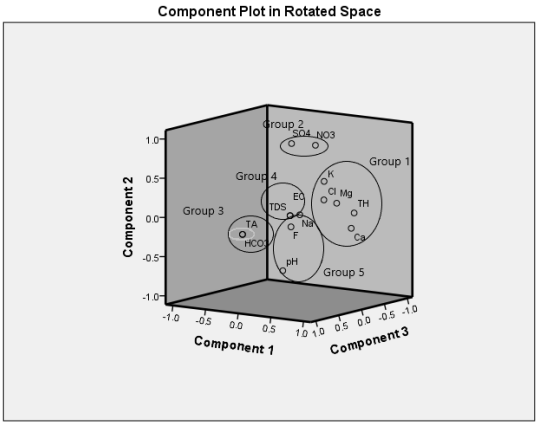

b)

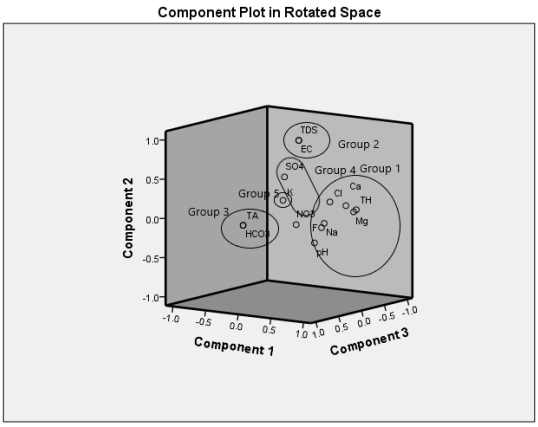

Grouping of parameters on the basis of the common characteristics of the Fig.5a) Dharmagarh and Fig.5b) Golamunda Blocks

DISCUSSION AND CONCLUSION

From the above analysis it can be concluded that on the basis of EC and TDS values, 17 and 9 regions of Dharmagarh block,28 and 1 regions of Golamunda blockindicate the initiation of problem andsevere problemrespectively. Groundwater from Golamunda and Dharmagarh blocksarehard and very hardtype. Fluoride concentration shows higher (>1.5mg/l) in 10 and 11 samples of the Dharmagarh and Golamunda blocks respectively (BIS 2012, WHO 2017).

F^- is strongly correlated withCa^2, Mg^{2+} in Dharmagarh region and with EC, Na^+ in Golamunda regionrespectively as shown in the fig.5a and 5b. The sequenceshown in the fig.2 bycations and anionsinn the groundwater of the respective proposed regions may be due to the intermixing of agricultural, pesticides and anthropogenic sources with the groundwater. Hydrogeochemical evaluation along with statistical approaches has proven more convenient to detect the water chemistry and the behaviour of dissolved contents for various purposes.

REFERENCES

APHA (1998) Standard Methods for the Examination of Water and Wastewater. 20th Edition, American Public Health Association, American Water Works Association and Water Environmental Federation, Washington DC.

Bureau of Indian Standards (2012) Indian standard drinking water-Specification (Second revision), IS 10500:2012.

Groundwater information booklet (2013) Ministry of Water resources, CGWB, SER

Molekoa, M.D., Avtar, R., Kumar, P., Minh, HVT. and Kurniawan, TA. (2019) Hydrogeochemical Assessment of Groundwater Quality of Mokopane Area, Limpopo, South Africa Using Statistical Approach.*Water*; 11(9):1891**.** https://doi.org/10.3390/w11091891

Swain, S., Sahoo, S. and Taloor, A. K. (2022) Groundwater quality assessment using geospatial and statistical approaches over Faridabad and Gurgaon districts of National Capital Region, India.Applied Water Science,12(4), 75.

World Health Organization (2017) Global diffusion of Health: making universal health coverage achievable: report of the third global survey on Health. World Health Organization.

VISTAS IN GEOLOGICAL RESEARCH
Special Publication in Geology (19), March 2023, pp. 134-141

Hydrochemical Facies and Groundwater Quality Assessment for Drinking Purpose in Kaniha Block, Angul District, Odisha

PRAGNYA PARAMITA DAS[1] AND NANDITA MAHANTA[2]*

[1]Department of Earth Sciences, Sambalpur University, JyotiVihar, Burla-768019
[2] Department of Geology, Utkal University, VaniVihar, Bhubaneswar-751004
*Corresponding Author, E-mail: nandita.mahanta12@gmail.com

Abstract: The present investigation is aimed to study the hydro-chemical facies and groundwater quality assessment for drinking purpose in Kaniha Block, Angul district, Odisha. Altogether 81 numbers of groundwater samples were collected from different tube wells and dug wells from the study area in Pre-monsoon season, 2022 and were analyzed for various physico-chemical parameters by following the standard analytical techniques.Average cation and anion chemistry stands in the orders of Ca^{2+}> Na^{+}> Mg^{2+} > K^{+} and HCO_3^{-}> Cl^{-}>SO_4^{2-}>NO_3^{-}respectively. The analytical results were evaluated in detail and compared with BIS 2012. The comparisons showed that majority of the samples are within the permissible limits except 4. The fluoride content is above the maximum permissible limit in these few locations. The analytical data was plotted in Gibbs diagram and Piper's diagram.The Piper plot indicates that Ca^{2+}-HCO_3^{-} is the dominant hydrogeochemical facies of the study area. Gibbs diagram shows that the samples are plotted in "rock dominance" field which indicate that the chemistry of the water is governed by rocks of that particular area.) On the basis of EC value, almost all the groundwater samples of the study area fall under the Type-I category (low salt enrichment except two samples which fall under the Type-II Category (medium salt enrichment). Moreover, it is found that in most part of the study area, the groundwater can be used for drinking purpose.

Key words: Fluoride contamination, Kaniha Block, Piper diagram

INTRODUCTION

Water is most precious natural resource on the earth. Plants, animals, and human beings all need water to survive. Water is a key resource of drinking, agriculture, industry and natural ecosystem. Groundwater is an important and vital component of our life support system which contributes 98% of drinking water resources on earth. There are several states in India where more than 90% of the population are dependent on ground water for drinking and other purposes. Due to tremendous increasing demand of groundwater, it is very necessary to assess the groundwater resources and manage the resource strategically. For the proper management of groundwater resources, proper understanding of the hydrogeological processes and regular monitoring of water quality are essential for sustainable development and effective management of groundwater resource. As the water quality directly affects human health, Bureau of Indian Standards (BIS, 2012) prescribed the standard limits for

different chemical variables for drinking purpose. The chemistry and quality of groundwater depends upon the type of geological formations, geochemical reactions and impacts of human activities. The objective of the present study is an attempt to study the hydrochemical facies and groundwater quality assessment in the Kaniha block, Angul district of Odisha.

STUDY AREA

The Kaniha block is situated on the northeastern part of the Angul district having geographical area of about 664.4 sq.km.The block lies between north latitude 21°00´47.942″and 21°15´10.896″ and east longitude 84°56´41.571″ and 85°12´35.663″, falling in Survey of India toposheetno.73G/4,73G/3,73C/15, 73C/16. The nearest town is Talcher. The area experiences the sub-tropical to tropical temperate monsoon climate. The south-west monsoon is the principal source of rainfall in the area. The average annual rainfall of the area for last 20 years is 1163.00 mm. The area of the block is characterised by both table landform as well as undulating topography. Elevations of the area vary between 72 m to 125 m above mean sea level. The general slope of the ground is from west to east. The main drainage is controlled by the Brahmani River through the Tikra jhora, Singhada jhora and Bhalutungri nala. The location map of the study area s given in Fig. 1.

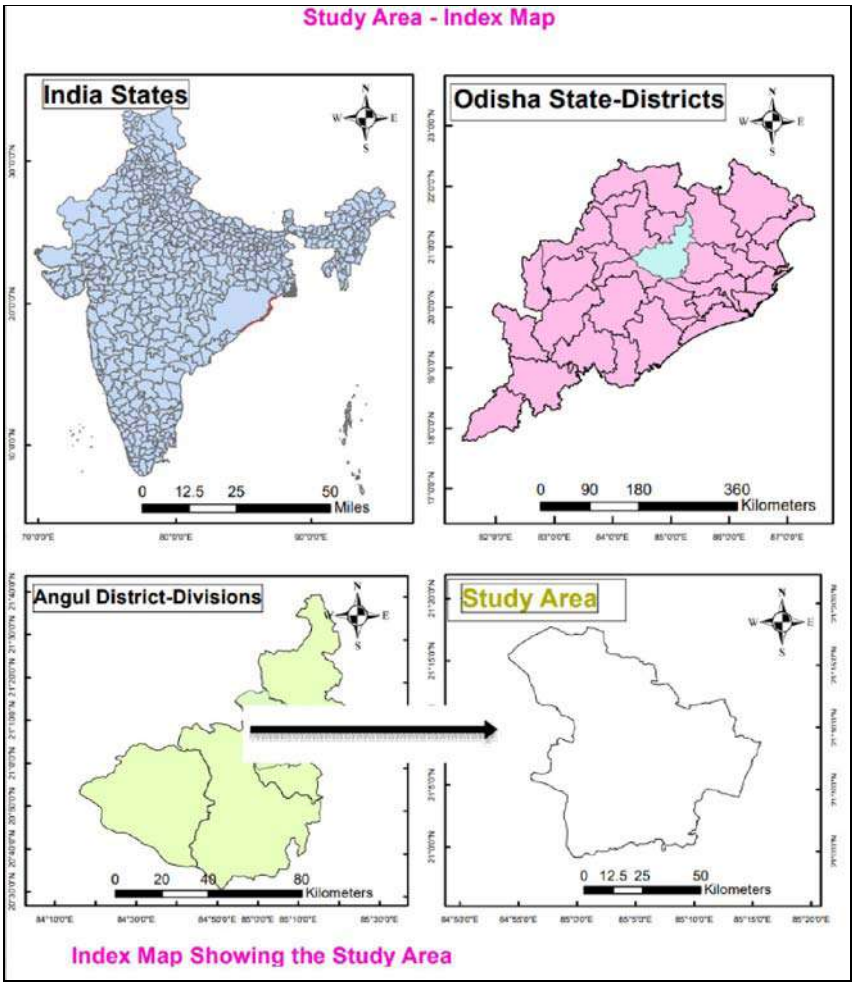

Fig. 1: Location map of the study area.

GEOLOGY AND HYDROGEOLOGY

The southern portion of the block is occupied by Gondwana Supergroup with sandstone, shale, coal, conglomerate and boulder beds. Barakar Formation is the main coal bearing formation with water bearing aquifer. The north and northeast portion of the block is occupied by charnockite, khondalite with granitic gneiss of Precambrian basement. The rocks of Iron-Ore Supergroup are exposed to the north of Brahmani River and central part of the block, consisting mainly of quartzites and mica schists. These rocks are devoid of primary porosity. The secondary porosity developed in the rocks is due to intense weathering and fracturing, which forms repository and passage for movement of ground water. Groundwater occurs under water table condition in the weathered residuum and in semi-confined to confined condition in fractured rocks at deeper depths. The alluvium occurs along the course of major rivers and streams and is having limited occurrence as pocket. The alluvium supports good yield. The major part of the area is occupied by “Alfisols” which includes red sandy soil, red loamy soil, and mixed red and black soils.

METHODOLOGY

Total 81 groundwater samples in pre monsoon season, 2022 were collected in 500 ml bottles (soaked with 1:1 HCl for twenty-four hours and washed twice with distilled water) from different bore wells and dug wells of the study areawhich are extensively used for drinking and other domestic purposes. Groundwater samples were analysed for hydrogen-ion concentration (pH), electrical conductivity (EC), total dissolved solids (TDS), and total hardness (TH) as CaCO3, calcium (Ca^{2+}), magnesium (Mg^{2+}), sodium (Na^{+}), potassium (K^{+}), bicarbonate (HCO_3-), chloride (Cl^{-}), sulphate (SO_4^{2-}), nitrate (NO_3^{-}), and fluoride (F^{-}), observing the standard procedures proposed by American Public Health Association (APHA 2012) in the laboratory. The concentration of all the chemical parameters were expressed in milligrams per litre, exceptpH (no units) and EC micros/cm.The ionic balance error percentage (IBE %) was checked for each groundwater sample which are within its satisfactory limit of ± 5% in the present study area.

RESULTS AND DISCUSSION

Groundwater Chemistry

The physical and chemical parameters including statistical measures such as minimum, maximum, average and standard deviation values are given in Table1.The groundwater of the study area is slightly acidic to alkaline as most of the samples have pH value greater than 7.00 with average 7.46. The EC Value of the groundwater of thestudy area is varying from 390.00 to 1543.00µS/cm with an average of 670.96µS/cm. The high EC value indicates high mineral content.Almost all the groundwater samples fall under the Type-I (EC<1500µS/cm; with low salt enrichment) except two samples which fall under Type-II (EC 1500 µS/cm - 3000 µS/cm; with medium salt enrichment (Rao et al. 2012). The total hardness in the groundwater is caused by the presence of calcium, magnesium and other metal ions

(Razowska-jaworeck 2014) and higher concentration TH value(>300 mg/L) may cause health issues (Jain et al. 2010). The ground water of the study area is moderately hard to hard but within permissible limit. From the data it is found that the order of abundance of cations are Ca^{2+}> Na^{+}> Mg^{2+}> $K^{+}$and anions are HCO_3^->Cl^-> SO_4^{2-}>NO_3^-in the study area. The abundance of the anions and cations are shown in the pie diagram given below.

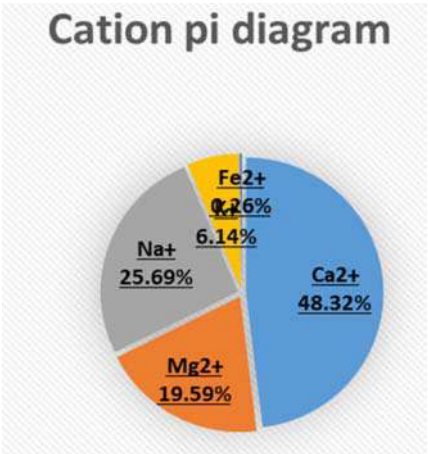

Fig. 2: Cation Pi diagram.

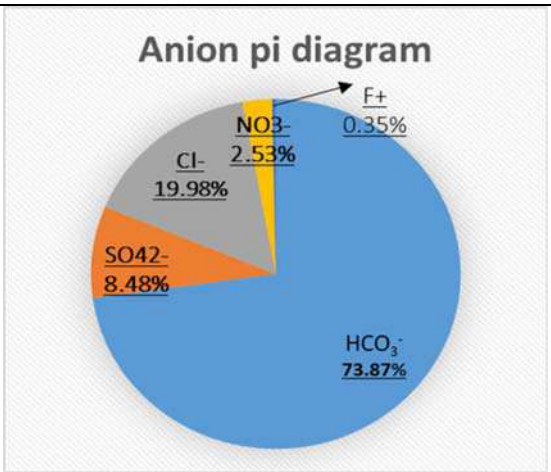

Fig. 3: Anion Pi diagram.

Table 1: Physico-Chemical parameters in the groundwater of the study area.

SI. No.	Parameters	Min	Max	Mean	Standard deviation
1	pH	6.30	8.7	7.46	0.33
2	EC	390.00	3388.78	670.96	280.83
3	TDS	247.04	2168.32	429.41	179.73
4	TA	70.00	299.00	179.50	52.49
5	TH	120.00	740.00	198.23	34.90
6	Ca^{2+}	34.00	205.00	47.15	8.18
7	Mg^{2+}	7.94	131.20	19.18	6.20
8	Na^{+}	12.34	65.00	25.51	11.63
9	K^{+}	0.19	11.78	5.99	3.03
10	Fe^{2+}	0.11	3.14	0.26	0.34
11	HCO_3^-	123.45	320.56	192.94	29.74
12	SO_4^{2-}	7.10	43.67	22.47	8.07
13	Cl^-	12.00	256.00	42.01	22.73
14	NO_3^-	1.45	67.00	6.82	4.16
15	F^-	0.23	2.70	0.82	0.42

Here, all the samples are express in mg/l except pH and EC. pH has no unit and EC is expressed as µS/cm.

Hydro-Chemical Facies

The hydrochemical facies analysis is used for determination of flow pattern and origin of mineral chemistry of groundwater. The geochemical interpretation of groundwater can be done by plotting the concentration of major cations and anions in the Piper Trilinear diagram (1944).On the basis of chemical analysis, the water samples can be divided into six facies such as Ca-HCO_3,Na-Cl,Mixed Ca-Na-HCO_3,Mixed Ca-Mg-Cl,Ca-Cl,Na-HCO_3 types.In the present study, the plotted data (Fig-4) shows that almost all the water samples fall in the Ca-HCO_3 type facies, only one sample fall in the Ca-Mg-Cl Facies which shows that Ca^{2+} is the major cation and $HCO_3^-$is the major anion. It suggests that alkaline earth metals exceed alkalies and weak acid HCO_3^- exceeded the strong acid. The high concentration of $HCO_3^-$and Ca^{2+} content is possibly due to weathering of carbonate minerals related to the flushing of CO_2 rich water from unsaturated zone, where it is formed by decomposition of organic matter degradation and silicate weathering.

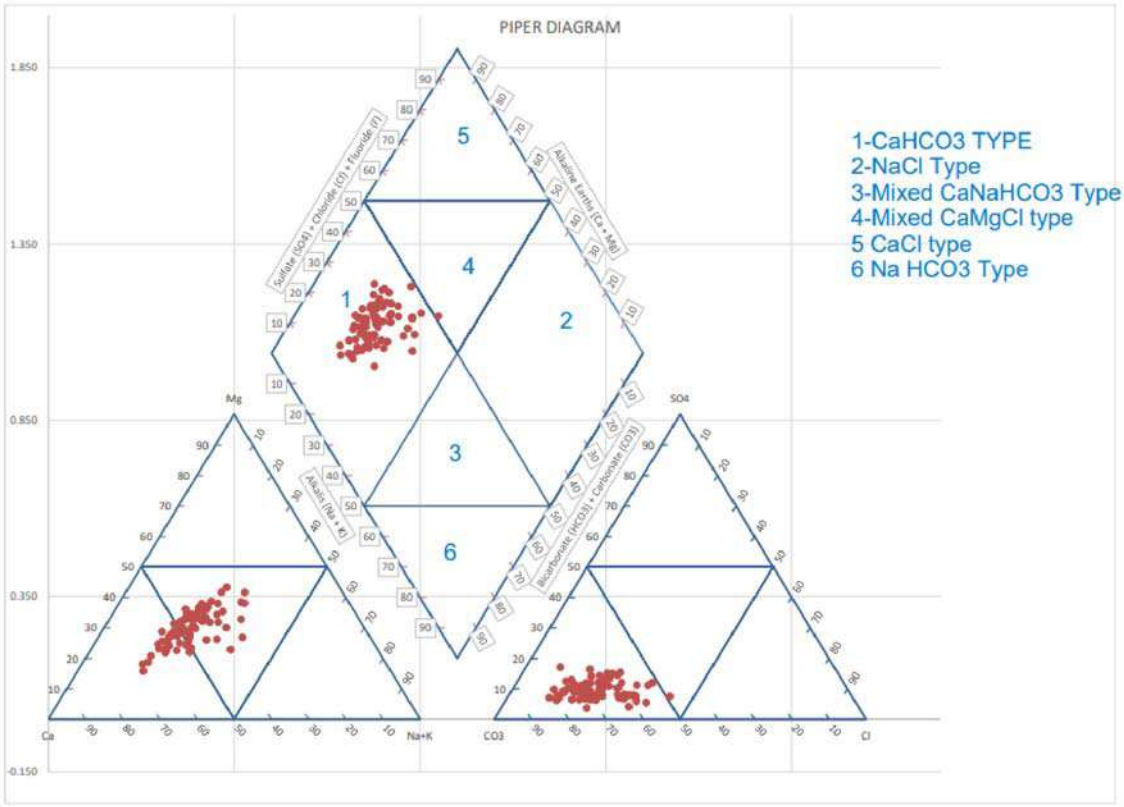

Fig. 4: Piper Trilinear Diagram showing geochemical classification of groundwater.

Gibbs Diagram and water rock interaction

Gibbs diagramindicate the origin chemical constituents in water with relation to rainfall (precipitation), rocks (lithology), and evaporation (climate) in groundwater system (Gibbs, 1970), using relationship of TDS vs $(Na^+ + K^+)/(Na^+ + K^+ + Ca^{2+})$ and TDS vs $(C1^{-})/(C1^{-} + HCO_3^{-})$. The Gibbs diagram (Fig5a and Fig. 5b) contain three fields such as precipitation dominance, rock dominance and evaporation dominance for finding the water chemistry mechanism. By plotting the chemical data of the present study area in Gibbs diagram, it is found that all the water samples fall in the rock dominance field indicating that the weathering of rocks is the dominant geochemical factor regulating the ion chemistry.

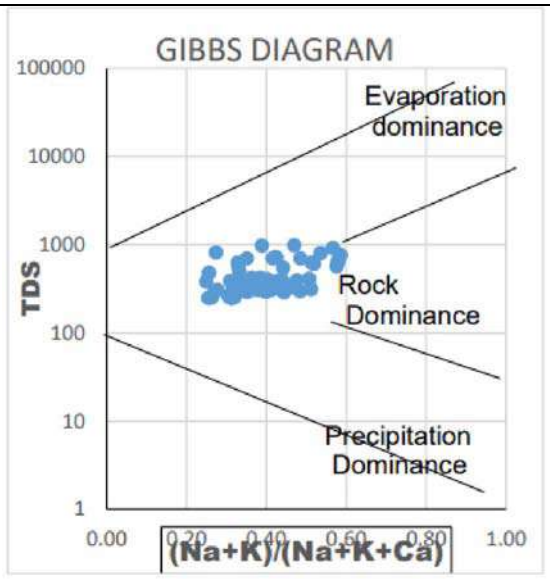

Fig.5a Gibbs diagram for cation

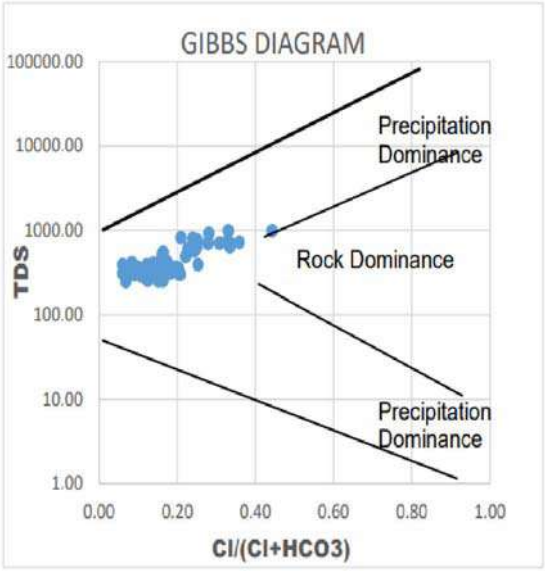

Fig.5b Gibbs Diagram for Anion

The scatter plot between $HCO_3^{-} + SO_4^{2-}$ and $Ca^{2+} + Mg^{2+}$ values a major indicator to identify ion exchange process. If ion exchange is the process, the points tend to shift to the right side of the plot due to an excess of $SO_4 + HCO_3^{-}$. If reverse ions exchange is the process, points tend to shift to the left side due to excess of $Ca^{2+} + Mg^{2+}$ over $SO_4 + HCO_3^{-}$. The plot of the $Ca^{2+} + Mg^{2+}$ vs $SO_4^{2-} + HCO_3^{-}$ (Fig3) in the study area shows that most of the groundwater samples are fall below the aquiline,indicating that the primary process involved in the geochemical evolution of groundwater sample was silicate weathering The molar ratio of Na/Cl values of study area ranging between 0.28 to 1.74. .The most of the samples have ratio less than one, which implies that the groundwater salinization is not only process but also other geochemical process operating at large scale which alter the ground water chemistry.

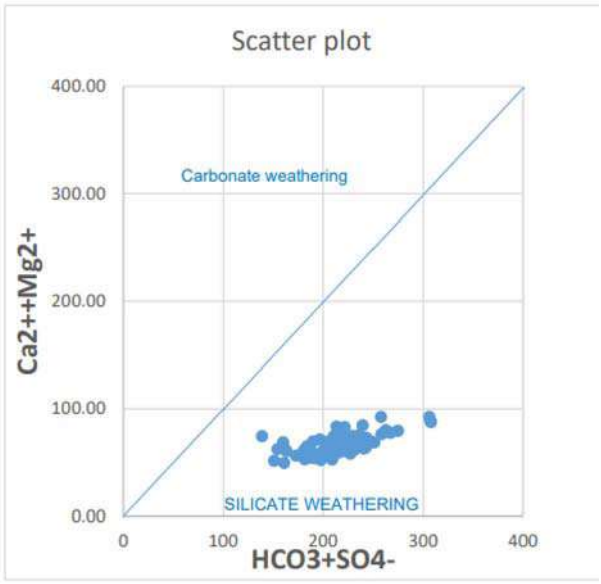

Fig. 6: Scatter plot between Ca^{2+}+Mg^{2+} vs. HCO_3^-+SO_4

Table 2: Comparison of post-monsoon groundwater quality with drinking water standards (IS 10500:2012)

Parameters	IS 10500:2012		No. of Samples exceeding acceptable limits	% of samples exceeding the acceptable limit	No of Samples exceeding permissible limits	% of Samples exceeding permissible limits
	Acceptable Limit	Permissible Limit				
pH	6.5-8.5	No relaxation	02	2.46	2	2.46
TDS	500	2000	19	23.45	1	1.23
TH	200	600	28	34.56	4	4.93
Ca^{2+}	75	200	10	12.34	1	1.23
Mg^{2+}	30	100	06	7.40	2	2.46
Cl^-	250	1000	01	2.46	Nil	0
SO_4^{2-}	200	400	00	0.00	Nil	0
NO_3^-	45	No relaxation	05	12.34	Nil	0
F^-	1	1.5	15	18.51	04	4.93

All the samples are express in mg/l except pH

The physical and chemical parameters of the groundwater of the study area are compared with the Indian standards (BIS 2012) for drinking purpose (Table-2). The table shows the acceptable and maximum permissible limit of various parameters. All the parameters are within the permissible limit except fluoride ion where 4 samples exceeded the permissible limit(>1.5mg/l). The fluoride content of the two tube wells at Kaniha and Samal are 2.70 and

1.70mg/L respectively whereas in the same locality in dug wells, the fluoride content is within the permissible value. The pH in 02 locations ,TDS concentration in 19 locations, TH concentration in28 locations, Mg^{2+} concentration in 06 locations, F^- concentration in 04 locations have values beyond the acceptable limit for drinking.The moderately high fluoride concentration may be due to geogenic processes such as leaching, weathering and ion exchange. However,the occurrence of high fluoride does not show any pattern in the study area. From the analysis result it reveals that the ground water of the study area is suitable for drinking and domestic use as most of the parameters are within the permissible limits except in some location due to high fluoride content.

CONCLUSION

The hydrochemical analysis of the study area (Kaniha Block, Angul district, Odisha) reveals that the groundwater of the region is moderately hard to hard type and are alkaline in nature. The order of the abundance of the major cations and anions are in the order Ca^{2+}> Na^+> Mg^{2+}> K^+andHCO_3^->Cl^-> SO_4^{2-}>NO_3^- From the Piper diagram, all the samples fall in the Ca^{2+}-Mg^{2+}-HCO_3^-facies. The Gibbs diagram indicates that the hydrochemistry of the groundwater samples of the study area is largely influenced by rock-water interaction and varied lithologies are dominant factor that controls its water composition. The comparison between the water qualities of the study area with the Bureau of Indian Standards (BIS, 2012) shows the groundwater of the study area is suitable for the drinking purposeexcept in some locations due to high fluoride content.

REFERENCES

APHA (2012) Standard methods for the examination of water and wastewater.American Public Health Association, Washington DC.

Bureau of Indian Standards (2012) Indian standard specifications for drinking water.10500: BIS: New Delhi, India

Dhakate, R. and VV S, G.R. (2015)Hydrochemical assessment of groundwater in alluvial aquifer region, Jalandhar District, Punjab, India.EnvironmentalEarthSciences, 73(12):8145-8153

Gibbs, RJ (1970) Mechanisms controlling worlds water chemistry. Sci., 170:1088–1090

Jain, C.K., Bandyopadhyay, A., Bhadra, A. (2010) Assessment of ground water quality for drinking purpose, District Nainital, Uttarakhand, India. Environmental Monitoring and Assessment, 166:663–676

Jaworeck, Razowska (2014) Distribution of Ca and Mg in groundwater flow systems in carbonate aquifers in Southern Latium Region (Italy). Implications on drinking water quality, Calcium and Magnesium in Groundwater, 1st Edition

Ramachandra, C. and Prasad, S. (2004) Impact of Urban Growth on Water Bodies: The Case of Hyderabad, India. Centre for Economic and Social Studies, Hyderabad. Journal of Water Resource and Protection, Vol.10 No.6

Rao, N.S.and Rao, P.S. (2012) Chemical characteristics of groundwater and assessment of groundwater quality in Varaha River Basin, Visakhapatnam District, Andhra Pradesh, India. Environmental Monitoring and Assessment, 184:5189–5214

VISTAS IN GEOLOGICAL RESEARCH
Special Publication in Geology (19), March 2023, pp. 142-147

Foraminiferal Assemblages of the Shella Formation from Silveta Area, Karbi-Anglong District, North-East India: Implication for Palaeoenvironmental Interpretation

SHILPIKA SAIKIA [1*] AND URBASHI SARKAR[1]

[1]Department of Earth Science, Assam University, Silchar – 788011
*Corresponding author saikiashilpika@gmail.com

Abstract : Eocene carbonate deposits from the Shella Formation in Karbi-Anglong district, Northeast India, are marked by rich assemblages of foraminifera and glauconite mineral. Palaeontological and palaeoenvironmental data from the Eocene carbonate succession are limited from Karbi-Anglong district of Assam. To address this research gap, 23 samples were collected from four different exposed sections of varying thickness from Silveta area. More than 3000 specimens of foraminifera have been handpicked from 23 samples. Abundance and diversity of the fossils exhibit a decreasing upward trend for section 1, 2 and 3 with a final unfossiliferous zone at the sandstone exposure. It shows an increasing trend for the last section. The samples are mostly dominant in benthic formainfera like Nummulites sp., Assilina sp., Caudammina sp., Quinqueloculina sp., Nonionella sp. along with ostracoda, molluscs, echinoid spines and other skeletal components. Thin section analysis revealed the composition of limestone as mainly biomicrite with minor amount of quartz and can be characterized as silty limestone and sandy limestone. Sandstones are also characterized by micrite cement. Partially broken, angular and fragmented shells together with high angular quartz grains suggest a short distance of transportation and partial sorting before their deposition. Glauconite is present as discrete grains in the matrix of the limestone and within the chambers of some larger foraminifera. Intra-granular occurrence of glauconite reveals a post depositional formation of the mineral. Foraminiferal assemblage suggests an open and shallow marine, inner shelf environment of deposition. Presence of glauconite indicates a continental shelf in neritic environment of deposition. From the analysis it can be inferred that the micrite limestone rich in foraminifera is likely to have been deposited in a shallow marine neritic to shelf environment.

Keywords: Eocene, Foraminifera, Nummulites, Palaeoenvironment, Glauconite, Karbi-Anglong, Silveta.

INTRODUCTION

The glauconite bearing carbonates of Karbi Hills (Mikir Hills) have formed at the time of Eocene Age (Das Gupta and Biswas, 2000) (Fig.1). Geologically the Mikir Hill Massif (MHM) is an eastern extension of the Shillong Plateau. Both the Shillong Plateau and the Mikir Hills had developed in a NW-SE stress which is evident from the predominant NE-SW structural trend of the Precambrian basement complex (Nandy, 2001). The carbonate

sediments belong to the Shella Formation of Jaintia Group. Based on field evidences, lithology and fossil evidences the Shella Formation was further subdivided into Sylhet Sandstone Member and Sylhet Limestone Member (Table1). Paleoenvironmental analysis uses microfossils among other indices to provide direct evidence for interpretation of ancient environments (Renema, 2002). The Sylhet Limestone Member of the area has wide variety of fossils including foraminifers, molluscs, ostracoda and echinoid spines (Sarma and Bora, 1999). The primary objective of the study is to infer paleoenvironmental factors of Shella Formation with the help of microfacies analysis and fossil assemblages.

Table 1: A Geological Succession of Silveta, Karbi-Anglong, Assam (Modified after Geological Survey of India, 1999).

Age	Group	Formation	Member
Recent	-	Newer Alluvium	
~~Unconformity~~~~~~~~~~~~~~~~~~~~~~~~~~			
Palaeocene to Eocene	Jaintia	Shella Formation	Sylhet Limestone Member Sylhet Sandstone Member
~~Unconformity~~~~~~~~~~~~~~~~~~~~~~~~~~			
Precambrian	Gneissic Complex	-	

SAMPLES AND METHOD

In the area under investigation, outcrops are exposed both at the river and road section of varying thickness (1.5-4) m. Twenty-three samples were collected both vertically and laterally at an interval of 1m from four sections (namely section 1, section 2, section 3 and section 4) marked in Fig.2. The samples were processed by using the traditional method and fossils were hand-picked under the Lieca EZ24 stereo zoom microscope. More than 3000 specimens have been picked from 23 samples and quantitative distribution of foraminiferal genera per 5 grams of the processed samples were recorded. The foraminiferas were identified and classified by following cf. Loeblich and Tappan, 1998. Standard thin sections were also prepared for petrographic analysis from Pradhan Enterprise, West Bengal and studied under Leica DM 4500P polarizing microscope to precisely define the microfacies. Both the micropalaeontological and petrographic analysis were carried out at the Department of Earth Science, Assam University, Silchar.

RESULTS

3.1. Lithofacies analysis

The Shella Formation is exposed in the Silveta area is made up of limestone and sandstone lithofacies.

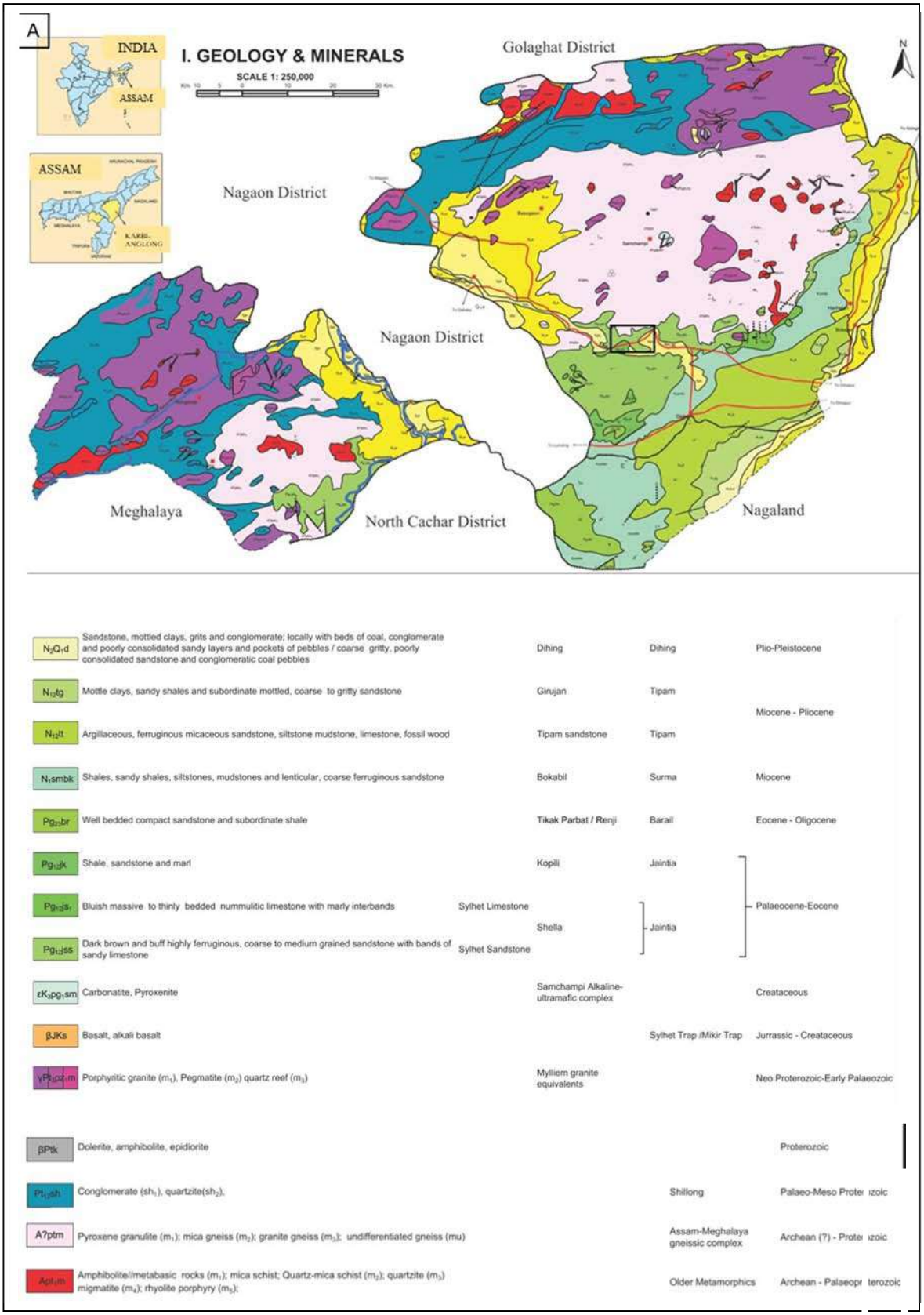

Fig.1: Lithological map of Karbi-Anglong district showing the study area marked in black box (Geological Survey of India, 2017).

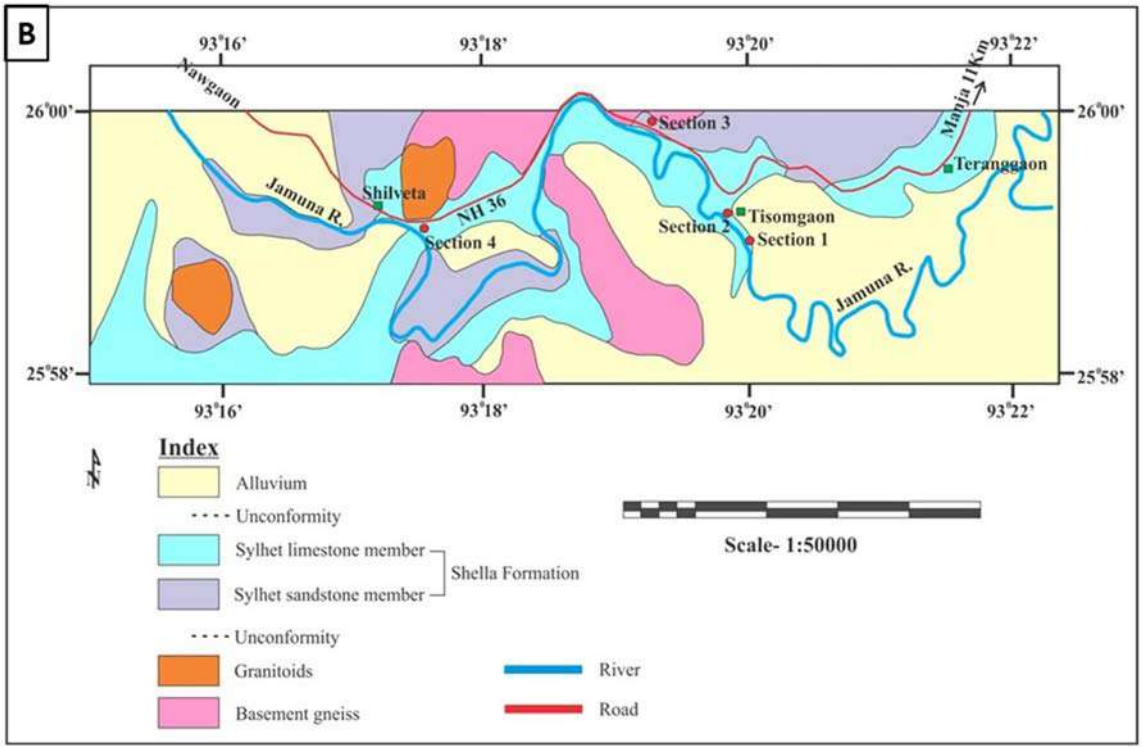

Fig. 2: Lithological map of the Silveta showing the different studied sections marked in red dot. (Modified after Geological Survey of India, 1999)

Sandstone: The Sylhet Sandstone Member in the locality has a thickness of 3.5m (Fig.3, Section - 3). It is a medium to coarse grained sandstone and is devoid of fossil. Under thin section, it is evident that sandstone is mostly dominant in quartz grains with microcrystalline calcite along with few plagioclase and mica grains. Both undulatory and non-undulatory quartz grains are observed. The quartz grains are sub rounded to angular in nature. The cementing materials are mostly calcareous with minor siliceous cementation around the grain margins. Primary structure bedding is indicated by the grain size variation of medium grained sandstone, alternating with coarse grained gritty sandstone unit.

Limestone: The Sylhet Limestone Member is exposed along both the river and road section with a thickness varying from (1.5-4m) (Section 1, 2 and 4) shown in Fig.2. Two varieties of limestone can be distinguished. First variety is found from section 1 and section 2. It is greyish in colour with moderate compactness and abundance of fossil. The other variety is observed in section 4. It is having brownish yellow colour limestone and are usually highly weathered and high in fossil abundance and diversity. The limestones occurring at different stations yielded a diverse larger benthic foraminiferal (LBF) assemblage of Nummulites, Assilina etc. Thin section study indicates that the limestone is composed of good amount of micrite with quartz having angularity and can be regarded as sandy and silty limestone. Shells of foraminifers and other fossils are enclosed in a matrix of micrite. Fossil shells are partially broken, angular and fragmented in nature. Calcite is the cementing material. Glauconite is seen to be distributed as discrete pellets in the matrix of the limestone. The green glauconite is also present within the chambers of these fossils. The limestone also bears other large fossils including bivalves, gastropods along with echinoids and ostracoda.

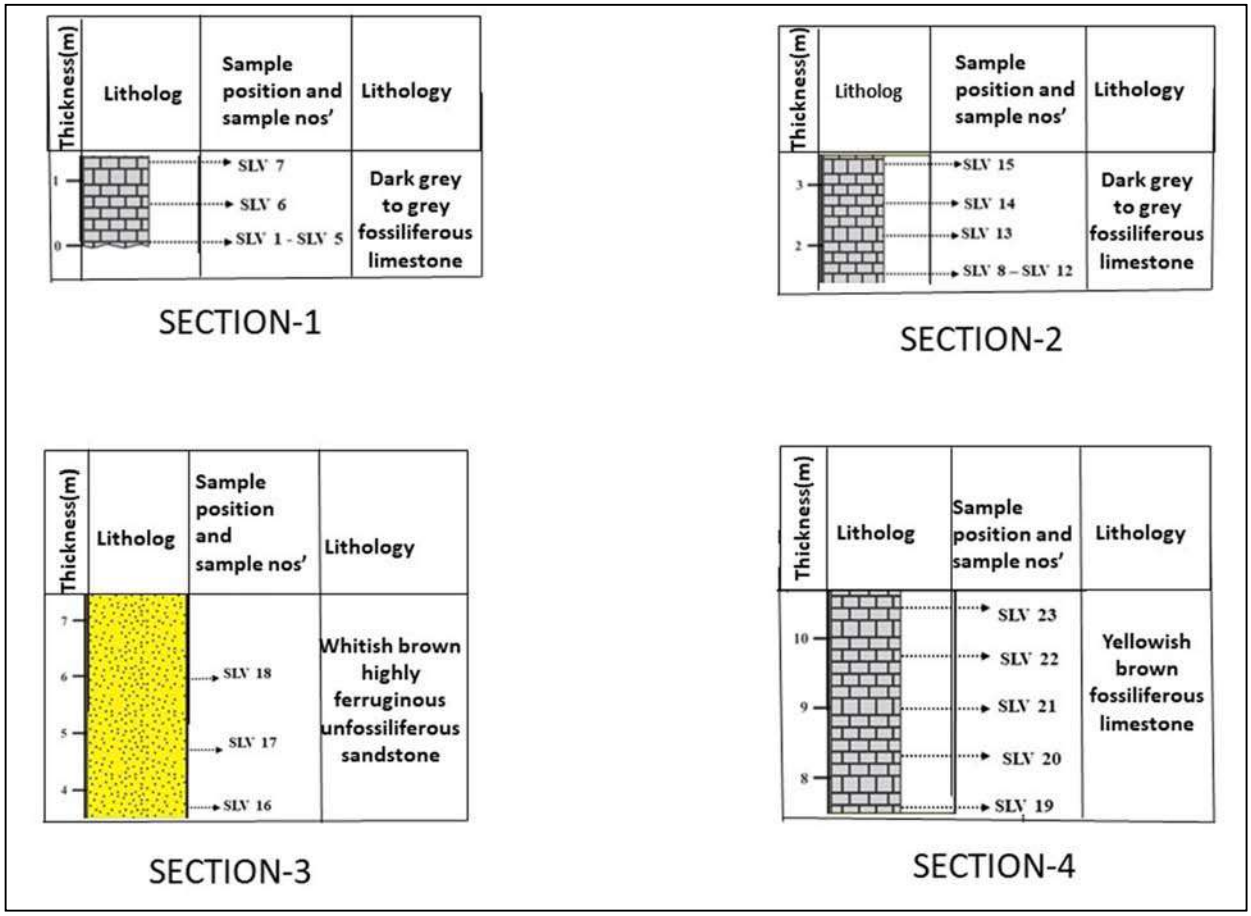

Fig. 3: Litholog of the four exposed study section marked from east to west (top to bottom) in the Silveta area map.

3.2. Foraminiferal Assemblages

The limestone samples from the Silveta outcrop sections dominantly yielded larger benthic foraminifers (LBF) such as Nummulites sp., Assilina sp. Nummulites of both small asexual A-forms and large sexual B-forms (Johnes, 2014) are present. In addition to larger benthic foraminifers, some smaller benthic foraminifers like Conotrochammina sp., Quinqueloculina sp., Nonionella sp., Cibicides sp., Cibicidoides sp., and Triloculina sp. are also present whose number increases from section 1 to section 4. The abundance and diversity of the fossils exhibit a decreasing upward trend for section 1 and section 2 with a final unfossiliferous zone at the sandstone exposure. The ratio of larger to smaller benthic foraminifera decreases in section 2. Again, the number of fossils increases in section 4 with high abundance of larger benthic foraminifera. Ostracoda, echinoids and invertebrates such as bivalves and gastropods are also found in the area. The presence of molluscs is higher in section 4 as observed with the naked eye in field and thin section. Some of the larger foraminiferal tests are also filled with glauconite.

DISCUSSION AND CONCLUSIONS

The Eocene carbonates of Karbi-Anglong is important as it yield wide variety of fossils including foraminifera, molluscs and osctracods. The foraminiferal assemblages record changes in abundance throughout the studied sections. For section 1, the abundance of Nummulites sp. is highest in most of the samples. Ostracoda is also present in good numbers in the samples. Ostracoda and benthic foraminifera have proven to be complementary indicators on river-influenced shelves. The samples in section 2 are mostly abundant in smaller benthic foraminifera like cibicides sp. with little or zero presence of Nummulites sp. High diversity of smaller benthic foraminifera and scarcity of larger benthic foraminifera suggest greater than normal levels of salinity and low incidence of light denoting the lower photic zone. In section 4, the abundance and diversity of foraminifera is higher along with other larger fossils like molluscs. Presence of Larger Benthic Foraminifera genera indicate shallower, oligotrophic, higher energy and upper photic zone corresponding to an inner shelf environment. Under thin section, it is evident that both limestone and sandstone are dominated by micrite cement. The dominance of Nummulites indicates the deposition of Sylhet Limestone in shallow shelf areas of carbonate sedimentation. The Partially broken, angular and fragmented shells suggest a short distance of transportation and partial sorting before their deposition. Together with, presence of glauconite mineral in the samples indicate the formation of the carbonates in continental shelves in neritic environment (Sarma and Basumalik, 1979). The quartz and glauconite is likely to form later than the fossils and got mixed with lime cement. The highly dominant presence of micrite (lime mud) with foraminifera and molluscan most likely suggest a lagoonal environment. On the basis of the faunal assemblage and glauconite, it can be inferred that the palaeoenvironment of Eocene carbonates ranged from open marine, shallow littoral neritic to shelf environment.

REFERENCES

Das Gupta, A.B., Biswas, A.K. 2000. Geology of Assam. Geological society of India ,11-26.

Johnes, R.W. 2014. Foraminifera and their Applications. Cambridge University Press. 105.

Loeblich, A.R., Tappan, H. 1988, Foraminiferal evolution, diversification and extinction. J.Paleontol.

Nandy, D.R. 2001. Geodynamics of Northeastern India and the Adjoining Region. ACB Publications, 111-130.

Renema, W. 2002. Larger foraminifera as marine environmental indicators. Scripta Geologica 124: 263 pp.

Sarma, J.N., Basumalik, S. 1979. Glauconites in some Eocene carbonate rocks of Mikir Hills, Assam. Indian Journal of Earth Sciences, Vol.6, No. 2.p. 186-19. 1979.

Sarma, H., Bora, A.K. 1999. Systematic Geological Mapping in Karbi Anglong District, Asaam. Assam Geology Project Operation: AMN North Eastern Region Guwahati. Geological Society of India.

VISTAS IN GEOLOGICAL RESEARCH
Special Publication in Geology (19), March 2023, pp. 148-157

Pre-Monsoon Ground Water Quality Assesment of Ghatagaon Block, Kendujhar District, Odisha, India using IDW (Inverse Distance Weighted) Interpolation Method

NISHANT KUMAR MOHAPATRA[1], PRABHU ABHISEK PANDA[2], RASHMI RANJAN MOHANTA[3] AND NANDITA MAHANTA[4*]

[1]P.G. Department of Earth Sciences, Sambalpur University, Jyoti Vihar, Burla-76801
[2]Department of Civil Engineering, RVS College of Engineering and Technology, Jamshedpur-831012
[3]Dept of Geography, Utkal University, Vani Vihar, Bhubaneswar-751004
[4]Dept of Geology, Utkal University, Vani Vihar, Bhubaneswar-751004
***Email:** nandita.mahanta12@gmail.com*

Abstract: In our life groundwater is an essential component and plays a vital role. Quality and quantity of groundwater for a particular area indicates its potentiality towards the society. People are using groundwater for many purposes like drinking, domestic, irrigation and industry etc. Therefore quality assessment of groundwater of a particular area is fully necessary. The groundwater quality of Ghtagaon Block, Kendujhar district, Odisha for the period of post-monsoon in 2018 has been studied to find out the suitability of groundwater for different uses. A total of 59 samples were collected from tube wells (51) and dug wells (5) from different locations of study area. It is analysed for various physical parameters such as pH, EC (Electrical Conductivity), and chemical parameters like Na^+, K^+, Ca^{2+}, Mg^{2+}, HCO_3^- ,CO_3^{2-}, SO_4^{2-}, Cl^- etc. It is found that the quality of groundwater is suitable for domestic purposes except some locations. For the evaluation of water quality, Q GIS Software was used to prepare the spatial distribution map and identifying the suitable and unsuitable zones. The Piper diagram shows that the groundwater is of carbonate hardness exceeding 50% and mixed type zone.

Keywords: Physico - Chemical parameters, Q GIS Software, Piper Trilinear Diagram

INTRODUCTION

Groundwater is one of the most important natural water resources used not only for drinking but also for irrigation and industrial purposes. It cannot be optimally used and sustained unless the quality of groundwater is assessed. So management of its quality is very important as the demand is increasing day by day. Ghatagaon is a block situated in Kendujhar district of Odisha, India. The main objective of the study is to understand the groundwater quality status of the Ghatagaon block, followed by attempts to investigate the spatial distribution of different analysed groundwater quality parameters and to identify the places containing potable groundwater. Spatial interpolation was carried out in a GIS environment to infer the lateral variation of the hydro-chemical variables (Das et al.2016).

STUDY AREA

The area selected for the research is the Ghatagaon Block of Kendujhar district, Odisha, India. The total area of the block is about 740.98 sq. km extends from latitude 21° 19'9"N to 21° 47' 5" N and longitude 85°38'30"E to 85°59'46"E. It lies in the Survey of India toposheet no. 73 G/10, 73 G/11, 73 G/14, 73 G/15.

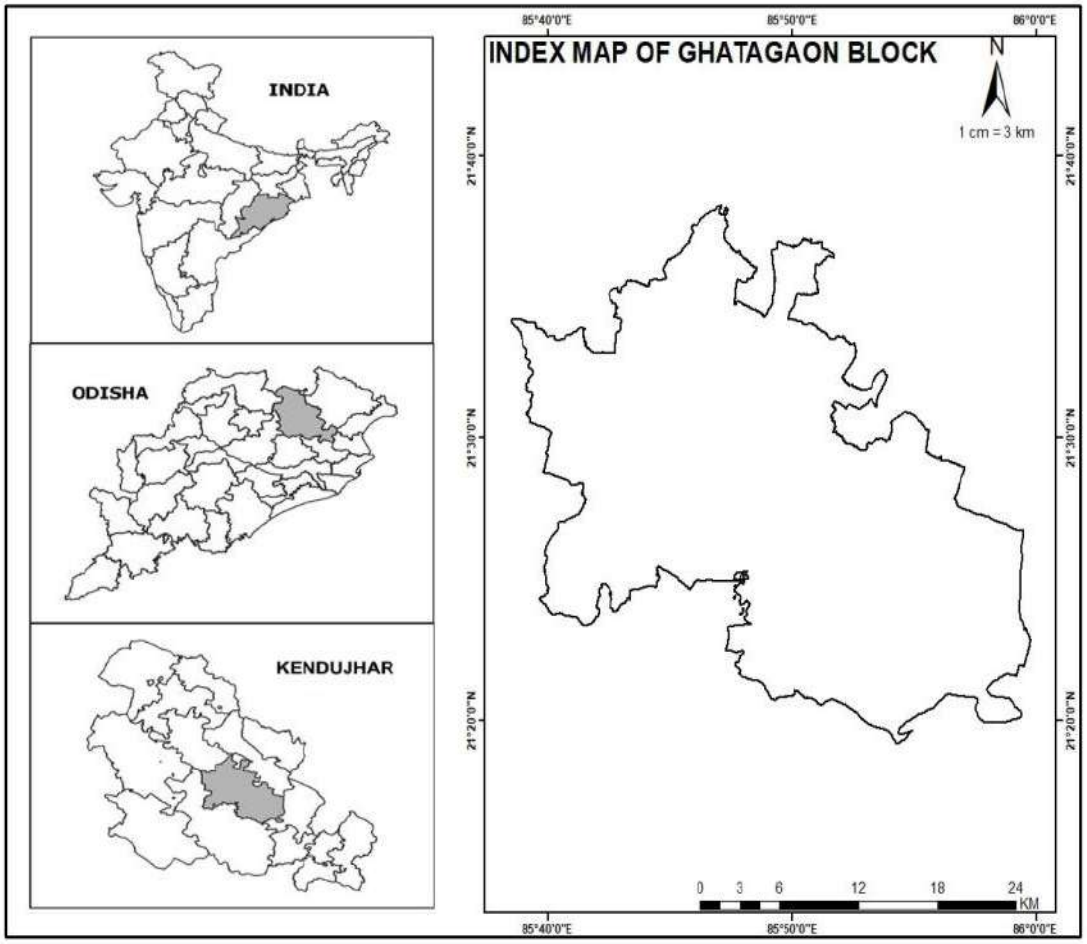

Fig. 1: Index map of the study area.

METHODOLOGY

Groundwater samples were collected systematically from 51 tube wells and 5 dug wells in 1 litre pre cleaned polythene bottles adopting standard procedure. Fig. 2 shows the sample location sites in the study area. The parameters such as pH, EC, TDS were measured in the field using portable instrument. Then the samples were taken to the laboratory for analyses of other parameters such as Ca^{2+}, Mg^{2+}, Na^{+}, K^{+}, HCO_3^{-}, CO_2^{-}, Cl^{-}, $SO^{4-,}$ F^{-} etc. The samples were analysed using standard procedure suggested by APHA, 1995, Brown et al. 1974, Trivedy and Goel, 1984 and Vogel, 1964.

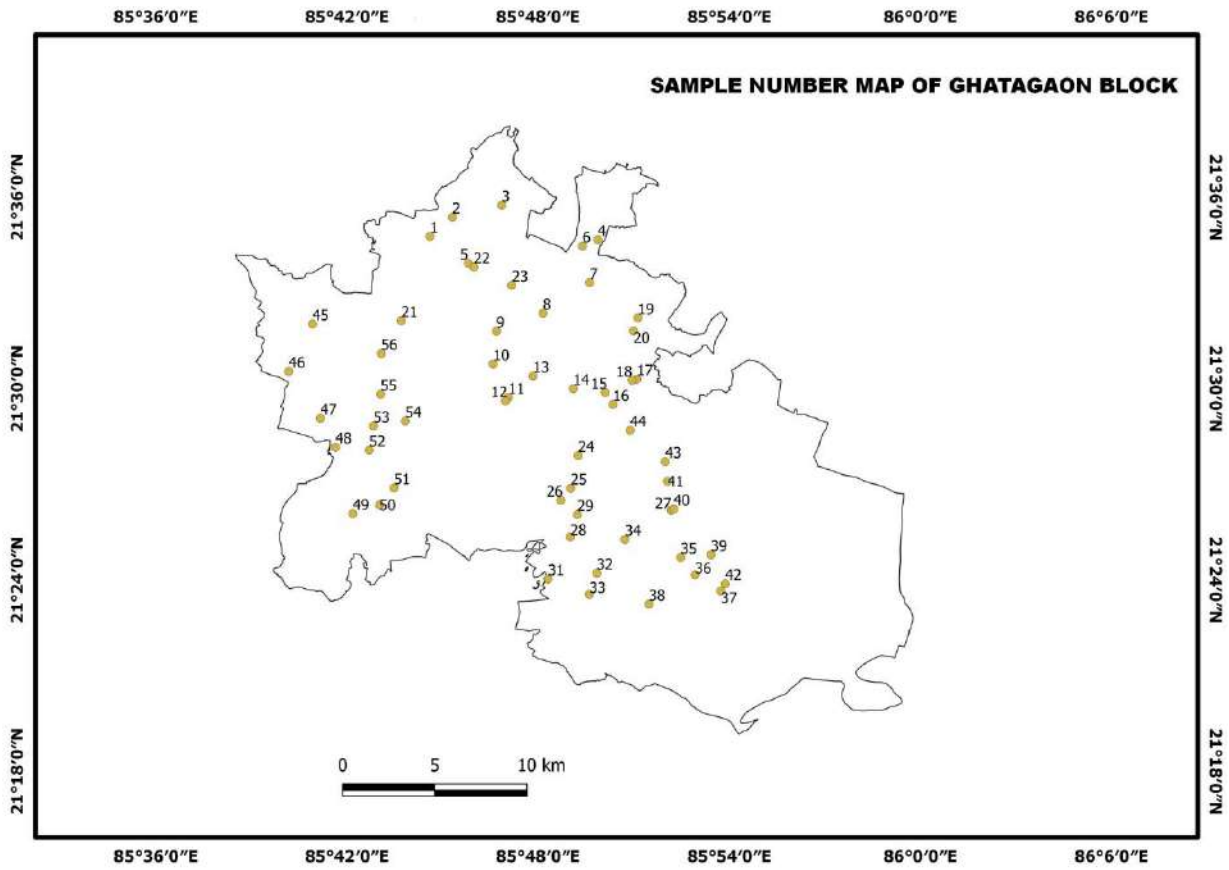

Fig. 2: Sample location sites of the study area.

Geospatial Analysis (Spatial Interpolation)

GIS can be a powerful tool for developing solutions for water resources problems like assessing water quality, determining water availability. Spatial analysis module in QGIS (version3.6.0) software was used for present study. The GIS interpolation tools were used to create a continuous surface to explain the similarities and differences between the measured and neighbouring sites. It also describes the level of spatial dependence and interrelationship (Khan et al., 2019) of predicting the values of attributes. In other words, spatial interpolation is a procedure of predicting the values of attributes at sites from measurement made at point locations within the same area. Spatial interpolation is a means of converting point data to surface data (Subramani et al., 2012). For this, the geospatial tool Inverse Distance Weightage (IDW) interpolation through QGIS 3.6.0 software was used in the present study.

RESULT AND DISCUSSION

The spatial interpolation maps for different parameters are given from Fig. 3 to Fig. 13.

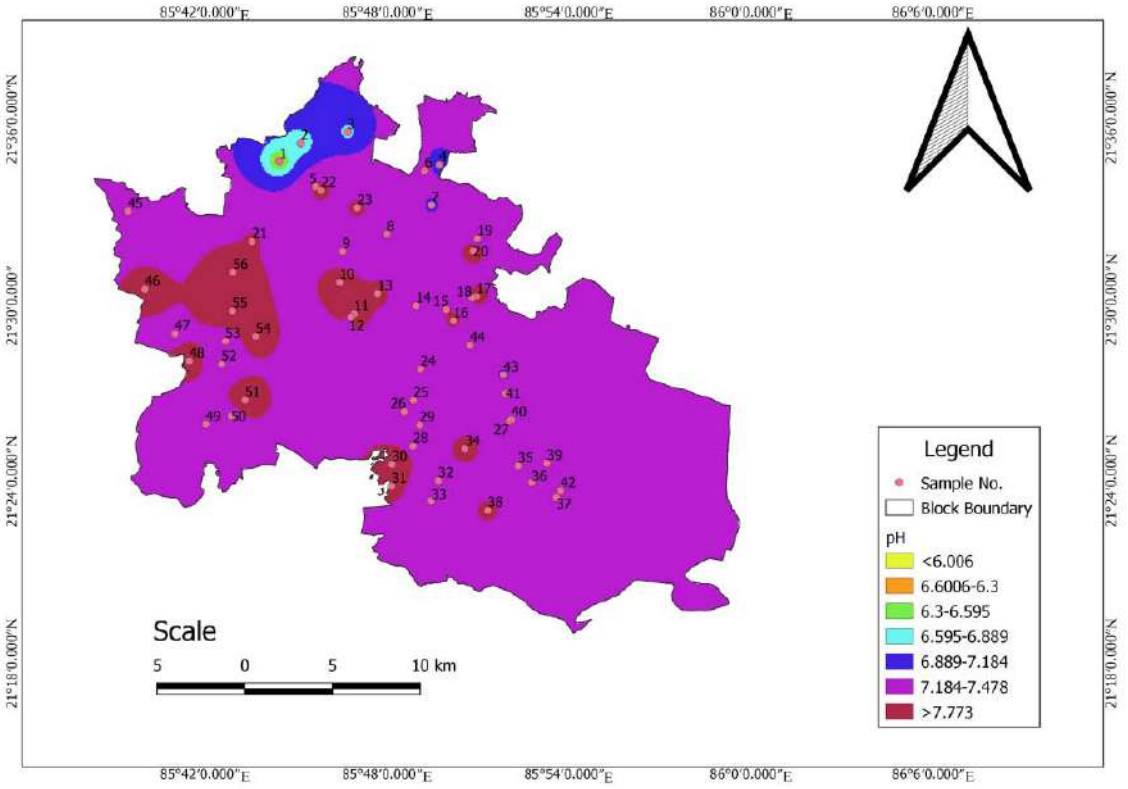

Fig. 3: Spatial interpolation map of pH.

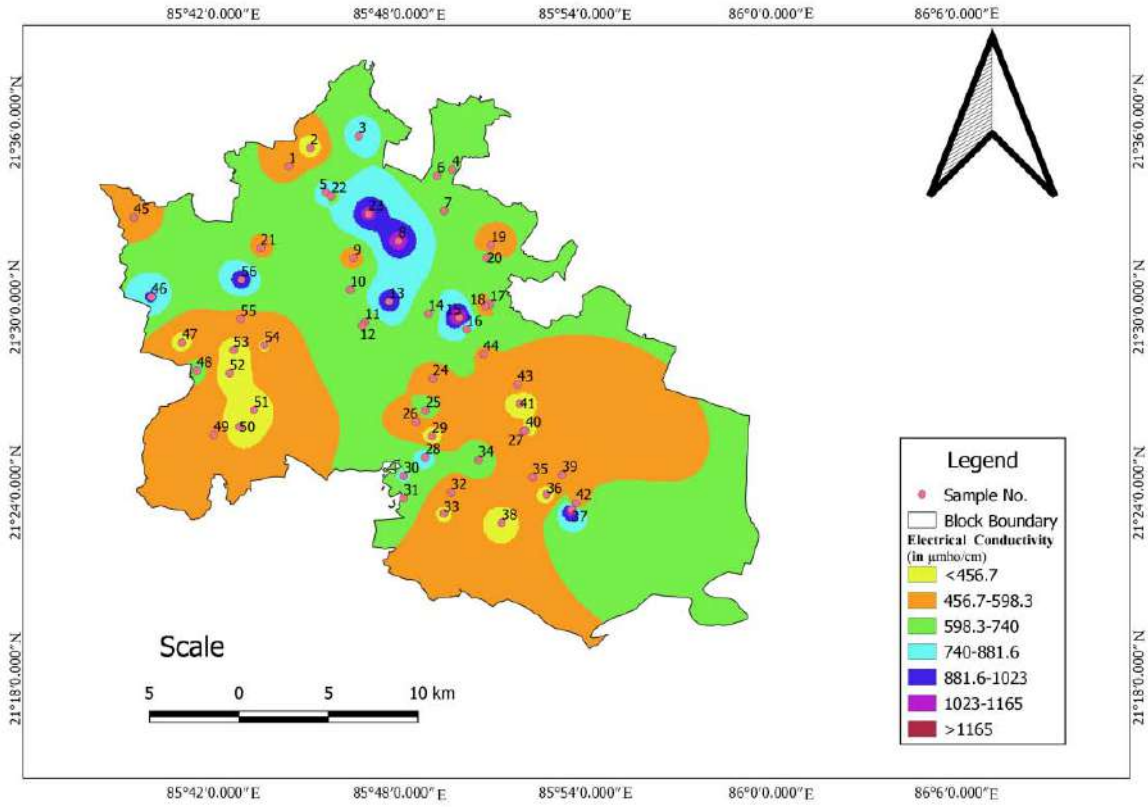

Fig. 4: Spatial interpolation map of EC.

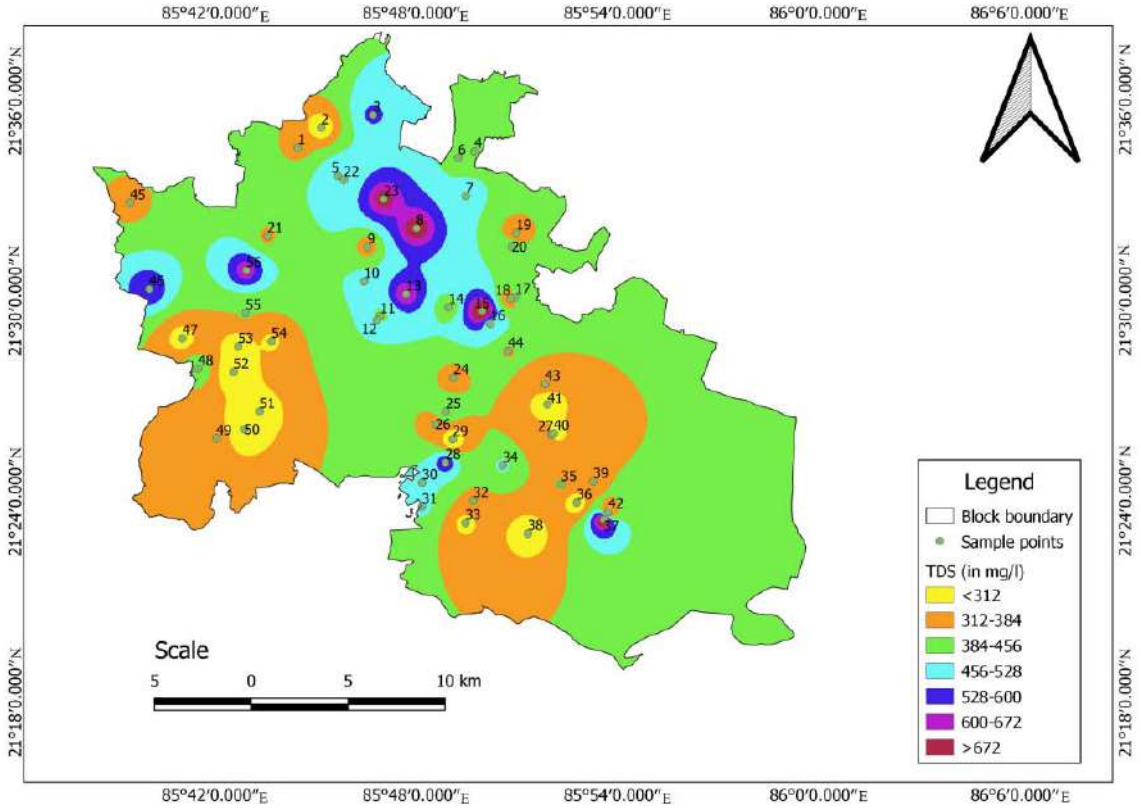

Fig. 5: Spatial distribution of TDS in the study area.

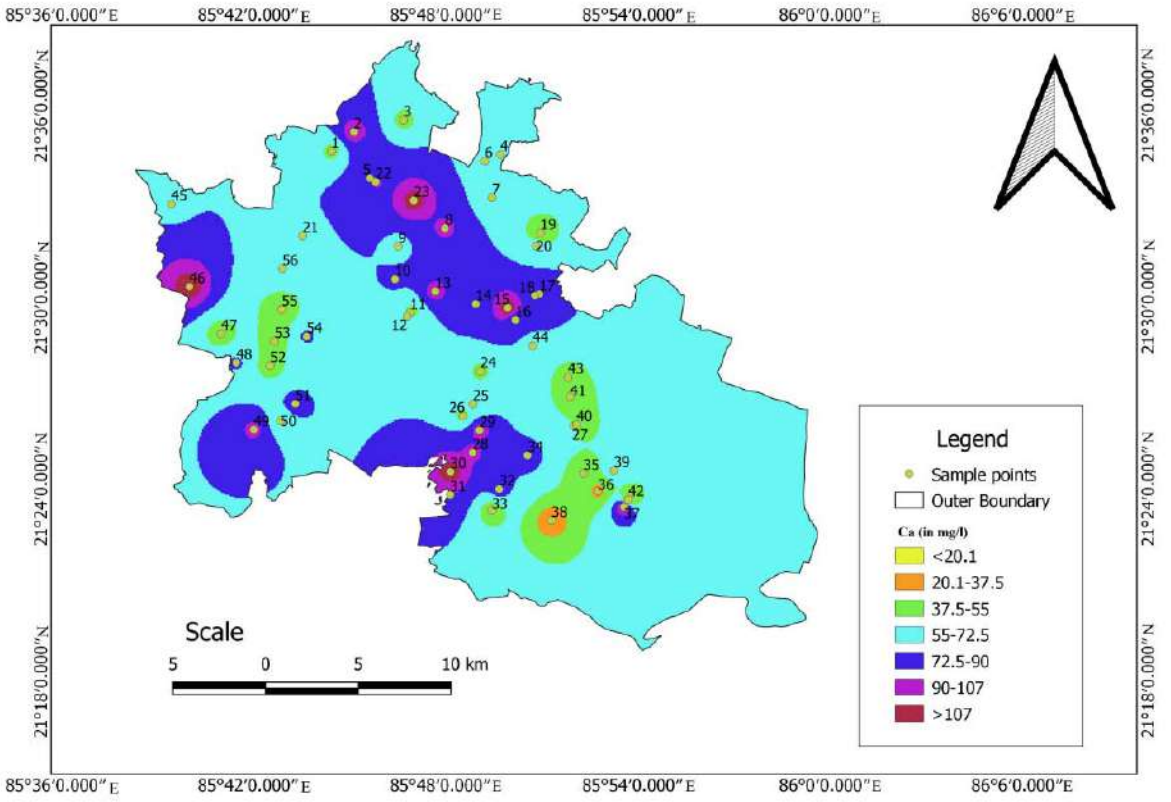

Fig. 6: Spatial interpolation map of Ca^{2+} .

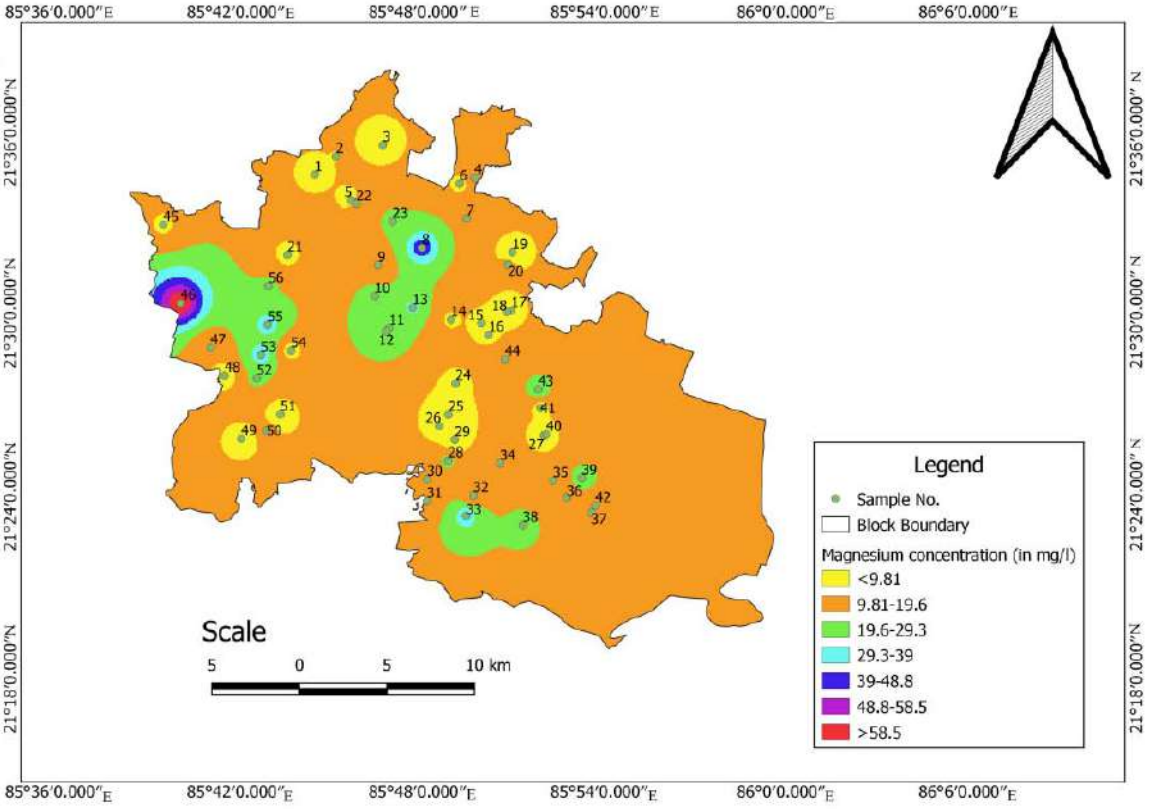

Fig. 7: Spatial interpolation of Mg^{2+} .

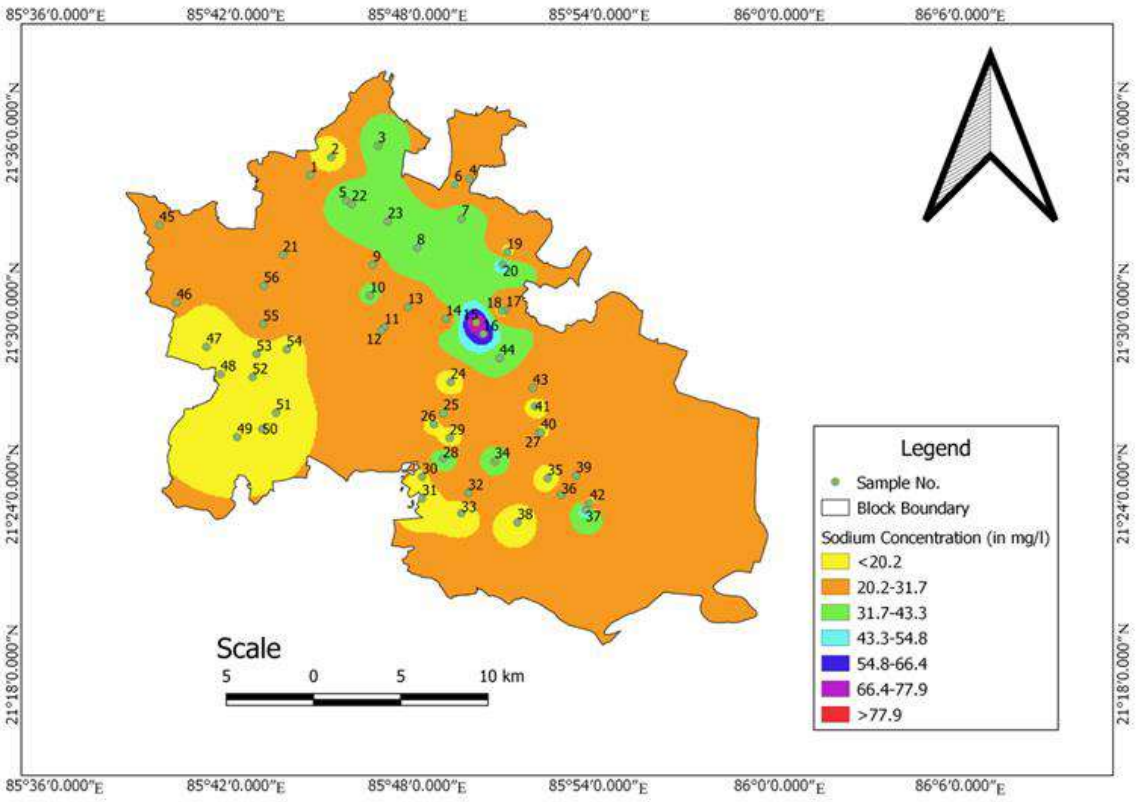

Fig. 8: Spatial interpolation map of Na^{2+} .

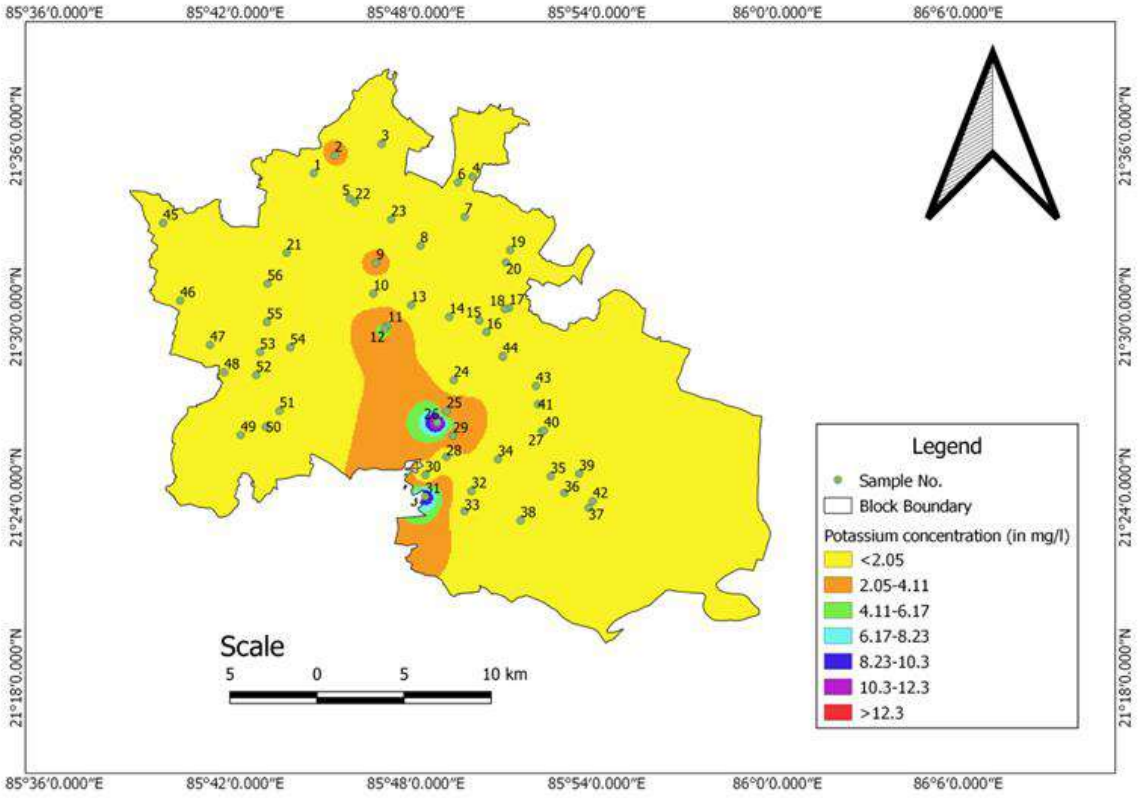

Fig. 9: Spatial interpolation map of K+ .

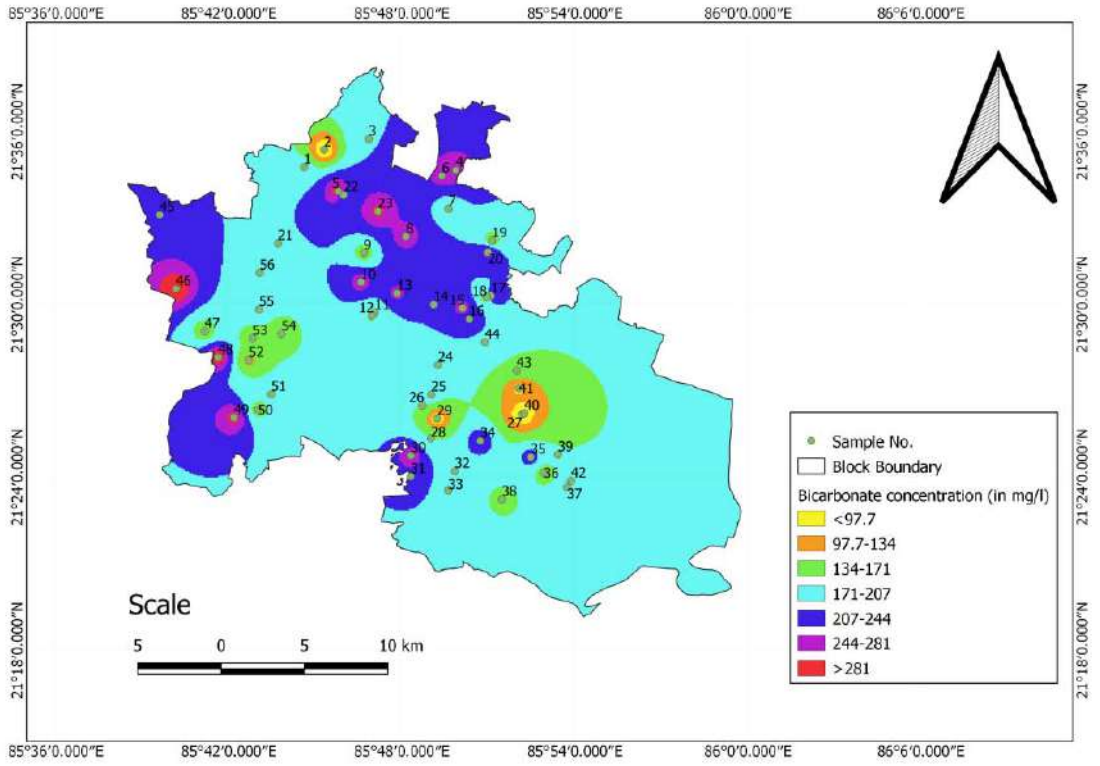

Fig. 10: Spatial interpolation of HCO_3^- in the study area.

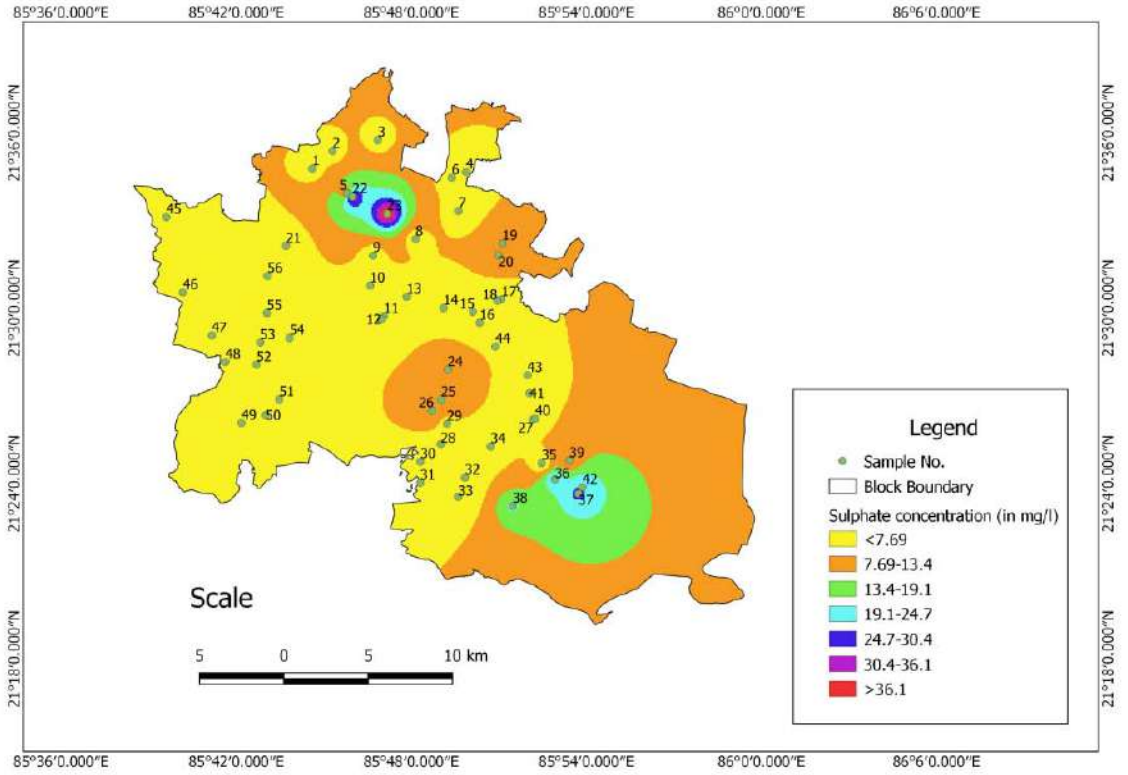

Fig. 11: Spatial interpolation of SO_4^{2-} in the study area.

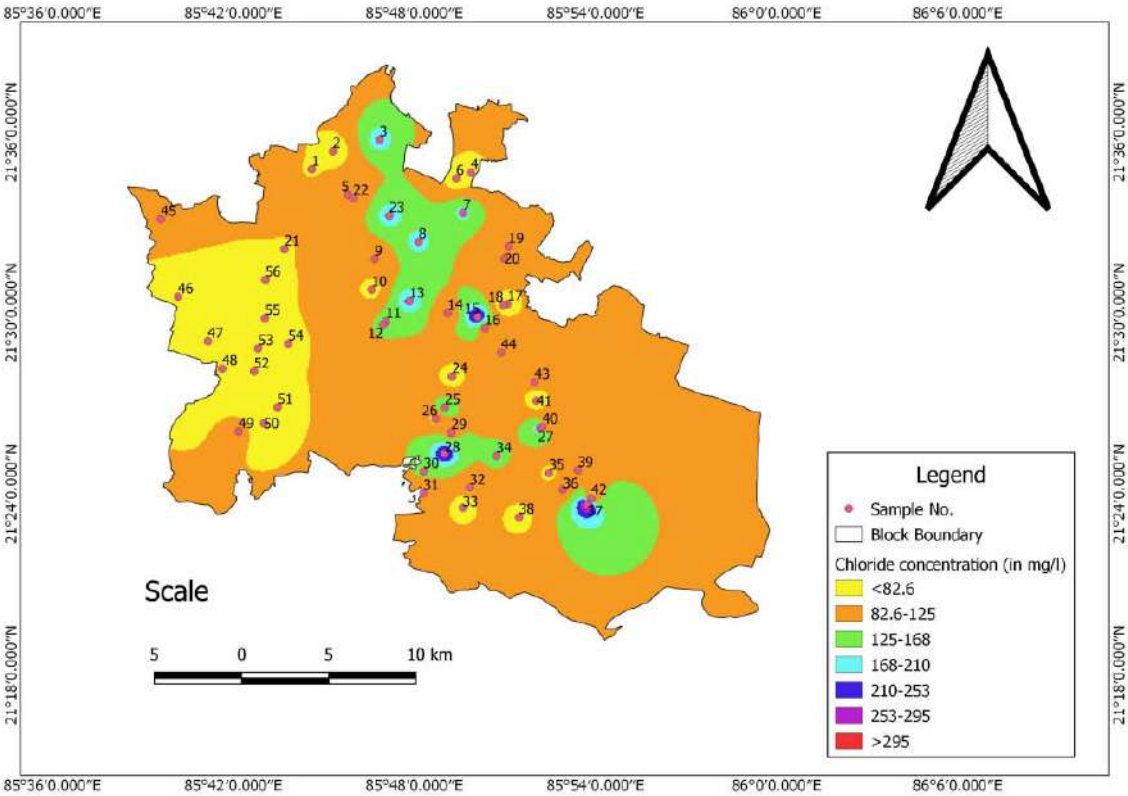

Fig. 12: Spatial interpolation of Cl^- in the study area.

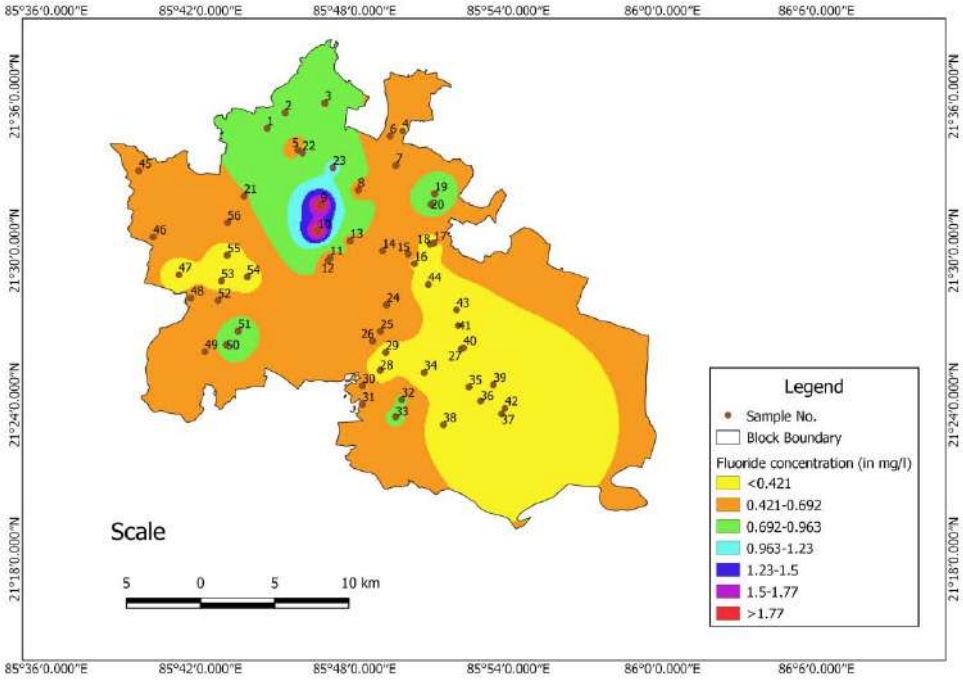

Fig. 13: Spatial distribution of F¯in the study area.

Piper Trilinear Digram

A Piper diagram is a graphic procedure proposed by Arthur M. Piper in 1944 for presenting water chemistry data to help in understanding the sources of dissolved constituent salts in water. The Piper diagram is suitable for comparing the ionic composition of a set of water samples. Water samples shown on the Piper diagram can be grouped in hydro chemical facies. The cation(s) and anion(s) triangles can be separated in regions based on the dominant cation(s) and anion(s) and their combination creates regions in the diamond shaped part of the diagram. The general form of Piper Trilinear Diagram with all its dominant ions is shown in Fig. 14. Fig. 15 shows plotting of groundwater quality data of Ghatagaon block. It is found that most of the samples are in two facies i.e. (a) Carbonate hardness exceeding 50% and (b) mixed type (transition zone).

CONCLUSION

The spatial interpolation diagram of the study area concludes that the groundwater quality is generally of potable category in many parts. In some locations, some parameters exceeded the acceptable limits but all are within the permissible limit except pH and fluoride. It is possible to identify the vulnerable zones due to high concentration of a particular parameter in the maps. So the groundwater of some areas is not suitable for drinking purpose. With respect to pH in the northern parts and with respect to Ca, Mg, F etc in central parts similarly, in some other locations, high TDS and high hardness values make the groundwater unsuitable for drinking purpose. The Piper diagram shows that the groundwater are of two types i.e. carbonate hardness exceeding 50% and mixed type.

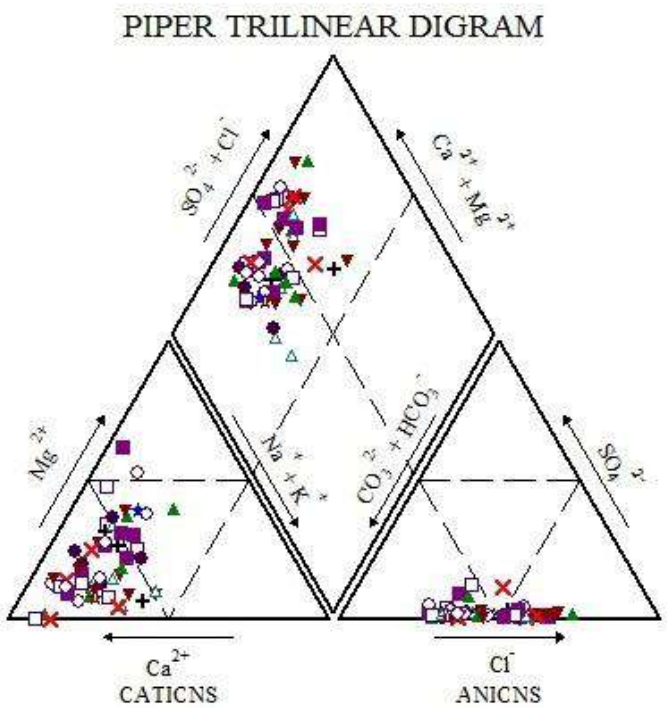

Fig. 14. Plotting of Groundwater quality data of Ghatagaon block on Piper Trilinear Digram.

REFERENCES

American Public Health Association (APHA) (1995) Standard methods for the examination of water and wastewater, U.S.A. 19th edition.

Brown, E., Skougstand, M.W. and Fishman, M.J. (1970) Methods of collection and analysis of water samples for dissolved mineral and gases. Techniques of water resources investigation of the U.S. Geological Survey 5.

Das, P.P., Mohapatra, P.P., Sahoo, H.K., Goswami, S. (2016) A Geospatial analysis of Fluoride contamination of Groundwater in Paradeep Area, Odisha, India. Environmental Geochemistry (ISSN 0972-0383)., Vol.19, No.1&2, pp. 11-14.

Khan, M.K., Ayoub, W., Saied, S., Hussai, M.M., Masood, S.S., Siddique, A., Khwaja, A. (2019) Statistical and Geospatial Assessment of Groundwater Quality in the Megacity of Karachi. Journal of Water Resource and Protection., v.11, pp.311-332.

Piper, A.M. (1944) A Graphic Procedure in the Geochemical Interpretation of Water Analyses.

Subramani, T., Krishnan, S., Kumaresan, P.K. (2012) Study of Groundwater Quality with GIS Application for Coonoor Taluk in Nilgiri District. International Journal of Modern Engineering Research (IJMAR), vol. 2(3), pp. 586-592.

Trivedy, R.K. and Goel, P.K. (1984) Chemical and biological methods for water pollution studies. Env. Publ., Karad, India, pp. 1-215.

Vogel, A.I. (1964) A Textbook of Quantitative Inorganic analysis (3rd edition), pp. 343.

VISTAS IN GEOLOGICAL RESEARCH
Special Publication in Geology (19), March 2023, pp. 158-165

Petrography and Microtexture of Chromite Ores from Asurabandha, Odisha, India

ANKITA BEHERA[1,2] AND BIBHURANJAN NAYAK[1,2*]

[1]CSIR-Institute of Minerals and Materials Technology, Bhubaneswar - 751013, India
[2]Academy of Scientific and Innovative Research (AcSIR), Ghaziabad - 201002, India
[*]Corresponding author e-mail: brn69@rediffmail.com

Abstract: Asurabandha chromite deposit is a small chromite deposit in Dhenkanal district of Odisha and forms a part of 'Sukinda Thrust Zone' (STZ) that lies in the tectonic contact zone between Eastern Ghats Group and Singhbhum Craton. The ore-bearing mafic-ultramafic rocks occur as irregular bodies and are highly silicified and lateritised. This research article focuses on petrographic and microtextural study of the chromitite samples that were done using optical petrological microscope. These samples were also investigated using scanning electron microscope (SEM), X-ray diffraction (XRD) and wavelength dispersive X-ray fluorescence (WD-XRF) spectrometer. Morphologically, the chromitites are massive, spotted and banded in nature and show various textures such as cumulus, chain, clot, cataclastic, corrosion etc. While the cumulus and chain textures reveal the primary magmatic nature of chromite, the cataclastic texture in chromite grains evidences post tectonic disturbances in this area during regional thrusting. The disseminated magnetite associated with host ultramafic rocks show exsolution, intergrowth textures with ilmenite and replacement textures while altering to hematite.

Keywords: Chromite; Petrography; Microtexture; Asurabandha

INTRODUCTION

Archean chromite deposits on earth occur either as stratiform or podiform deposits (Murthy et al., 2011; Papp and Lipin, 2001). In India, stratiform chromite deposits are confined to the ultramafic intrusives of Archaean or Precambrian lithosequences of low or high metamorphic grade. Stratiform type of chromite deposits in low-grade greenstone sequences are found in Odisha, Jharkhand, and Karnataka, while in Tamil Nadu and Andhra Pradesh, they were emplaced in high-grade granulite lithopackages. Manipur, Nagaland, and Ladakh sectors of the Himalayan belt as well as in the Andaman Islands of the Indo-Burma arc are known to host Tertiary ophiolite sequences with ultramafic rocks and podiform chromite. The most significant chromite-bearing ultramafic bodies of the Archean greenstone belts in the Indian shield are the Baula-Nuasahi and Sukinda chromite deposits. Approximately 98% of India's total chromite resources and 2.5% of the world's chromite resources come from these two chromite ore deposits (Tripathy et al., 2014). In addition to these two complexes, several minor chromiferous ultramafic rocks have been discovered southeast of the Sukinda complex in the granulite tract, north of Maulabhanj Parbat in the west and Asurabandha in the east (Banerjee et al.,1962). In this paper we present the detailed petrographic and microtextural characters of chromite ores of Asurabandha area. The study area forms a part of the Sukinda

Thrust Zone (STZ), which is a contact region between the Eastern Ghats Group and Singhbhum Craton.

Geological Setting

The ultramafic-mafic bodies of the Mesoarchean Sukinda ultramafic complex occur towards the southern boundary of the Singhbhum Craton (SC). The 'Sukinda Thrust Zone' marks the contact zone between the Eastern Ghats Group in the south and the Singhbhum Craton in the north (Prasad Rao et al., 1964; Saha, 1994) and unveils rocks belonging to Iron Ore group as well as the granulites (Tripathy et al., 2014). This tectonized zone has also facilitated the emplacement of granitoids and ultramafics into it. Many ultramafic bodies have been reported from Nilgiri (in northeastern part SC) to Deogarh (in southwest) through large ultramafic bodies in the southeastern margin of the craton, i.e. Boula-Nuasahi ultramafic complex (BNUC) and Sukinda ultramafic complex (SUC). Sukinda massif is the largest ultramafic body in this craton having length of about ~25 km and width of ~400m. The Sukinda complex covers an area of about 42 km^2 and occurs in the form of a south-westerly plunging synform having a moderately dipping north limb (40°-50°) and a sub-vertical south limb (Page et al., 1985). The chromite bearing ultramafics in Sukinda valley follows NE-SW orientation and shows pocket type chromite bodies of various sizes, generally associated with the dunite-peridotite types of rocks of stratified nature (Chakraborty and Chakraborty, 1984) and extends from Kansa in the east to Kathpal in the west.

Outside Sukinda valley, chromite bearing mafic-ultramafic intrusives have been recognized in Bhuban-Asurabandha, Maulabhanja-Kamakhyanagar area in the west of Sukinda valley in WNW-ESE trend (Rath and Mohanty, 1986). A huge number of chromite clasts have been identified in two dispersed circular to elliptical chromiferous lateritic exposures near Bhuban area (Tripathy et al., 2014). The chromitites occur as dissemination and small pods both in weathered silicified serpentinite and talc-tremolite schist. The ultramafic/mafic rocks comprise pyroxenite, gabbro, gabbroic anorthosite and anorthosite and chromite-bearing weathered peridotite (Tripathy et al., 2014). The exposure of chromite ores is very limited due to the extensive lateritic overburden in this area. Due to strike-slip faults, shears, and fractures, these chromitite units within the Eastern Ghats granulites are believed to be a tectonically separated component of the Sukinda Ultamafic Complex (Mondal et al., 2006).

MATERIALS AND METHODS

For our primary investigation, polished sections of the collected chromite ores were prepared using conventional techniques, i.e. mounting in araldite followed by grinding and polishing with diamond paste. The prepared sections were investigated using reflected light optical microscope (Leica DM4P) for petrological study. The sections were further examined in a ZEISS EVO-18 Scanning Electron Microscope (SEM) with an accelerated voltage of 15 kV. The X-ray patterns of well-grounded ore samples were obtained using PANalytical XPERT-PRO X-ray diffractometer with CuK_α radiation at 40 kV and 30 mA current. The bulk geochemical compositions for major and minor elements were measured by wavelength-

dispersive X-ray Fluorescence (WD-XRF) Spectrometry by a PANalytical ZETIUM (Minerals Edition) spectrometer.

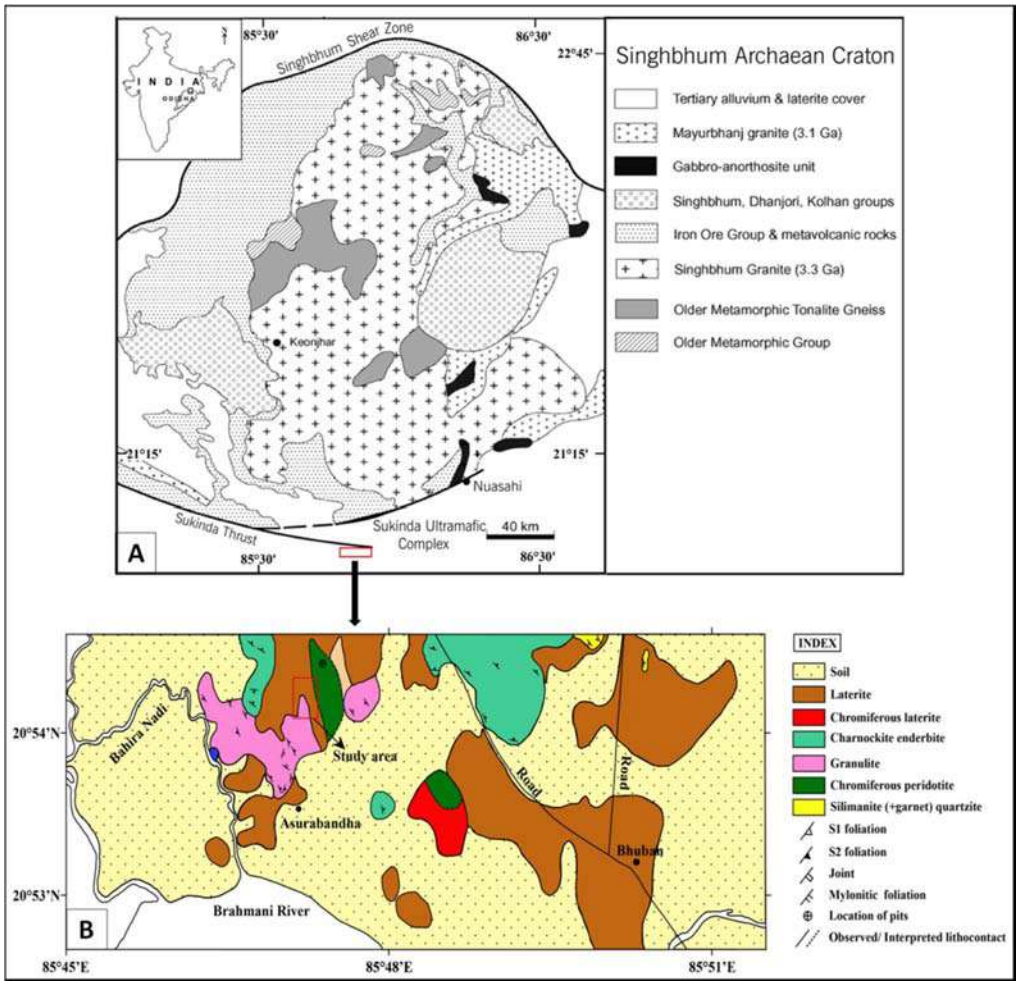

Fig.1: A- Regional geological setting of Singhbhum Craton locating Asurabandha (modified after Saha, 1994; Mondal et al., 2001); B- Detailed geological map of the Bhuban-Asurabandha area (modified after Arasada et al., 2020).

RESULTS AND DISCUSSION

At Asurabandha, chromite is found in altered ultramafic rocks as lenses and sporadic pockets. The chromitite bodies also display layered stratiform nature with thin serpentine and chert veins that cut across them (Singh et al., 2005). The ores are greyish in colour with brownish hue and sometimes found to be lateritic. The chromite ores of the study area can be categorized into massive, spotted and banded types based on their morphology. The Massive ores are medium grained, steel-grey coloured and very hard and compact in nature with very low to no intergranular space. The chromite grains are of various sizes ranging between ~ 150-500 µm. As the concentration of gangue minerals increases, the massive chromitite grades into spotted and banded varieties. The spotted type chromite ore is an intermediate of massive and banded type with the light coloured ultramafic minerals present in oval to rounded form within chromitite matrix to give it a spotted look. The ore contains subhedral to

euhedral chromite grains with sizes ranging from ~100 to 400 µm. The banded ore types have alternate layers of chromite grains and altered ferro-magnesian silicate minerals and the size of chromite grains vary from <100 µm to 400 µm. Due to the severe weathering and silicification process in this region, all of the major ferro-magnesian silicate minerals in the examined chromite ores have been replaced by opal and quartz.

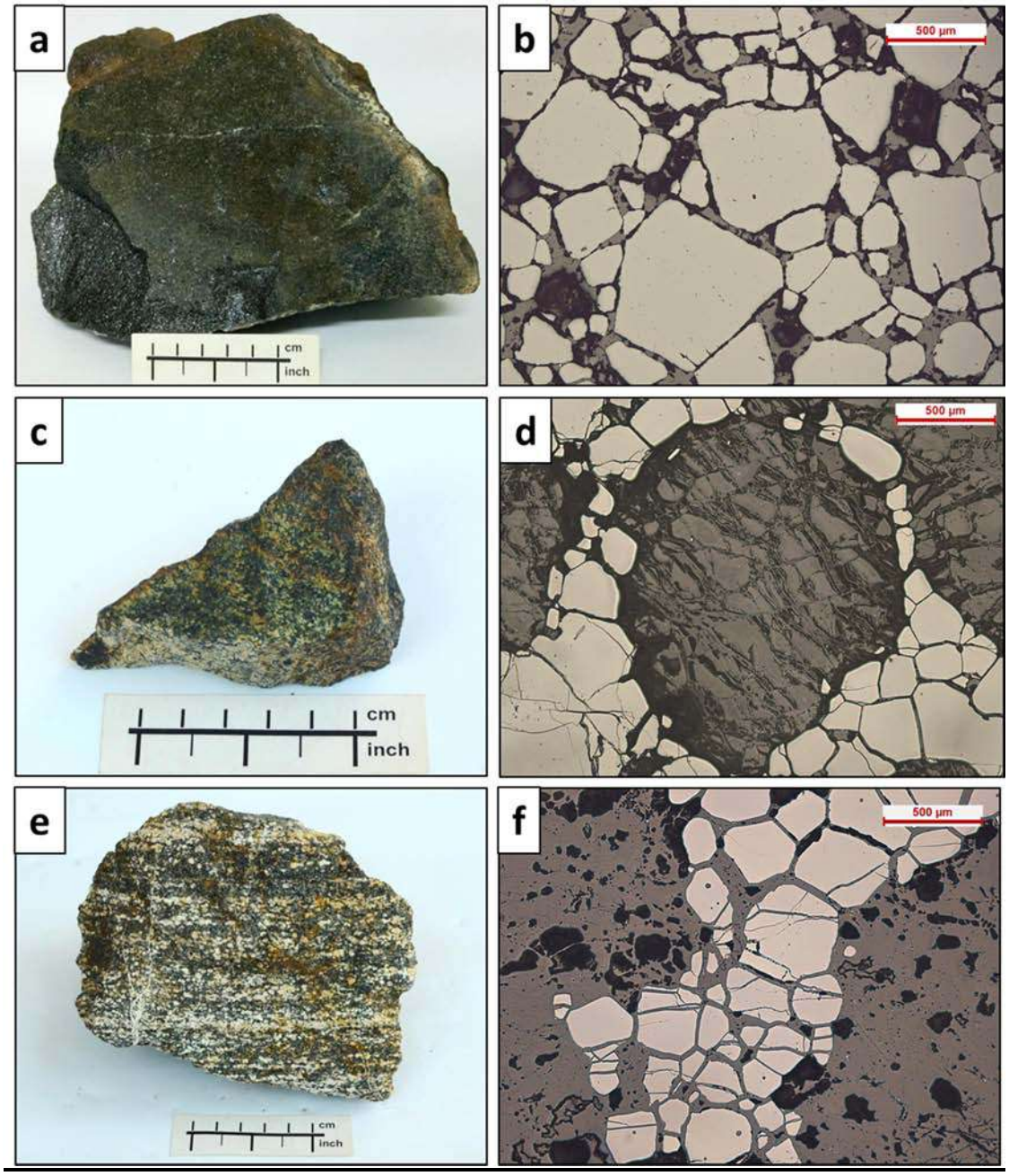

Fig.2: Different varieties of chromite ores based on morphology; (a) Massive medium-grained chromitite, (c) spotted chromite ore, (e) banded chromite ore; Optical photographs of three different types of chromite ores: (b) massive variety having euhedral to subhedral chromite grains exhibits cumulus texture, (d) Spotted chromite ore showing clot of altered ultramafic minerals surrounded by chromite grains, (f) Band of fractured chromite grains in altered silicate matrix.

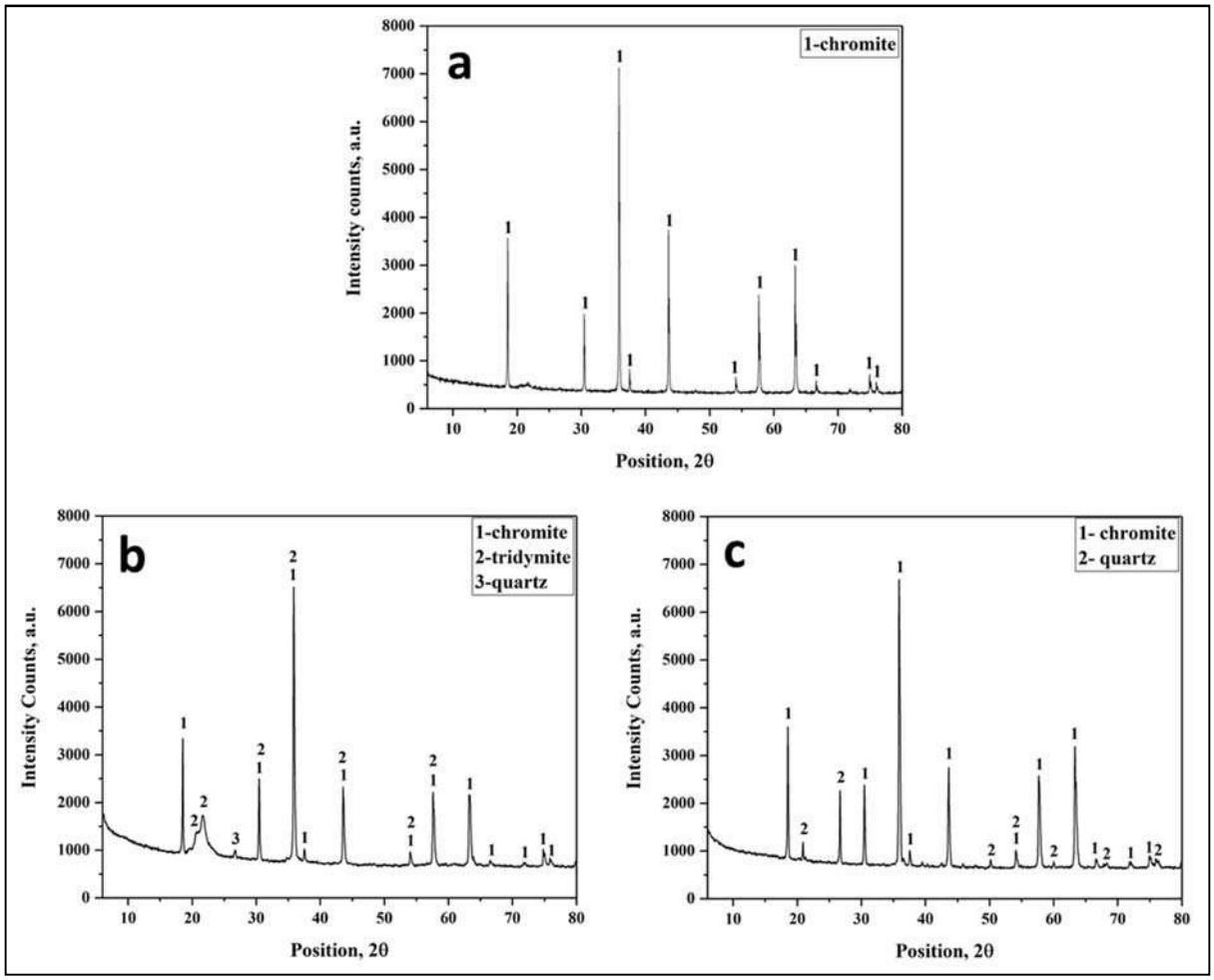

Fig.3: PXRD peaks of three different types of chromite ores; (a) massive ore, (b) spotted ore, (c) banded ore

For identification of mineral phases in XRD, the samples were pulverised to <45 micron size. In massive variety, only chromite phase was identified from the diffraction pattern. In spotted type of ore, chromite along with tridymite and quartz are found to be present while only chromite and quartz were identified in banded type. SEM-EDAX analysis was also done for the confirmation of the phase compositions. Wavelength dispersive XRF spectroscopy was used to obtain the bulk geochemical composition of the ores as shown in table 1. The SiO_2 composition (in wt. %) in massive ore is 17.24, which gradually increases in spotted and banded types i.e., 47.73 and 56.31 respectively. The percentage of Cr_2O_3 is found to be inversely proportional to SiO_2. The source of MgO and Al_2O_3 in the ores is from chromite grains only as other ultramafic minerals have completely altered to some forms of SiO_2 (eg. Quartz and opaline silica). Hence, the percentage of MgO and Al_2O_3 is high in massive variety and low in spotted and banded type with decrease in chromite content.

Table.1: Distribution of major and minor elements in the three types of chromite ores obtained from WD-XRF spectroscopy

	Massive Ore	Spotted Ore	Banded Ore
SiO_2	17.24	47.73	56.31
Cr_2O_3	51.97	29.57	26.48
Fe_2O_3	12.69	13.07	8.75
MgO	10.38	4.6	4.71
Al_2O_3	7.21	3.49	3.56
CaO	0.14	0.2	0.04
TiO_2	0.19	0.1	0.09
NiO	0.19	0.15	-
P_2O_5	-	-	0.02
LOI	0	1.1	0
Total	100.01	100.01	100

The study area has undergone extensive tectonic disturbances because of intense shearing and faulting, indicated by some cataclastic textures like brecciation and shearing of chromite grains (Fig. 4 a & b). Some chromite grains show development of parallel fractures, known as pull-apart texture (Fig. 4c). The corroded margins of chromite grains evidences weathering and alteration process by hydrothermal fluids in the study area (Fig. 4d). Magnetite is frequently found to be present within the ultramafic rocks. Different textures and structures of the magnetite have been observed, and in most cases, it is altered to martite. Magnetite and ilmenite occasionally exhibit intergrowth texture, where development of ilmenite lamellae is found within magnetite grain (Fig. 4e). Additionally, magnetite exhibits replacement texture along its weak cleavage planes, where martitization occurs (Fig. 4f). Martitization is the pseudo-hematitization of magnetite grains along the weak zones, such as edges, fissures, fracture planes and cleavages. The chromitite bodies occur as bands in Sukinda Ultramafic Complex, while in Asurabandha area, chrome-bearing ultramafic rocks within granulite rocks occur in the form of solitary and lensoidal bodies. However, the ultramafic rocks and chromites of both the areas are highly similar in terms of their mineralogical composition (Arasada et al., 2020). In addition to previous studies, we have also found textures like pull-apart, shearing and brecciation in chromite grains which might be due to tectonic disturbances in this area. Hence, according to petrographic evidences, the isolated chromiferous masses of Asurbandha area can be viewed as tectonically separated and displaced rocks from the main Sukinda Ultramafic Complex, related to regional thrusting and strike-slip movement.

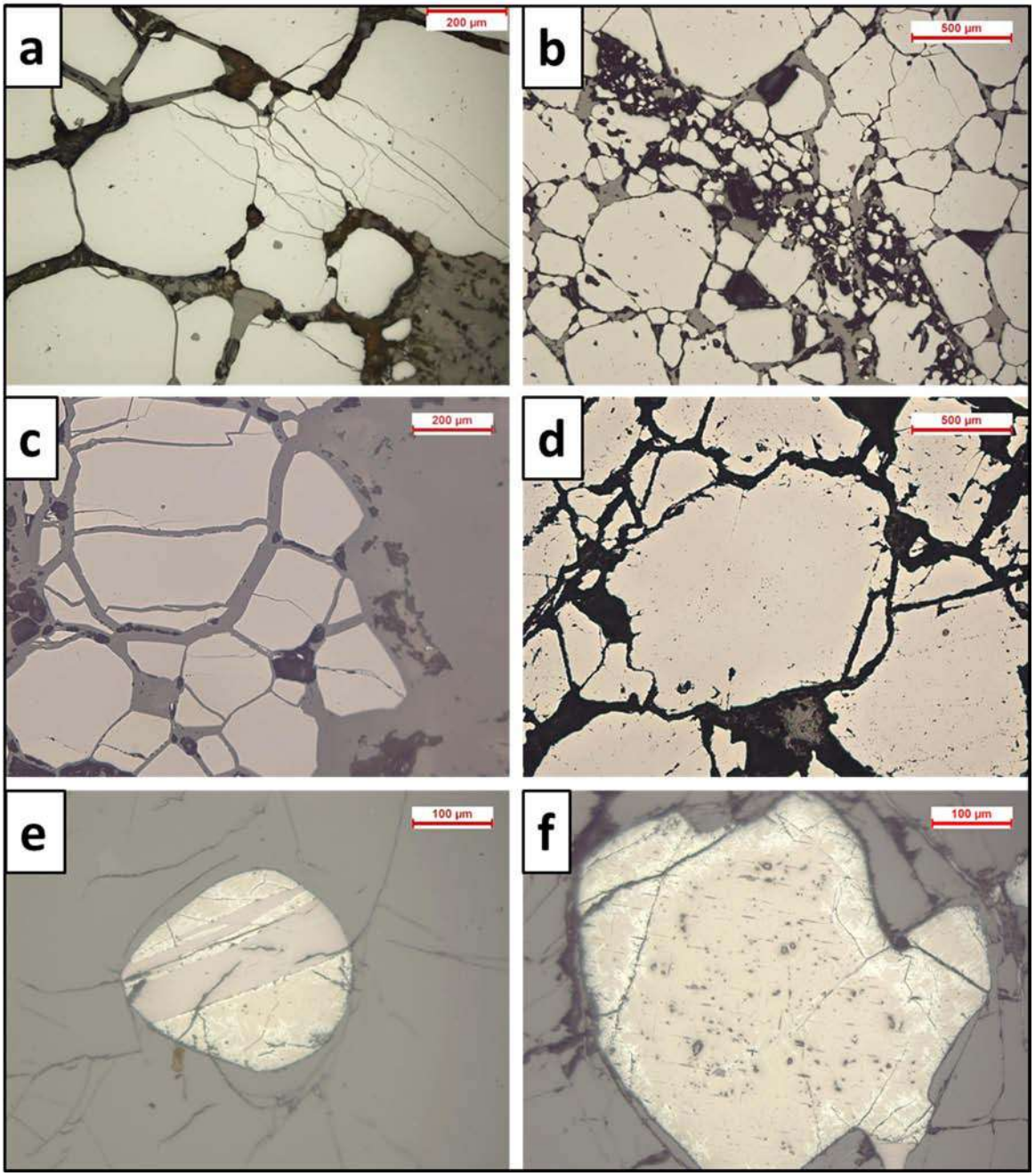

Fig.4: Reflected light optical microphotographs showing (a) Shear strain in chromite grains, (b) Brecciation of chromite grains may be due to faulting, (c) Pull-apart texture in chromite grains as a result of parallel fractures, (d) Corrosion of chromite grains from grain boundary resulting in uneven margins, (e) Intergrowth of ilmenite lamellae in a magnetite grain, (f) Gradual replacement of magnetite grain by hematite.

ACKNOWLEDGMENTS

This is a part of A. Behera's PhD work, which is supported by the University Grants Commission, New Delhi in terms of a research fellowship. The authors are grateful to M/s Real India Consultancy Ltd. for permitting to collect rock and ore samples from their Asurabandha chromite leasehold. The authors are thankful to the Director, CSIR-IMMT, Bhubaneswar for permitting to publish this paper.

REFERENCES

Arasada, R.C., Srinivasa Rao, G., Sahoo, P.R., 2020. Integrated geological and geophysical studies for delineation of laterite covered chromiferous ultramafic bodies around Bhuban, southwestern part of Sukinda ultramafic complex, Odisha. Ore Geology Reviews 119, 103402. https://doi.org/10.1016/j.oregeorev.2020.103402

Banerjee, P.K., Nag, P., Pattanayak, R.N., 1962. A report in the regional assessment of chromite deposits in Cuttack, Dhankanal and Keonjhar districts, Orissa. Unpublished Report. Geol. Surv, India.

Chakraborty, K.L., Chakraborty, T.L., 1984. Geological Features and Origin of the Chromite Deposits of Sukinda Valley, Orissa, India. Minerallium Deposita. 19, 256–265. https://doi.org/10.1007/BF00204378

Mondal, S.K., Baidya, T.K., Gururaja Rao, K.N., Glascock, M.D., 2001. PGE and Ag mineralization in a breccia zone of the precambrian Nausahi ultramafic-mafic complex, Orissa, India. The Canadian Mineralogist 39, 979–996. https://doi.org/10.2113/gscanmin.39.4.979

Mondal, S.K., Ripley, E.M., Li, C., Frei, R., 2006. The genesis of Archaean chromitites from the Nuasahi and Sukinda massifs in the Singhbhum Craton, India. Precambrian Research. 148, 45–66. https://doi.org/10.1016/j.precamres.2006.04.001

Murthy, Y.R., Tripathy, S.K., Kumar, C.., 2011. Chrome ore beneficiation challenges & opportunities - a review. Minerals Engineering. 24, 375–380.

Page, N.J., Banerji, P.., Haffty, J., 1985. Characterization of the Sukinda and Nausahi ultramafic complexes, Orissa, India by platinum-group element geochemistry. Precambrian Research. 30, 27–41. https://doi.org/10.1016/0301-9268(85)90027-0

Papp, J.F., Lipin, B.R., 2001. Chromium. Report: USGS Numbered Series. Open-File Rep. 2001–2381.

Prasad rao, G.H.S.V., Murty, Y.G.K., Deekshitulu, M.N., 1964. Stratigraphic relations of Precambrian iron formations and associated sedimentary sequences in parts of Keonjhar Cuttack, Dhenkanal and Sundergarh districts of Orissa, India. Proc. 22nd Int. Geol. Cong. India Sec. X, 72–87.

Rath, S.C., Mohanty, A. K., 1986. Report on the investigation of ultramafic bodies in parts of Dhenkanal district, Orissa. (For additional chromite resources). Geol. Surv. India, Unpubl. Rep. F.S. 1983-84.

Saha, A.K., 1994. Crustal evolution of Singhbhum North Orissa. Eastern India. Mem. Geol. Surv. India 27, 341.

Singh, P., Das, M., Acharya, D., Acharya, S., 2005. On Some Traits of The Chromite and Magnetite Around Moulabhanj, Dhenkanal District, Orissa. Vistas in Geological Research U.U. Spl. Publ. Geol. 126–131.

Tripathy, A., Sahoo, K., Chaudhuri, T., Sar, R., Mohanty, M., Das, M., 2014. PGE-bearing chromite cumulates from boninitic ultramafic parentage in Bhuban Ultramafic Complex (BUC), Odisha. Indian Journal of Geosciences. 68.

VISTAS IN GEOLOGICAL RESEARCH
Special Publication in Geology (19), March 2023, pp. 166-169

Pre Monsoon Groundwater Chemistry of Bolagarh Block, Khordha District, Odisha

PINALI MOHAPATRA AND DURGA SHANKAR PATTANAIK

P.G. Department of Geology, Utkal University, Bhubaneswar-751004

Abstract: Twenty seven water samples were collected during pre monsoon period 2022 and analyzed for physico-chemical parameters. The pH values of the studied samples vary from 6.28 -7.6 indicating that the ground water is slightly acidic to slightly alkaline in nature. The groundwater of the area exhibits medium to high inland salinity in few locations as evidenced from the electrical conductivity values. It comes under hard to very hard category on the basis of Total Hardness values. High fluoride contamination is indicated in few locations. Majority of the water samples contain iron above the BIS permissible limit for drinking water. The groundwater of the study area is therefore not generally suitable for drinking purposes without proper treatment.

Keywords: Groundwater quality, Bolagarh block, drinking water.

INTRODUCTION

Groundwater is important for human water supply and in Asia alone 1 billion people are directly dependent upon this resource (Foster 1995).In India, groundwater resources support nearly 50% of irrigated agriculture and more than 80% of freshwater demand for domestic use. As a result, there is incessant pressure on the groundwater resources, which affects both the quality and quantity of groundwater (Singh et al. 2017). However, use of groundwater is advantageous as it is comparatively fresh and widely distributed unlike the surface water. Threats to groundwater have been increasing everyday due to rise in population and their needs. Because of geogenic and anthropogenic reasons the presence of low or high concentration of certain ions is a major issue as they make the groundwater unsuitable for drinking, domestic, agricultural, and industrial uses. The groundwater quality depends on its physical and chemical parameters evolved due to weathering, decomposition and changes occur with respect to time and space (Venkatesan D et al. 2016). The present study has been conducted for assessment of groundwater quality for domestic and agricultural activities.

STUDY AREA

The study area covers Bolagarh block of Khordha district, Odisha stretching from20^0 6’ 52”N to 20^0 17’ 2” N latitudes and85^0 12’ 4” E to 85^0 27’ 27” E longitudes. This area forms a part of Eastern Ghats Super Group and the major rock types of the area are granite gneiss, charnokites and its derivatives. The Bolagarh block is characterized by a population of 90,794 living in 157 villages (Census report, 2011).

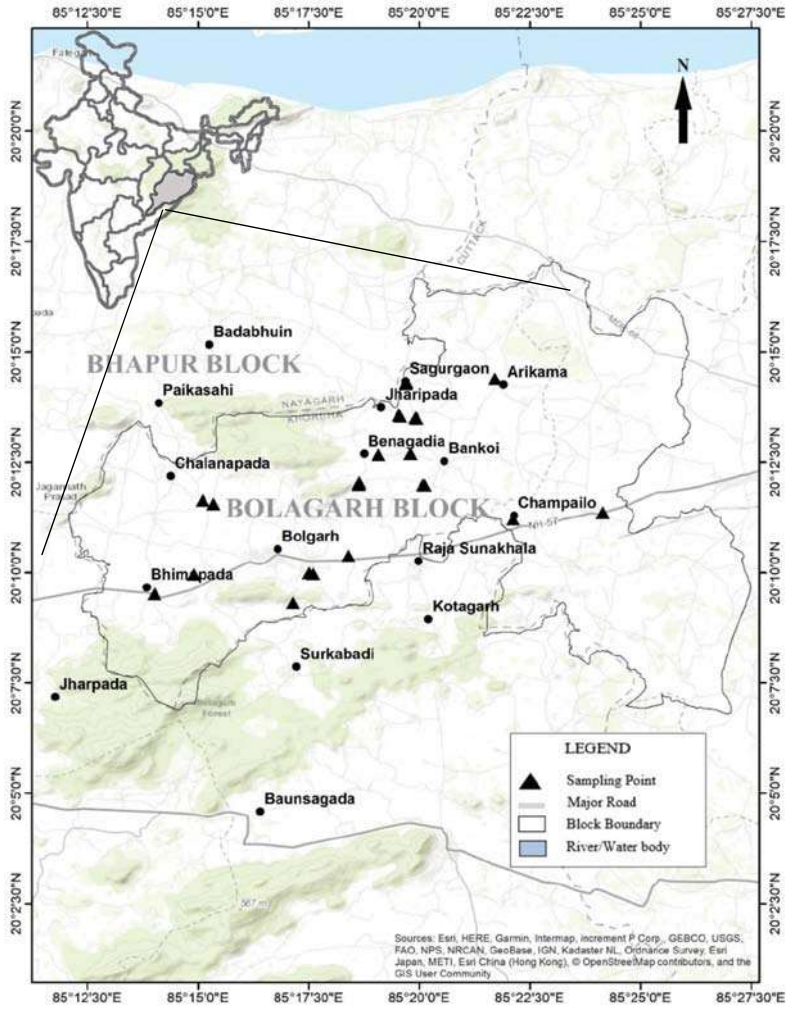

Fig. 1: Map of study area showing sample locations.

MATERIALS AND METHOD

Twenty seven (27) groundwater samples were collected during pre-monsoon period of 2022 from different parts of study area using cleaned polyethylene bottles as per the standard procedure (APHA, 2005) to avoid contamination and change in chemical characteristics. Field parameters such as pH, Electrical conductivity (EC) & Total dissolved solid (TDS) of water samples were measured using portable meters. Concentration of major cations (Ca^{2+}, Mg^{2+}, $Na^{+}$and K^{+}), anions (CO_3^{2-}, HCO_3^{-}, Cl^{-} and SO_4^{2-}), total alkalinity and total hardness of the water samples were determined following standard analytical procedures (APHA, 2005& BIS,2012). Na^{+} and K^{+} were determined by flame photometer. Ca^{2+}, Mg^{2+}, CO_3^{2-}, HCO_3^{-}, Cl^{-}, TA (total alkalinity) and total hardness (TH) were determined by volumetric titrations and NO_3^{-}, SO_4^{2-} were estimated by spectrophotometer. Iron was estimated by atomic absorption spectroscopy (AAS) and F^{-} by ion selective electrode method.

RESULTS AND DISCUSSION

The physio-chemical characteristics of the groundwater samples were evaluated in accordance with the Bureau of Indian Standards Specifications for drinking water (BIS, 2012) and World Health Organisation for Drinking water quality (WHO,2004). The pH of the groundwater samples of the study area varies from 6.28 to 7.66, which indicates that the groundwater is slightly acidic to slightly alkaline in nature. The EC of the water samples varied from 330 to 3750 µS/cm, which indicates medium to high salinity (Handa, 1969). The TDS is in between 214.5 to 2437.5 mg/l which is under permissible limit except in few locations with high values.93% of water samples of the study area come under hard to very hard category after Sawyer and McCarthy (1967) hardness classification and thus require water softening treatment.The concentrations of cations, such as Ca^{2+}, Mg^{2+}, Na^{+} and K^{+} are within the maximum permissible limits for drinking except for few water samples. Ca concentration varies from 30.46 to 243.69 mg/l and Mg concentration varies from 1.94 to 79.7 mg/l. Na and K concentration varies from 18.71 to 671mg/l and 0.02 to 613.3 mg/l respectively. High fluoride values are indicated in few locations. Most of the samples contain iron above the permissible limit; hence water should be used for drinking after removal of excess iron content. Chloride content of the samples are in the range of 20 to 772 mg/l. Bicarbonate concentrations vary from 136.64 to 756.4 mg/l. Sulfate concentration varies from 0.43 to 225.08 mg/l. The parameters show values above desirable limit but within the permissible limit.

Table 1. Physico-chemical analysis of Groundwater samples from the study area.

Water Quality Parameters	Unit	IS 10500: 2012		Minimum	Maximum	Mean	Standard Deviation
		Acceptable limit	Permissible limit				
pH		6.5-8.5		6.28	7.66	7.08	0.36
EC	(µS/cm)	500	1000	330	3750	1461.55	870.84
TDS	(mg/l)	500	2000	214.5	2437.5	950.01	566.04
TH	(mg/l)	200	600	108	768	319.55	182.1
TA	(mg/l)	200	600	112	620	326.37	121.81
Fe	(mg/l)	0.3		0.08	20.54	2.27	4.12
Ca	(mg/l)	75	200	30.46	243.69	80.81	53.21
Mg	(mg/l)	30	100	1.94	79.7	28.65	20.72
Na	(mg/l)	200	-	18.71	671	158.58	167.08
K	(mg/l)	-	-	0.02	613.3	73.88	160.84
Cl	(mg/l)	250	1000	20	772	231.41	206.5
F	(mg/l)	1	1.5	0.15	2.53	0.63	0.46
NO_3	(mg/l)	45	100	0.02	169.24	38.1	47.11
SO_4	(mg/l)	200	400	0.43	225.08	47.39	47.63
HCO_3	(mg/l)	-	-	136.64	756.4	398.17	148.61

CONCLUSION

Groundwater quality and its suitability for drinking purposes were studied in the Bolagarh block of Khordha district, Odisha.The hydro-chemical analysis shows the groundwater of the study area shows considerable variation. On comparison with BIS (2012), it indicates that except iron, all chemical parameters are within permissible limit except few samples. However iron content is quite high in many samples. Hence, water should be used for drinking after removal of excess iron.

REFERENCES

APHA (2005) Standard methods for the examination of the water and waste water, American Public Health Association.

BIS (2012) Indian Standard Drinking water – Specification (Second Revision), Bureau of Indian Standards, IS 105000:2012.

Foster SSD (1995) Groundwater for development: An overview of quality constraints. In: Nash H, McCall GJH (eds) Groundwater quality, 17th Special Report, Chapman and Hall, London United, pp1-3.

Handa, B.K., 1969. Description and classification of media for hydro-geochemical investigations. In: Symposium on Ground Water Studies in Arid and Semiarid Regions, Roorkee.

Singh R, Syed TH, Kumar S, Kumar M, Venkatesh A.S (2017) Hydrogeochemical assessment of surface and groundwater resources of Korba coalfield, Central India: environmental implications. Arab J Geosci 10:318. doi: 10.1007/s12517-017-3098-6.

Sawyer GN, McCartly DL (1967) Chemistry of sanitary engineers, 2ndedn. McGraw-Hill, New York, pp 518.

Venkatesan D, Suresh Gandhi M, Thivya C (2016) Quality of Groundwater and hydrogeochemical processes in hard rock region of Salem taluk, Tamilnadu. EnviroGeoChimica Acta (2016) 3(1): 63-70.

WHO (2004) Guideline of Drinking water quality in Health criteria and other supporting information. World health Organisation, 2:336.

VISTAS IN GEOLOGICAL RESEARCH
Special Publication in Geology (19), March 2023, pp. 170-176

Erosion-Deposition Framework for Detrital Iron-Ore Deposit (DID) of Chamkpur-Inganjharan area of Keonjhar District, Odisha

A. PARIDA* AND D. BEURA

P.G. Department of Geology, Utkal University, Bhubaneswar-751004
* amiya009@gmail.com

Abstract: Chamakpur-Inganjharan area in Keonjhar district, Odisha is known for the iron ore conglomerates, which is termed as Detrital Iron Ore Deposits (DID). Both the areas Chamakpur and Inganjharan lying on opposite sides of River Baitarani in the eastern side of Joda East iron formation are occupied with DID of varying spatial horizons. The area comes under the Survey of India Toposheet no.F45H8 (73 F/8), lying between the North Latitude 22°00′00″- 22°02′30″and the East Longitude 85°27′30″- 85°30′00″. DID comprises of fragments of iron formation of varying sizes and shapes cemented by fine grained hematite, goethite, kaolinite and limonite matrices. The source for this detrital iron ore is the western IOG i.e. iron formation of Joda East belonging to the eastern limb of the Bonai-Keonjhar belt. Joda East Iron formation as provenance supplied the eroded iron materials in form of colluvium and alluvium deposited as DID in Chamakpur-Inganjharan area. Cobbles and boulder sized materials are deposited in Chamakpur area because of high altitude difference between source and deposition site. Weathered materials at the source travelled under gravity along high angle sloping terrain and deposited at Chamakpur area. Rock fragments along with iron ore are deposited in this way known as colluvium. However, alluvial sediments of pebble and gravel size are deposited to form the DID in Inganjharan area. Morphology of DID of Inganjharan shows rounded clasts of iron formation whereas sub-rounded to angular clasts are noticed in DID of Chamakpur area.

Keywords: Detrital Iron Deposits (DID), Chamakpur-Inganjharan area, Colluvium, Alluvium

INTRODUCTION

Odisha is the largest producer of high grade iron ore in India. There are three distinct iron ore bearing provinces together constitute the Iron Ore Super Group (IOSG) of Odisha (Beura and Singh, 2005; Nanda and Beura, 2021; Beura et al., 2023) accounting for the maximum iron ore resources. Badampahar-Gorumahisani-Suleipat belt (BGS belt), Bonai-Keonjhar belt (BK belt) and Daitari-Tomka belt (DT belt) are the designated IOGs flanking the North Odisha Iron Ore Craton in eastern, western and southern sides respectively. Banded iron formation hosting the iron ores is the dominating litho-horizon of IOSG. Chamakpur - Inganjharan area in the Keonjhar district, Odisha lying in the eastern limb of 'U'-shaped BK belt is one of the few localities where detrital iron ore deposits (DID) are noticed. The area comes under the Survey of India Toposheet no. F45H8 (73 F/8), lying between the North Latitude 22°00′00″- 22°02′30″and the East Longitude 85°27′30″- 85°30′00″.Chamakpur and Inganjharan are two

separate localities lying on opposite sides of River Baitarani in the eastern side of Joda East iron formation. DID with morphological differences in these areas are of common composition that include pebbles and cobbles of hematite, goethite, BHJ, jasper/quartz and shale cemented by fine matrix of goethite/hematite and varying amount of lateritic masses. Iron formation of Joda East in the western side of the area might have supplied the clasts and matrix materials in form of colluvium and alluvium deposited as DID. Cobbles and boulders of mostly iron formation fragments form DID in Chamakpur area are poorly sorted colluvial masses. However, DID in Inganjharan area constitutes alluvial derived sediments of rounded to sub-rounded pebbles and gravels. Since the Joda East provenance maintains high altitude with respect to Chamakpur, the masses might have been derived under gravity as colluvium, which are characterized by size, shape and sorting of sediments Turner (1996) and Morris et al., (2003). In contrast, alluvium is transported through the drainage system to reach the depositional site at Inganjharan.

GEOLOGY

The detrital iron ore deposits of Chamakpur and Inganjharan areas are located at the north-eastern part of the eastern limb of Bonai-Keonjhar belt (Fig.1). The Bonai-Keonjhar belt, the youngest Iron Ore Group in the Iron Ore Super Group of Odisha, is designated as BIF-III (Acharya 1984, 2000) that occupies a distinct 'U'-shaped pattern in the western flank of the NOIOC resting over the Dhanjori quartzite (Misra 1961; Iyengar and Murthy 1982). The Precambrian IOG largely contains BIF in addition to the other volcano-sedimentary rocks forming a significant portion of the North Odisha Craton. The litho-associations of this area comprises of banded hematite jasper, banded hematite quartz/chert, banded shale, banded manganese formation and ferruginous shale. The banded iron formation consists of predominantly iron oxide minerals such as hematite, magnetite, martite, specularite, and the silica as chert, jasper and quartz. The litho-assemblages of this youngest Iron ore belt are un-metamorphosed and lack of intrusive. The general structural disposition of the rocks of the area shows a synclinorium trending NNE-SSE direction having low plunge towards NNE.

The detrital iron deposit occurs as small horizons in discontinuous manner along with bedded iron formation in many parts of the BK belt. They occur at Chamakpur and Inganjharan area on both sides of the river Baitarani and are being mined in good. The DID consisting of pebbles/cobbles of hard laminated hematitic ore, irregular fragments of BIF, shale, chert and jasper are cemented mostly by hematite/goethite matrix. The matrix may also include fine to medium grained clastic quartz and silica.The disposition of DID masses in form of mounds and upheaval patches in the area remain aligned with the general trend of B-K belt i.e., NNE-SSW. A north-south fault along the course of Baitarani River has separated Chamakpur area from Inganjharan. Apart this several east-west aligned faults have also been noticed in this region.

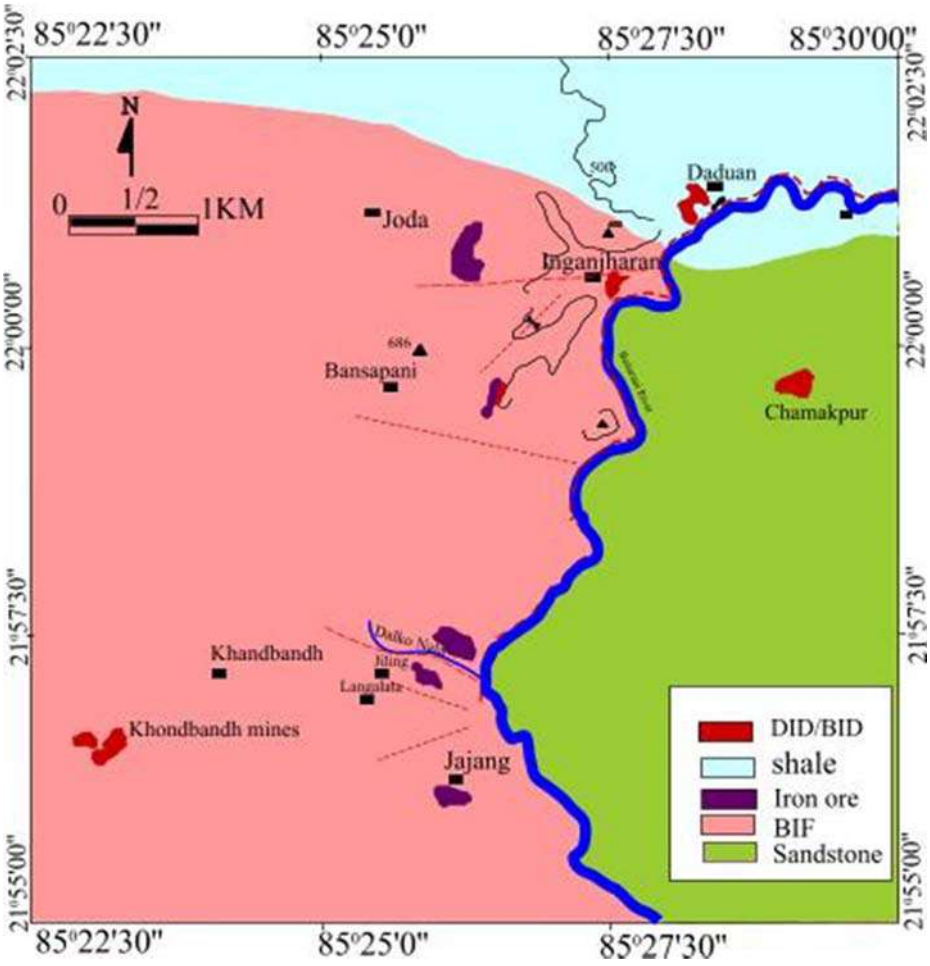

Fig.1: Geological map showing the DID deposits of Chamakpur-Inganjharan area of Bonai-Keonjhar belt.

MODE OF OCCURRENCE

The DID of Chamakpur-Inganjharan area overlie a succession comprising of medium to coarse grained subarkosic sandstone and itself overlain by a succession of cross stratified sandstone Mukhopadhyay et al., (2007) and Mohapatra et al., (2008). In Chamakpur area, DID occurs as separate entity covering an area about 3 km^2 in form of segregated heaps and mounds with limited deep rooting of 3-4 meters (Fig.2.A). Also, it extends as short ridges and elongated loads having about 200 m length and 30m of thickness (Fig.2.B). Mining of iron ores from DID horizons of Chamakpur area is being done sporadically, since continuity and ore reserve estimation is yet to be assessed. In Inganjharan area DID occurs as horizontal stretches with varying relief covering an area about 2 km^2. These are commonly found along the banks of River Baitarani (Fig2.C) and nearby foothills (Fig. 2.D). Isolated patches and DID boulders are often encountered in the surrounding area. Size, shape and sorting of clasts are the major differentiating parameters between the DID of Chamakpur and Inganjharan area.

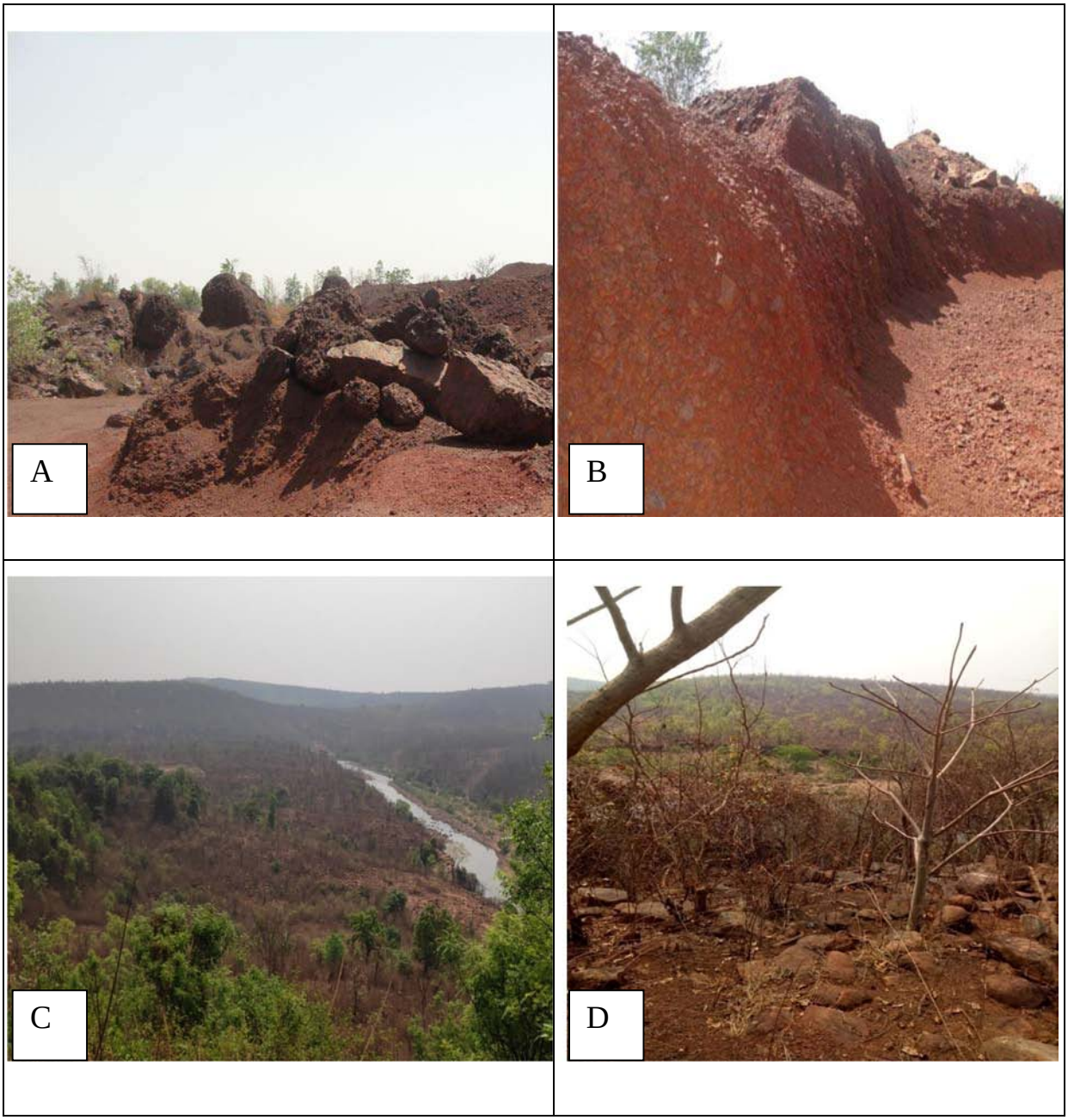

Fig. 2: Field photographs showing
A. DID of Chamakpur in form of segregated heaps and mounds.
B. DID of Chamakpur showing short ridges and elongated loads topography, comprising of angular to subrounded clasts.
C. DID of Inganjharan deposited near banks of River Baitarani.
D. DID of Inganjharan found nearby foothills.

EROSION-DEPOSITION FRAMEWORK

DID of the study area is formed by erosion and deposition of colluvial/alluvial materials from the source area i.e. the iron formation of Joda East. According to Morris (1994) colluviums or colluvial materials are loose, heterogeneous and incoherent mass of soil material and /or rock fragments deposited by rainwash, sheetwash or slow continuous down slope creep usually concentrated at the base of gentle slopes or hill sides. Alluvium is deposited by surface runoff or sheet erosion usually at the base of a slope. DID of Chamakpur comprise of colluvium whereas alluvial materials form the DID of Inganjharan (Fig.3). Physiographic setting, compositional similarity of material and path of transportation indicate that Banded Iron Formation of Joda East is the provenance to supply material for the DID formation of Chamakpur-Inganjharan area. Joda East crop up as higher elevated area of altitude (675 meter) while Chamakpur and Inganjharan area lies at altitudes of 440 m and 460 m respectively. Higher altitude differences and topographic configuration between source and depositional site favours colluviums to be deposited in Chamakpur.

Colluvial material comprising of larger fragments of ironformation from the provenance have been crawled down under gravity and transported to Chamakpur area maintaining the momentum till the loss of their inertia.Clasts of larger diameter attain greater momentum and tend to travel larger distancein comparison to smaller fragments. This might be the process by virtue of which boulder sized DID outcrops are noticed in Chamakpur area (440 Msl).

Inganjhan area exhibits DID formed by the alluvial materials comprising cobble and granule. Eroded clast of iron formation is transported from the Joda East provenance through different orders of streams which pour out the alluvium deposited as DID. Here the smaller fragments could be able to reach the destination site as the carrying capacity of channels suited their transportation. The larger fragments could not be transported to a long distance while smaller fragments are carried away in channel through surface runoff.

CONCLUSION

Dominated by the bedded type of iron formation, the BK belt also exhibits detrital and brecciated type of iron deposits at some localities. Chamakpur and Inganjhan are two such localities in the eastern limb of the Horseshoe shaped belt that exposes detrital iron deposits. Morphologically the DID of the two areas are different though the composition remain almost same. Larger fragments with angular to subrounded shapes comprising of rocks of iron formation, jasper and shale are cemented by the hematitic matrix mainly to form the DID in Chamakpur area. The erosion-depositional framework has been studied to be fit to colluvial type of material supported by factors like size, sorting and transporting mode. Inganjharan DID differs from the DID of Chamakpur area with regards to the size and sorting. Alluvial materials transported through channels are deposited in form of horizontal stretch in Inganjharan.

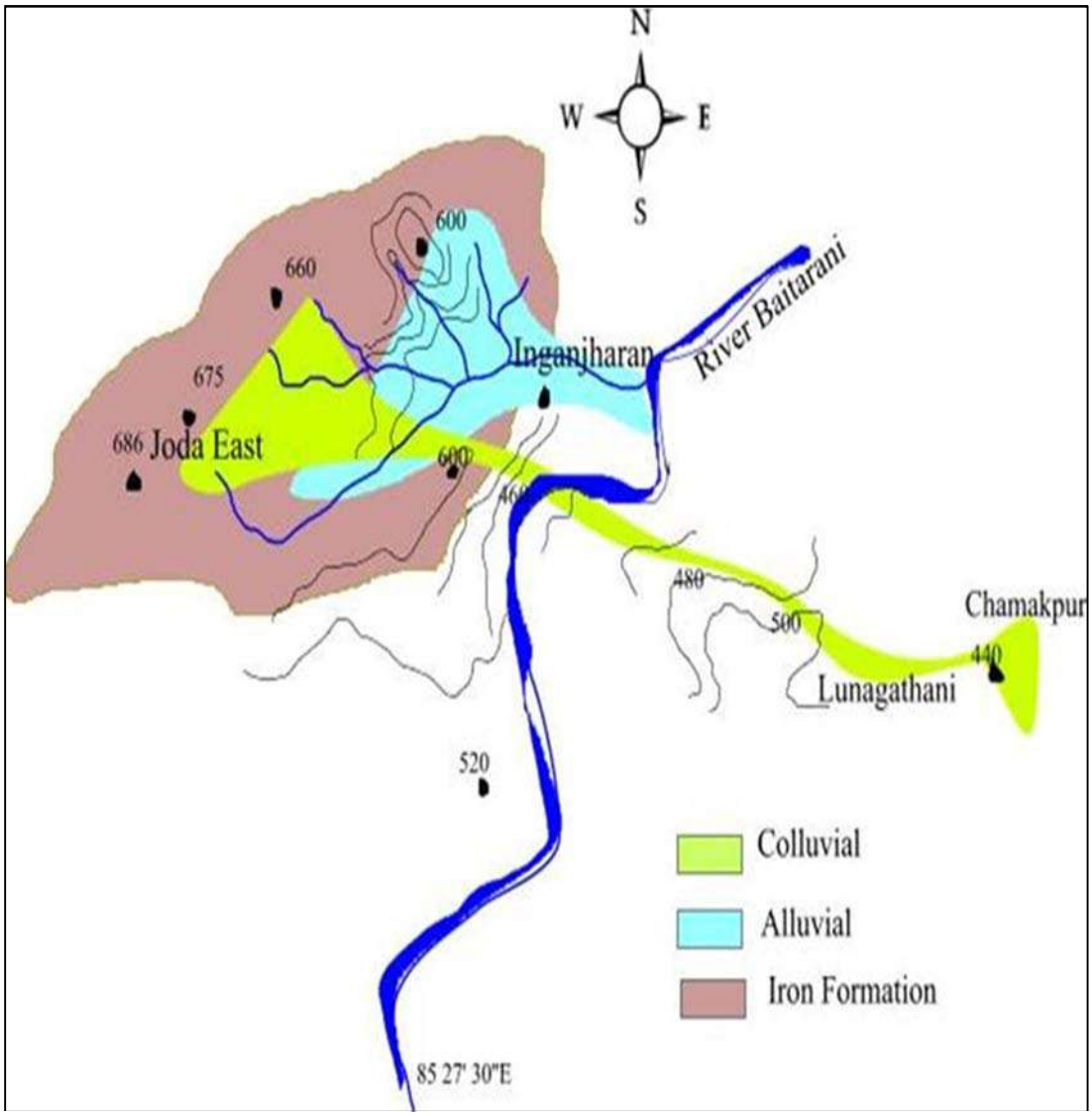

Fig. 3: Schematic diagram of Chamakpur-Inganjharan colluvial/alluvial iron ore deposits

REFERENCES

Acharya, S. (1984) Stratigraphy and structural evolution of the rocks of Iron Ore Basin in Singhbhum-Orissa Iron Ore Province. Ind. Jour. Earth Sci., Seminar v.1, pp.19-28.

Acharya, S. (2000) Some observations on parts of the Banded Iron Formations of Eastern India.

President. Address, 87th Session, Ind. Sci. Cong., v.1, pp.1-34

Beura, D. Singh, P. (2005) Geological setting and mineral deposits of Archaean schist belt-A case study around Badampahar belt, North Orissa, India. Proc. Internatl. Sem., Khon Ken University, Thailand, pp. 326-329.

Beura, D. Singh, p. Satpathy, B. Behera, S. and Nanda, S.K. (2016) Field Relationship among the Three Iron Ore Groups of Iron Ore Super Group Encircling the North Odisha Iron-

Ore Craton, India; A Comparision Study. Journals of Geosciences and Geomatics. 4(3), 53-60.

Beura, D. Nanda, S. K. Parida, A. Pattanayak, L. (2023) Deformation Episodes in Iron Formations of Eastern Province of North Odisha Iron Ore Craton, Eastern India, Journal of Geosciences Research. Vol.8, No.1, pp. 38-42

Iyengar, S. V. P and Murthy, Y. G. K. (1982) The evolution of the Archean proterozoic crust in parts of Bihar and Orissa eastern India. Rec. Geol. Surv. India; v 112, pp.1-6.

Misra, G. B. (1961) A note on stratigraphy of Joda area, Keonjhar. Quarterly Journal of the Geological, Mining and Metallurgical Society Of India 33, 15-22

Mohapatra, B. K. Singh, P. Mishra, P. P. Mahant,K. (2008) Detrital iron-ore deposits in the Iron Ore Group of rocks, northern Orissa, eastern India, Australian Journal of Earth Sciences. An International Geoscience Journal of the Geological Society of Australia, 55:8, 1139-1152

Morris, R.C. (1994) Detrital Iron Deposits of the Hamersley Province, CSIRO/AMIRA Iron Ores of the Hamersley Province Project P75G, Exploration and Mining Restricted Report 76R.

Morris, R. C. Ramanaidou, E. R. and Horwitz, R. C.(2003) Channel iron deposits of the Hamersley Province. CSIRO, Division of Exploration and Mining, AMIRA Project P75G, Restricted Report No. 399G

Mukhopadhyay, J. (2007). Precambrian Colluvial Iron Ores in the Singhbhum Craton:

Implications for Origin, Age of BIF-Hosted High-Grade Iron Ores and Stratigraphy of the Iron Ore Group. Journal of the Geological Society of India. 70. 34-42.

Nanda, S.K. and Beura, D. (2021) Implicating the Origin and Depositional Environment of Banded Iron Formation (BIF) of Bonai-Keonjhar Iron Ore Belt in Eastern India from its Petrography and Geochemistry.Geology of Ore Deposits. Vol. 63, No.6, pp. 497-514

Turner, A.K. (1996) Colluvium and Talus, Landslides; Investigation and Mitigation. Chapter-20, p. 525-554http://onlinepubs.trb.org/Onlinepubs/sr/sr247/sr247-020.pdf

VISTAS IN GEOLOGICAL RESEARCH
Special Publication in Geology (19), March 2023, pp. 177-163

Textural Development in Minerals of Iron Formation of Eastern India: Importance for Downstream Processing

JYOTIRMAYEE MAHANTA[1,2,*], DEVANANDA BEURA[3], CHITA RANJAN MAHANTA[4] AND PRABHAS CHANDRA BEURIA[1,2]

[1]CSIR-Institute of Minerals and Materials Technology, Bhubaneswar 751013, India
[2]Academy of Scientific and Innovative Research (AcSIR), Ghaziabad 201002, India
[3]Department of Geology, Utkal University, Bhubaneswar 751004, India
[4]Department of Applied Geology, Indian Institute of Technology (Indian School of Mines) Dhanbad
*Corresponding author: jyotirmayee.21@immt.res.in

Abstract: The Precambrian Bonai-Keonjhar (BK) Iron Ore Group (IOG) is the major Iron Formation in eastern India to serve the Iron & Steel industries of the nation and abroad. Banded Iron Formation of BK belt hosts the iron ores of this region epigenetically formed by supergene enrichment. The most common Iron ore minerals present are magnetite (Fe_3O_4), hematite (Fe_2O_3) and goethite (FeOOH), confirmed through chemical and mineralogical characterization. Unlike other processes, textural characterization is significant in beneficiating iron ores by optimising downstream processing. Magnetite is found to be the primary iron oxide mineral that evolved to other minerals like martite, hematite and goethite though the crystallization/alteration as evidenced by various textures. Banded Hematite Japer (BHJ) proto-ore mostly consists of alternate bands of iron and silica where martite hematite bands have been transformed from magnetite. BHJ contains less Fe(T) 25 - 45 Wt.%, which is difficult for processing. According to the ore variant nomenclature of iron ore based on strength, hard massive/laminated ore are high grade and are least matured ore due to the presence of dense martite, martitized magnetite and goethite. These least mature ore produces less fines in comminution process. Soft laminated ore, though high grade with same mineral composition as hard massive/laminated ore, produce more fines due to the presence of skeletal textures deformed/altered crystals containing goethitic materials represented by colloform textures. The biscuity ore contain more microplaty hematite and martite-goethite grains. In due course of time, part of this martite either may convert to fine-grained hematite (microplaty hematite), increasing the textural complexity, which requires more attention before putting them in to beneficiation. Thus, ores with the same chemical and mineral composition may behave very differently during downstream processing because of the presence of textural variations. Texture of iron ore determines the geometallurgical characteristics applicable for selection of ore and controlled production of fines in a comminution circuit.

Keywords: BK Belt, Iron Formation, Texture, Geometallurgy, Beneficiation

1. INTRODUCTION

The majority of the world's present iron ore resources and production are found in deposits hosted by the Banded Iron Formations, and they are hematitic in nature. High-grade hematite iron ore occurring in Bonai-Keonjhar iron ore basin of the Precambrian age is the major resource of raw materials for the iron and steel industries in eastern India(Beura 2016; Nanda 2020). According to their physical strength, high-grade ores are categorized in terms of mining as hard, soft, biscuity, powdery, or blue dust ore (Figueiredo e Silva et al. 2013; Goldring 2003). The enrichment of the Precambrian iron formations led to the formation of these hematitic iron ore deposits. Mostly the ore is derived from the BIF through successive enrichment by supergene activity and subsequently altered to the present form(Morris 1985). An in-depth understanding of the formation of high-grade hematite iron ore deposits can be obtained by field research combined with systematic mineralogical and textural characterization study(Morris 1980; Donskoi et al. 2016). This paper describes the mineralogical and textural evolution of minerals from BHJ to iron ores. The texture of iron ore can be used to determine the grade as well as the mineralogy of the ore. It can also be used to identify different types of ore and to choose the best way to process them. The findings of this study provide a better understanding of the evolution of ore textures and their alteration in facilitating the subsequent mineral processing.

2. MATERIALS AND METHODS

Samples were collected from Nuagaon Iron ore mine. The mine is present in the Eastern limb of Bonai-Keonjhar Iron ore belt. Five types of representative samples were selected on the basis of their variations in megascopic features and primary physical properties. The samples represent BHJ, high grade Hard Laminated ore (HLO), Soft Laminated Ore (SLO), Biscuity Ore and Blue dust Ore. For the mineralogy and textural study of the sample, polished sections were prepared by conventional techniques by mounting. Optical microscopy study was performed by using Leica DM4P. Polished sections were coated with Gold (Au) rays (20 nm thick) and analysed using a ZEISS EVO18 electron microscope for the SEM study. For various analyses, representative sections of the ore samples were ground using a pulveriser to a grain size smaller than 45 microns. The bulk geochemical analysis of the samples was carried out for major and minor elements by wavelength- dispersive X-ray Fluorescence (WD-XRF) analysis using PANalytical ZETIUM (Mineral edition) spectrometer. To determine the primary mineral phases, powder X-ray diffraction (XRD) was performed using a Rigaku Ultima IV diffractometer with CuK radiation operating at 40 kV and 30 mA.

3. MINERALOGICAL AND TEXTURAL STUDY

Mostly magnetite, hematite and goethite comprise ore components and jasper or quartz, kaolinite and gibbsite constitute the gangue components in iron ore. The minerals and their textural features in BHJ and iron ores are described in the following sections.

3.1. Banded Hematite Jasper (BHJ)

Iron ore minerals associated with the Precambrian BHJ are mainly found in three oxy-hydroxy phases as hematite, martite, and goethite, shown in fig.1-B. The major mineral phases present in BHJ are quartz and hematite (fig.1-A). In banded hematite jasper, hematite and martite are characterized by alternating bands with jasper. Primary hematite and quartz are showing salt and pepper texture, and some of the martitized magnetite present with association of silica grains. Those martitized magnetite grain (fig.1-C) having relict magnetite phase, which is the indication of magnetite source. The selected BHJ sample contain Fe_2O_3 41.46Wt%, SiO_2 54.73Wt% and LOI of 1.90.

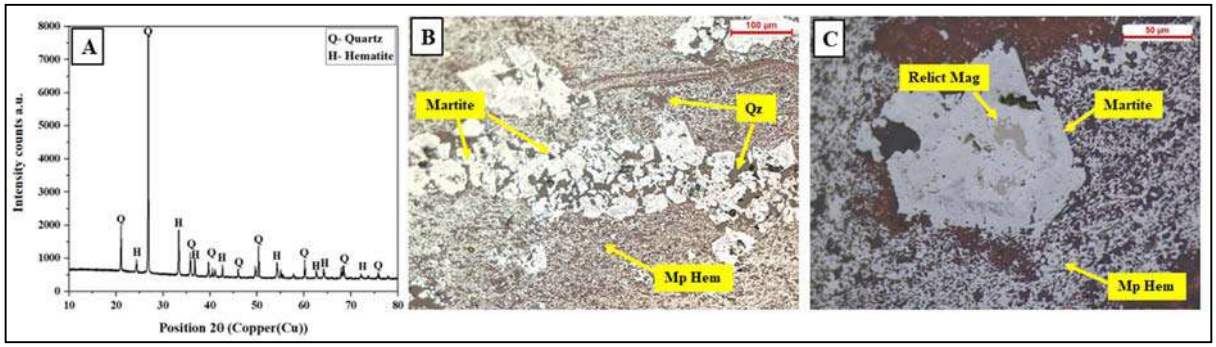

Fig. 1: (A) XRD of BHJ, Photo micrograph showing (B) banding of jasper/quartz (Qz) and martite chain, (C) Martite grain having relict magnetite, where the relict magnetite surrounded by Micro platy hematite (Mp Hem)

3.2. Hard Laminated Ore (HLO) and Soft Laminated Ore (SLO)

Hard Laminated Ores are compact and tightly packed (fig.2-A). The mineral phases in HLO and SLO are hematite, and minor goethite is also present. They are mostly high grade, HLO having 95.5 Wt.% Fe_2O_3, 0.4 Wt.% SiO_2, 0.26 Al_2O_3 and LOI 0.99. SLO having 94.01Wt.% Fe_2O_3 ,0.45Wt.% SiO_2, 3.12 Wt.% Al_2O_3 and LOI 1.97. Removal of silica from bands and successive enrichment of iron by leaching resulted in the formation of martite-goethite (fig.2-B, C). Hard Laminated Ore contains a compact mass of fine-grained, densely packed hematite granules. Dense martite is very common in HLO. Fine-to-medium grained martite, and microplaty crystals of hematite (fig. 2-F) are intricately associated with each other leaving very fine intergranular micro pore spaces as seen in hand specimen (fig. 2-A). Precipitation of goethite in the voids has resulted due to the leaching out of pre-existing minerals in the martite grain. Due to the consistent sequence of alteration of martite and silica, martite-goethite and colloform goethite are formed. Some of the martite grain was altered by hydration to goethite (fig. 2-E). Subsequent leaching of this goethite in preference to martite leads to a variety of skeletal textures (fig. 2-F) which may help identify the original magnetite, which gradually produces void skeleton of martite grain. Destruction happens due to recrystallisation of martite lamellae. Due to the deformation of martite grains, voids increase gradually in the ore, which leads to an increase in porosity of the ore and forming soft laminated ore (fig. 2-D).

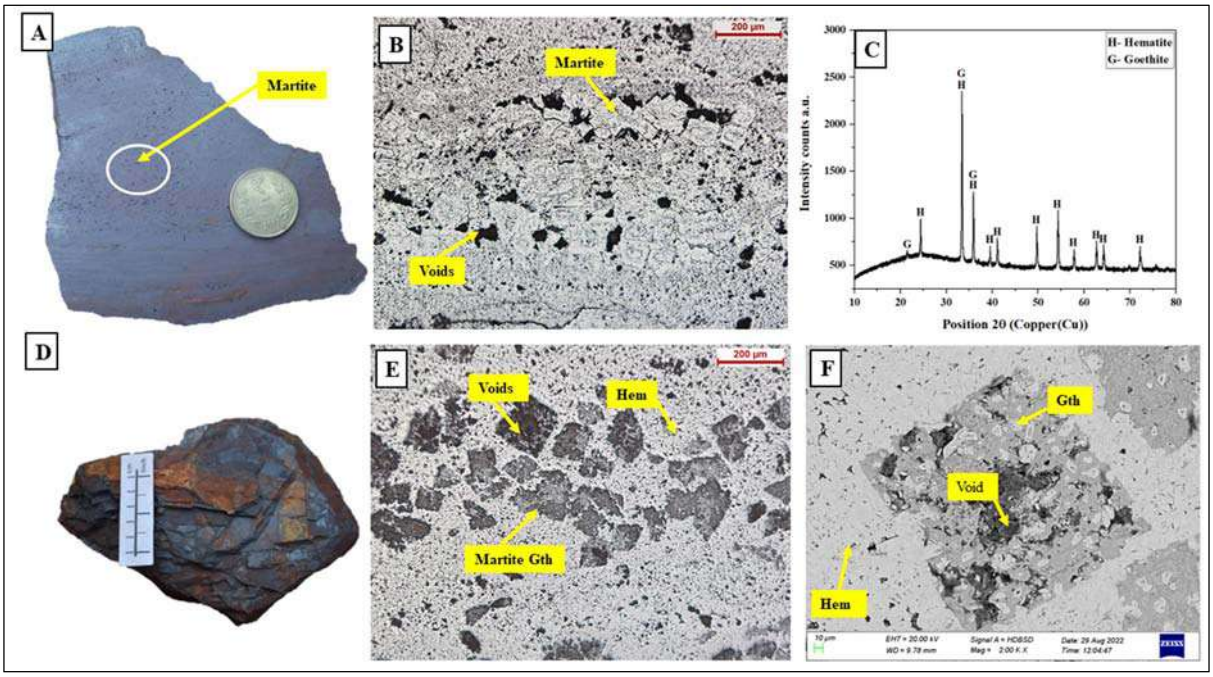

Fig. 2: Photograph showing (A) Fine inter granular micro pores in hand specimen of Hard Laminated Ore (HLO), the image having the marker coin is 23mm (B) Martite and Dense martite in HLO (C) XRD of HLO (D) Hand specimen of Soft Laminated Ore (SLO) (E) Skeletal martite grain and their bands having colloform goethitic texture (F) Goethite replacing the skeletal martite.

3.3. Biscuity and Blue Dust Ore

Biscuity ores are always present in association with blue dust ore (fig.3-A, D). Blue dust is steel grey in colour and occurs as minor pockets. In Nuagaon iron ore mine, the controlling Environment may not be suitable for leaching, so the blue dust availability is significantly less in this area. The biscuity and blue dust ores mainly composed of microplay hematite and martite (fig.3-B, C). Presence of martite in blue dust indicates their origin by desilisification process from banded iron ore. They mostly contain hematite as major mineral phase and goethite and quartz as minor mineral phase (fig.3-E). The biscuity ore contains more microplaty hematite and martite-goethite grains. In due course of time, part of this martite either may convert to fine-grained hematite (microplaty hematite), and produce blue dust. The later generation microplaty hematite has grown randomly through intergranular pore spaces and bridged the courser grains (fig.3-F). This second generation microplaty hematite are nanometre thick and they are also more mature than the primary microplaty hematite.

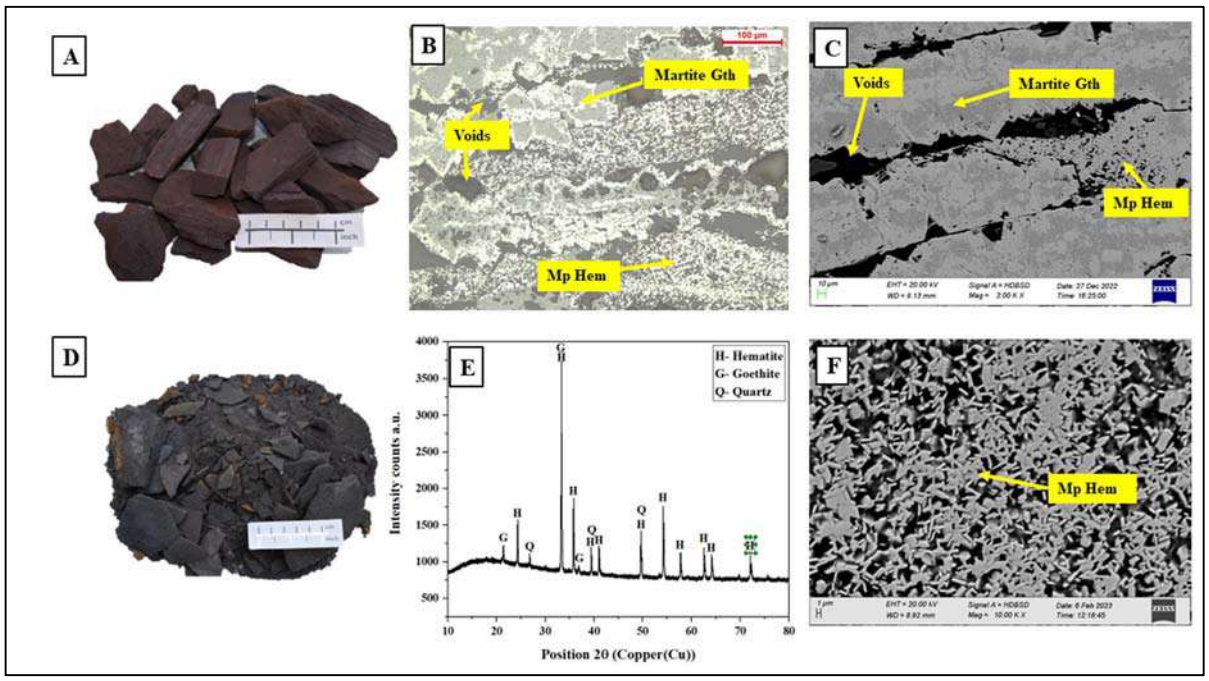

Fig. 3: Image showing (A) Megascopic image of Biscuity Ores (B) Banding of Martite-Goethite (Martite Gth) (C) Martite Gth bands and micro platy hematite (Mp Hem) with pores (D) Blue dust association with Biscuity ore (E) XRD of Blue dust ore (F) Secondary microplaty hematite in blue dust.

4. DISCUSSION

Banded Hematite Jasper (BHJ) is the least altered, unweathered, protolith of Banded Iron Formation (BIF). The interlocking of iron and quartz in BHJ is challenging to process. Due to insignificant leaching, martite grains are found to be preserved in the iron ore bands of the Nuagaon iron ore mines. According to mineralogy, HLO, SLO, Biscuity, and blue dust ore are high-grade hematitic ore. But all are texturally different. The first stage of processing for high-grade hematitic ores is crushing and screening. According to the production requirements, run-of-mine high-grade ore is crushed and screened into +10mm to -30mm lump for blast furnace feed (J. M.F. Clout 2006; Nomura et al. 2014). HLO contains martite goethite and the least mature microplaty hematite. Because HLO has a lower porosity, it has a less weak zone and can be used directly in a blast furnace. SLO mostly contain martite-goethite grains, and gradually, those martite grains form void due to the leaching of goethite. Due to the void this ore produced more fines during processing(John M.F. Clout 2003; Mahanta et al. 2022). The fine ores mostly go for agglomeration. The high-grade biscuity ore is more fragile than the soft laminated ore. In the further evolution of martite and hematite they evolved micro platy hematite (Mp-Hem); these secondary Mp-Hem are more mature. These mature Mp-Hem mostly produces the blue dust fines. It is evident that the majority of grains may not respond to mineral processing as they are smaller than 25 µm and may report to slime. From geometallurgical point of view extreme care should be taken for the secondary mature Mp-Hem in a mineral processing circuit.

5. CONCLUSION

The ore derived from banded iron formation in Nuagaon Iron ore mine represent evolution series from parent rocks to most mature ore. The least mature ore contain residual oxides, and the later form due to enrichment. The mature ores have more secondary mineral phases and texture, because of that porosity increases, strength decreases. As a result of textural variations, ores with the same chemical and mineral composition can behave very differently during downstream processing. Textural analysis shows that the ore will behave consistently and predictably during processing. Texture of iron ore defines the geometallurgical characteristics applicable for selection of ore and controlled production of fines in a comminution circuit.

REFERENCE

Beura, Devananda. 2016. “Technological Upgradation For Mineral Development: In Context with Iron Ore Mineral.” International Journal of Scientific Research 4 (7).

Clout, J. M.F. 2006. “Iron Formation-Hosted Iron Ores in the Hamersley Province of Western Australia.” Transactions of the Institutions of Mining and Metallurgy, Section B: Applied Earth Science 115 (4): 115–25. https://doi.org/10.1179/174327506X138931.

Clout, John M.F. 2003. “Upgrading Processes in BIF-Derived Iron Ore Deposits: Implications for Ore Genesis and Downstream Mineral Processing.” Transactions of the Institution of Mining and Metallurgy, Section B: Applied Earth Science 112 (1): 89–96. https://doi.org/10.1179/0371745032501153.

Donskoi, Eugene, Andrei Poliakov, Ralph Holmes, Steven Suthers, Natalie Ware, James Manuel, and John Clout. 2016. “Iron Ore Textural Information Is the Key for Prediction of Downstream Process Performance.” Minerals Engineering 86: 10–23. https://doi.org/10.1016/j.mineng.2015.11.009.

Figueiredo e Silva, Rosaline Cristina, Lydia Maria Lobato, Carlos Alberto Rosière, and Steffen Hagemann. 2013. “Petrographic and Geochemical Studies At Giant Serra Norte Iron Ore Deposits in the Carajás Mineral Province, Pará State, Brazil.” Geonomos, no. February 2013. https://doi.org/10.18285/geonomos.v19i2.54.

Goldring, D. C. 2003. “Iron Ore Categorisation for the Iron and Steel Industry.” Transactions of the Institution of Mining and Metallurgy, Section B: Applied Earth Science 112 (1): 5–17. https://doi.org/10.1179/0371745032501162.

Mahanta, Jyotirmayee, Subhabrata Mishra, Madhusmita Baliarsingh, and Prabhas Chandra Beuria. 2022. “Mineralogical Study of Low and Lean Grade Iron Ore Fines during Slow and Rapid Reduction Roasting.” Journal of the Geological Society of India 98 (8): 1159–65. https://doi.org/10.1007/s12594-022-2138-3.

Morris, R. C. 1980. “A Textural and Mineralogical Study of the Relationship of Iron Ore to Banded Iron-Formation in the Hamersley Iron Province of Western Australia.” Economic Geology 75 (2): 184–209. https://doi.org/10.2113/gsecongeo.75.2.184.

Morris, R.C. 1985. Genesis of Iron Ore in Banded Iron-Formation By Supergene and Supergene-Metamorphic Processes – a Conceptual Model. Regional Studies and Specific Deposits. Second Edi. ELSEVIER B.V. https://doi.org/10.1016/b978-0-444-42497-6.50006-0.

Nanda, S K. 2020. "Recovery of Iron Values through Conventional Beneficiation Techniques from Banded Hematite Jasper of Eastern India with Special Reference to Mineralogical and Chemical Characterization." Indian Journal of Science and Technology 13 (38): 3960–69. https://doi.org/10.17485/ijst/v13i38.681.

Nomura, Tsutomu, Norihito Yamamoto, Takeshi Fujii, and Yuta Takiguchi. 2014. "Beneficiation Plants and Pelletizing Plants for Utilization of Low Grade Iron Ore." R and D: Research and Development Kobe Steel Engineering Reports 64 (1): 8–13.

VISTAS IN GEOLOGICAL RESEARCH
Special Publication in Geology (19), March 2023, pp. 184-193

Remote Sensing Techniques using EO-1 Applied for the Detection of Iron ore Deposits in Odisha, India

SMRUTI REKHA SAHOO* AND DEEPIKA PATRA

Department of Geology, Fakir Mohan University, Balasore – 756089
Corresponding Author: srsahoo.geol@gmail.com

Abstract: In recent years remote sensing techniques and digital image processing have enabled use of Spectral bands with distinctive spatial/spectral statistics for estimation of mineral identification and exploration. This combines imaging and spectroscopy in a single system which often includes large data sets and require new processing methods. The techniques available for classification of different features present in the satellite imagery are beneficial. The hyperspectral image needs to be processed with the steps such as Bad line removal, radiometric correction, atmospheric correction using FLAASH (Fast Line-of-Sight Atmospheric Analysis of Hypercubes module). The spectral classification is done by the Spectral Angle Mapper classification (SAM) according to the given steps: i) Spectral reduction by Minimum Noise Fraction (MNF), ii) Spatial reduction by the Pixel Purity Index (PPI) and iii) manual identification of the end members using the N-Dimensional Visualizer (N-D Visualizer). The results of the spectral matching technique indicate the accurate sites for the discrimination of iron ore minerals by the Hyperion data. The present study focuses on the iron ore detection using these techniques related to Hyperion image (EO-1) of part of Keonjhar district, the northern part of Odisha, India. The combination of remote sensing and field investigations can lead to generate the high accuracy mineralogical map.

KEY WORDS: Hyperspectral, Mineral Mapping, Remote Sensing

INTRODUCTION

Mineral Exploration is the process of searching for evidence of any mineralisation hosted in the surrounding rocks, main purpose of this is to identify ore bodies and promising deposits to get an overview over the available mineral resources for mining. Minerals and rocks generally have diagnostic spectral absorption bands in the spectral range of 400–2500 nm. Hyperspectral remote sensing can effectively capture spectral characteristics. Mineral composition information can be inverted and identified according to the spectrum.Nowadays, this is becoming increasingly difficult, especially in obtaining ground access to sensitive or remote areas. Spectral Remote Sensing methods can be used in such circumstances and provide detailed study. This information is useful for mapping potential host rocks, alteration assemblages and regolith characteristics. Solar radiation scattered from the Earth's surface interacts with atmosphere before reaching to any space based or airborne remote sensing sensor (Rani et al., 2017). The spectral signatures of land surface, derived from imagery, can be used to identify and even quantify mineralogical entities of exploration significance.

Hyperspectral images have wide applications in several fields such as geology, mineral

exploration, environmental science, agriculture etc. due to their narrow band width with numerous channels. The common theme in all of these applications is the requirement for classification of each pixel in the scene, and reduction of data volume to tractable levels. This is a rapidly developing technology and allows for fast and systematic mineral mapping, facilitating exploration of the Earth's surface at various scales on a variety of platforms. Recently, Space based hyperspectral images have found wide use in mineral mapping in various geological units (Kruse et al., 2003). The present work is an experiment to characterize the iron ore deposits of the study area using Hyperion data (EO-1).

STUDY AREA

The study area comprises part of Keonjhar district which is situated at the northern part of Odisha, India. The area is bounded by latitudes 21^0 45' to 22^0 05' North and longitudes 85^0 05' to 85^0 25' East and forms a part of the 'horse shoe' shaped synclinorium of the well-known Precambrian Iron Ore Group (IOG) of Odisha and Jharkhand. The figure (Fig.1) shows the key map for the study area with Hyperion image (FCC R:40 G:30 B:20). The selected area experiences a tropical climate with maximum temperature of 45^0C and minimum temperature of 23^0C and average annual rainfall is 1534.5 mm. The hills present in this area are upto 800 meters height. Keonjhar is one of the premier minerals producing district in Odisha. The district occupies a prominent place in the mineral map of the Country. Iron ore formations occupy most part of the district which can be traced from the state of Jharkhand in the north to the Jajpur district of Odisha in the south. In field, the lithological association includes banded hematite jasper/quartzite/chert, banded magnetite quartzite with characteristics banded nature (Sahoo et al., 2015). Because of their resistant to weathering, they form linear ridges (Rajendran et al., 2011).

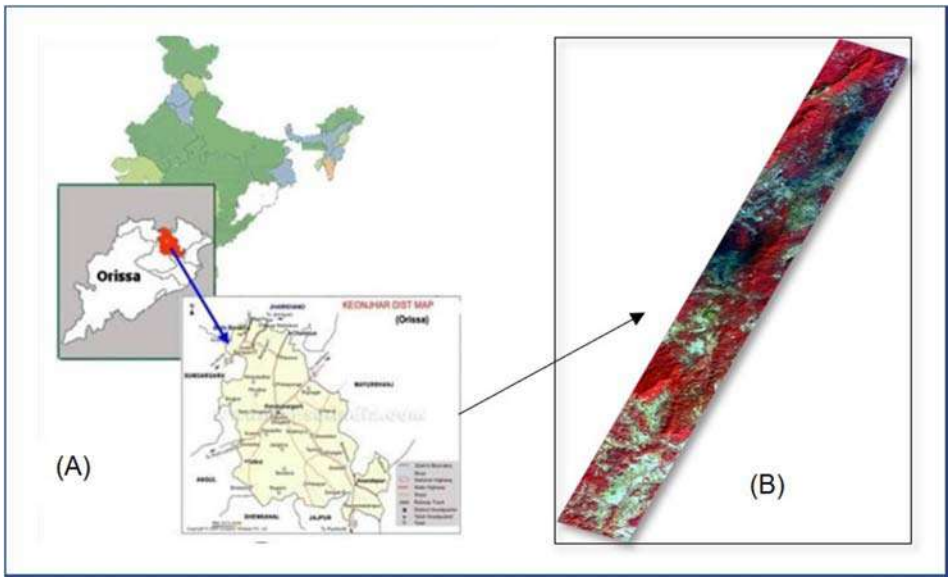

Fig. 1: (A) Study area (part of Keonjhar district), (B) Hyperion image showing the study area (FCC 40 30 20)

Geological Setting

Keonjhar district, in the north-eastern parts of Odisha state, is quite in its geology. Most of the high-grade (>60 wt. % Fe) iron ores in eastern India are located within the Archean Iron Ore Group of the Singhbhum craton (Fig. 2). The Iron Ore Group (IOG), occurs within the Singhbhum Granite (>3.1Ga) along its western (Noamundi-Jamda-Koira), eastern (Gorumahisani-Badampahar) and southern (Tamka-Daitari) margins. The Bonai-Keonjhar (BK) belt (Fig.2) is one of the most important iron formation belts that form a part of the Archean supracrustal of Iron Ore Super Group (IOSG) of Odisha (Behera et al., 2019). Iron ore is generally found in the form of magnetite (Fe_3O_4), hematite (Fe_2O_3), goethite (FeO(OH)), limonite ($FeO(OH)nH_2O$) or Siderite ($FeCO_3$) (Sengupta et al., 2018). Remote sensing and GIS can be applied in exploration and resource management of iron deposits by integrating spatial and non-spatial data of the satellite images taken in different times.

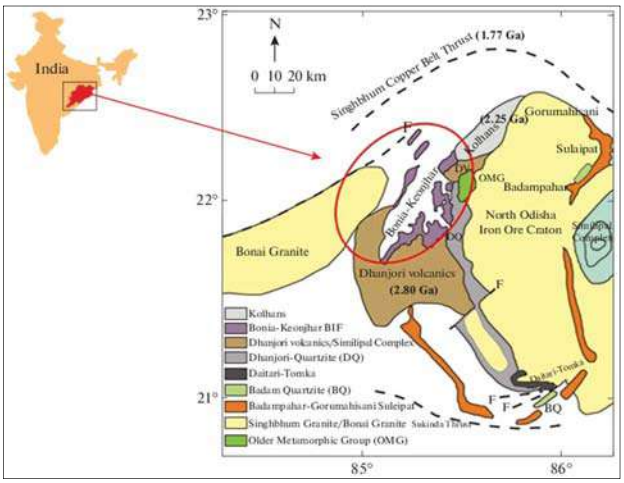

Fig. 2: Implicating the Origin and Depositional Environment of Banded Iron Formation (BIF) of Bonai-Keonjhar (Source-Nanda, 2022).

Data Processing

The data used for the study are Hyperion Level 1R and Level 1Gst images, Geological Map of the study area and Spectral Library (USGS). Hyperion data onboard EO-1 satellite acquired on Dt-16/01/2006, at 04:28:35 GMT is used for this study. The Hyperion is a push-broom Imager with 242, 10 nm bands covering the spectrum from 400 nm–2400 nm. The flowchart (Fig. 3) appended below shows the overall methodology for the present study.

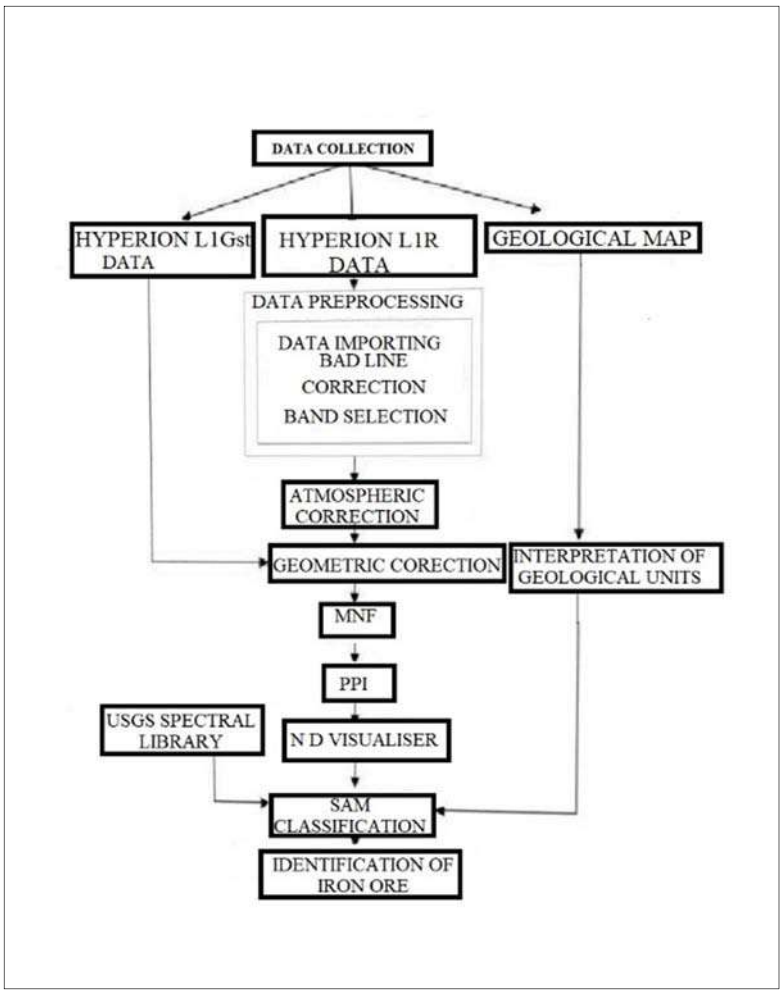

Fig. 3: Step-by-Step processes Depicted in the given flowchart.

Most of the surface exhibits diagnostics spectral signature in VNIR and SWIR of the electromagnetic spectrum which enables their detection on the basis of characteristics of Spectral signature (Yitagesu et al., 2011, Hewson et al., 2012). Processing of high dimensional hyperspectral data is a challenging task and the computational complexity is a result of vast data volume in numerous spectral bands. Hyperion (L1R and L1Gst) sensor operates from a space platform United States Geological Survey (USGS) with modest surface signal levels and a full column of atmosphere attenuating the signal, the data demand careful processing to manage sensor noise. The Hyperion image consist of 242 spectral bands in the wavelength of electromagnetic spectrum. However, in this study, only bands have been processed due to the poor signal to noise ratio using ENVI Software. The errors are said to be caused due to calibration differences in the detector array. The Hyperion dataset has to be corrected for abnormal pixels, stripping and smiling, bad columns prior to atmospheric correction. Preprocessing of hyperspectral image is required not only for removing sensor errors during acquisition but also for display, band selection (to reduce the data dimensionality) and to reduce computational intricacy.

Band Selection and Bad Line Correction

Several vertical lines with no information can be produced by detectors in Hyperion sensor. The information from these areas can be covered by replacing their pixel values with the average pixel values of their neighboring pixels. To reduce the errors caused by the stripping effect, all spectral bands are screened and manually rejected a total of 54 bands with apparent stripping effects from VNIR + SWIR spectral range. A spatial subset was taken to focus on the study area. The raw image has some dark and bright columns occurring due to change in the calibration or failure of some detectors in the CCD array at the time of capturing the image. Bad lines in Hyperion level 1R data appear as dark vertical lines. The bad lines were replaced by taking average of the previous and next column (Fig. 4).

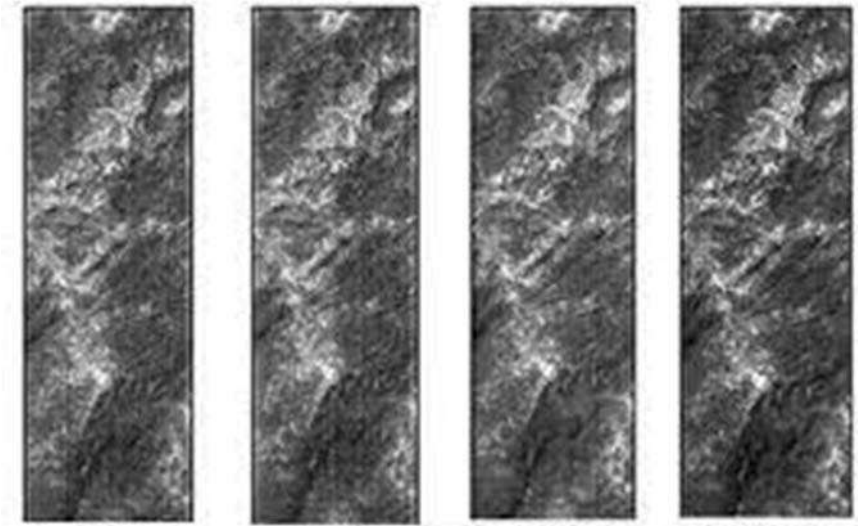

Fig. 4: Before Striping and after De-striping of bands of Hyperion data module using ENVI Software.

Atmospheric Correction with (FLAASH) Module

Different levels of preprocessing are available to correct the original hyperspectral images including geometric and atmospheric correction. Atmospheric correction becomes a necessary pre-requisite for any further processing and accurate interpretation of spectra of different surface object. Radiometrically calibrated hyper spectral imagery contains information relating to the material properties of a surface target and the atmospheric layers between the surface target and the sensor. FLAASH (Fast Line-of-sight Atmospheric Analysis of Spectral Hypercubes) is rigorous atmospheric algorithm requires the input radiance image (Fig. 5 Hyperion image after FLAASH corrected) containing calibrated radiance data in a floating point, long integer (4- byte signed), or integer (2-byte signed or unsigned) data type having units W/cm² * nm* steradian. The image should have BIL or BIP format.

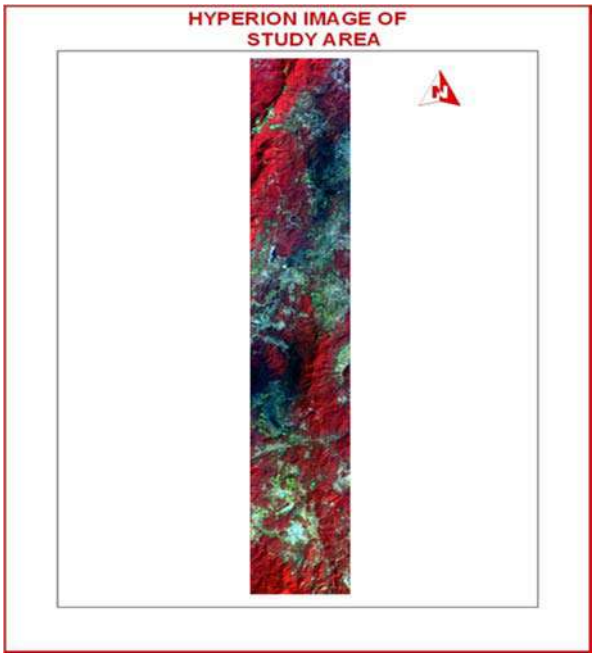

Fig. 5: FLAASH Corrected Hyperion Image of Study Area.

Georeferencing of Hyperion Data

The FLAASH output image is georeferenced by using the L1Gst Hyperion data (UTM/WGS 84 zone 45N) of the same area. In order to avoid spectral interpolation, nearest neighborhood resampling method is used.

Hyper Spectral Analysis and Selection of Image End-Members

The following procedures of hyper spectral analysis were employed to map iron ore from the Hyperion image of the study area including the Minimum Noise Fraction (MNF) transformation for reducing spectral data, the Pixel Purity Index (PPI) for identifying those extreme or spectrally pure pixels, and the N-Dimensional Visualizer for determining the endmember directly from the image. Spectral Angle Mapper (SAM) was applied to estimate abundances of each endmember to produce final map.

Minimum Noise Fraction

The minimum noise fraction (MNF) transform has been extensively used in multispectral and hyperspectral data for feature extraction, noise whitening and spectral data reduction (Kumar et al., 2015). It is used to determine the inherent dimensionality of image data, to segregate noise in the data, and to reduce the computational requirements for subsequent processing. (Fig. 6 MNF data). The MNF transform is essentially two principal component transformations.

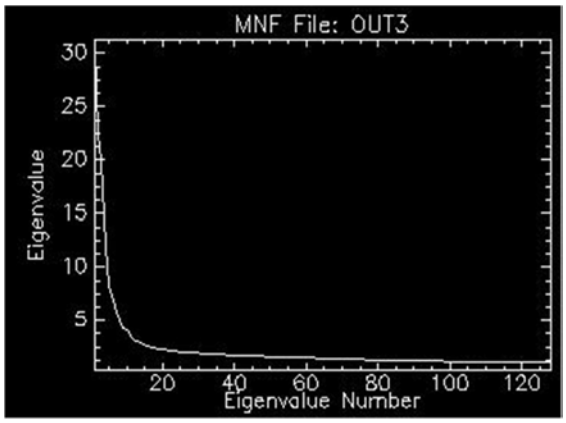

Fig. 6: MNF Algorithm implemented on Hyperion data.

Pixel Purity Index (PPI)

All remotely sensed images contain a phenomenon known as mixed pixels. These are pixels that contain a mix of features (e.g., grass, forest, water). The pixel purity index is a way of finding the most spectrally pure pixels in images. The PPI stipulates how many times the pixel is extreme in the simplex. The most spectrally pure pixels typically correspond to spectrally unique materials. The PPI procedure generates an image where pixel values correspond to the number of times that this pixel was recorded as extreme which results in further spatial reduction.

N-Dimensional Visualizer

The N-Dimensional Visualizer is an interactive tool that allows the user to select end members in n-space, this procedure generates clusters of points related to the pixels in N-dimensional space defined by the MNF components (Fig. 7 in different colours). It rotates interactively the data cloud by which the user is able to see the spectral data in different dimensions from several angles. The selected classes were exported to region of interest (ROI) and used as input for further spectral analysis.

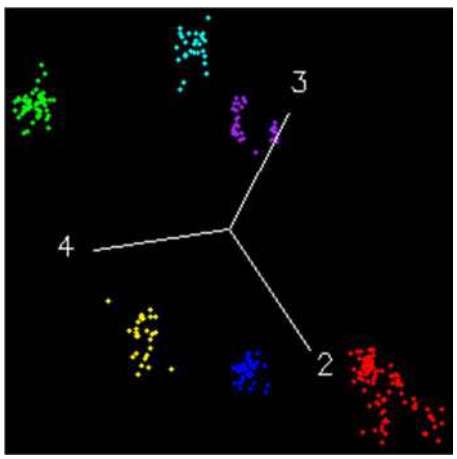

Fig. 7: The ROI selected from N-dimensional visualizer showing different colours.

Spectral Angle Mapper (SAM) Classification

The Spectral Angle Mapper Classification (SAM) is an automated method for directly comparing image spectra to known spectra (usually determined in a lab or in the field with a spectrometer) or an endmember. This method treats both (the unknown and known) spectra as vectors and calculates the spectral angle between them. This method is insensitive to illumination since the SAM algorithm uses only the vector direction and not the vector length. The result of the SAM classification is an image showing the best match at each pixel

Result and Discussion

Different methods have been adopted in the study to obtain the best possible results, which helped for interpretation directly or indirectly. Hyperion (EO-1) data has been used to extract the mineralogical information through SAM for identifying the hematite in the part of study area. The MNF transformation is a linear transformation which essentially likes two cascaded Principal component analysis (PCA). Forward MNF has been run on the Hyperion dataset. Several trials of Minimum noise fraction transformation have been applied to get the optimum result. The resulted eigenvector and eigenvalue are used for the Keonjhar dataset. Only 4832 number of pure pixels is resulted after the Pure Pixel Index (PPI) processing of the Hyperion EO-1 image of the Keonjhar study area. These pixels are processed further for the selection of endmembers from the atmospherically corrected image, the coordinates of the points in N-D space consist of ‘n’ spectral radiance or reflectance values in each band for a given pixel. The distribution of these points in N-D space estimates the number of spectral endmembers and their pure spectral signatures. Endmembers in a Spectral Data Cloud are located when pixel data are plotted in a scatter plot that uses image bands as plot axes, the spectrally purest pixels always occur in the corners of the data cloud, while spectrally mixed pixels always occur inside of the data cloud. The spectral angle mapper algorithm determines the spectral similarity between two spectra by calculating the angle between the spectra and treating them as vectors in a space with dimensionality equal to the number of bands.

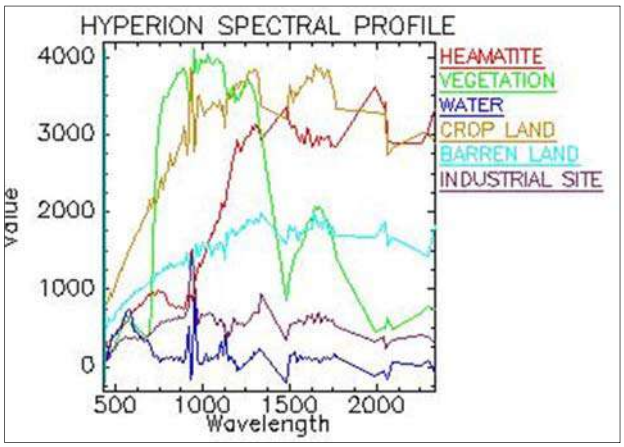

Fig. 8: The spectral values of different features including spectral plots of Iron ore (Hematite,Red line).

The output from SAM is a classified image and a set of rule images (one per endmember). The pixel values of the rule images represent the spectral angle in radians from the reference spectrum for each class. The SAM classification method was applied to the Keonjhar data set and iron ore endmember spectra was given as the reference spectra (Fig. 8). The results of the SAM mapping method for the Odisha dataset indicates that the lowest radian measurement (angle between the reference spectra and the target) have been registered for the iron ore, indicates the similarity in the spectra of the reference and target spectra. This indicates that the SAM mapping method has given good results in the mapping of iron ore in Keonjhar. Because of the lack of access to spectral library or field measurements of spectral properties of land cover types of interest, endmember data of the known ground cover types were extracted from the Hyperion data. Six endmembers including Iron ore (Hematite), Vegetation, Water body, Crop land, Barren land, industrial site is extracted from the Hyperion image of the study area. The final map created using six rule classifiers is shown in the figure (Fig. 9, A).

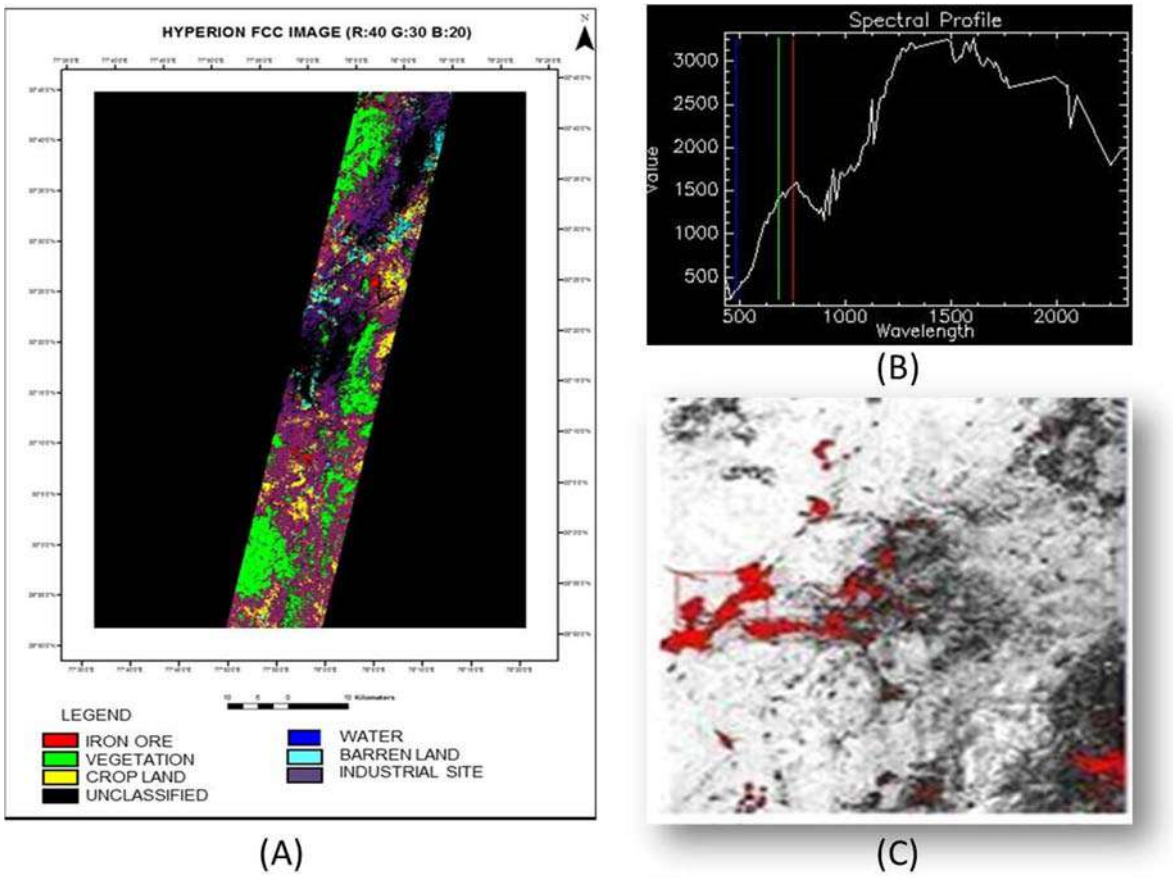

Fig. 9: (A) The figure shows Hyperion FCC image, (B) Spectral profile of Iron ore deposits after comparing with USGS Library, (C) The Figure shows the presence of Iron Ore in red colour.

CONCLUSION

It can be said that the low signal to noise ratio of Hyperion (Fig. 9, A) and presence of smile effect in the image and the use of laboratory spectra of these minerals from the standard spectral libraries as the reference affected the classification results and their accuracies. Image processing and analysis was ended in the spectral and spatial domain with keeping an eye on the objective of the study. Atmospheric correction technique has given the corrected image of the study area from which the endmembers are selected by different techniques like MNF, PPI, and N-dimensional visualizer. The areas having Iron ore in the study area are mapped by the help of spectral matching with USGS spectral library (Fig.9, B) and then the image is classified with spectral angle mapper classification. Hence it can be concluded that an integrated approach of several mapping techniques will lead to the successful mapping of iron ore (Fig.9, C). Hyperspectral data contains number of image bands hence, the volume of information it gives, are enormous and the challenges it poses for researcher is also ample.

Acknowledgements: This work is funded by OURIIP, OSHEC, Government of Odisha.

REFERENCES

Nanda, S.K. Implicating the Origin and Depositional Environment of Banded Iron Formation (BIF) of Bonai-Keonjhar Iron Ore Belt in Eastern India from its Petrography and Geochemistry. Geology of ore deposits 2022; 63(6):497-514.

Behera, R., Beura, D. Lithology and Petrography of Iron Formation of Bonai-Keonjhar Belt with Special References to Jajang Area, Odisha. Vistas in Geological Research 2019; 17:88-97

Sengupta, A., Adhikari, M.S., Maiti, S., Maiti, S.K., Mahanta, P., Bhaumick, S. Identification and mapping of high -potential iron ore alteration zone across joda, Odisha using ASTER and EO-1 hyperion data. Journal of Spatial Science 2018; 64(3):491-514.

Rani, N., Mandla, V.R., Singh, T. Evaluation of atmospheric Corrections on Hyperspectral data with special references to mineral mapping. Geoscience Frontier 2017;8(4):797-808.

Sahoo, S.R., Panda, P.K., Champati ray, P.K. Hyperspectral Image analysis for Iron Ore discrimination in Keonjhar district, Odisha. International Journal of Remote Sensing and Geoscience 2015:4(2); 2319-3484.

Kumar, C., Shetty, A., Raval, S., Sharma, R., Champati ray, P.K. Lithological Discrimination and Mapping using ASTER SWIR Data in the Udaipur area of Rajasthan, India. Procedia Earth and Planetary Science 2011; 11:180-188.

Rajendran, S., Thirunavukkarasu, A., Balamurugan, G., Shankar, K. Discrimination of iron ore deposits of granulite terrain of southern peninsular India using ASTER data. Journal of Asian Earth Sciences 2011; 41(1):99-106.

Yitagesu, F.A., Meer, F.V.D., Werff, H.V.D., Hecker, C.A. Spectral characteristics of clay minerals in the 2.5-14µm wavelength region 2011. Applied Clay Science 53(4):581-591.

Kruse, F.A., Boardman, J.W., Huntington, J.F. Comparison of airborne hyperspectral data and EO-1 Hyperion for mineral mapping. IEEE Transactions on Geoscience and Remote Sensing 2003; 41(6):1388-1400.

USGS EARTH EXPLORER : https://earthexplorer.usgs.gov

www.spweather.com/enviuser/tutorial/hyperspectral_tools.

VISTAS IN GEOLOGICAL RESEARCH
Special Publication in Geology (19), March 2023, pp. 194-206

Organo-Petrographic Facets of Ib-River Coal Basin, Odisha

AKHANDAL SAHOO[1*], VIVEKA NAND JHA[1], ATUL KUMAR VARMA[1], SUREN NAYAK[2] AND NIRASINDHU DESINAYAK[3]

[1]Department of Applied Geology, Indian Institute of Technology (Indian School of Mines), Dhanbad-826004, Jharkhand, India.
[2]Department of Geology, Utkal University, Vani Vihar-751004, Bhubaneswar, Odisha, India.
[3]Department of Geology, Ravenshaw University, Cuttack-753003, Odisha, India.
*Corresponding author/Presenting author

ABSTRACT: Twenty-two coal samples from Ib-River coal basin have been studied by means of physical properties, microlithotypes, proximate analysis, ultimate analysis, and micro-petrographic analysis for the characterization of coal and depositional history of the basin. These coal samples are black to grey in color and thinly laminated, consisting dominantly fusain bands which may indicate the paleo-fire event in the basin. Cleat intensity of the bright band with respect to the dull band shows the richness of volatile and other organic gases in coal. Moisture content, Ash yield, and carbon content vary from 0.90-9.30 wt%, 6.53-26.51 wt%, and 39.74-64.20 wt%, respectively. Volatile matter content and Fuel ratio values vary from 29.68 to 42.89 wt% and 1.29-2.37 in these samples indicates sub-bituminous to bituminous rank. The elemental analysis shows that carbon varies from 56.53 to 83.92 wt%; hydrogen is between 3.15 and 5.21 wt%; nitrogen is between 0.46 and 1.47 wt%; and oxygen is between 11.39 to 39.12 wt%. H/C ratio in the study is quite significant and they range from 0.58-0.96 to produce hydrocarbon. In micro-petrographic study, the macerals viz, vitrinites, liptinites as well as inertinites are observed with a significant amount. A high proportion of structured inertinite (viz. semifusinite and fusinite) in the maceral study shows that the peats are from a relatively oxidizing environment. The high value of the Tissue Preservation Index (TPI) has been noticed, while the Gelification Index (GI) values are substantially low. The plot of VI vs. GWI demonstrates swamp to swamp forest depositional environment. The high calorific values and low moisture of the coals from this basin substantiates the industrial use of coal.

Keywords: Fusain; Inertinite; Tissue Preservation Index; Gelification Index; Cleat intensity

INTRODUCTION

A significant coal basin in India is the Ib-River coal basin, which is a portion of the Mahanadi master basin. The Ib-River coal basin has attracted a lot of attention with respect to petrographic and geochemical characterisation since it is the third-highest coal resource in India. Due to the numerous practical uses for coal from this coal basin, petrographic and geochemical properties of these coals have attracted a lot of research. Additionally, interest has grown among attention-seeking scientists, researchers, and fuel geologists in unconventional oil resources to find ways to increase raw material output. Following Varma et al., 2019 synthesis of carbon nano-products from low-rank coal from this coal basin, curiosity has been created for detailed petrographic analysis. The value of these low-rank

coals from this coal basin has been added besides power generation. Several investigations had been carried out on the Ib valley Basin and Mahanadi master Basin. Pareek (1958) has studied for the first time the microstructure and petrological compositions of the Rampur coal seam and found that these coals consist of fibrous fusain and fine-grained durain. Further Navale (1967) and Navale & Tiwari (1968), Behera and Chandra (1995), and several researchers have investigated on nature of the formation, petrographic contents, and lithotypes of the Ib-River coal basin. But no systematic and comprehensive work yet has been carried out in the form of understanding of coal genesis, depositional environment, correlation of the coal seams as well as assaying the hydrocarbon generation potential in Ib-River coal basin. The amount, type, and maturity of the inherent organic matter have a deep impact on hydrocarbon generation potential (Sykes and Snowdon, 2002; Tissot and Welte, 1978). The geochemical study of coals from this Basin gives significance to hydrocarbon generation which is the prime interest of this research. Twenty-two (22) representative coal samples were selected from different seams of Ib-River coal basin to study the petrographic composition and to document the depositional environment. In this study an effort has been made to carry out detailed petrographic studies of the coal samples drawn from all seams covering both Barakar and Karharbari Formation of the Ib-River coal basin which signifies the novelty of our study.

GEOLOGICAL SETTING

The Ib-River coal basin is located in the southeast of the Mahanadi master basin, which has a NW-SE trend, between 21°30′ and 22°06′N latitude and 83°37′ to 84°10′E longitude. The Ib-River coal basin derives its name from the Ib-River which is a tributary of the Mahanadi River (Varma et al., 2015; Goswami et al., 2006; Tewari et al., 2009). The Mahanadi Master Basin, which is long and parallel to the structural alignment of the underlying Precambrian rocks, contains the Ib-River coal basin. A significant NW-SE lineament forms this Master Basin's southern border. A north-western descending synclinal flexure is what gives the Ib-River coal basin its distinctive appearance. A fault that juxtaposes the Barren Measures and Raniganj formations with Precambrian rocks forms the basin's southern limit. (Goswami et al., 2006; Tewari et al., 2009) To the north-west, the Ib-River Coalfield continues into the Mand-Raigarh Coalfield. The coal basin has not been known to have any igneous intrusions (Anand Alwar, 1977). Coals in the basin are typically non-caking type with high moisture, ash and volatile matter production (Anand Alwar, 1977). In light of previous research (Ball, 1871; Mehta and Anandalwar, 1960; Raja Rao, 1982; CMPDI, 1987; Chaudhury, 1988; Mukhopadhyay, 1987, 1989; Pal et al., 1992; GSI, 1997) the stratigraphic succession is shown (GSI, 1997) in Table 1. Major coal bearing Formations are recorded in Barakar and Karharbari Formation in Ib-River coal basin (GSI, 1997). There are 5 coal seams in Ib-valley coalfield on the status (Manjrekar et al., 2006) out of which 3 major coal seams are named Ib seam, Lajkura seam and Rampur seam. Rampur seam is the younger while Ib seam is the older seam. Stratigraphically Ib seam belongs to Karharbari formation and other two belongs to Barakar formation. First geological map of Ib-vally Coalfield was prepared by V. Ball in 1871and then regional exploration was done by GSI on 1964-65. Detailed exploration in this coalfield was done by Govt. of Odisha on behalf of CMPDI since 1974-75. The Geological map of the Ib-River coal basin area is shown in (Figure 1).

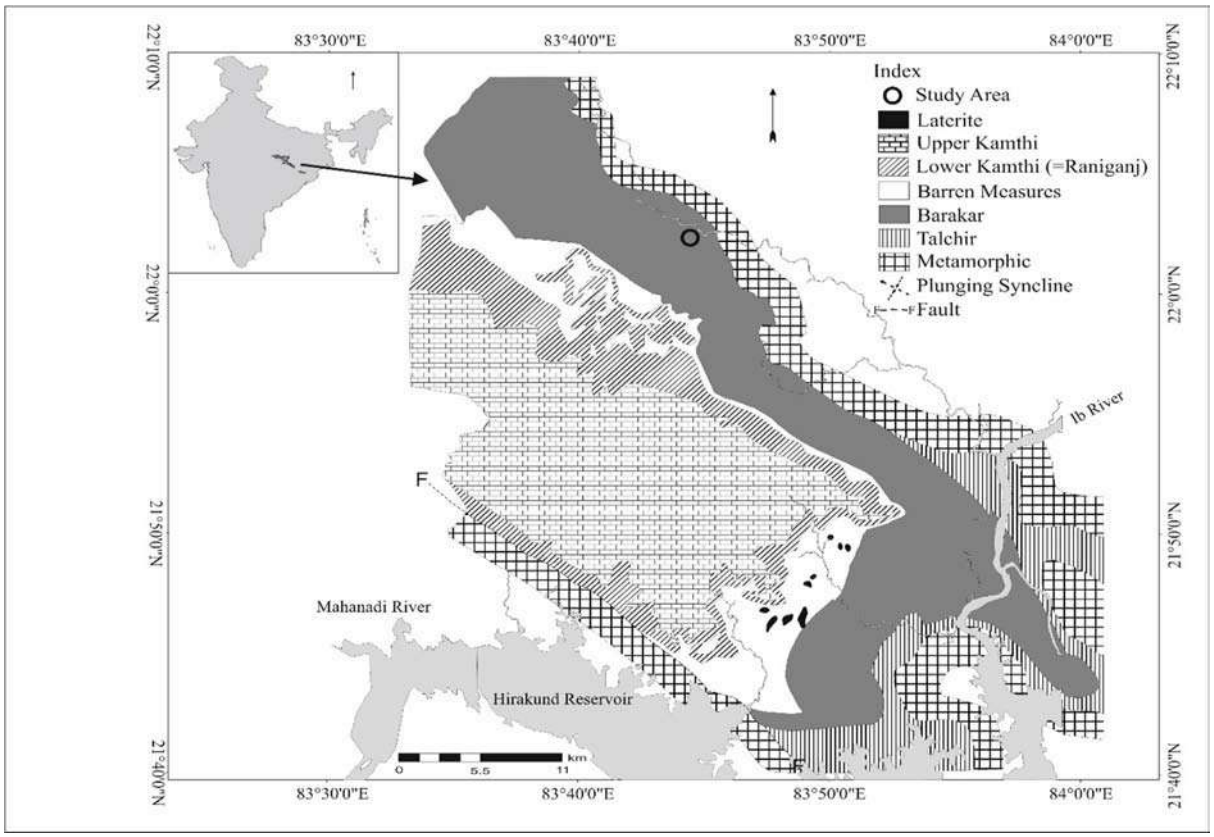

Fig. 1: Geology map of IB valley basin after GSI 1997 and CMPDI, KOLKATA.

Table 1: Geological succession of Ib-River coal basin, Odisha (GSI, 1997).

Age	Group	Formation/Thickness	Lithology
Holocene		Alluvium/Laterite	Gravel and conglomerate
Early to Middle Triassic	Upper Gondwana	Upper Kamthi(150 m+)	Conglomerate, red shale, coarse ferruginous-sandstone with clasts.
Unconformity			
Late Permian	Lower Gondwana	Lower Kamthi Raniganj	Fine-medium grained well sorted sandstone, siltstone, clay bed, coal, shale
Middle Permian		Barren Measures (250 m+).	Grey shale, carbonaceous shale, fine to coarse-grained sandstone, clay and ironstone nodules/shale.
Early Permian		Upper Barakar	Feldspathic sandstone, grey and carbonaceous shales
		Lower Barakar	Feldspathic sandstone, grey and carbonaceous shales
Early Permian		Karharbari(30–65 m).	Conglomerate, carbonaceous sandstone with fresh feldspar grains containing thin coal bands, only along the NW margin of the basin
		Talchir(130 m+).	Diamictite, greenish sandstone, olive green colored needle shales and rhythmites
Unconformity			
Precambrian			Granites, gneisses, amphibolites, migmatites

MATERIALS AND METHODS

Coal samples are collected (CG#1801, CG#1802, CG#1803, CG#1803, CG#1804, CG#1805, CG#1806, CG#1807, CG#1808, CG#1809, CG#1810, CG#1811, CG#1812) from West Basundhara open cast mine and (CG#1812, CG#1813, CG#1814, CG#1815, CG#1816, CG#1817, CG#1818, CG#1819, CG#1820, CG#1821, CG#1822) from Kulda open cast mine of Mahanadi Coalfields Limited, Odisha. Stratigraphically all samples belong to both Barakar and Karharbari Formation. First 11 coal samples are taken from Rampur seam and last 11 coal samples are from the top and bottom seam of Ib seam of Mahanadi coal field. Physical properties of collected samples were studied. Lithotype study is done following standard measures (Dissel, 1965).

The number of cleats, presence of master cleat was also investigated. The samples are crushed at -72 mesh (212 µm) size for proximate analysis, 1 mm size was used for making pellets. Proximate analysis of the coal samples was carried out by the Indian Standard method (I.S.1977) to determine the percentage of moisture, volatile matter, and ash as well as fixed carbon content at Dept. of Applied Geology, IIT(ISM) Dhanbad. The ultimate analysis has been done with CHNS (O) Analyser FLASH EA 1112 series at SAIF, IIT, Bombay. The analysis includes the determination of carbon, hydrogen, sulfur and nitrogen in the material, as found in the gaseous products on its complete combustion and the calculation of oxygen by difference following standard ASTM D3178-84 (1979). The results of proximate and ultimate analysis have been given in Table 2. For petrographic analysis the samples were crushed to 1mm sizes to prepare polished pellets which were studied under both reflected and fluorescent light in “Leica DM 2700 P” microscope under 50x oil immersion objective following standard procedures (ICCP 1971, 1998, 2001) at Coal Geology and Organic Petrology Laboratory, Department of Applied Geology, Indian Institute of Technology (Indian School of Mines), Dhanbad, India. Macerals were identified following ICCP classification of macerals (ICCP 1971, 1998, 2001, ASTM, 1994). The microscope was attached with software MSP-200 and image workstation with LAS (Leica Application Suite) software, following ISO 7404-3; 1994 (E) and 7404-5: 1994 (E) for viewing and capturing the photomicrographs of macerals and minerals. More than 1000 points were counted with the help of point counter system fixed with the microscope for each pellet with keeping the spacing of points or field of view approximately half the diameter of the largest particle followed by the standard (ISO, 1994). Therefore, volume percentage of macerals and mineral matter were calculated. The vitrinite reflectance of the samples were measured in oil immersion under “Leica DM4500 P” following (ASTM, 2015).

RESULTS AND DISCUSSIONS

The physical properties of the coal samples were studied, and the coals of these areas were found banded in nature with black to grey in color having lustre varying from silky to sub-vitreous. The cleat intensity in these samples varies from 2 to 6 per cm. Tertiary cleats are developed in few samples. Higher values of cleat intensity in bright band indicate high degree of volatile matter present in the area. Cleat intensity of various samples are shown in Table 3. Lithotypes of Ib seam studied thoroughly can be described as fusainic-vitrinic-clarainic type.

Table 2: Technological properties of coal samples from Ib-River coal basin.

SN	A^a (wt%)	W^a (wt%)	VM^a (wt%)	FC (wt%)	Fuel ratio	A^d (wt%)	VM^{daf} (wt%)	CV
CG#1812	21.9	2.49	27.21	48.40	1.78	22.46	35.99	4948.01
CG#1813	25.1	5.31	29.85	39.74	1.33	26.51	42.89	4539.07
CG#1814	15.91	2.60	32.63	48.86	1.50	16.33	40.04	5313.08
CG#1815	14.6	7.11	30.34	47.95	1.58	15.72	38.75	5107.68
CG#1816	15.31	2.89	32.53	49.27	1.51	15.77	39.77	5333.78
CG#1817	24.57	2.50	30.30	42.63	1.41	25.20	41.55	4754.52
CG#1818	15.00	1.20	30.13	53.67	1.78	15.18	35.95	5484.25
CG#1819	7.40	3.60	34.16	54.84	1.61	7.68	38.38	5808.01
CG#1820	10.40	2.69	30.44	56.47	1.86	10.69	35.02	5696.69
CG#1821	17.30	1.80	31.26	49.64	1.59	17.62	38.64	5278.38
CG#1822	20.82	1.90	29.66	47.62	1.61	21.22	38.38	5043.19
CG#1801	18.48	1.69	32.40	47.43	1.46	18.80	40.59	5204.25
CG#1802	8.50	3.40	26.60	61.50	2.31	8.80	30.19	5846.13
CG#1803	12.78	9.30	34.10	43.82	1.29	14.09	43.76	5085.55
CG#1804	12.70	2.50	35.20	49.60	1.41	13.03	41.51	5528.33
CG#1805	18.03	3.00	33.30	45.67	1.37	18.59	42.17	5149.13
CG#1806	7.10	1.60	27.10	64.20	2.37	7.22	29.68	6068.79
CG#1807	7.89	1.50	27.70	62.91	2.27	8.01	30.57	6005.42
CG#1808	16.08	0.90	33.30	49.72	1.49	16.23	40.11	5412.73
CG#1809	10.50	3.80	27.50	58.20	2.12	10.91	32.09	5654.84
CG#1810	10.57	2.40	34.60	52.43	1.52	10.83	39.76	5674.83
CG#1811	6.20	5.10	29.57	59.13	2.00	6.53	33.34	5834.44

Explanation: A^a= ash yield in analytical state, W^a=moisture content (analytical state), VM^a= volatile matter yield in analytical state, FC= fixed carbon content, A^d=ash yield (dry basis), VM^{daf}=volatile matter yield (dry ash free basis), CV=calorific value (estimated)

On the basis of lithotypes the coal samples of Ib seam can be defined as fusainic coal indicate a palaeo-fire in the depositional history. Lithotypes of various samples are shown in Table 4. From the technological analysis it is observed that the volatile matter yield (VM^{daf}) of the samples ranges from 29.68 wt% to 42.89 wt%. The ash yield (Ash^d) of the samples vary from 6.53-26.51 wt%. Moisture content present in the coal sample is very low and varies from 0.90-9.30wt%. The fuel ratio varies varies from 1.29-2.37. From the above technological properties, the coal samples appear to be of bituminous to sub-bituminous rank. Technological properties of coal samples are mentioned in Table 2. Macerals analysis provide a wealth of information towards defining depositional environment especially the presence of facies. Critical macerals such as telinite is derived from woody tissue and so the presence of telinite making most of the vitrinite composition of the studied coal samples indicate the presence of both wood-producing plants and non-woody organic matters.

Table 3: Cleats distribution of coal samples from Ib-River coal basin.

Sample no.	No of Cleats Bright Band	No of Cleats in Dull Band	Cleat Intensity in Bright Band	Cleat Intensity in Dull Band
CG#1812	40	0	4.0	0.0
CG#1813	36	11	6.4	2.3
CG#1814	44	12	3.4	1.2
CG#1815	12	4	1.6	0.8
CG#1816	34	4	3.4	0.6
CG#1817	19	7	1.2	0.6
CG#1818	28	2	3.2	0.7
CG#1819	27	0	3.6	0.0
CG#1820	26	6	2.3	0.6
CG#1821	24	4	2.3	0.9
CG#1822	6	0	1.2	0.0
CG#1801	32	2	3.2	1.0
CG#1802	18	5	6.0	0.6
CG#1803	28	11	4.6	0.5
CG#1804	12	8	5.2	0.6
CG#1805	19	7	2.6	0.4
CG#1806	16	6	4.5	0.7
CG#1807	26	8	5.1	0.4
CG#1808	23	9	3.5	0.8
CG#1809	11	13	4.6	0.3
CG#1810	19	11	2.8	2.5
CG#1811	16	7	3.6	1.4

The macerals group of composition is shown in Table 5. The vitrinite macerals group (V^{mmf}) varies from 23.11 to 49.84 vol%; the inertinite (I^{mmf}) content placed in range of 51.19 to 86.06 vol% whereas the liptinite content has a narrow in range of 9.08 vol% to 20.72 vol%. The vitrinite macerals group is differentiated into telinite, collotelinite, collodetrinite, vitrodetrinite, gelinite and corpogelinite and their variation is noted in various coal samples. The inertinite maceral group is differentiated into micrinite, macrinite, oxyfusinite, pyrosemifusinite, oxyfusinite, pyrofusinite and inertodetrinite. The mineral matter varies from 8.92 to 32.99 vol. % which is dominantly composed of clay minerals with minor amounts of oxide, sulphides, carbonates and silicates. A small amount of pyrites is found in the samples. The different types of macerals observed in the analysis are given in Figure 2. The presence of high proportion of structured inertinite macerals (fusinite and semifusinite) i.e. very low V/I ratio also indicate woody vegetation but under relatively dry condition i.e. relatively low water-table conducive to the formation of pyrofusinite and oxyfusinite under oxidizing condition. Presence of inertodetrinite in samples further establishes a woody

precursor as they form from disintegration of structured inertinite and has the same origin as them.

Table 4: Lithotypes distribution of coal samples from Ib-River coal basin.

Sample No.	Fusain (vol%)	Vitrain (vol%)	Clarain (vol%)	Duro-clarain (vol%)	Claro-durain (vol%)	Durain (vol%)
CG#1812	100.00	-	-	-	-	-
CG#1813	55.55	-	-	-	44.44	-
CG#1814	64.28	26.19	-	9.52	-	-
CG#1815	50.00	-	15.51	-	-	34.48
CG#1816	65.62	-	-	-	-	-
CG#1817	70.00	30.00	-	-	-	-
CG#1818	28.57	17.85	-	25.00	28.57	-
CG#1819	25.39	-	-	-	49.20	25.39
CG#1820	34.37	21.87	43.75	-	-	-
CG#1821	48.50	20.30	31.20	-	-	-
CG#1822	64.21	-	35.78	-	-	-

Fig. 2: Microphotographs of some identified macerals from Ib-River Coal Basin.

Explanation- A, B=Sporinite under fluorescent light; C, D: semifusinite reflected light; E, H: Fusinite under reflected light; F: Collotelinite under reflected light; G: corpogelinite under reflected light.

Table 5: Petrographic composition of coal samples collected from Ib River coal basin in mineral matter free basis.

SN	CG#1812	CG#1813	CG#1814	CG#1815	CG#1816	CG#1817	CG#1818	CG#1819	CG#1820	CG#1821	CG#1822	CG#1801	CG#1802	CG#1803	CG#1804	CG#1805	CG#1806	CG#1807	CG#1808	CG#1809	CG#1810	CG#1811
Te	0.93	1.24	3.47	0.62	4.18	3.03	5.77	2.90	5.65	2.86	2.99	8.65	1.75	3.14	9.64	4.22	4.44	5.77	13.43	5.65	7.72	2.78
Co	14.48	13.93	12.81	17.26	16.30	12.07	18.58	11.00	13.24	10.01	10.11	18.43	14.29	36.05	15.67	18.63	20.29	18.58	29.85	13.24	21.44	20.63
CoD	6.30	6.24	3.11	6.10	5.13	4.86	0.35	4.34	7.42	6.68	5.98	3.34	3.76	0.01	1.44	0.74	1.11	0.35	3.88	7.42	6.68	1.19
Ge	0.46	1.07	0.00	0.00	0.00	0.20	0.17	0.57	0.17	0.24	0.37	0.26	1.00	0.50	0.24	0.99	0.55	0.17	1.19	0.17	0.42	0.00
CoP	0.70	1.24	0.54	0.41	0.93	0.40	3.25	0.87	1.24	0.47	0.56	0.00	0.00	0.00	0.00	0.00	0.00	3.25	0.00	1.24	0.00	0.00
Vd	3.98	4.64	4.39	3.57	3.72	3.81	0.54	4.63	5.82	2.86	4.11	0.00	0.00	0.01	0.89	1.49	2.22	0.54	1.49	5.82	0.00	0.00
Vt	26.84	28.35	24.32	27.95	30.26	24.38	28.66	24.29	33.55	23.11	24.11	30.68	20.81	39.71	27.88	24.73	28.60	28.66	49.84	33.55	36.26	24.59
Spo	6.07	6.24	3.29	6.10	5.36	3.81	0.89	6.07	5.65	5.48	3.18	0.19	1.25	0.07	0.00	0.49	0.01	0.89	0.00	5.65	1.28	0.78
Cu	0.23	4.99	4.02	9.88	7.45	0.63	0.54	3.18	2.99	2.86	3.66	0.00	0.50	4.02	0.00	7.45	0.27	0.54	0.00	2.99	0.00	0.00
Al	0.46	3.03	3.29	1.46	2.79	6.76	2.34	0.28	0.35	4.77	2.25	0.00	0.00	0.00	0.00	0.00	0.00	2.34	0.00	0.35	0.00	0.00
Re	2.32	3.03	4.02	0.84	5.13	2.54	3.78	6.07	6.18	3.09	4.11	0.00	0.00	0.00	0.00	0.00	0.00	3.78	0.00	6.18	0.00	0.00
L	9.08	17.30	14.62	18.28	20.72	13.75	7.55	15.61	15.17	16.20	13.20	0.19	22.56	4.10	0.00	7.93	0.28	7.55	0.00	15.17	37.53	25.38
Mic	4.66	1.42	14.10	0.62	3.95	1.47	0.35	3.18	2.11	0.71	2.25	0.51	0.75	0.00	0.00	0.00	0.27	0.35	0.00	2.11	0.00	0.00
Mac	2.79	1.24	1.28	1.46	1.62	0.20	1.83	0.57	2.29	1.66	2.61	1.61	2.01	0.00	0.00	0.49	0.27	1.83	0.00	2.29	0.00	0.00
Fu	24.28	21.77	20.32	22.51	24.46	19.05	26.09	24.91	17.66	27.91	24.33	37.13	32.59	37.80	33.75	40.49	37.23	26.09	33.73	17.66	27.87	37.29
Sf	23.59	23.04	21.24	25.46	24.69	37.69	31.22	36.80	23.84	25.29	28.26	27.64	28.83	25.62	28.21	35.28	35.84	31.22	47.37	23.84	30.88	36.90
InD	8.64	6.78	4.02	3.57	6.29	3.59	4.33	4.92	5.29	5.00	5.05	2.51	0.00	4.02	0.72	0.00	3.59	4.33	4.92	5.29	3.42	0.00
I	63.96	53.00	60.96	53.63	61.01	62.01	63.73	69.81	51.19	60.58	62.50	69.08	86.06	67.44	62.91	76.25	77.21	63.73	86.02	51.19	62.18	74.17

Explanations: Te: Telinite, Co: Collotelinite , Sf: Semifusinite , Fu: Fusinite, CoD: Colodetrinite , Mac: Macrinite, Ind: Inertodetrinite, Vd: Vitrodetrinite, CoG: Corpogelinite, Vt: Vitrinite, Ge: Gelinite, MM: Mineral Matter content, Su: Suberinite, Re: Resinite, Al: Alginite, Lid:Liptodetrinite, Spo: Sporinite, Cu:Cutinite, CoP: Corpogelinite, Cu: Cutinite, Al: Alginite, Re: Resinite, Mic: Micrinite, Mac: Macrinite, InD: Inertodetrinite.

Tissue preservation index (TPI), gelification Index (GI), groundwater index (GWI), and vegetation index (VI) are calculated and given in Table 6. The plot between VI and GWI is plotted in (Figure 2) (Calder et al., 1991). It evaluates coal depositional environment. Also, the plot between TPI and GI in Figure 3 (Lamberson et al., 1991) indicates a correlation between coal facies indicators and the environment of coal formation. The higher value of TPI index of the samples indicates higher proportion of woods that has contributed to the peat. Presence of high amount of conifers is also possible. Well preserved plant tissue, high proportion of arboreal vegetation and aerobic condition are also indicated by TPI index. The low value of Gelification index (GI) indicated deposition at dry basin margins. GI value can also be considered as inverted oxygen index i.e., low GI indicating high oxidation conditions and here the low values indicate high oxidation conditions. The plot of TPI vs GI also indicates a dry forest swamp to telmatic environment of deposition. The plot of VI vs GWI indicates swamp to swamp forest depositional environment. Various types of petrographic ratio are presented below;

$$TPI = \frac{(Te + Co + CoG + Sf + F)}{(CoD + Ge + InD + Vd)}$$

$$GI = \frac{(Co + CoG + Ge + CoD)}{(Te + VoD + I)}$$

$$VI = \frac{(Te + Co + Re + Sub + F + Sf)}{(InD + Alg + Ld + Spo + Cut + CoD)}$$

$$GWI = \frac{(CoG + Ge + CoD + MM)}{(Te + Co = Vd)}$$

$$SF/F = (Osf+PsF)/ (OF+PF)$$

$$T/F = (Vt)/ (OsF+PsF+OF+PF)$$

$$IR = (OsF+PsF+OF+PF)/ (InD+Mac+Mic)$$

$$WD = (Te+Co+OsF+PsF+OF+PF)/ (Al+Spo+InD)$$

$$SD = (Te+Co+OsF+PsF+OF+PF)/ (Al+Spo+InD+Vd+Ge+CoG+CoD)$$

$$VA/VB = (Te+Co)/(Al+Spo+InD+Vd+Ge+CoG+CoD)$$

(Explanation: TPI: Tissue Preservation Index, GI: Gelification Index, GWI: Groundwater Index, Te: Telinite, Co: Collotelinite , Sf: Semifusinite , Fu: Fusinite, CoD: Colodetrinite , Mac: Macrinite, Ind: Inertodetrinite, Vd: Vitrodetrinite, CoG: Corpogelinite, Vt: Vitrinite, Ge: Gelinite, MM: Mineral Matter content, Su: Suberinite, Re: Resinite, Al: Alginite, Lid:Liptodetrinite, Spo: Sporinite, Cu:Cutinite, CoP: Corpogelinite, Cu: Cutinite, Al: Alginite, Re: Resinite, Mic: Micrinite, Mac: Macrinite, InD: Inertodetrinite)

Table 6: Petrographic ratios of coal samples from Ib valley coal basin.

SN	CG# 1812	CG# 1813	CG# 1814	CG#18 15	CG# 1816	CG#18 17	CG#18 18	CG# 1819	CG# 1820	CG# 1821	CG# 1822	CG# 1801	CG# 1802	CG#18 03	CG#18 04	CG#18 05	CG#18 06	CG#18 07	CG#18 08	CG# 1809	CG#18 10	CG#18 11
GWI	2.14	1.90	1.32	1.45	1.56	2.39	0.90	2.79	1.48	2.44	2.11	1.20	2.22	0.24	1.15	1.11	1.17	0.90	0.77	1.48	1.14	0.94
VI	3.02	2.31	3.49	2.46	2.77	3.79	10.11	4.35	3.07	2.79	3.47	15.21	14.06	12.64	40.40	11.36	19.64	10.11	14.13	3.07	7.72	49.54
GI	0.52	0.57	0.56	0.57	0.58	0.41	0.49	0.37	0.77	0.43	0.46	0.48	0.37	0.59	0.44	0.33	0.38	0.49	0.58	0.77	0.58	0.33
TPI	2.82	2.98	4.34	4.36	3.94	5.59	7.93	4.93	2.74	3.96	3.59	12.31	13.42	25.40	28.61	36.26	13.60	7.93	12.09	2.74	8.70	82.02
VA/VB	1.35	1.15	2.02	1.77	2.09	1.63	5.65	1.34	1.29	1.26	1.19	7.52	3.37	75.37	9.85	7.10	6.37	5.65	6.60	1.29	4.11	19.67
SF/F	0.97	1.06	1.05	1.13	1.01	1.98	1.20	1.48	1.35	0.91	1.16	0.74	0.88	0.68	0.84	0.87	0.96	1.20	1.40	1.35	1.11	0.99
V+L/I	0.56	0.86	0.64	0.86	0.84	0.61	0.57	0.57	0.95	0.65	0.60	0.45	0.50	0.65	0.44	0.43	0.37	0.57	0.58	0.95	1.19	0.67
VL/IMM	0.40	0.62	0.49	0.63	0.59	0.41	0.44	0.39	0.69	0.46	0.45	0.32	0.37	0.57	0.31	0.33	0.28	0.44	0.44	0.69	0.84	0.53
T/F	0.56	0.63	0.59	0.58	0.62	0.43	0.50	0.39	0.81	0.43	0.46	0.47	0.34	0.63	0.45	0.33	0.39	0.50	0.61	0.81	0.62	0.33
IR	2.98	4.75	2.14	8.49	4.14	10.79	8.80	7.12	4.28	7.22	5.31	13.99	22.25	15.78	86.06	154.63	17.69	8.80	16.48	4.28	17.18	0.00
WD	4.17	3.74	5.46	5.92	4.82	5.07	10.80	6.71	5.35	4.33	6.27	34.02	61.97	25.09	121.21	201.27	27.17	10.80	25.28	5.35	18.70	125.13
SD	2.38	2.05	3.10	3.10	2.87	3.07	6.88	3.49	2.33	2.59	3.06	14.58	12.89	22.26	26.53	26.58	13.07	6.88	10.83	2.33	7.45	49.54

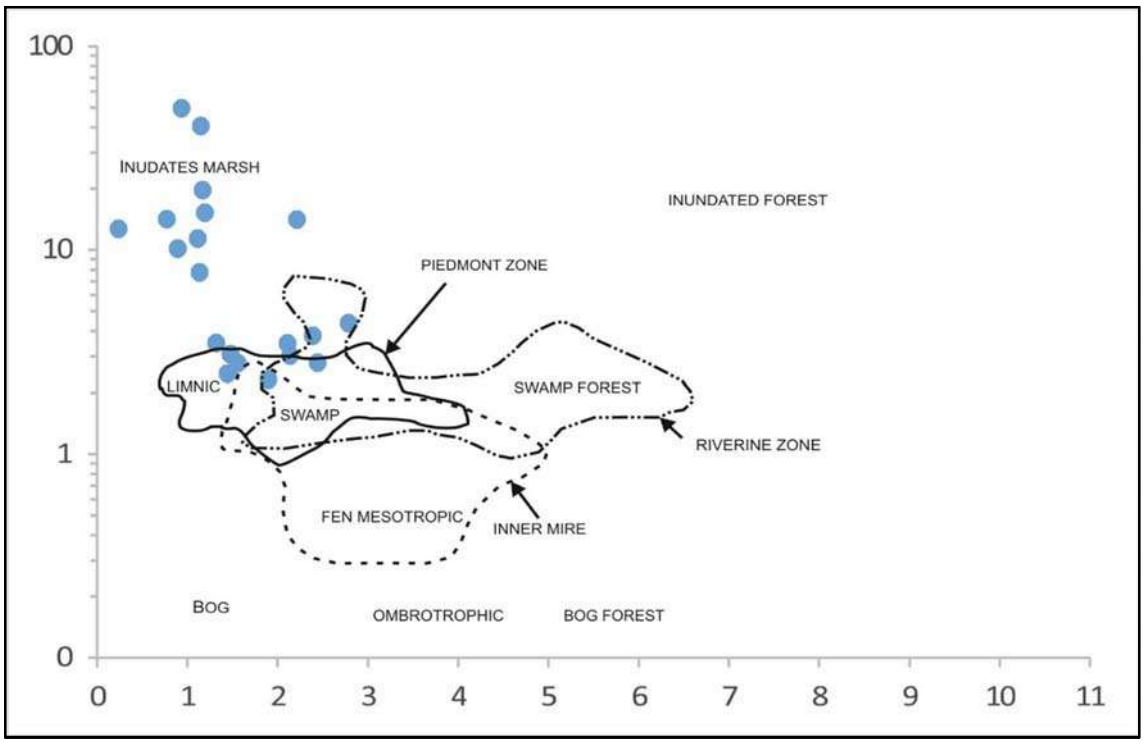

Fig. 3: Relation between vegetation index (VI) and groundwater index (GWI).

Explanations: Samples from Rampur seam indicates inundates marsh environment and samples from Ib seam belongs to swamp-to-swamp forests depositional environment.

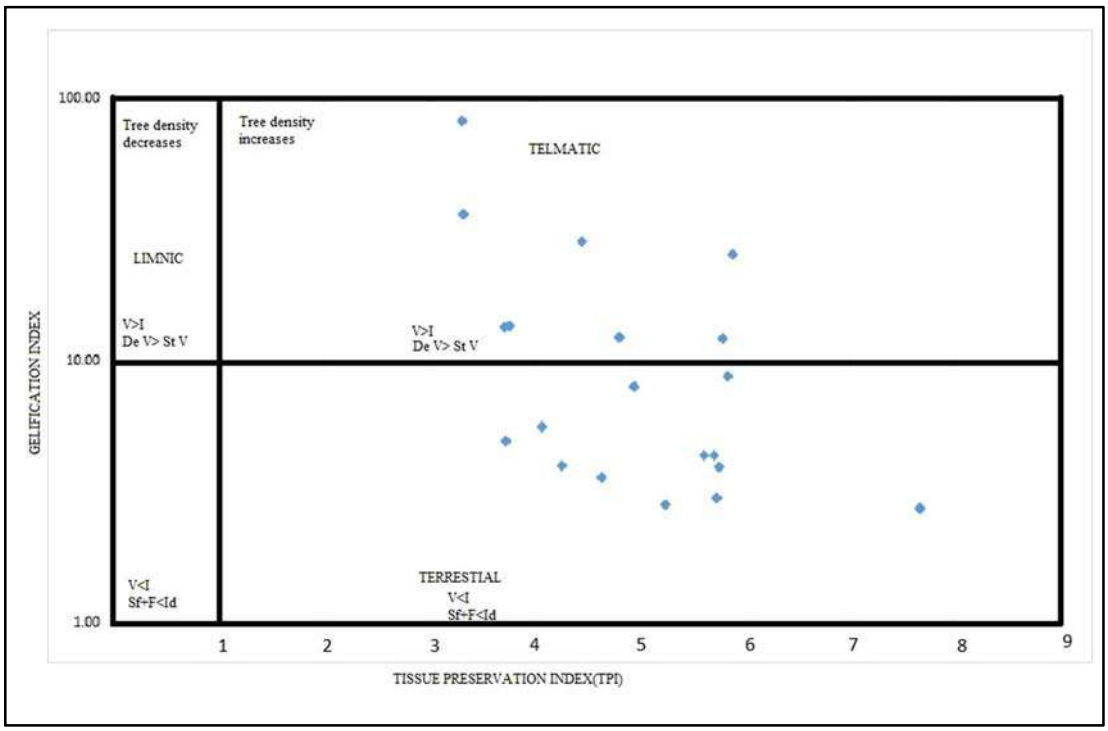

Fig. 4: Relation between Tissue preservation index (TPI) vs Gelification Index(GI).

Explanations: Samples from IB seam showing terrestrial environment of formation while samples from Rampur seam showing telmatic environment.

CONCLUSIONS

Ib valley coal basin was studied with respect to physical characters, proximate, ultimate and micropetrographic characterization. Following conclusions can be made on the basis of results obtained from the analysis done.

1. From the physical properties the coals of Ib-River coal basin were found to be composed of alternate bright and dull bands with rich mineral matter
2. From the lithotype study the coals of Ib-River coal basin is mostly fusinic indicating the evidence of palaeo-fire in depostional history.
3. From the proximate and ultimate analysis, the coals are rich in ash and fixed carbon content. From the volatile matter and moisture content the rank of the coals is found to be sub-bituminous to bituminous in stage.
4. Micro-petrographic analysis indicates enrichment of vitrinites and significant amount of liptinites which promote oil and gas potential.
5. The relation between different petrographic indices, TPI vs GI indicates palaeomire was generated by herbaceous plants and in wet forest swamp environment. Moreover, groundwater index (GWI) and vegetation index (VI) suggest that coal samples have been originated by bog forest under ombrotrophic hydrological conditions.

REFERENCES

Anand Alwar, M.A., 1977. Coal resources of India. Mem. Geol. Surv. India 88, 217–221.

ASTM, 1979. D3178-84 Standard Test Methods for Carbon and Hydrogen in the Analysis Sample of Coal and Coke, p. 418-423.

ASTM, 2015. Standard test method for microscopical determination of the reflectance of vitrinite dispersed in sedimentary rocks. In: Annual Book of ASTM Standards: Petroleum Products, Lubricants, and Fossil Fuels; Gaseous Fuels; Coal and Coke, Sec. 5, v. 5.06. ASTM International, West Conshohocken, PA.

Ball, V., 1871. The Ramgarh and Himgir Coalfield. Rec. Geol. Surv. India 4 (4), 89–139.

Behera, P. and Chandra, D. (1995) Spontaneous Combustion of the Ib Valley Coals of Orissa (India)—A DTA Study. Minetech, 16, 52-57.

Calder J. H., Gibling M. R., and Mukhopadhyay P. K. (1991), "Peat formation in a Westphalian B piedmont setting, Cumberland Basin, Nova Scotia: implications for the maceral-based interpretation of rheotrophic and raised paleomires," Bulletin—Societe Geologique de France, vol. 162, no. 2, pp. 283–298, 1991.

Chaudhury, P.N., 1988. Report on the geology and the coal resources of Gopalpur area, Hingir Valley. Ib-River Coalfield. Report Geological Survey of India.

CMPDI, 1987. Master Plan for Ib-River Coalfield, SECL. (Unpublished).

Diessel, C.F.K., 1965. Correlation of macro- and micropetrography of some New South Wales coals. In: Woodcock, J.T., Madigan, R.T., and Thomas, R.G. (Eds.), Proceedings-general, vol 6, 8th Commonwealth Mineral and Metallurgy Congress, Melbourne, p.669 – 677.

Goswami, S., Das, M. and Guru, B.C. (2006) Permian Biodiversity of Mahanadi Master Basin, Orissa, India and Their Environmental Countenance. Acta Palaeobotanica, 46, 101-118

GSI, 1997. Recent Advances in stratigraphy and tectonics of Ib-Himgir Valley Gondwana Basin, Orissa. An Unpulished Guide for traverses in the field workshop held during 15th to 17th February, 1997,

ICCP (1971) International Hand book of Coal Petrology. Supplement to 2nd Edition, International Committee of Coal Petrology, cent., Natl., Sci., Paris.

ICCP (1998) The New Vitrinite Classification (ICCP System, 1994). Fuel, 77, 349-358.

ICCP (2001) The New Inertinite Classification (ICCP System, 1994). Fuel, 80, 459-471.

Indian Standard (1977) Methods of Test for Coal and Coke, Part-I, Proximate Analysis. 1st Revision, 2nd Reprint.1977.

ISO 7404-5:1994, Methods for the petrographic analysis of bituminous coal and anthracite — Part 5: Method of determining microscopically the reflectance of vitrinite.

Lamberson M. N., Bustin R. M., and Kalkreuth W. (1991), "Lithotype (maceral) composition and variation as correlated with paleo-wetland environments, Gates Formation, northeastern British Columbia, Canada," International Journal of Coal Geology, vol. 18, no. 1-2, pp. 87–124, 1991.

Manjrekar, V.D., Choudhury, V. and Gautam K.V.V.S. (2006) Coal. In: Mahalik, N.K., Ed., Geology and Mineral Resources of Orissa, Society of Geoscientists and Allied Technologist, Bhubaneswar, 205-226.

Mehta, D.R.S., Anandalwar, M.A., 1960. The Ib-River (Rampur – Himgir) Coalfield. Rec. geol. Surv. India 86 (3), 421–551.

Mukhopadhyay, S.K., 1987. Geology around Kanika and Rohini area, Southern part of Ib-River Basin, Sundargarh and Sambalpur dists., Orissa. Unpublished Progress Report, Coal Wing, Geol. Surv. India, Field Season 1984-85.

Mukhopadhyay, S.K. (1989) Geology of Northeastern part of Ib-River Coalfield, Sambalpur District, Orissa. UnPublished Progress Report, Coal Wing, Geol. Surv. India, Field Season 1986-87.

Navale, G.K.B. (1967) Microconstituent Analysis of Coal Seams in Hingir-Rampur Coalfield, U.G.C. Sponsored Symposium: "Coal; A Pterographic Approach".

Navale, G.K.B. and Tiwari, R.S. (1968) Palynological Correlation of Coal Seams, Their Nature and Formation in Rampur Coalfield, Lower Gondwana (India). The Review of Palaeobotany and Palynology, 6, 155-169. p. 1–10.

Pal, A.K., Chaudhury, P.N., Bose, S., Ghosh, R.N., 1992. A Middle Triassic age for the Kamthi (Himgir) Formation of the Lower Gondwana Ib-Himgir Basin, Orissa, India, New Palaeobotanical evidence. Newsl. Stratigr. 27 (1/2), 33–39.

Pareek, H.S. (1958) A Note on the Petrology of Ib-River Coals. Quart. Jour. Geol. Min.Met. Soc. Ind, 9.

Raja Rao, C.S., 1982. Coalfields of India, II. Coal resources of Tamilnadu, Andhra Pradesh, Orissa and Maharashtra. Bull. geol. Surv. India Ser. A. 45, 1–101.

Sykes, R., & Snowdon, L. R. (2002). Guidelines for assessing the petroleum potential of coaly source rocks using Rock-Eval pyrolysis. Organic geochemistry, 33(12), 1441-1455.

Tissot, B. P., Welte, D. H., Tissot, B. P., & Welte, D. H. (1978). Sedimentary processes and the accumulation of organic matter. Petroleum Formation and Occurrence: A New Approach to Oil and Gas Exploration, 55-62.

Tewari, R., Mehrotra, N.C., Meena, K.L., Pillai, S.S.K., 2009. Permian megaspores from Kuraloi Area, Ib-River Coalfield, Mahanadi Basin, Orissa. J. Geol. Soc. India 74, 669–678.

Varma, A. K., Sahoo, A., Saikia, B. K., & Das, T. (2019). Petrographic controls of coal from Ib valley Basin for carbon nano-products formation. International Journal of Coal Geology, 211, 103211.

VISTAS IN GEOLOGICAL RESEARCH
Special Publication in Geology (19), March 2023, pp. 207-215

Heavy Metal Pollution and its Indexing Approach in Pre-Monsoon Groundwater of Baliapal Block, Balasore District, Odisha, India

PRITAM KUMAR BARIK[1], NANDITA MAHANTA[2*] AND H.K. SAHOO[2]

[1]Dept. Of Geology, Fakir Mohan University, Balasore, Odisha-756089
[2]Dept. of Geology, Utkal University, Vani Vihar, Bhubaneswar, Odisha-751004
***Corresponding Author:** nandita.mahanta12@gmail.com

Abstract: The present study aims to find out the heavy metal pollution index of Baliapal block of Balasore District of Odisha during the Pre-Monsoon season of 2022. A total of 100 ground water samples were collected to know the details about the concentration of heavy metal present in water. The Atomic Absorption Spectrophotometer (AAS) is used to analyse heavy metals like Iron, Copper, Manganese, Chromium, Nickel and Arsenic. As per Bureau of Indian Standards (BIS) 2012, 5% of water samples exceeded the acceptable limit for Iron (300 µg/l) where as 3% of samples had manganese concentration above the acceptable limit (100 µg/l). 4% samples of chromium have exceeded the acceptable limit (50 µg/l). 3% samples of arsenic has exceeded the acceptable limit(10 µg/l) where as no sample is beyond the acceptable limit with respect to copper and nickel as its limit is 50 µg/l and 20µg/l respectively. The mean HPI value of groundwater of the study area is 55.11. The heavy metal pollution index of 97% samples have value below 100(Critical Index) and 3% have value above the critical level, which is due to agricultural, industrial and urban activity. The average MI value of the area of study is 0.38.

Key words: Heavy Metal Pollution Index, Balasore District, Drinking Water Quality,

INTRODUCTION

Water is a most precious and necessary resource and plays an extremely important role in the sustain of life. The demand for water increases due to over population, irrigation and industries. Because of the erratic rain fall there is a scarcity of surface water. The term quality indicates the importance of both surface and ground water whether it is useful or not. Hence, the study of surface and ground water is essential for human developmental activities as it not only affect our health, but also society and economy. Saltwater intrusion is the movement of saline water into freshwater aquifers, which can lead to groundwater quality degradation, including drinking water sources, and other consequences. Saltwater intrusion naturally occurs in coastal aquifers, owing to the hydraulic connection between groundwater and sea water.

STUDY AREA

An area of about 200 sq km was studied in Baliapal Block which is situated in Balasore District; Odisha It is located at 21.6504°N, 87.2804°E falling in Survey of India Toposheet numbers F45P/2, P/3 and P/6. This region is famous for red crabs found in beach

sand. The study area is surrounded by a number of blocks such as Bhograi, Jaleswar, Basta and Balasore.

ROCK TYPES

The area forms a part of to east-coast coastal plain which consists of sand, silt and clay. The soil of this area is marshy and saline contain high amount of sodium, potassium, calcium, magnesium, iron and less in nitrogen and phosphorous. The index map of the investigated area is given in Fig.1.

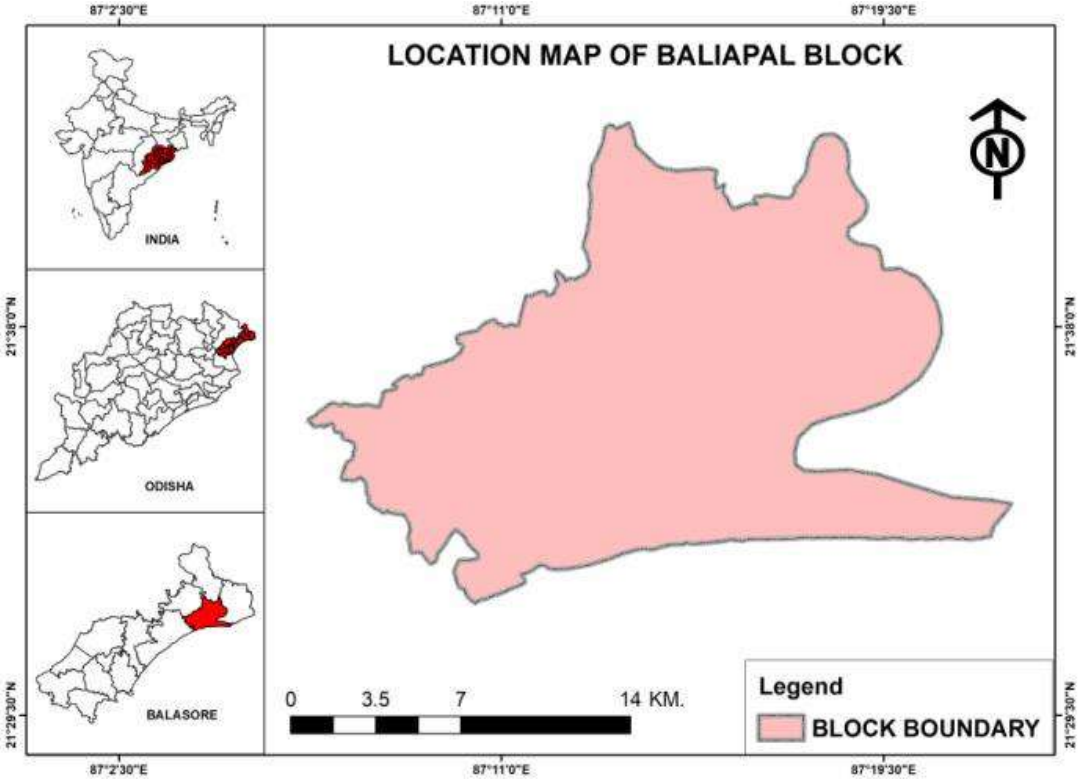

Fig. 1: Index map of the study area.

MATERIALS AND METHOD

To study the quality of groundwater in details, 100 numbers of water samples from tube wells were collected in pre-monsoon, 2022. The samples were collected from the entire investigated area with more emphasis on the residential area, agricultural sectors, various industrial sites, etc. The sample location map is given in Fig.2. The various physicochemical parameters such as pH, temperature, total dissolved solids (TDS), electrical conductivity (EC), total alkalinity (TA), total hardness (TH), calcium (Ca^{2+}), magnesium (Mg^{2+}), sodium (Na^{+}), potassium (K^{+}), sulphate (SO_4^{2-}), chloride (Cl^{-}), carbonate(CO_3^{2-}), bicarbonate (HCO_3^{-}), nitrate (NO_3^{-}), fluoride (F^{-}) etc. were determined by standard procedure followed by APHA (1995). Heavy metal concentrations like Iron (Fe), Copper (Cu), Manganese (Mn), Chromium (Cr), Nickel (Ni) and Arsenic (As) were determined by Atomic Absorption Spectrophotometer (AAS) to know about the metal contamination in water.

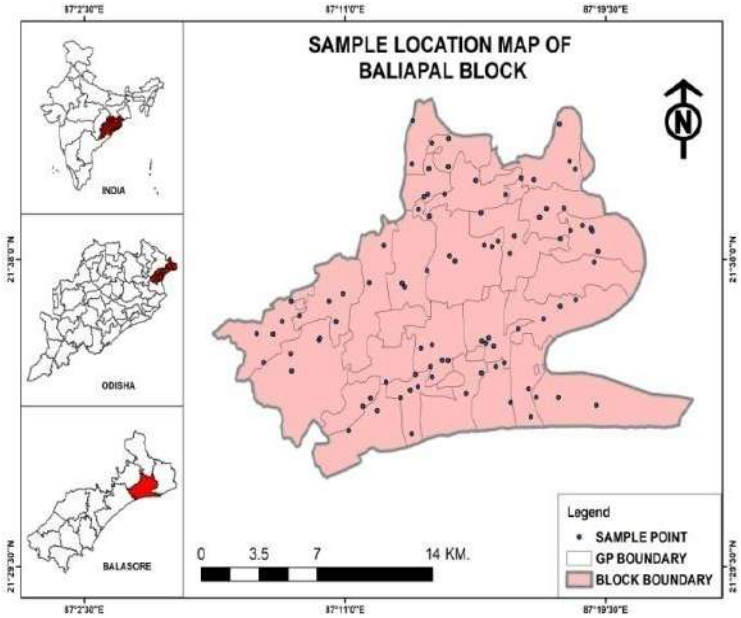

Fig. 2: Sample location map.

HEAVY METAL SPECIFICATION

Iron (Fe)

The iron concentration of the collected water varied from 15 to 1783 µg/l with an average of 179.55 µg/l. As per Bureau of Indian Standard (2012), the acceptable limit of iron is 300 µg/l. There are 57 locations where the value exceeded the acceptable limit. The high concentration of iron is because of the discharge of waste effluents on land and weathering of rocks. The iron iso-concentration map of the area is given in Fig.3. The 57% of samples exceed the acceptable limit of iron (BIS, 2012) for drinking purposes. The minimum, maximum, mean and standard deviation of the heavy metal concentration of the area of study is given in Table: 1 and comparison with.BIS, 2012 is given in Table 2.

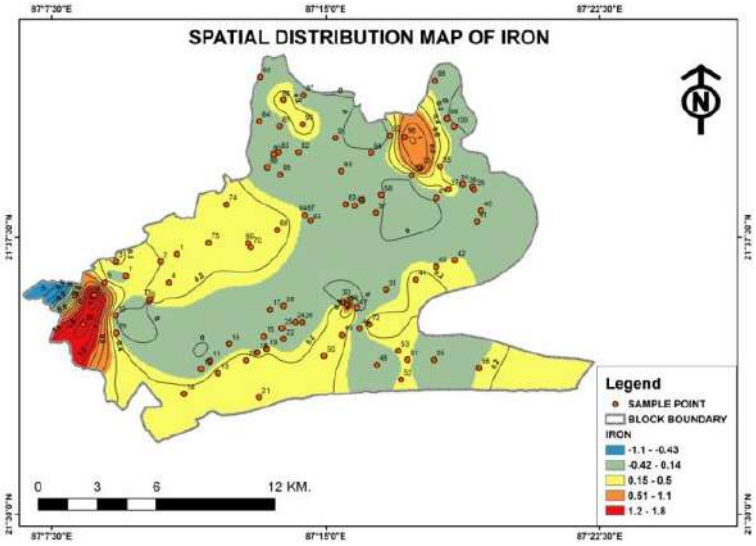

Fig.3a: Spatial distribution map of Iron.

Table 1: Statistical data of heavy metal of water samples of the area of study.

Parameter	Minimum	Maximum	Average	SD
Fe	15	1783	179.59	272.00
Mn	12	817	40.73	85.30
Cr	11	86	28.14	12.88
Cu	2	36	11.56	8.47
Ni	3	66	10.88	9.54
As	2	24	6.68	2.73

Here, all the values are expressed in μg/L.

Table 2: Comparison of Chemical quality of groundwater with BIS for drinking and domestic purposes.

Parameters	BIS 10500:2012		No. of Samples exceeding acceptable limits	% of samples exceeding acceptable limit	No. of Samples exceeding Permissible Limit	% of samples exceeding Permissible Limit
	Acceptable Limit	Permissible Limit				
pH	6.5	8.5	99	99	Nil	0
TDS	500	2000	67	67	1	1
TH	200	600	68	68	1	1
Ca^{2+}	75	200	14	14	1	1
Mg^{2+}	30	100	68	68	6	6
HCO_3^-	200	600	91	91	0	0
Cl^-	250	1000	46	46	1	1
SO_4^{2-}	200	400	1	1	0	0
NO_3^-	45	No relaxation	6	6	Nil	0
F^-	1.0	1.5	Nil	0	Nil	0
Fe	0.3	No relaxation	5	5	Nil	0
Cu	0.05	No relaxation	Nil	0	Nil	0
Mn	0.1	0.3	1	1	2	2
Cr	0.05	No relaxation	4	4	Nil	0
Ni	0.02	No relaxation	Nil	0	Nil	0
As	0.01	No relaxation	3	3	Nil	0

All units are in mg/l., except pH.

Copper (Cu)

The copper value of the analyzed sample is ranged between 2 and 36 μg/l and average is 11.56 μg/l. Analysis of samples collected from Baliapal block shows that 7 samples were above the acceptable limit i.e. 50 μg/L for drinking water. The locations where the value exceeded the acceptable limit are Jhinkiria, Bhanreswar, Talanendua, Balarampur, Betana, Purusottampur, Keshdiha. The isoconcentration map of copper is given in Fig.4.

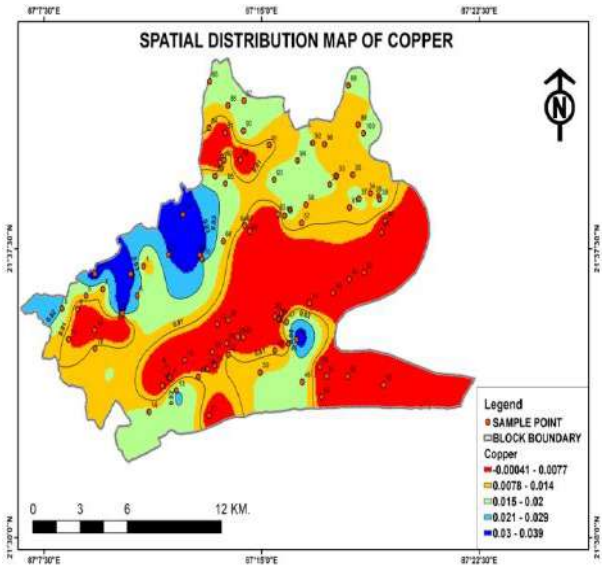

Fig. 4a: Spatial distribution map of Copper.

Manganese (Mn)

Manganese is found in form of various minerals and salts and is commonly found with iron compounds. The low concentration of manganese in groundwater is because of geochemical control [Jain et al. 2010]. According to BIS, the acceptable limit of manganese is 100μg/ l and the permissible limit is 300μg/ l. The concentration of manganese in groundwater samples ranged between 2 and 817 μg/ l with a mean of 40.73 μg/ l. There are 32 samples were above the permissible limit.

Chromium (Cr)

The chromium value of the analyzed sample is ranged between 11 and 86 μg/ l and average is 28.14μg/ l Analysis of samples collected from Baliapal block shows that 70 samples were above the acceptable limit i.e. 50 μg/ l for drinking water.

Arsenic (As)

The arsenic value of the analyzed sample is ranged between 2 and 24μg/ l and average is 6.68 μg/L. Analysis of samples collected from Baliapal block shows that 45 samples were above the acceptable limit i.e. 10 μg/l for drinking water.

COMPUTATION OF HPI AND MI

Heavy Metal Pollution Index (HPI)

The method of rating which shows the composite influence of individual heavy metals on the overall quality of water is known as the Heavy Metal Pollution Index (HPI) (Sheykhi and Moore 2012).

It is formulated by,

$$HPI=\frac{\sum_{i=1}^{n} WiQi}{\sum_{i=1}^{n} Wi}$$

Where Wi = Unit weightage of ith parameter
Qi = Sub-index of the ith parameter
n= Number of parameters
The sub-index (Qi) of the parameter is determined by the following formula.

$$Qi = \sum_{i=1}^{n} \frac{|Mi - Ii|}{Si - Ii} \times 100$$

Where, Mi= Monitored value of the heavy metals of the ith parameter
Ii = Ideal value of ith parameter
Si = Standard value of the ith parameter.

In the indexing of heavy metal pollution, the rating value of Wi is an arbitrary value between 0 and 1 given for each metal. The rating is based on the relative importance of individual quality considerations and is inversely proportional to the recommended standard (Si) for each parameter. Water quality and its suitability for drinking may be examined by determining its quality index [Mohan *et al*. 1996,] [Prasad and Mondal 2008]. The computational method for calculating HPI is given in Table- 3.The critical pollution index of HPI value for drinking water is 100. Water quality can be classified into three categories based on HPI. These are low heavy metals pollution (<100), threshold risk (=100), high heavy metal pollution (>100) [Ghaderpoori et. al, 2018]. It is found that only three numbers of groundwater samples have a high HPI value (>100). 97% samples have a low value of HPI. The higher values of HPI were observed particularly in the area of Indipada (PT-6), Kalajathia (PT-66), and Baramahisadi (PT-96) (Ref. Table:4).

Table 3: Calculation of Heavy Metal Pollution Index (HPI) for groundwater sample.

Heavy Metals	Mean Value(Mi) in ppb	Standard Permissible Value(Si) in ppb	Highest Desirable Value (Ii) in ppb	Unit Weightage (Wi)	Sub Index (Qi)	Wi×Qi
Fe	179.55	300	---	0.003	59.85	0.179
Cu	11.56	50	---	0.02	23.12	0.462
Mn	40.73	300	100	0.003	13.58	0.041
Cr	28.14	50	---	0.02	56.28	1.126
Ni	10.88	100	---	0.01	10.88	0.109
As	6.68	10	---	0.1	66.80	6.68
				ΣWi=0.156		ΣWiQi =8.597

Heavy metal Pollution Index (HPI)= 8.963/0.163=55.11

Table 4: Water quality classification using HPI (Ghaderpoori et. al, 2018).

HPI	Characteristics	% of samples
<100	Low heavy metals pollution	97
=100	Threshold risk	0
>100	High heavy metals pollution	3

Table 5: Calculation of Metal Index (MI) for groundwater sample.

Heavy Metals	Concentration(Ci) in (ppb)	Maximum Allowable Concentration.(MAC)	MI= $\sum_{i=1}^{N} \frac{Ci}{(MAC)i}$
Fe	179.55	300	0.60
Cu	11.56	50	0.23
Mn	40.73	300	0.13
Cr	28.14	50	0.56
Ni	10.88	100	0.11
As	6.68	10	0.67
			Mean= 0.38

Metal Index

The metal index is defined as evaluating the water quality based on the content of heavy metals present in water. If the metal concentration is higher than the MAC value, then the quality of the water is worse. The water cannot be used if the concentration of the element is higher than the respective MAC value (MI>1). In groundwater presences of several elements have smaller concentrations but close to the respective MAC values will also decrease the overall quality of water because of an additive effect. Thus, the metal index value 1 is the threshold of warning, even in the case where *Ci* is smaller than MAC*i* for all the elements (Tamasi and Chini, 2004).

MI can be express by the equation-

$$MI= \sum_{i=1}^{N} \frac{Ci}{(MAC)i}$$

Where MI = metal index,
C = concentration of each element in solution,
MAC = maximum allowed concentration for each element
Subscript i = the i^{th} sample.

The computational method for calculating metal index (MI) for groundwater sample is shown in the Table-6. If the concentration of metals for MAC (Maximum Allowed Concentration) value is high, the water became worse quality. Therefore, the value of 1 for MI is a threshold of warning even in the case where Ci is less than MACi for all elements. (Where Ci is the mean concentration of each metal and MACi is maximum allowable concentration) (Balakrishnan and Ramu 2016). The average value of the metal index (MI) of the study area was found 0.38. The classification based on MI show that there are four village Indipada (PT-6), Kalajathia (PT-66), Bisikadeipur (PT-78) and Baramahisadi (PT-96) have MI values >1 and is slightly affected. Among the rest of the samples, 57% samples are pure and 39% samples are very pure with respect to MI (Caerio et al., 2005).

Table 6: Water quality classification using MI after Caerio et al. 2005.

MI	Characteristics	Class	Total No. of Sample
<0.3	Very pure	I	**39**
0.3-1.0	Pure	II	**57**
1.0-2.0	Slightly affected	III	**04**
2.0-4.0	Moderately affected	IV	--
4.0-6.0	Strongly affected	V	--
>6.0	Seriously affected	VI	--

CONCLUSION

From the above studies, it is found that the average value of the heavy metal pollution index (HPI) of the area is 55.11 and metal index (MI) is 0.38. The HPI and MI values of the groundwater are used to evaluate the overall pollution level of groundwater. It is found that only six numbers of samples (3%) have a high HPI (>100), which is found in Indipada, Kalajathia, Baramahisadi. Similarly the four villages Indipada, Kalajathia, Bisikadeipur, and Baramahisadi are slightly affected by metal index where as 39% samples are very pure and 57% samples are pure variety depending upon MI values. As per Bureau of Indian Standards (BIS) 2012, 5% of water samples were exceeded the acceptable limit for Iron (300 µg/l) where as 3% of samples had manganese concentration above the acceptable limit (300 µg/l). 4% samples of chromium have exceeded the acceptable limit (50µg/l). 3% samples of arsenic has exceeded the acceptable limit(10 µg/l) whereas no sample is beyond the acceptable limit with respect to copper and nickel as it's permissible limit is 50 µg/l and 100 µg/l respectively. The overall quality of groundwater is suitable for drinking purposes with respect to heavy metal pollution index except few locations.

REFERENCES

Balakrishnan,A. and Ramu, A. (2016) Evaluation of heavy metal pollution index(HPI) of ground water in and around the coastal area of gulf of mannar biosphere and palk strait J. Adv. Chem. Sci. v.2(3),pp. 331–333.

BIS (BUREAU OF INDIAN STANDARDS) (2012) Specification for drinking water IS 10500: 2012, New Delhi, India.

Caeiro S, Costa M.H., Romas T.B.,Fernandes F.,silveria N.,Coimbra A, Medeiros G., Painho M. (2005) Assessing heavy metal contamination in Sado Estuary sediments :an index analysis approach .Ecol Indic 5:051-169.

Ghaderpoori, M., Kamarehie, B., Jafari, A., Ghaderpoury, A., and KaramI, M.(2018) Heavy etals analysis and quality assessment in drinking water – Khorramabad city, Iran, Elsvier, doi: 10.1016/j.dib.2017.11.078**,** pp-685- 692.

Jain, C.K., Bandyopadhyay, A.and Bhadra, A. (2010) Assessment of ground water quality for drinking purpose, District Nainital, Uttarakhand, India. Environment Monitoring Assessment, v.166, pp. 663-676.

Mohan, S.V., Nithila, P.and Reddy, S.J. (1996) Estimation of heavy metal in drinking water and development of heavy metal pollution index. J Environ Sci Health A v.31 (2), pp.283–289

Prasad, B.and Mondal, K.K. (2008) The impact of filling an abandoned opencast mine with fly ash on ground water quality: a case study. Mine Water Environ v.27 (1), pp.40–45

Sheykhi, V.and Moore, F. (2012) Geochemical characterization of Kor River water quality, Fars Province, Southwest Iran. Water Qual Expo Health v.4, pp.25–38

Tamasi, G. and Cini, R. (2004) Heavy metals in drinking waters from Mount Amiata (Tuscany, Italy) Possible risks from arsenic for public health in the province of Siena, Sci. Total Environ. V.327, pp.41-51.

VISTAS IN GEOLOGICAL RESEARCH
Special Publication in Geology (19), March 2023, pp. 216-222

Geospatial Distribution and Assessment of Groundwater Quality in Coastal blocks of Balasore District, Odisha, India

UTSAV DAS AND ROSALIN DAS

P. G. Department of Geology, Fakir Mohan University, Balasore - 756089, Odisha
Corresponding author e-mail: rosalindas.geology@gmail.com

Abstract: This research article investigates the geospatial distribution of groundwater quality in the Balasore Sadar and Remuna blocks of Balasore district, located in the eastern state of Odisha, India. A total of 60 groundwater samples were collected from tube wells and dug wells during the pre-monsoon period of 2022 and were analysed for physico-chemical parameters such as, pH, electrical conductivity, total dissolved solid, carbonate, bicarbonate, calcium, magnesium, potassium, sulphate, chloride, fluoride etc using standard methods of APHA. The geospatial interpretation of the analysed value has been made using GIS software. The results are compared with WHO and BIS water quality standards. The results show that both blocks have relatively good water quality, with few cautions. The study suggests that the water is mostly alkaline and hard but many parameters excluding F^- are within the permissible limit. Piper tri-linear diagram reveals that groundwater of the study area are Ca-Mg-HCO_3 type followed with Ca-Na-HCO_3 and Na-Cl type. This suggests the intrusion of saline water in most of the coastal villages. The study emphasizes the need for continued monitoring of groundwater quality to ensure the safety and sustainability of water resources in the region.

Key words: Groundwater quality, Geospatial distribution, Balasore Sadar block and Remuna blocks

INTRODUCTION

Groundwater is a significant resource for human needs, agriculture, and industry. However, its quality is often affected by anthropogenic activities and natural processes. Coastal regions are particularly vulnerable to contamination due to their proximity to the sea and intensive human activities. Balasore is a coastal district located in the eastern state of Odisha, India. The district is known for its aquifer systems, which are the primary source of drinking water and irrigation. The present study aimed to assess the geospatial distribution of groundwater quality in the coastal blocks, Balasore Sadar and Remuna blocks of Balasore district.

STUDY AREA

The study area is located 21°04’ to 21°58’ North latitude and 86°16’ to 87°29’ East longitude in the district of Balasore at an elevation of 600m above the MSL. The study is spread over 786Sq.Km (Remuna block 309Sq.Km and Balasore block for 477Sq.Km). A major part of the district is underlain by tertiary and quaternary alluvium with basement Precambrian Nilgiri granites (Mahalik and ananda 2006) and granitic genies with minor pegmatite and quartz veins. Budhabalanga and its tributaries are the main drainage of the area. Flattering of topography near by the coast. The region enjoys humid subtropical climate

with an average of 250mm-290mm rainfall receives during rainy season. During pre-monsoon, depth of the water level remained within 6m – 8m below ground level (BGL). In hard rock area and transition zone it may 10m below the ground level. (CGWB)

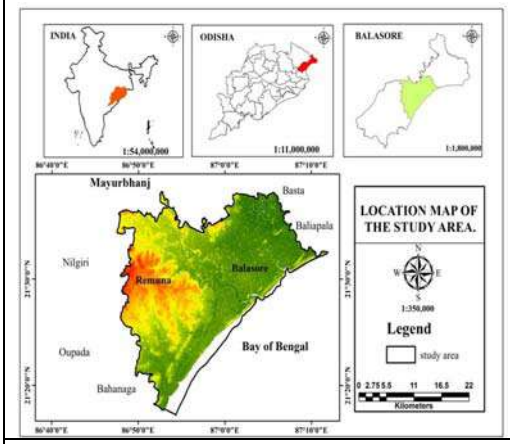

Fig.1. Location of Study area

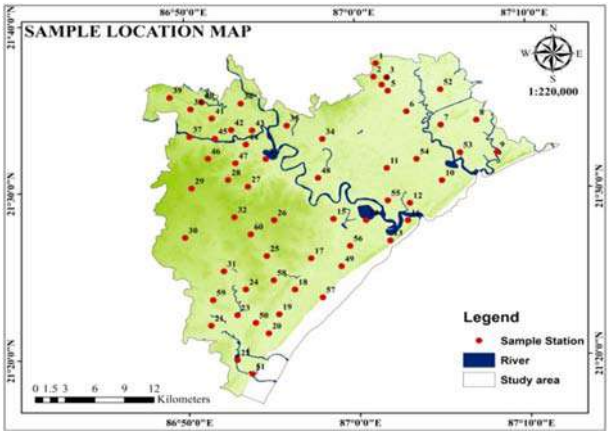

Fig.2. Sampling Points

METHODOLOGY

The study was conducted in the Balasore Sadar block and Remuna blocks of Balasore district. A total of 60 groundwater samples were collected from hand pumps and dug wells during the pre-monsoon season (March-April 2022). The samples were analyzed for physico-chemical parameters such as pH, electrical conductivity (EC), total dissolved solids (TDS), alkalinity, hardness, nitrate, chloride, fluoride, by standard analytical procedure (APHA 2012). The EC and PH are measured insitu using handheld PH and EC meter (HANNAHI-9828). Ca^{2} , HCO^{-}, Mg^{2}, Cl^{-} and TDS by volumetric titration method. Na , K ion is measured by flame photometer while F^{-} and SO^{2-}_{4} determined by Spectro-photometric techniques.

The collected data was processed using the Geographical Information System (GIS) software. The spatial distribution of physico-chemical parameters was mapped using the Kriging interpolation method. The interpolation surfaces were classified based on the Standard for Drinking Water (WHO) to identify the areas with poor water quality.

RESULTS AND DISCUSSION

Comparison with reliable standards and geospatial mapping

The analysed vaues of groundwater parameters are compared with WHO (2017) and BIS (2012) to assess the suitability of water for drinking purpose (Table.1). The results showed that hydrogen ion concentration (pH) varies from 6.70 to 8.40 with an average value of 7.47 indicating mostly alkaline nature of the groundwater. The Electrical conductivity (EC) depends upon temperature, concentration and types of ions present in the water (Das et al., 2011, 2015, 2016). Electrical conductivity (EC) is the measure of capacity to convey the

electric current. Worth mentioning, Electrical conductivity (EC) is used to explain the salinity of water; the concentration of dissolved salts is a metric to determine the EC of groundwater. The electrical conductivity from different locations varies from 476.92 µmho/cm to 1361 µmho/cm with an average value of 772.44 µS/cm, whereas the permissible limit is 300 µmho/cm recommended by USPHS. High EC at some places indicate introduction of sewage in groundwater at these sites. The result shows that most of the samples exceeded the permissible limit of salinity, particularly along the coastal tract (Alam et al., 2017). The effect of high EC water on crop productivity is the inability of the plant to compete with ions in the soil solution for water. The higher the EC, the less water is available to plant (Das, 2022) The total dissolved solids (TDS) ranges from 310 – 885 mg/L with an average value of 504.03 mg/L signifying contributions from both geogenic and non-geogenic sources (Subba Rao et al., 2017). Increased shrimp farming in the agricultural land along the coast causes salinisation of soil as well as salinity of groundwater of the adjacent area (Mahmuduzzaman et al., 2014; World Health Organization, 2017). Continuous use of saline water can be a great threat to human consumption and irrigation.

Table.1. Comparison of water quality of the study area with WHO and BIS 10500 standards

Parameter	Ranges	WHO (2004)	BIS 10500 (ISI.1995)	
			Highest desirable	Maximum desirable
pH	6.7-8.4	6.5-8.5	6.5	8.5
EC	476.92-1361.54	400-2000	-	-
TDS	310- 885.00	500-1000	500	2000
Alkalinity	135.00 -315.00	-	200	600
Total Hardness	125.00-350.00	-	300	600
Calcium	30.00 -70.00	100-200	75	200
Magnesium	8.38 -51.64	30-50	30	100
Sodium	22.18-172.28	20-1756	-	-
Potassium	0.58 -14.80	10-12	-	-
Carbonate	6.00 -24.00	-	-	-
Bicarbonate	110.00- 232.00	-	200	600
Chloride	35.00 - 255.00	25-600	250	1000
Fluoride	1.04- 5.48	-	1.0	1.5
Sulphate	15.64 - 78.27	25-250	200	400
Nitrate	15.63-42.32	50	45	

The geospatial mapping of various water quality parameters is carried out to visualize their variations, which helps to demarcate the contaminated regions. The spatial variation of pH, EC, TDS, TH, alkalinity, sodium, chloride, fluoride, sulphate, and salinity over the study area are presented in Fig.3. It can be observed that groundwater of the coastal portions is highly saline in nature with increased concentration of EC, sodium, chloride, and salinity. The groundwater over a significant portion of the study area is affected by very high EC and TDS. In many cases, the F - concentrations are more than the recommended limit of 1.5 mg/L (BIS, 2012 and WHO, 2017). The GIS-based analysis revealed that the coastal areas of both Balasore Sadar and Remuna blocks show relatively high salinity.

The abundance sequence of cations in the groundwater is $Na^+ > Ca^{2+} > Mg^{2+} > K^+$. The dominance of Na^+ in groundwater points to the prolific weathering and dissolution of the basement rocks as well as anthropogenic inputs and saline water intrusion. The abundance sequence of anions is $HCO_3^- > Cl^- > SO_4^{2-} > NO_3^- > CO_3^{2-} > F^-$.

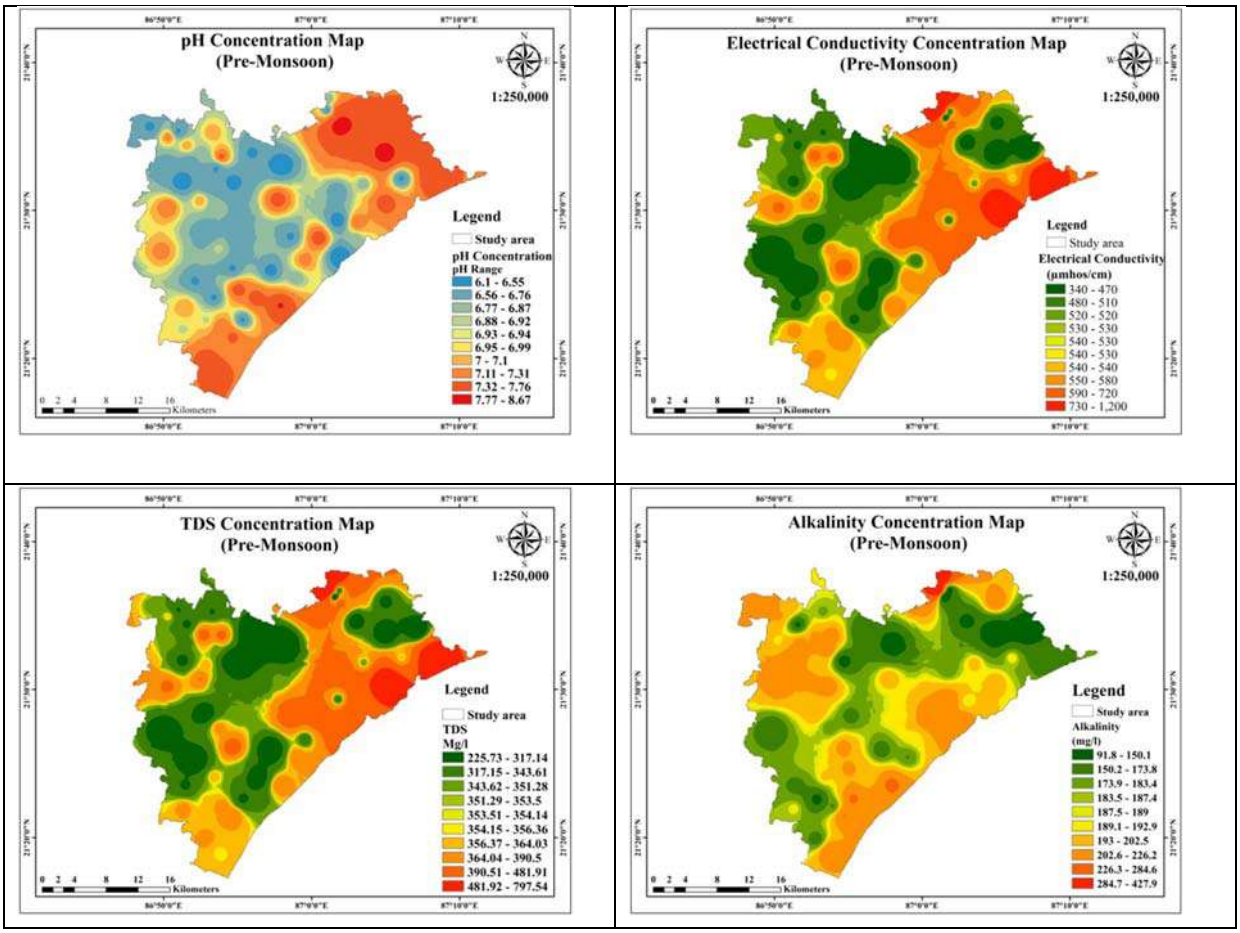

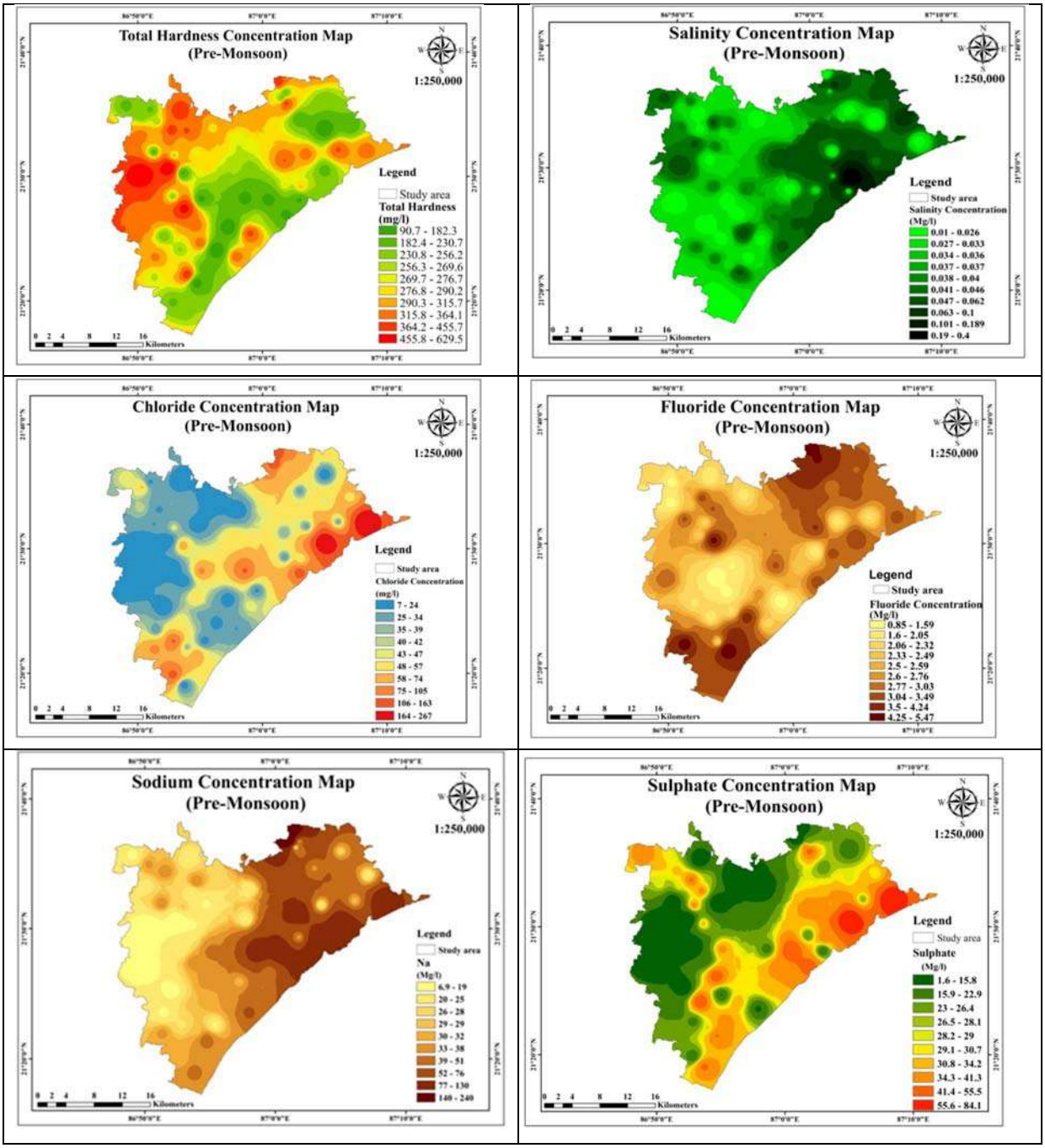

Fig. 3. Spatial distribution of pH, EC, TDS, TH, Alkalinity, Salinity, Sodium, Chloride, Fluoride and Sulphate

Hydrochemical facies

The hydrochemical facies of the study area are determined based on Piper's Trilinear diagram. The groundwater type varies from coast towards inland. The important groundwater types are Ca^{2+}-HCO_3^- (73.05%), Na^+- Cl^- (21.18%), Ca^{2+}-Mg^{2+}- Cl^- (5.45%), and Mg^{2+}- HCO_3^- (0.32%) as exhibited by the Piper diagram (Fig.4). It suggests that Ca^{2+}-HCO_3^- type gradually changes to Na^+- Cl^- type through Ca^{2+}-Mg^{2+}- Cl^- type mixed waters, which might be an indication of change of hydrogeological conditions or different processes

like rock-water interaction, anthropogenic activity (Subba Rao et al. 2019a) or seawater intrusion. The groundwater in the recharge zone will have Ca^{2+}- HCO_3^- type water while in the discharge zone it may have higher mineral composition due to the long residence time and prolonged contact with aquifer matrix (Nawale et al. 2021). This suggests the intrusion of saline water in most of the coastal villages.

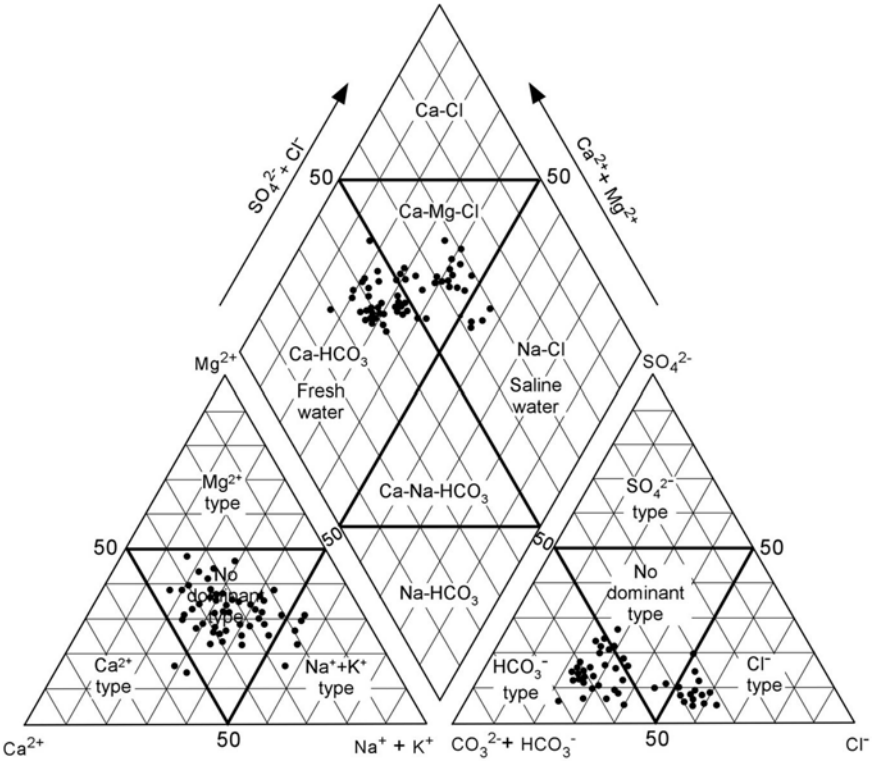

Fig. 4. Piper's Trilinear diagram.

CONCLUSION

The present study provides an assessment of the geospatial distribution of groundwater quality in the Balasore Sadar and Remuna blocks of Balasore district. This coastal part of Odisha is densely populated and sustains intense agricultural activity, as a result of which the coastal aquifers are affected by geogenic, anthropogenic and seawater intrusion processes including fluorosis problem. The study suggests that the water is mostly alkaline and hard but many parameters excluding F^- are within the permissible limit. Change of groundwater types from Ca-HCO_3 (fresh water) → Ca-Mg-Cl → Na-Cl (saline water) as well as increase of TDS in seaward direction indicates the effect of seawater intrusion in the study area. The impact of non-geogenic sources is often superimposed on the geogenic factors resulting in wide variation of the groundwater chemistry. However, it is important to monitor the groundwater quality in these blocks regularly to ensure the continued safety and sustainability of the water resources. Rainwater harvesting techniques like surface water storage, recharge pits, check dams, etc., should be erected to improve the groundwater quality and quantity for sustainable development and management of groundwater resources.

REFERENCE

Alam, M. Z., Carpenter-Boggs, L., Mitra, S., Haque, M. M., Halsey, J., Rokonuzzaman, M. 2017. Effect of Salinity Intrusion on Food Crops, Livestock, and Fish Species at Kalapara Coastal Belt in Bangladesh. J. Food Qual, Pp 1–23. Article ID 2045157. doi:10.1155/2017/2045157

APHA (2012) Standard methods for the examination of water and wastewater, 19 th edn. American Public Health Association, Washington DC.

BIS (2012) Bureau of Indian Standards: Drinking water specifications. IS 10500: 2012, New Delhi, India

Das, R. 2011. Hydrogeochemistry of Banki Sudivision, Cuttack district Orissa. The Bioscan, pp.35-42.

Das, R. 2022. Monitoring the seasonal variation of groundwater chemistry and quality assessment for agricultural and industrial purpose of Athgarh basin, India, Journal of Environment, Ecology and Conservation, Eco. Env. & Cons. 28 (1), pp. 298-309, Copyright@ EM International, ISSN 0971–765X, DOI No.: http://doi.org/10.53550/EEC.2022.v28i01.043

Das, R., Das, M. and Goswami, S. 2016. Groundwater quality Assesment for drinking and industrial purpose of Rourkela, Sundergarh District, Odisha, India. International Journal of Earth Science and Engineering. (6), pp. 314-321.

Das, R., Goswami, S., Das, S., Das, M. 2015. Hydrogeochemistry and Groundwater quality assessmentfor irrigation purpose in and around Rayagada Town, Odisha, India. International Journal of EarthScience and Engineering 8 (2), pp.611- 616. (SJR:0.15) (ISSN:0974- 5904), http://cafetinnova.org/journals/ ijee/about- journal/) SCOPUS UGC No.2901 incorporating the first addendum. Geneva. 541p.

Mahalik, N.K. and Nanda, J.K. (2006). Precambrians. In: Geology and mineral resources of Orissa (eds:Mahalik, N.K. Sahoo, H.K, Hota, R.N., Mishra, B.P, Nanda, J.K. and Panigrahi A.B.). Society of Geoscientists and Allied Technologies, Bhubaneswar 3rd edition.

Mahmuduzzaman, M., Ahmed, U. Z., Nuruzzaman, A. K. M., and Ahmed, R. S. F. 2014. Causes of Salinity Intrusion in Coastal Belt of Bangladesh. Int. J. Plant Res. 4 (4A), pp.8–13. doi:10.5923/s. plant.201401.02

Nawale, V. P., Malpe, D. B., Marghade, D. and Yenkie, R. (2021) Non-carcinogenic health risk assessment with source identification of nitrate and fluoride polluted groundwater of Wardha sub-basin, central India. Ecotox. Environ. Safety, v.208, p.111548.https://doi.org/10.1016/j.econv.2020.111548

Piper, A. M. (1953) A graphic procedure in the geo-chemical interpretation of water analysis. USGS Groundwater Note No.12.

Subba Rao N (2017) Hydrogeology - Problems with solutions. PHI Learning Pvt. Ltd., Delhi.

Subba Rao, N., Sunitha, B., Sun, L., Spandna, B. D. and Chaudhary, M. (2019a) Mechanisms controlling groundwater chemistry and assessment of potential health risk: A case study from south India. Geochemistry, https://doi.org/10.1016/j.chemer.2019.125568

World Health Organization (2017) Guidelines for drinking-water quality: fourth edition.

VISTAS IN GEOLOGICAL RESEARCH
Special Publication in Geology (19), March 2023, pp. 223-230

Active Fault Studies In and Around Mandi, Himachal Pradesh, India

BHABANI SHANKAR SETHI, SANTISWARUP SAHOO [*], JITUNANDAN PRADHAN

[1] P. G. Department of Geology, Utkal University, Vani Vihar, Bhubaneswar,751004
** Corresponding author:sahoosantiswarup@gmail.com*

Abstract: Our study is focused in and around Mandi, Himachal Pradesh, which is a part of meizoseismal zone of 1905 Kangra earthquake (Mw 7.8). A new active strike-slip fault has been identified from the interpretation of high-resolution CORONA satellite data (1.8 m). A 20 km long active strike slip fault having dextral movement has been identified in the vicinity of Mandi. Prominent offset of streams, pressure ridge, linear valley was delineated. Offset of streams were measured from the satellite image having variation of length from 274m to 833m. The calculation of slip rate was done using D\L ratio (Matsuda,1975) and found to be 5.19 mm/year, which suggests that it is accumulating more strain. Based on the length of the fault, magnitude was calculated to be 6.5 Mw using the empirical relationship by Wells and coppersmith, 1994. The newly identified active strike-slip fault in a thrust regime is a result of oblique convergence between the Indian and Eurasian plate. This identification will certainly help towards seismic hazard assessment (SHA) of the region.

Keywords: Active fault, Steam Offsets, River Sinuosity, Slip Rate, Rupture Length, Earthquake-magnitude.

INTRODUCTION

The Indian subcontinent is more vulnerable to various kinds of natural hazards such as earthquakes and tsunamis. These catastrophic disasters have posed threat to mankind. The increasing population at a high rate and very poor understanding leads to an exponential growth of infrastructure in the last decade which indicates that more no of the population is seized under highly vulnerable areas. Highly vulnerable area indicates both near and far-field forms of the shores of natural hazards.

The Himalayas spreads its venue along the northern side of the Indian continent and stands by the restless giant structure. The structure is a result of the ongoing crustal collision and the convergence between the Indian and Eurasian plates. These mighty events have made the Himalayas one of the most seismic-active regions in the world. The most promising large magnitude earthquakes not only shake the restless giant landmass but also leave its footprints in world scenarios for its vulnerable index. In the last 100 years, the arc has witnessed several large-magnitude earthquakes. These major earthquakes which make this region both interesting and dangerous, are 1905 Kangra (7.8 Mw),1934 Bihar-Nepal (8.1 Mw),1950 Upper Assam (8.4Mw) and recent 2005 Muzaffarabad (Mw7.6) Nepal earthquake of 2015 (Mw7.8) (Seeber and Armbruster,1981; Yeats et al.,1997; Ambraseys and Bilham,2000; Ambraseys and Douglas,2004, Yeats and Hussain,2006, Kenda at el.,2008). It is evident that more than 45% of the Himalayan arc has ruptured during the last 200 years and the remaining

undeformed regions are under high seismic risk and categorized under seismic gaps. These potential areas can trigger large-magnitude earthquakes in the near future (Bilham et al.,2001). To study properly more about Seismic Hazard Assessment (SHA) of the seismically active regions identification of active faults is necessary for it because the active faults are considered the sources of large magnitude earthquakes in near future and pose a hazard to near-field and far-field areas (Yeats et al.,1997; McCalpin,1996: Malik et al.,2010).

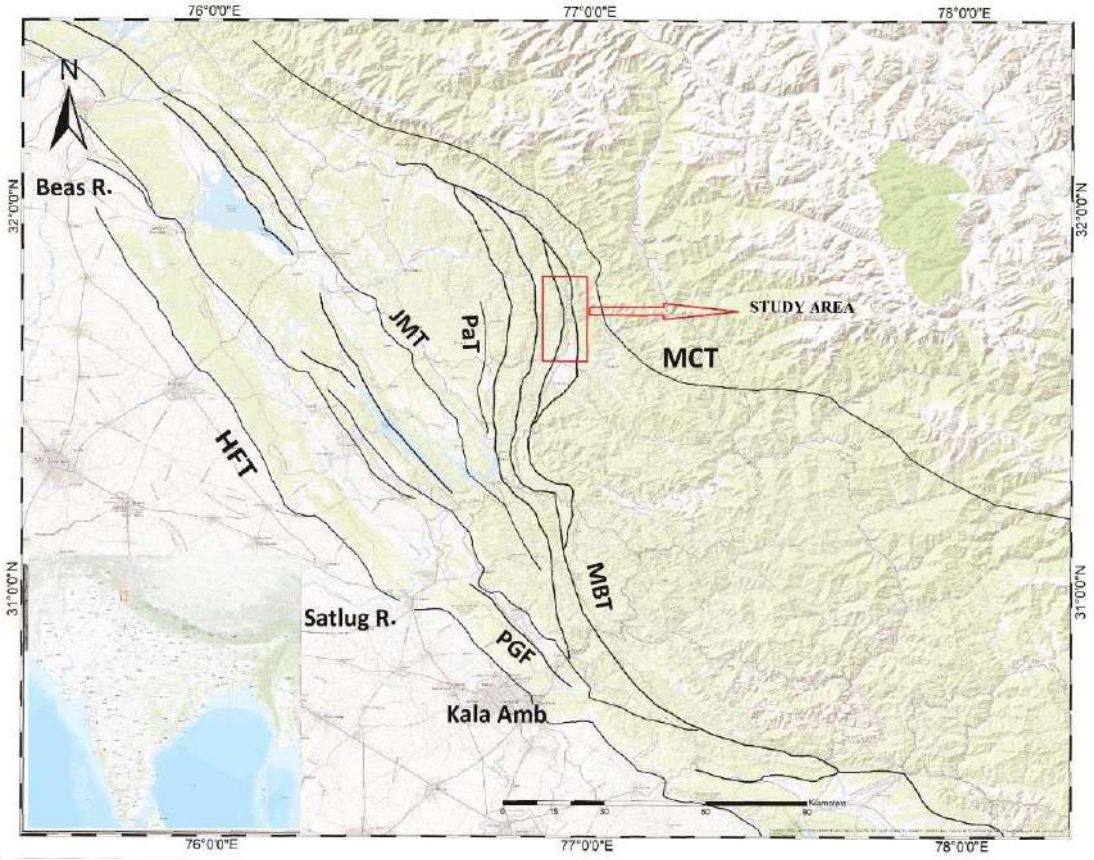

Fig. 1: Topographic relief map of the study area illustrating major faults marked by continuous lines. The red box shows the area where the study was concentrated. The major faults are after Gansser (1964), Valdiya (2001) and Powers et al. (1998). The inset shows the DEM of India with the location of the NW Himalaya.

General Geomorphic Setting

The present study area is part of northwest Himalaya, it is the upper part of the historical Kangra valley and part of the Main Boundary Thrust (MBT). The area lies between the Main central thrust (MCT) and Himalayan frontal thrust (HFT). It falls in a part of the Main Boundary Thrust (MBT) which acts as a transition zone of lesser Himalayan and higher Himalayan rock. It is the part of north Himalaya having coordinates between 76.9179E-31.7609N to 76.9115E- 31. 6262N.Mandi is a bowl-shaped tableland on the banks of the river Beas, surrounded by the high hill ranges of Gandharv Hills, Motipur Dhar, Rehra Dhar, and Tarna Hill. Geologically, the city is in seismic Zone No. IV is near a fault line and is prone to earthquakes.

Beas River is the major drainage system in this district, and it bifurcates into two near Mandi town. The rock formations occupying the district range from the Pre-Cambrian to the Quaternary period. A major part of the district lies in the lesser Himalayan region, which presents a rugged mountainous terrain composed of crystalline, metamorphic, and unfossiliferous sedimentary rocks of the oldest system. The lithologies vary from the southwestern part consisting of Siwalik sediments with scarped slopes, a few small intermontane valleys of fluvial systems having younger alluvial plains, prominent among them is the Sunder Nagar valley south of Mandi town.

The dynamics of the Himalayas are not only known for their long-extending mountain chain but also known for their physiological variation from north to south. Four major principal tectonic zones play the main role in it; they are higher Himalaya, lesser Himalaya, sub-Himalaya, and Indo-Gangetic plain (IGP) (Nakata,1972; power et al.,1998). They are as follows (Malik and Mohanty, 2007).

1. Folded mountain range
2. Intermontane valley
3. Sub-Himalayan hill range (Siwalik)
4. Indo-Gangetic plain (IGP)

The main boundary thrust in the south (MBT) and Main Central Thrust (MCT) in the north are the two major tectonic elements along with the lesser Himalayan domain. The geology of Lesser Himalaya has been rendered challenging by its characteristic complexities such as:

1. The presence of rocks of a wide spectrum of stratigraphic ranges from Precambrian to Tertiary.
2. The complex structural juxtaposition of the number of in-sequence thrust sheets.
3. Superposition of several thermal and tectonic events.

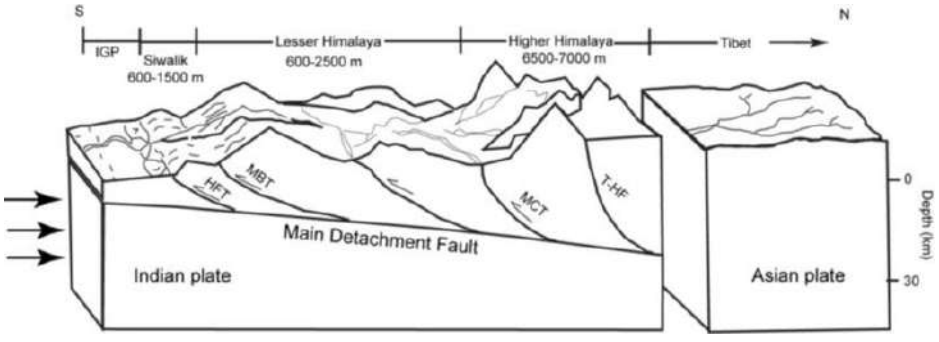

Fig. 2: Generalized schematic model showing major structural features and physiographic divisions of the Himalayas (after Jackson and Bilham, 1994; Burbank and Anderson, 2001). IGP – Indo-Gangetic Plain; HFT-Himalayan Frontal Thrust, MBT-Main Boundary Thrust, MCT-Main Central Thrust, THF-Trans Himadri Fault. Reference: - Active Fault and Paleoseismic studies in Kangra Valley, NW Himalaya, (Sahoo,2014)

Active faulting in the vicinity of Mandi

Endeavour has been made towards the identification of active fault traces in and around the Mandi region. In the present study high resolution satellite data i.e., corona satellite photos (stereo pair), CartoDEM and Google earth data were used. These data sets are used towards the identification and measurements. There are several software such as ArcGIS, and Google earth pro are also used for data sets to view 3D the terrain model of the desired area with a broader preview. Satellite data interoperation helps the identification of geomorphic indicators/markers such as linear valleys, stream offsets, and triangular forests and helps in calculating the Beas River sinuosity. This geomorphic indicator indicates the ongoing active fault topography in the study area.

Stream offsets

The area selected for research lies near Main Boundary Thrust and the portion of the Beas River is flowing on this prominent trend. There is the presence of a linear valley along the river which extends from Kathayana to Bhatwar. The presence of four sets of stream offsets is found along the fault. They are distributed from Beer to Bhanwar near about 20 km. The first set of stream offset (S1) is found near Kayathana and Dhryanaarea. The first offset is found in the northwest direction of Mandi town having coordinates 31°43’31’’N, 76°55’11’’E in Kathayana and Dharayana area. The area shows gentle warping of the strata along with triangular facets and a linear valley shown as a geomorphic indicator. Along the offsets, the Beas is meandering from its original path and moving towards southwest with depositing sand. The second offset (S2) is located 1.5 km towards the south direction of offset 1 having coordinates 31°42’46’’N, 76°55’11’’E in the Satohal area.

The area shows gentle warping of the strata along with triangular facets and linear valleys as geomorphic indicators. Along the offsets, the Beas meanders its original path and moves towards the southwest with depositing sand. This area clearly shows the deformation. The third offset (S3) is found at 1.6 km towards the south direction of offset 2 having coordinates 31°42’17’’N, 76°55’03’’E in Lakhwan area. The area shows gentle warping of the strata along with triangular facets showing a geomorphic indicator. Along the offsets, the Beas River is bifurcated, and it is part of a linear valley. The fourth offset (S4) is found 800m west of the third offset showing maximum deformation in the area.

The Faulting placed and warped the lesser Himalayan sediments, developing Sharp vertical scarlets facing towards the Beas River. The most prominent deformation shows along MBT (Main Boundary Thrust) on the bank of Beas River. There are 4 sets of stream offsets are identified in satellite imagery. The fault has a downthrown side to the west to south-west reassembling the pattern of strike slip faulting.

Fig. 3: Corona satellite imagery (resolution 1.8m) of Main Boundary thrust, Mandi region, Himachal Pradesh, India. White arrows indicate the trace of the fault. The white arrow indicates consistent right-lateral offsets of steam drainage crossing the fault. Note: sharpness of the fault traces, which suggests the recent activity.

DISCUSSION

The offset of strike-slip fault by channel and its preservation involves both the interaction of erosion and sedimentation (Wallace, 1968). On the other hand, tectonic movements i.e., Fault displacement and warping or tilting processes are part of catastrophic and relatively continuous. The rates of the two sets of processes are, in general of the same order of magnitude; for example, fault slips are measured in meters in the same period that channel erosion or sedimentation is measured in meters.

The main aim of the present study is to determine the rate and the nature of the movements. Straight channels have formally crossed the fault are shown in the figure-3 and it experienced no vertical movement. The streams flow in their original straight path before the movement. After the movement has progressed the stream deviates from its original path .and other channels are brought into this alignment (Wallace, 1968). As a result, the stream flows right to the adjacent.

Based on the stream offsets, an attempt has been made to calculate the slip rate of the fault. A relationship between long-term slip rate (S) along with a lateral slip of fault and offset ratio (a = D/L) has been roughly calculated as S (m/1000 years), i.e., 10 a (Matsuda, 1975). Off-set

ratio ($a = D/L$), where D is the amount of stream offset along the fault and L is the upstream length of the displaced stream (Matsuda, 1966 , Malik and Nakata,2003).

After the 3D terrain visualisation of corona satellite data with the help of a mirror stereoscope the offsets are marked, and the same offsets are identified in Figure-3. The upstream and offset lengths are measured, and the offset and upstream Ratios are calculated along with slip rate. The ratio is plotted in logarithmic scale through MS Excel.

Table 1: Calculation of slip rate with help of amounts of stream offset along the fault and upstream length from the fault trace.

Sl. No	L (Upstream Length) in meter	D (Offset ength) in meter	D/L	Mean	10a=slip rate (mm)
S1	1257	883	0.7024	0.5191	5.19
S2	948	746	0.7869		
S3	1817	392	0.2157		
S4	738	274	0.3712		

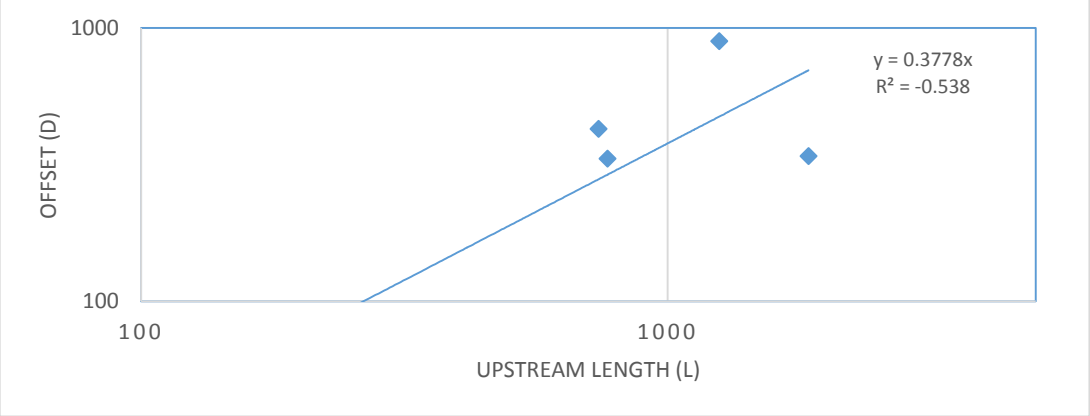

Fig. 4: Relationship between amounts of stream offset along the fault and upstream length from the fault trace.

Calculation of Magnitude

From the given (Wells and Coppersmith,1994) formula for calculation of magnitude all around the world given by

M = 5.08 + 1 .1 6*1og (SRL)

where M is the moment magnitude

SRL is surface rapture length.

In our study area, the length of the fault is nearly equal to 20 KM.

*M= 5.08 + 1 .1 6*1og (20) =5.08+1.508=6.58 Mw*

CONCLUSIONS

Our investigation enlightened towards the identification of active fault in a thickly populated area such as Mandi. The identification of geomorphic indicators evidence and identification of stream offsets indicating towards the activeness of the area. A 20 Kilometre dextral active strike slip is identified in the Mandi area. The presence of a strike slip fault in a thrust region envisages that there is a slip partitioning among thrust and strike slip faults resulting due to oblique convergence between the Indian and Eurasian plates.

From the presence of a 20 Kilometre dextral active strike slip identified in the Mandi area, we calculated magnitude using a formula which universally accepted for strike slip faulting (Wells, D. L., Coppersmith, K. J., 1994), which will be a great help towards the seismic hazard assessment of thickly populated area like Mandi. The estimated slip rate using the D/L ratio (Matsuda, 1975) suggests that the area is accumulating more strain which may experience a large magnitude earthquake in the near future.

REFERENCES

Ambraseys, N., Bilham, R., 2000, A note on the Kangra Ms = 7.8 earthquake of 4 April 1905. Current Science, v. 79 (1), pp. 45–50.

Ambraseys, N., Douglas, J., 2004. Magnitude calibration of north Indian earthquakes. Geophysical Journal International, v. 158, pp. 1–42.

Bilham, R., Gaur, V. K., Molnar, P., 2001. Himalayan seismic hazard. Science, v. 293, pp. 1442–1444.

Burbank, D. W., Anderson, R. S., 2001. Tectonic Geomorphology. Blackwell Science, pp. 274.

Gansser, A., 1964. The Geology of the Himalaya. Wiley Interscience, New York, pp.189.

Jackson, M., Bilham, R.,1994. Constraints on Himalayan deformation inferred from vertical velocity fields in Nepal and Tibet. Journal of geophysical

research, vol. 99, no. B7, pages 13,897-13,912.

Kaneda, H., Nakata, T., Tsutsumi, H., Kondo, H., Sugito, N., Awata, Y., Akhtar, S. S., Majid, A., Khattak, W., Awan, A. A., Yeats, R. S., Hussain, A., Ashraf, M., Wesnousky, S. G., Kausar, A. B., 2008. Surface rupture of the 2005 Kashmir, Pakistan, earthquake and its 181 active tectonic implications. Bulletin of the Seismological Society of America, v. 98 (2), pp. 521–557.

Malik, J. N., Nakata, T., 2003. Active faults and related Late Quaternary deformation along the northwestern Himalayan Frontal Zone, India. Annals of Geophysics, v. 46 (5), pp. 917–936

Malik, J. N., Mohanty, C., 2007. Active tectonic influence on the evolution of drainage and landscape: geomorphic signatures from frontal and hinterland areas along Northwestern Himalaya, India. Journal of Asian Earth Sciences, v. 29 (5–6), pp. 604–618.

Malik, J. N., Shah, A. A., Sahoo, A. K., Puhan, B., Banerjee, C., Shinde, D. P., Juyal, N., Singhvi, A. K., Rath, S. K., 2010a. Active fault, fault growth and segment linkage

along the Janauri anticline (frontal foreland fold), NW Himalaya, India. Tectonophysics, v. 483, pp. 327–343.

MATSUDA, T. (1966): Strike-slip faulting along the AteraFault, Japan, *Univ.* Tokyo.

MATSUDA, T. (1975): Active fault assessment for IrozakiFault System, Izu Peninsula, Report on the Earthquakeof the Izu Peninsula, 1974, 38, 409.

McCalpin, J. P., 1996. Paleoseismology; Academic Press, New York, p 588.Meghraoui, M., Camelbeeck, T., Vanneste, K., Brondeel, M., Jongmans, D., 2000. Active faulting and paleoseismology along the Bree fault, lower Rhine graben. Belgium Journal of Geophysical Research, v.105, pp. 13809–13841.

Nakata, T., 1972. Geomorphic History and Crustal Movements of the Foothills of Himalayas. Sendai, Institute of Geography, Tohoku University, pp. 77.

Powers, P. M., Lillie, R. J., Yeats, R. S., 1998. Structure and shortening of the Kangra and Dehra Dun Reentrants, Sub Himalaya, India. Geological Society of America Bulletin, v. 110, pp .1010–1027.

Seeber, L., Armbruster, J. G., 1981. Great detachment earthquakes along the Himalayan arc and long-term forecasting. In: Simpson, D. W., Richards, P.G. (Eds.), Earthquake Prediction: An International Review AGU 4, pp. 259–279.

Sahoo, Santiswarup., 2014. - Active Fault and Paleoseismic studies in Kangra Valley, NW Himalaya:An attempt to identify the surface rupture of 1905 Kangra earthquake. Unpublished PhD thesis.

Valdiya, K. S. 2001. Reactivation of terrain-defining boundary thrusts in central sector of the Himalaya: Implications. Current Science, v. 81 (11), pp.1418–1431.

Wallace E.R.,1968, Notes on stream channels offset by the San Andreas fault, southern coast ranges, California*, U.S. geological survey, Menlo Park, California

Wells, D. L., Coppersmith, K. J., 1994. New empirical relationships among magnitude, rupture length, rupture width, rupture area, and surface displacement. Bulletin of the Seismological Society of America, v. 84(4), pp. 974–1002.

Yeats, R. S., Sieh, K., Allen, C. R., 1997.The geology of earthquakes: Oxford University

Yeats, R. S., Hussain, A., 2006. Surface Features of the Mw 7.6, 8 October 2005 Kashmir earthquake, northern Himalaya, Pakistan: Implications for the Himalayan Front. Abstract, Seismological Society of America.

VISTAS IN GEOLOGICAL RESEARCH
Special Publication in Geology (19), March 2023, pp. 231-240

Hydrogeochemical Characterization and Irrigation Quality Assessment of Groundwater in Puintala Block of Balangir District, Odisha

BABITA BAKHARA[1], NANDITA MAHANTA[2*] AND H.K. SAHOO[2]

[1]Department of Earth Sciences, Sambalpur University, Jyoti Vihar, Burla-768019
[2]Department of Geology, Utkal University, Vani Vihar, Bhubaneswar-751004
*Corresponding Author, E-mail: nandita.mahanta12@gmail.com

Abstract: Groundwater is the main source used for domestic and agricultural purposes. The demand for the water increases due to rapid population growth, increased industrialization and irrigational activities. Therefore, management of this resource is very important. In groundwater resource evaluation, quality is as important as quantity. The aim of the study is to assess the suitability of groundwater in relation to irrigation, domestic and drinking uses. A total of 25 water samples (21 tube wells and 04 dug wells) were collected from different localities of Puintala block, Balangir district, Odisha. The samples were then analyzed for various physicochemical attributes like temperature, Electrical Conductivity (EC), Total Dissolved Solids (TDS), Total hardness (TH), Total alkalinity (TA), Calcium (Ca^{2+}), Magnesium (Mg^{2+}), Sodium (Na^{+}), Potassium (K^{+}), Chloride (Cl^{-}), Sulphate (SO_4^{2-}), Bicarbonate (HCO_3^{-}), Nitrate (NO_3^{-}), Fluoride (F^{-}) etc. and compared with the Bureau of drinking water standard (BIS, 2012). As per this standard, 40% of the samples exceed the acceptable limit for the total dissolved solids (TDS). 44% of samples for TH, 8% samples for Ca^{2+}, 32% samples for Mg^{2+}, 12% samples for Cl^{-}, and 8% for SO_4^{2-} exceed the acceptable limit for drinking purposes but all the samples have values within permissible limit. The value of sodium adsorption ratio (SAR) depicts that the groundwater resources of Puintala block is excellent for irrigation. From the Residual sodium carbonate (RSC) value, it is observed that 88% of the groundwater samples are safe for irrigation. Kelly's ratio (KR) value revealed that maximum numbers of water samples are of good to moderate category for irrigation. With respect to Percent sodium (%Na), maximum numbers of samples are "good" to "permissible" for irrigation purpose. With respect to %Na values, 9 samples are "good", 13 samples are "permissible" and only one sample fall in "doubtful" category Further, Piper trilinear diagram classified the maximum number of the samples from the study area under Ca^{2+}–HCO_3^{-} type followed by mixed Ca^{2+}–Mg^{2+}–Cl^{-} type.

Keywords: Hydrochemical analysis· Puintala block· Correlation coefficient, irrigation.

INTRODUCTION

Water is an indispensable natural resource on earth. Safe drinking water is the primary need of every human being. Freshwater has become a scarce commodity due to over-exploitation and pollution of water. Groundwater is the major source of drinking water in both urban and rural areas (Gupta et al., 2009). It is the most important source of water supply for drinking, irrigation and industrial purposes. The increasing population and its necessities have led to

the deterioration of surface and subsurface water Groundwater is believed to be comparatively much clean and free from pollution than surface water. But the prolonged discharge of industrial effluents, domestic sewage, use of fertilizers and pesticides, and waste dumping cause the groundwater to become polluted and create health problems (Ramakrishnaiah et al., 2009). The rapid growth of urban areas has further affected groundwater quality due to the overexploitation of resources and improper waste disposal practices. Hence there is always a need for concern over the protection and management of groundwater quality (Singh et al., 2012). Considering the above aspects of groundwater contamination, the present study is undertaken to investigate the possible impact on the groundwater quality of some tube wells and dug wells of Puintala block of Balangir district, Odisha. Thus, in this research work, an attempt has been made to assess the physical and chemical properties of groundwater for drinking and irrigation purposes.

STUDY AREA

The present study has been carried out in Puintala block of Balangir district, which is the western part of Odisha bounded by latitude 20º35´68´´N to 20º50´58´´N and longitude 83º30´56´´ to 80´40´16´´ E which comes in Survey of India Toposheet nos. 64P/5, 64P/9 and 64P/10. The block is bounded by the Subarnapur district on the east, Balangir block by west, Loisinga and Deogaon blocks by north and south respectively. The Puintala village has population of 2838 of which 1436 are males while 1402 are females as per Population Census 2011. The location map of the study area is shown in Figure 1.

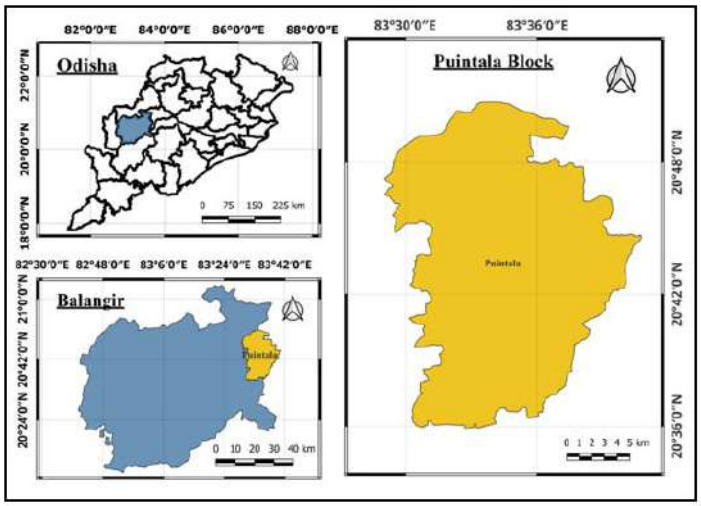

Fig. 1: Location map of study area.

MATERIAL AND METHODS

Groundwater Sampling

A total of 25 groundwater samples were collected from different locations of the study area during the post-monsoon season in 2017. The collected samples and the sample location map from different villages are shown in Figure 2. All the samples were collected in 1 liter polyethylene bottles. Each bottle was rinsed with distilled water and before sampling, the

tube wells were pumped for 5 minutes to purge the aquifer and to avoid contamination in the water samples. The bottles were labeled and made airtight to prevent leakage.

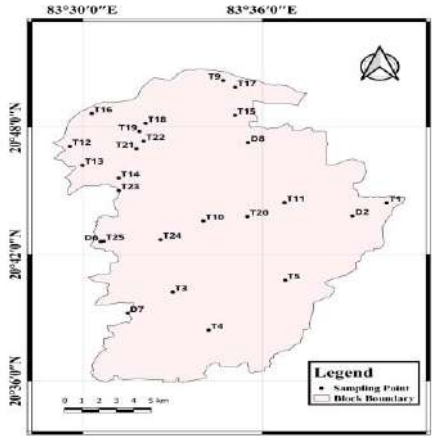

Fig. 2. Sample location map.

Analytical Techniques

Temperature, EC, TDS were measured in the field and other parameters such as Ca^{2+}, Mg^{2+}, Na^{+}, K^{+}, HCO_3^{-}, Cl^{-}, SO_4^{2-}, NO_3^{-}, F^{-}, TA and TH, were analyzed in the laboratory. The ion balance error equation was used for checking the accuracy of the analysis and found to be ± 5% for all the ion concentrations. The results were compared with the drinking water quality standard given by BIS (2012). The hydrochemical results were interpreted using Piper (1944), Wilcox (1955) and Richards (1954) diagrams to infer the suitability of groundwater for irrigation purposes.

RESULT AND DISCUSSION

The statistical analysis of physicochemical parameters, which were analyzed in the post-monsoon season, in 2017, has been shown in Table 1. The comparison of groundwater quality data with BIS standards has been shown in Table 2. At the time of sample collection, the water temperature varies from 24ºC to 29 ºC with an average of 27.8 ºC, implying that the water is not influenced by any form of geothermal water. The pH value of water samples in the study area ranged from 6.62 to 7.81 with average of 7.03. The pH of all samples is within the acceptable limit as prescribed for drinking water standards, BIS (2012). The permissible limit of TDS in drinking water is 2000 mg/l (BIS, 2012). TDS values of the study area highly fluctuated from 222.3 to 1928.19 mg/l. There are 10 numbers of samples exceeding their acceptable limit and the value of all the samples are below the permissible limit. The electrical conductivity (EC) of water samples of the study area varies between 317 and 2819 µ mho/cm with an average of 905.96 µ mho/cm. In the drinking water samples, the calcium content varies from 8.01 to 136.67 mg/l and average is 37.20 mg/l. The results indicate that two samples of the site have the concentration of calcium above the acceptable limit. The magnesium content ranges from 11.66 to 60.7 mg/l with an average 30.44 mg/l. There are 8 samples exceeding their acceptable limit. The main source of magnesium in the study area

may be due to weathering of olivine, augite, biotite, hornblende, diopside etc. of the aquifer material. The values of sodium were confined between 21.11 and 222.22 mg/l and average is 78.11 mg/l in the study area. High concentrations of sodium in groundwater may due to the weathering of feldspar bearing rocks and saltwater intrusion. But the study area is not surrounded by any ocean, the lithology is the main source of sodium present in groundwater. The potassium ion concentration fluctuates from 0.29 to 29.55 mg/l. BIS and WHO have not prescribed any limit for potassium ions in drinking water but it is useful for total ionic balance as well as an important nutrient for the human body (Tyagi, S. et al., 2014). Minimum value of bicarbonate is 86.37 and maximum is 433.12 mg/l in the groundwater samples of the study area. Chloride (Cl^-) is an essential anion found in water. According to BIS, the maximum permissible limit for chloride is 1000 mg/l. Three samples of villages Bramhanipali, Lukapada and Nuapada had exceeded their acceptable limit of 250 mg/l. The rest of the samples are all within the acceptable limit. Fluoride concentration ranged from 0.18 to 1.34mg/l with average of 0.60 mg/l. Three samples of villages Athgaon, Chhatamakhana and Jamsara have fluoride values beyond their desirable limit of 1.0 mg/l. Sulphate may come into groundwater through industrial or anthropogenic additions in the form of Sulphate fertilizers (Rao et al. 2013). Sample no.T-9 and T-24 have values above the acceptable limit whereas the rest of the samples are observed within the acceptable value of sulphate. Nitrate is soluble in water very easily so it can move into the drinking water supply through rock and soil (Saba et al., 2006). The Nitrate of groundwater in the study area ranged from 1.2 to 140.7 mg/l with an average of 30.5 mg/l. Six samples have values both acceptable and permissible limit. The range of total hardness was found in between 45.2 to 584.81 mg/l, 11 numbers of samples exceeded their acceptable limit. Alkaline water may decrease the solubility of metals. Alkalinity values in the analyzed water samples were found to be 86.37 to 433.12 mg/l and average 218. 80 mg/l.

Table 1: Statistical analysis of physicochemical parameter.

Parameter	**Minimum**	**Maximum**	**Average**
Temperature	24	29	27.8
pH	6.62	7.81	7.03
TDS	222.3	1928.19	614.16
EC	317	2819	905.96
Ca^{2+}	8.01	136.67	37.20
Mg^{2+}	11.66	60.7	30.44
Na^{+}	21.11	222.22	78.11
K^{+}	0.29	29.55	3.072
HCO_3^-	86.37	433.12	218.80
Cl^-	7.09	411.22	100.49
F^-	0.18	1.34	0.60
SO_4^{2-}	1.24	342.2	55.1
NO_3^-	1.2	140.7	30.5
TH	45.2	584.81	214.10
TA	86.37	433.12	218.80

All the parameters are express in mg/l except pH, temp. and EC. The EC is expressed in µmho/cm,and temperature is express in ºC.

Table 2: Comparison of post-monsoon groundwater quality with drinking water standards (IS 10500:2012)

Parameters	IS 10500:2012		No. of Samples exceeding acceptable limits	% of samples exceeding the acceptable limit	No. of Samples exceeding permissible limits	% of Samples exceeding permissible limits
	Acceptable Limit	Permissible Limit				
pH	6.5-8.5	No relaxation	00	0	Nil	0
TDS	500	2000	10	40	Nil	0
TH	200	600	11	44	Nil	0
Ca^{2+}	75	200	02	8	Nil	0
Mg^{2+}	30	100	08	32	Nil	0
Cl^-	250	1000	03	12	Nil	0
SO_4^{2-}	200	400	02	08	Nil	0
NO_3^-	45	No relaxation	06	06	Nil	0
F^-	1	1.5	03	12	Nil	0

All the samples are express in mg/l except pH.

The radar chart is used for the displaying of the major ion concentrations of each and every sample. The radar chart of all 25 samples is given in Figure. 3 in the radar diagram. It is found that sodium and bicarbonate ions have a higher value in comparison to other ion concentrations.

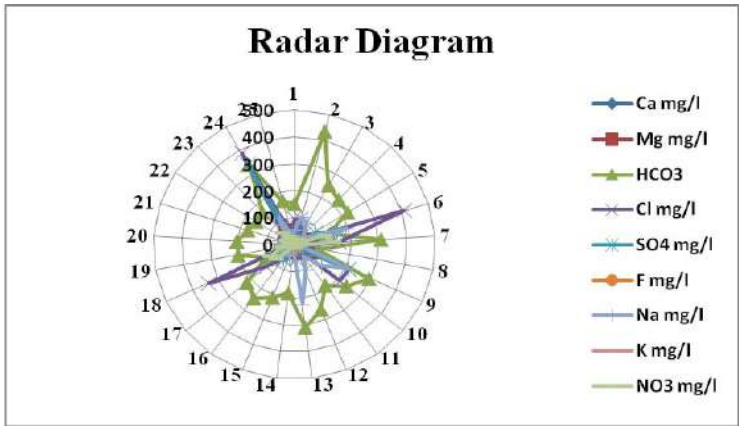

Fig. 3: Radar diagram of ion concentration.

In this study, groundwater has been classified as per Piper trilinear diagram (Piper 1944) to understand the hydrochemical facies of groundwater resources, which is shown in Figure. 4. The majority of the samples belonged to Ca^{2+}–Mg^{2+}–HCO_3^- and Ca^{2+}-Mg^{2+}–SO_4^{2-}–Cl^- representing temporary hard water and permanently hard water and only a few samples fall under Na^+–HCO_3^-, Ca^{2+}–Cl^- and mixed Ca^{2+}– Mg^{2+}–Cl^- type.

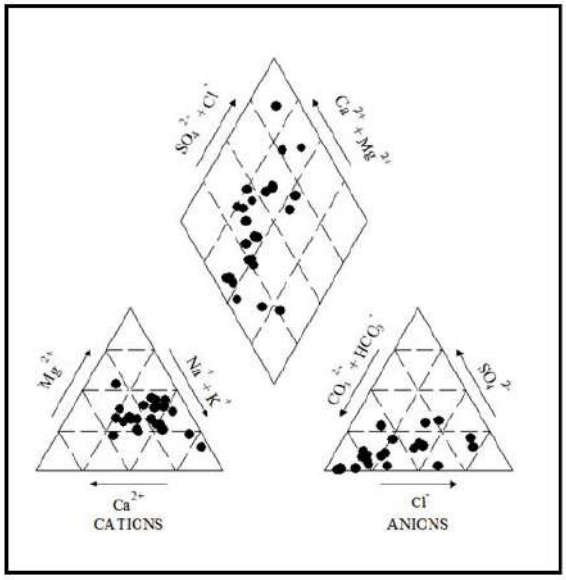

Fig. 4. Piper diagram.

Gibbs (1970) has proposed to scatter diagram method illustrating three important natural mechanisms controlling the major ion chemistry of the groundwater such as 'water-rock interaction', 'evaporation' and 'atmospheric precipitation'. The majority of the samples collected fall in "rock dominance" field and a few groundwater samples fell into evaporation dominant field, (5a and 5b) indicating that the chemistry of groundwater is controlled by the chemical composition of the aquifer.

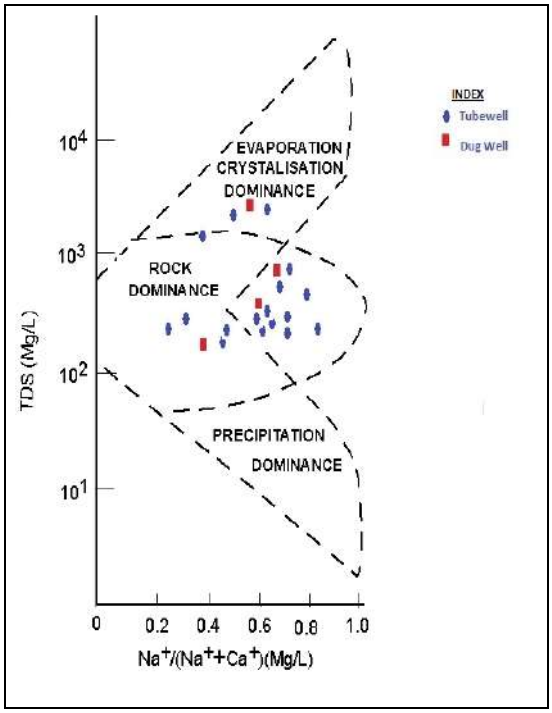

Fig. 5a. Gibb's Diagram for Cation

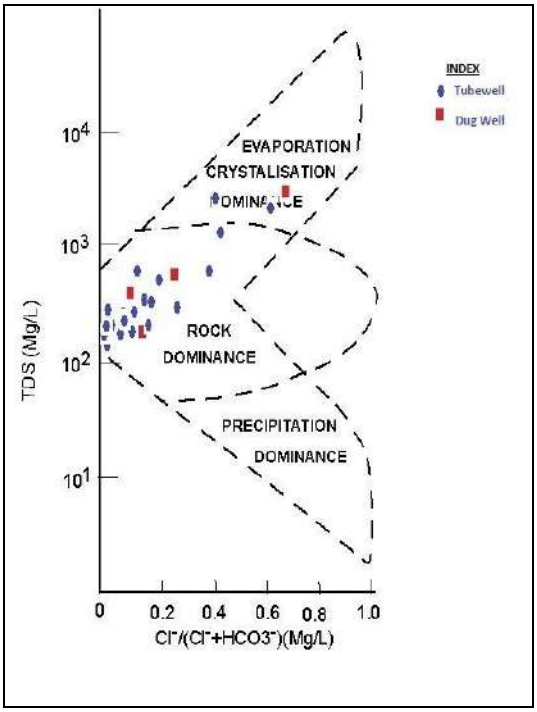

Fig. 5a. Gibb's Diagram for Anion

WATER QUALITY CLASSIFICATION FOR IRRIGATION

As the groundwater is being used for irrigation in the Puintala block, it is necessary to determine the parameters for irrigation water quality. The important parameters to know the quality of water for irrigation purposes are Sodium adsorption ratio (SAR), Percent sodium (%Na), Magnesium ratio (MR), Kelly's ratio (KR) and Residual sodium carbonate (RSC).According to classification by Richards (1954), the classification based on SAR values (Table 3), all the samples were found to be "excellent" for irrigation.

Table 3: Classification of groundwater samples of the study area for irrigation purposes

		Range	Class	Samples
SAR	$\frac{Na^+}{\sqrt{(Ca^{2+}+Mg^{2+})}/_2}$	<20	Excellence	25
		20-40	Good	--
		40-60	Permissible	--
		60-80	Doubtful	--
		>80	Unsafe	--
%Na	$\frac{(Na^+ + K^+)*100}{(Ca^{2+}+Mg^{2+}+Na^+ + K^+)}$	>20	Excellent	1
		20-40	good	9
		40-60	Permissible	13
		60-80	Doubtful	1
MR	$\frac{Mg^{2+}}{Ca^{2+}+Mg^{2+}} \times 100$	<50	Suitable	19
		>50	Unsuitable	6
RSC	$(HCO_3^- + CO_3^-) - (Ca^{2+} + Mg^{2+})$	<1.25	Safe	22
		1.25-2.50	Permissible	2
		>2.50	Unsuitable	1
KR	$\frac{Na^+}{Ca^{2+}+Mg^{2+}}$	<1.0	Suitable	19
		>1.0	Unsuitable	6

According to %Na, 13 samples were found to be "permissible" for irrigation. 9 numbers of samples are "good" and only one sample fall in the "unsuitable" category. Based on MR, most of the samples (19 samples) are suitable for irrigation. During the present study, the RSC values (Table 3) clearly indicate that 88% of the groundwater sample of Puintala is safe for irrigation. KR values (Table 3) indicate that the groundwater of Puintala is suitable for irrigation except few. There are 19 samples under suitable category and 6 samples under unsuitable category out of 25 samples. (Table 3). The plot of data on the U.S. salinity diagram(Richards,1954) in which the EC is taken as salinity hazard and SAR as alkalinity hazard majority of the water samples fall in the category C2-S1 followed by C3-S1, indicating medium salinity and low alkali and high salinity and low alkali water respectively. Minimum numbers of samples were in the zone of C4-S1 indicating very high salinity and low alkali water (Figure. 6).

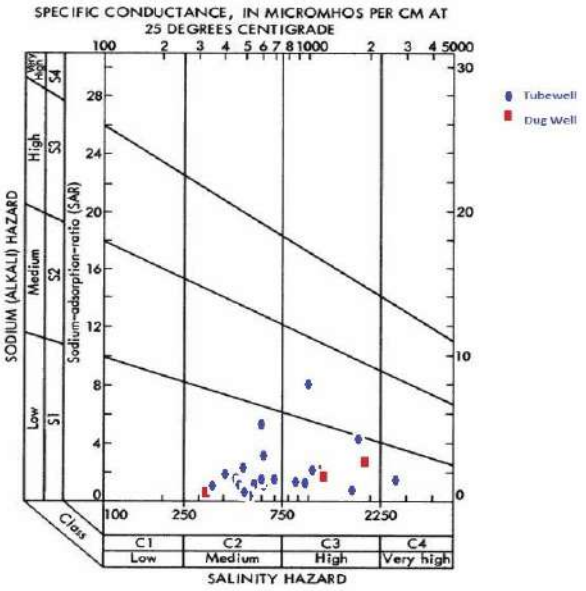

Fig. 6: U.S Salinity Diagram.

The analytical data plotted on the Wilcox diagram (Figure. 7) illustrates that except a few samples, most of the groundwater samples fall in "good and permissible" categories and can be used for irrigation.

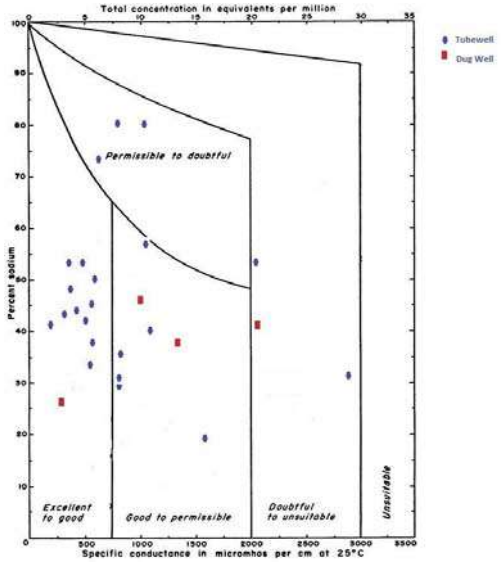

Fig. 7: Wilcox Diagram.

CONCLUSION

The majority of water samples were found to have values within acceptable limits as prescribed by Bureau Indian standards for drinking water (BIS, 2012). Among 25 numbers of samples, 10 samples exceeded their acceptable limit of TDS. 44% of water samples had exceeded their TH value. The 8% and 32% of water samples fall beyond the acceptable limit for calcium and magnesium respectively. of the samples. 12% of chloride, 8% of sulphate, 24% of nitrate and 12% of fluoride have crossed their acceptable limit. In case of nitrate 24% of the samples have values beyond the permissible limit. All the analyzed physicochemical parameters are within the drinking water permissible limit except nitrate. It is concluded that TDS, TH, and nitrate value is found to be more in comparison to other parameters. It is interpreted to be the result of weathering of rock and domestic solid waste leachet. The parameters like percent sodium (%Na), sodium adsorption ratio (SAR), Kelly's ratio (KR) and magnesium ratio (MR) were calculated from the chemical data. As per the results obtained, SAR revealed the excellent quality of groundwater for irrigation. Among the %Na value, maximum numbers of samples are good to permissible for irrigation purposes whereas, MR and KR values showed that the majority of water samples are suitable for agriculture and domestic uses. According to the RSC value, there are 88% of samples are suitable. Further, Piper trilinear diagram classified the maximum number of the samples from the study area under Ca^{2+}–HCO_3^- type followed by mixed Ca^{2+}–Mg^{2+}–Cl^- type. The majority of samples fall in the “rock dominance zone” according to Gibb's (1970) plot indicating that the lithology plays an important role in controlling the overall quality of groundwater apart from various other local environmental conditions. From this study, it is concluded that the majority of groundwater in the study area is chemically suitable for domestic and agricultural uses.

REFERENCES

Bureau of Indian Standards (2012) Indian standard specifications for drinking water 10500: BIS: New Delhi, India.

Gibbs, R. J. (1970) Mechanism controlling water world chemistry. Science 170:1088–1090

Gupta, D.P. Sunita and Saharan, J.P. (2009) Physiochemical analysis of groundwater of selected area of Kaithal City (Haryana) India. Researcher. V.1(2), pp.1-5.

Piper, A.M. (1944) A graphic procedure in the geochemical interpretation of water analysis Trans Am Geophys Union v.25, pp.914–923.

Ramakrishnaiah, C. R., Sadashivaiah, C., and Ranganna, G. (2009) Assessment of Water Quality Index for the Groundwater in Tumkur Taluk, Karnataka State, India. E-Journal of Chemistry, 6(2), pp.523-530. http://dx.doi.org/10.1155/2009/757424.

Rao.J. D., Babu. H. B, Swami, A.V.V.S and Sumithra, S. (2013) Physico-Chemical Characteristics of Ground Water of Vuyyuru, Part of East Coast of India Universal Journal of Environmental Research and Technology. v.3(2), pp.225-232.

Richards, L. A. (1954) Diagnosis and improvement of saline and alkali soils, Vol. 78, No. 2, p. 154. LWW

Saba, H.B., Thureau, P., Ancian, B. and Thevand, A. (2006) Combined use of Overhauser spectroscopy and NMR diffusion experiments for mapping the hydration structure of nucleosides: structure and dynamics of uridine in water, Magn. Reson. Chem.v. 44, pp. 1109–1117.

Singh, M. K., Jha, D. and Jadoun, J. (2012) Assessment of Physico-chemical Status of Groundwater Samples of Dholpur District, Rajasthan, India. International Journal of Chemistry. v. 4(4).

Tyagi, S., Dobhal, R., Kimothi, P.C., Adlakha, L.K., Singh, P., Uniyal, D.P. (2013) Studies of river water quality using riverbank filtration in Uttarakhand, India. Water Quality Exposure and Health,v. 5, pp.139-148.

Wilcox, L.V. (1955) Classification and use of irrigation waters. U.S. Department of Agriculture. Circ, Washington, DC, pp 969.

Printed @ ankitagraphics, Bhubaneswar
09437077337, saroj77337@gmail.com